Impacts to stock abundance indices due to offshore wind development-driven changes to fishery-independent survey effort: a thesis in Marine Science and Technology - Living Marine Resources Science and Management.

Miller, Angelia M

University of Massachusetts Dartmouth

School for Marine Science and Technology

Impacts to stock abundance indices due to offshore wind development-driven changes to fishery-independent survey effort

A Thesis in

Marine Science and Technology--Living Marine Resources Science and Management

by

Angelia M. Miller

Submitted in Partial Fulfillment of the

Requirements for the Degree of

Master of Science

August 2025

We approve the thesis of Angelia M. Miller

Date of Signature

Gavin Fay
Associate Professor, Department of Fisheries Oceanography
Thesis Advisor

Steven X. Cadrin
Professor, Department of Fisheries Oceanography
Thesis Committee

Catherine Foley
Fishery Biologist, Northeast Fisheries Science Center, NOAA Fisheries
Woods Hole, MA
Thesis Committee

Geoff Cowles
Graduate Program Director, Marine Science and Technology
Chairperson, Department of Fisheries Oceanography

Kevin Stokesbury
Dean, School for Marine Science and Technology

Tesfay Meressi
Associate Provost for Graduate Studies

ABSTRACT

Impacts to stock abundance indices due to offshore wind development-driven changes to fishery-independent survey effort

by Angelia M. Miller

Offshore wind energy development is occurring throughout the Northeast Large Marine Ecosystem and will interact with many marine use sectors, including fisheries. Wind areas overlap spatially with the footprint of the National Marine Fisheries Service (NMFS) Northeast Fisheries Science Center (NEFSC) multispecies bottom trawl survey, which has been conducted since the 1960s, and provides data that are relied upon for the assessment and management of many fisheries stocks in the Northeast U.S. This fishery-independent survey is confronted by potential preclusion of trawl sampling due to the spatial conflict arising from offshore wind energy development. My thesis quantifies the impacts of preclusion to survey operations and how changes to species distributions and abundances within wind areas could jointly affect downstream data products, such as stock abundance indices, and fisheries management advice. The first phase of my study uses the empirical data to serve as a proxy for expected impacts to survey data products when the survey is precluded from sampling within offshore wind energy areas (wind-precluded survey effort). Findings suggest that abundance indices are impacted most for species where there were larger differences in their catch rates in and outside of wind areas. The second phase of my study used survey data for summer flounder (*Paralichthys dentatus*) and Atlantic mackerel (*Scomber scombrus*) as case studies to fit spatiotemporal generalized linear mixed effects models (GLMMs), simulate survey data, calculate indices of abundance and population trends, and compare survey outcomes with and without preclusion from wind development areas. The results of the modeling indicate that spatiotemporal models can be used to simulate new survey data and evaluate impacts to the survey (and survey data products) when it is precluded from offshore wind energy areas. Further employing the species distribution operating models, I conducted a simulation study to examine changes in fish density under

assumed changes in species productivity within wind areas, and their effects on survey catch rates under wind-precluded survey effort. Findings conclude that estimates of abundance indices and population trends will be most biased if species experience enhanced productivity and survey effort is precluded within these areas. Thus, it is important that the losses in survey effort and data be mitigated to maintain at a minimum the existing understanding of species' relative abundance. This study contributes directly to implementation of the Federal Survey Mitigation Strategy for the Northeast U.S. Region as a part of the Survey Simulation Evaluation and Experimentation Project, which aims to assess potential impacts to the bottom trawl survey operations and data products and identify mitigation strategies to maintain data integrity. Furthermore, this study contributes to the current knowledge surrounding the impacts that offshore wind energy development can have on fishery-independent surveys, which globally is scarce.

ACKNOWLEDGMENTS

I would like to acknowledge the village that has supported me through this journey. To my husband, Zach, for picking me up when my R code was kicking me down. To my family, for supporting this crazy dream of counting fish for a living. To the School for Marine Science and Technology (SMAST) community, and all the people I have met and close friends I have made - I feel truly lucky and humbled to have had the chance to work alongside and get to know so many genius people. A special shout out to the members of the Fay Lab, who were my first friends here, whether it was because of forced proximity or by choice, there is no other group I would rather parody the statistical impacts of a beer challenge with. To the Survey Simulation Evaluation and Experimentation Project (SSEEP) team and its funding partners for the countless reviews and meetings that made this work possible and afforded me the opportunities to present it on national and international scales. To my committee members, Dr. Cadrin for being the whole cheer squad for every student that walks these halls and setting the standards for post-Wednesday seminars, and to Dr. Foley, for taking me under your wing at conferences and on the fall survey; and being a beacon of what it means to support women in Science, Technology Engineering and Mathematics (STEM). Lastly and most importantly to my advisor, Dr. Fay, for believing in me when I had no prior quantitative fisheries experience and pushing me out of my comfort zone. Without you I would not have met all these great people, had all these unforgettable experiences and the opportunity to pursue this dream.

To each and every one of you, I am eternally grateful.

TABLE OF CONTENTS

LIST OF FIGURES

LIST OF TABLES

ABBREVIATIONS

AIC	Akaike's Information Criterion
ASMFC	Atlantic States Marine Fisheries Commission
BIWF	Block Island Wind Farm
BOEM	Bureau of Ocean Energy Management
BTS	Bottom trawl survey
CPUE	Catch-per-unit-effort
CV	Coefficient of variation
EEZ	Exclusive Economic Zone
ELPD	Expected log predictive density
FMP	Fishery management plan
GLMM	Generalized linear mixed effect model
IID	Independent and identically distributed
MAB	Mid-Atlantic Bight
MAE	Mean absolute error
MAFMC	Mid-Atlantic Fishery Management Council
MARE	Mean absolute relative error
MCMC	Markov Chain Monte Carlo

MPAs	Marine protected areas
MRE	Mean relative error
NEFMC	New England Fishery Management Council
NEFSC	Northeast Fisheries Science Center
NESLME	Northeast Shelf Large Marine Ecosystem
NMFS	National Marine Fisheries Service
NOAA	National Oceanic and Atmospheric Administration
SDM	Species distribution model
SSEEP	Survey Simulation Experimentation and Evaluation Project
TMB	Template model builder

1 INTRODUCTION

To ensure the sustainable production of fisheries over time, fisheries management employs a suite of stock assessment and decision-making tools. Particularly, stock assessments often rely on indices of abundance, which are assumed proportional to a stock's size, to reflect changes in a stock's trend (Harley et al., 2001; Hilborn & Walters, 1992). Indices of abundance are derived primarily from data that collects catch numbers and weight. Common types of data collection include catch-per-unit-effort (CPUE) data from commercial and recreational, or fishery-dependent, sources, tag and recapture data, cooperative research studies with industry vessels, and fishery-independent surveys (hereafter "surveys"). Indices of abundance are most often produced from CPUE data or survey data. Surveys use statistical sampling designs to ensure a random sampling of a stock's distribution relative to its population (Cochran, 1977; Kotwicki & Ono, 2019; Ducharme-Barth et al., 2022), though often at a costly price point. Once indices of abundance are generated from the data, they can be used within stock assessments to help provide advice for implementing fishery management plans (FMPs) with specific management measures for the sustainability of a given stock (Large et al., 2013; Gill et al., 2020).

In the Northeast United States (US), the National Marine Fisheries Service (NMFS) Northeast Fisheries Science Center (NEFSC) has conducted bi-annual fishery-independent multispecies bottom trawl surveys since 1963 (fall) and 1968 (spring) along the US' Continental Shelf Large Marine Ecosystem (NESLME; Politis et al., 2014). The NESLME is a temperate system that encompasses an area of approximately 260,000 km^2 from Cape Hatteras in the south to the Gulf of Maine in the north (Kleisner et al., 2017). This area was incorporated into the US exclusive economic zone (EEZ) as part of the Magnuson-Stevens Fishery Conservation and Management Act of 1976 and is cooperatively managed by two of the eight regional councils established in the act, the New England Fishery Management Council (NEFMC) and the Mid-Atlantic Fishery Management Council (MAFMC). Both the New England and Mid-Atlantic regions are experiencing declines in seafood production and commercial fishery profits, with mixed trends in ecological stability (i.e., fish diversity, fecundity, decreased length at maturity; Caracappa et al. 2025, Gaichas et al. 2025). There is also evidence of shifting distributions and changes in migration and spawning times in response to changing climate and oceanography metrics

(Caracappa et al. 2025, Gaichas et al. 2025). With potential regime shifts and shifting species distributions to the northeast (Caracappa et al. 2025, Gaichas et al. 2025), long-running standardized surveys such as the NEFSC multispecies bottom trawl survey and its data sets are an invaluable source of fisheries information.

The NEFSC bottom trawl survey employs a stratified random sampling design where strata are defined by depth and latitude and stations are randomly selected before leaving port and sampled within each stratum, and is designed to produce relative and unbiased abundance indices (Politis et al., 2014). Survey stations are allocated proportionally to strata area with a minimum of three sets conducted in each stratum to ensure the calculation of a stratified variance and coefficient of variation (CV) which is used to assess the survey's accuracy and precision in estimating a stock's relative abundance. Sometimes, the pre-selected station locations are unable to be sampled due to the presence of fixed gear or difficult habitats such as rocky or hard-bottom substrates. In these instances, a different pre-selected station is sampled in its place, effectively reallocating the survey effort to another location within the same stratum.

Other survey designs include simple random sampling, where each station has an equal probability of being sampled and is chosen at random, or systematic sampling, where a station is selected at random and each subsequent station is selected based on another randomly-selected unit of distance apart from the first (Cochran, 1977). There is extensive research into the performance of each design and comparison among designs (Simmonds, 1996; Overholtz et al. 2006; Blanchard et al., 2008; Liu et al. 2009, 2011; Yu et al., 2012; Hyun & Seo, 2018; Zhao et al., 2018; Von Szalay et al., 2023). However, each sampling strategy has its tradeoffs related to the objective of the survey at hand, and while a function of their chosen sampling strategy and standardized sampling protocols, surveys are also at the mercy of natural species variability, composition, and behavior. The size of the survey area and the timing of the survey can impact observations of trends in a species' spatial distribution or seasonal migration if the survey area is too small compared to the actual spatial distribution or the distribution changes over time; if the survey occurs within a species migration pattern; or if the population is only surveyed during the day when it is more active at night (Godo, 1994; Hjellvik et al., 2002; Rago, 2005; Henderson et al., 2017; Nichol et al., 2019). Henderson et al. (2017) found that species distributions and

biomasses along the northeast shelf were affected by the timing of spring and fall transitions indicated by chosen thresholds of sea surface temperature. More specifically, they found that species like Atlantic mackerel and summer flounder were more responsive to extreme spring transitions and would have a more northward distribution during the fall survey with longer summers or later fall transitions (Henderson et al., 2017). Henderson et al. (2017) also noted variable timing of the NEFSC bottom trawl survey over the course of its time series. Earlier shifts in distribution or prolonged residence time within sampling areas could affect the availability of fish to the survey and even its ability to detect those changes, thereby affecting the reliability and robustness of relative abundance indices (Blanchard et al., 2008; Thorson & Barnett, 2017). When coupled with the logistical constraints of a standardized fishery-independent survey, sources of uncertainty in stock abundance indices have the potential to be confounded.

To minimize the effect of uncertainty on survey data products, scientists and researchers maintain consistency of the survey design and comparability of its data products by sampling the same spatial coverage in time, employing the same gear to standardize catchability (von Szalay & Somerton, 2005; Miller et al., 2010), and optimizing the effort allocation and time spent transiting between stations (Liu et al., 2011; Oyafuso et al., 2021; Rhodes & Jonzén, 2011; Xu et al., 2015). For this reason, fishery-independent surveys are much more costly than their fishery-dependent counterparts and are more readily susceptible to effort reduction through various means such as funding and labor shortages, vessel maintenance and repairs, and no-transit zones in response to environmental and animal protections, among many others (Dennis et al., 2015). Reductions in survey effort can increase measures of uncertainty and relative bias in abundance trends (Zimmermann & Enberg, 2017; Kotwicki & Ono, 2019; ICES, 2020), leading to bias in stock assessment outcomes, failure to track population changes, and overfishing (Kotwicki et al., 2014; Kotwicki & Ono, 2019). Ongoing research efforts strive to prepare scientists and surveys to respond to both planned and unplanned reductions and changes to survey designs and sampling strategies (ICES, 2020, 2023). For example, Yalcin et al. (2023) found that spatiotemporal models can make up for survey lost effort. Oyafuso et al. (2021, 2023) developed an approach to optimize survey designs that included the flexibility to adapt easier in the face of

unavoidable survey changes, and many others have studied the potential to combine data streams to derive representative distribution maps and indices of abundance that could be used to supplement gaps in survey effort (ICES 2020, 2023).

A source of particular interest regarding survey effort reduction is offshore wind energy development. The offshore wind industry is expected to interact with many marine use sectors and to impose at least four impacts to fishery-independent surveys associated with sound and vibration, electromagnetic fields, habitat changes, and fishing practice changes (Lipsky et al., 2016; BOEM, 2019; Haggett et al., 2020, 2021; Methratta et al., 2020; Hare et al., 2022). In Europe, offshore wind areas have been in operation since the early 1990s, and changes to commercial fishing practices as a result of preclusion from wind areas has occurred in Germany and Belgium (Berkenhagen et al., 2010; Schupp et al., 2021). Government research vessels have tended to be an exemption from these preclusions (Coates et al., 2016; Gill et al., 2020). Much of the research on impacts of offshore wind to fisheries has been through the lens of commercial fishery preclusion, and the resulting socioeconomic and ecological impacts (including displacement of fishing effort). Due to the forced exclusion of all fishing vessels during construction or operation in Europe, wind energy areas have become quasi-marine protected areas (MPAs) or No Take Zones (Inger et al., 2009). Berkenhagen et al. (2010) found that the preclusion of fishing operations equated to a 50 percent loss of fishery catch. Large socioeconomic losses of that magnitude for the fishing industry in a given area could shift the allocation of that effort to less resilient habitats and populations (Bergström et al., 2014), which would only exacerbate the importance of the fishery-independent surveys to track changes in population abundances.

Unfortunately, little research has been done to understand impacts to fishery-independent survey effort within the offshore wind energy development areas despite a demonstrated need to understand and quantify such impacts. As of August 2023, initial phases of construction began on over 22 million acres, 10,000 turbines, and 33,000 miles of submarine cables slotted for development along the NESLME (BOEM, n.d.), which imposes a potential 30-percent spatial overlap with the NMFS NEFSC bottom trawl survey footprint. The bottom trawl survey, along with twelve other federal surveys in the region, will experience a spatial conflict driven by the

potential preclusion of scientific monitoring and trawling efforts from areas designated for offshore wind energy development. The current survey vessel will be unable to sample in wind areas. To minimize the impacts felt across the suite of NEFSC surveys, and to sustain consistent sampling designs that are conducive to predicting species' abundances and distributions, NMFS has partnered with the Bureau of Ocean Energy Management (BOEM) to produce the Federal Survey Mitigation Implementation Strategy for the Northeast Region (hereafter Mitigation Strategy; Hare et al., 2022).

The first goal and objective of the Mitigation Strategy is to reduce and rectify impacts of offshore wind on NOAA Fisheries surveys by developing and implementing survey-specific plans to address four identified impacts: preclusion, impacts to survey design, changes to habitat and airspace, and reduced sampling productivity (Hare et al., 2022). To achieve this goal, collaborators between NOAA Fisheries, BOEM, Fishery Applications Consulting Team, and the University of Massachusetts Dartmouth School for Marine Science and Technology (UMassD SMAST) initiated a project, Survey Simulation Experimentation and Evaluation Project (SSEEP), to develop a spatially explicit simulation tool that emulates NMFS' fishery independent surveys and assess the statistical performance of alternative survey designs and sampling scenarios guided by a set of stakeholder workshops (Guyant et al., 2022a, 2022b, 2023).

This thesis contributes to the Mitigation strategy, SSEEP, and the limited studies available for the impacts to federal surveys around wind energy areas by considering the impacts that the preclusion of fishery-independent survey effort within the wind areas will have on survey operations, survey performance, and estimates of stock abundance indices that directly affect fisheries management advice. More specifically, I developed a general framework to quantify estimates of annual abundance indices derived from existing federal survey operations and compared them to estimates of annual abundance indices that were calculated under the assumption that the survey would be unable to conduct tows within wind energy areas and would not be able to reallocate the lost effort to other pre-selected stations within the same sampling unit. I then focused the application of this general framework in the context of the NEFSC multispecies bottom trawl survey (BTS), and further on two case study species.

The two case study species considered in this work include summer flounder (*Paralichthys dentatus*) and Atlantic mackerel (*Scomber scombrus*), which were identified in the stakeholder workshops as two of 11 species of commercial and recreational importance and of key interest identified by industry, academic, and management stakeholders (Guyant et al., 2022a, 2022b, 2023) to understand impacts of wind preclusion on the multispecies bottom trawl survey. They were chosen as the case study species, in part due to their commercial importance and stakeholder interest, but also to compare the variation in impacts between two species with differing behavioral characteristics and interactions with the bottom trawl survey.

The geographic distribution of both summer flounder and Atlantic mackerel has extended from North Carolina to the U.S-Canadian border (NEFSC, 2019, 2021), a spatial range that includes the full extent of the wind area installation space within the mid-Atlantic as of June 2022. Summer flounder is jointly and cooperatively managed by the MAFMC and the Atlantic States Marine Fisheries Commission (ASMFC). Although summer flounder does not currently have an overfished stock status, it is experiencing overfishing (NEFSC, 2023). It is a sandy bottom-dwelling fish that has historically been found inshore in the late-summer to early-fall and on the outer shelf in the spring both of which are areas that are proposed for offshore wind development. Additionally, it is thought to be very well sampled by the fall and spring survey.

Atlantic mackerel is also managed by the MAFMC and has been declared overfished with overfishing occurring (NEFSC, 2021). In contrast to summer flounder, it is a pelagic fish and has a much patchier spatial distribution that extends throughout the survey area. The spring survey is generally much better at sampling Atlantic mackerel than the fall survey. However, recently, the spring survey has been observing a change in Atlantic mackerel availability due to changes in habitat availability including a decline in observations on the outer shelf in the mid-Atlantic Bight (MAB) and an increase in observations on the inner shelf of the MAB, Gulf of Maine, and Georges Bank (McManus et al., 2018).

An increase in the magnitude of observations of Atlantic mackerel inshore could overlap spatially with the planned wind areas in the mid-Atlantic. However, their patchier distribution leads to lower encounter rates which incurs a higher variance around the annual abundance

indices. Thus, it is expected that the impacts from wind areas for Atlantic mackerel will be different than those impacts identified for summer flounder when the same impact analysis is applied to both species. Additionally, because of their interactions with the survey, the analysis is applied to the fall and spring survey data for summer flounder, and only the spring survey data for Atlantic mackerel, which also coincides with the seasonal annual NEFSC bottom trawl survey abundance indices used in their stock assessments.

Both species have experienced distributional shifts poleward related to reduced fishing pressures or climate pressures (Nye et al., 2009; Overholtz et al., 2011; Bell et al., 2014, 2015; Henderson et al., 2017; McMahan et al., 2020), and have been the subject of initial studies related to their interactions and uses within offshore wind farms. It is hypothesized that offshore wind turbines could act much like an artificial reef due to the scour protection and artificial rocky bottoms installed around the monopiles, with either increases to fish abundance within these areas according to the attraction-production hypothesis (Mavraki et al., 2021; Reubens, Braeckman, et al., 2013; Reubens, Vandendriessche, et al., 2013); or decreases in abundance due to changes in availability of preferred habitats. Mavraki et al. (2021) found that while present within the wind areas in the North and Baltic Sea, Atlantic mackerel were not using these areas as feeding habitats. Wilber et al. (2022) found a reduction in overall fish condition of summer flounder within areas of the Block Island Wind Farm (BIWF), which could translate to a less preferred habitat and imply impacts to abundance index calculations if wind energy areas are precluded from survey monitoring efforts.

My work considers those impacts under scenarios where offshore wind areas could result in local changes to fish density, like the attraction production hypothesis. My thesis attempts to answer three questions: (1) what would the effect on previous stock abundance indices have been if wind areas prevented bottom trawl survey effort, (2) can species distribution models be used to analyze potential impacts of offshore wind areas on survey operations and changes in abundance, and (3) how do the impacts to abundance indices as a result of wind-precluded survey effort change when there are changes in species productivity and fish density due to the presence of wind turbines.

2 METHODS

The NMFS NEFSC bottom trawl survey actively samples 82 strata encompassing the Gulf of Maine, the western Scotian Shelf, Georges Bank, and the mid-Atlantic Bight (MAB), has conducted an average of 350 tows per season, and has observed 488 species since 1963. For the analyses in this thesis, I focused on data from 2009 to 2021 to allow for the continuity of data related to vessel, depth and the strata sampled, which has changed throughout the time series (Sosebee & Cadrin, 2006; Bell et al., 2015). The survey was conducted on the NOAA ship *Albatross IV* up until 2008 at which point it was retired and the *Henry B. Bigelow* was commissioned for the survey. The data and subsequent analyses focus on the period in which the *Henry B. Bigelow* has been in operation.

Incomplete survey years were also removed from the data sets to account for pre-existing survey effort reduction. For instance, the 2017 fall survey was conducted on the sister NOAA ship *Pisces* due to scheduled maintenance of the *Henry B. Bigelow* and the survey only completed half of the stations (n = 128 tows) during the season. In 2020, the COVID-19 pandemic placed a halt on all non-essential operations including the 2020 spring survey such that the spring survey only completed 132 of its planned 377 tows. While the survey was able to operate by the 2020 fall survey, its efficiency was still significantly impacted by the pandemic and only completed half of the stations during this season. Thus, the 2017 fall survey and 2020 survey year were removed from the data.

Wind energy planning areas and leases are updated periodically and are available online through BOEM as a geographic information systems (GIS) geodatabase or shapefile. For this thesis, I used the shapefiles of the wind planning and lease areas (hereafter "wind areas") from June 2022 (https://www.boem.gov/renewable-energy/mapping-and-data/renewable-energy-gis-data) which was the most recent data available at the start of the project and included the lease areas within the Mid-Atlantic and the Central Atlantic planning areas (Figure 1).

Using the trawl survey database and the wind planning area information, I developed a general framework to assess the impact on survey data and data products used for stock assessments in the Northeast U.S. in two phases.

2.1 An empirical analysis of potential impacts on survey data

The first phase aimed to identify potential impacts to sample sizes and estimates of seasonal stratified random mean biomass indices (hereafter "annual abundance indices") by removing historical survey tows from data analysis if they were identified as overlapping proposed wind areas. The wind areas were spatially overlayed with the locations of survey tows from 2009-2021, and tows intersecting a wind area were denoted as wind-area tows while those that did not intersect a wind area were denoted as outside tows. The quantified impacts to historical sample sizes and to annual abundance indices were then used as a proxy for information loss due to wind-precluded survey effort.

The impacts on sample size were quantified across two groups: (1) each species that was encountered by the survey, and (2) species identified by stakeholders during two Survey Simulation Experimentation and Evaluation Project (SSEEP) workshops to be of research interest (hereafter "stakeholder-selected species"). The impacts on indices of abundance were quantified across three groups: (1) spatially-filtered species that met minimum catch criteria (below), (2) stakeholder-selected species, and (3) Atlantic mackerel and summer flounder as the case study species.

Two participatory workshops were held in January and February 2022 and hosted by the SSEEP project team with the aim to understand stakeholders' interests in potential impacts of wind preclusion on survey operations and data products. During these workshops, industry, academic, and management stakeholders were asked to identify a set of species that were of regional importance to evaluate in context of potential impacts from survey preclusion due to offshore wind (Guyant et al., 2022a, 2022b, 2023). Participants suggested that the focal species should be selected based on the quantity of existing data, the performance of their stock assessments, and the variability in efficiency of the bottom trawl survey for each species (Guyant et al., 2022a, 2022b, 2023). From these discussions and guidelines, eleven (11) species were selected that

spanned regional significance across the three fisheries management bodies, the NEFMC, MAFMC, and ASFMC, including: a skate complex (barndoor skate, winter skate, clearnose skate, little skate), Atlantic herring, Atlantic mackerel, black sea bass, butterfish, longfin squid, silver hake, spiny dogfish, summer flounder, winter flounder, and yellowtail flounder.

2.1.1 Impacts on sample sizes

For each species encountered by the survey, I calculated the percentage of survey tows that caught each species and that would be precluded if it occurred within a wind area, as well as the percentage of individuals of that species that were observed by the survey tows designated as a wind-area tow. The percentage of survey tows expected to be precluded by wind areas, $PE_{j,w}$, for a species, j, was calculated by:

$$PE_{j,w} = \frac{\sum_{w}^{W} n_{j,w}}{\sum_{h}^{H} n_{h,j}} * 100 \qquad \text{(Equation 1)}$$

where $n_{j,w}$ is the total number of positive tows for a given species, j, observed in a wind area, w, and $n_{h,j}$ is the total number of positive tows, observed in a wind-overlapped stratum, h. Similarly, the percentage of individuals of that species, PQ_j, within the wind areas was calculated as:

$$PQ_j = \frac{\sum_{w=1}^{W} N_{j,w}}{\sum_{h=1}^{H} N_{h,j}} * 100 \qquad \text{(Equation 2)}$$

where $N_{j,w}$ is the total number of individuals observed within a wind area, w, while $N_{h,j}$ is the total number of individuals observed within a wind-overlapped stratum, h.

2.1.2 Impacts on indices of abundance

I estimated and compared the annual abundance index under two survey effort scenarios: (1) status quo survey effort, where all the historical observations were used in the index calculation; and (2) wind-precluded survey effort, where wind-area tows were removed in each year of the dataset representing a reduction in seasonal survey effort. Calculations were performed for all species that met a minimum set of criteria in a particular season: (1) the species was observed in

three or more strata, (2) the species was observed in three or more years, and (3) the species was observed in at least one stratum proposed for overlap with offshore wind development. This minimum catch selection allowed analyses to focus on the species that would be most impacted by offshore wind developments rather than species rarely observed by the survey.

For each of the species that met the minimum catch criteria, I created seasonal spatial footprints and sampling frames such that the annual abundance indices were driven by a species' distribution and not overly influenced by survey tows that occurred in areas where the species is never found. For each species, I found the strata that contributed to a threshold of the cumulative catch (in biomass) observed in the time series and to remove influence of strata where the species has rarely been observed, with additional adjustments to create a contiguous area.

The thresholds used were either the 95th or 99th percentile of the cumulative biomass, depending on the species of interest. For summer flounder, I adjusted the 95th percentile cumulative biomass sampling frame for each season to include additional strata that were in a similar depth range or accounted for the full extent of wind area overlap with their seasonal distributions (Figure 10). The sampling frame for Atlantic mackerel consisted of the full survey area and all 82 strata due to minimal differences between the 95th and 99th percentile cumulative biomass sampling frames, and the lack of a contiguous area in either case (Figure 16).

The annual abundance indices were estimated according to Cochran (1977) for each survey effort scenario as:

$$\hat{I}_{j,k,t} = \frac{\sum_{h=1}^{H} A_h \bar{I}_{h,j,k,t}}{\sum A_h} \qquad \text{(Equation 3)}$$

where, $\hat{I}_{t,j,k}$, is the stratified random mean per sampling unit for a given species (j), season (k), and year (t). A_h is the size of stratum, h, and $\bar{I}_{h,j,k,t}$ is the observed mean biomass observed in the same stratum. The total survey area is denoted by $\sum A_h$.

With every observed mean biomass calculated in each stratum ($\bar{I}_{h,j,k,t}$), the estimated variance of observed data ($x_{i,j,k,t}$) from the mean in the same stratum was calculated by:

$$v^2_{h,j,k,t} = \frac{\sum(x_{h,i,j,k,t} - \bar{I}_{h,j,k,t})^2}{n_{h,j,k} - 1} \quad \text{(Equation 4)}$$

which was then used to quantify the precision of the estimated abundance by the annual stratified variance (Cochran, 1977) given by:

$$\text{Var}\,(\hat{I}_{j,k,t}) = \sum_{h=1}^{H} \frac{r_h v^2_{h,j,k,t}}{n_{h,j,k}} \left(1 - \frac{n_h}{\sum A_h}\right) \quad \text{(Equation 5)}$$

where r_h is the relative stratum weight, $v^2_{h,j,k,t}$ is the observed variance, $n_{h,j,k,t}$ is the sample size. Some analyses and stock assessments tend to use a bootstrap resampling method to derive the variance quantities which has shown to be more precise than the conventional point estimate in some respects (Magnusson et al., 2013), but similar in others (Anderson et al., 2024).

The precision of the survey was quantified as the coefficient of variation (CV; Cochran, 1977) and given by:

$$CV(\hat{I}_{j,k,t}) = \frac{\sqrt{Var(\hat{I}_{j,k,t})}}{\hat{I}_{j,k,t}} \quad \text{(Equation 6)}$$

In addition to quantifying the magnitude of abundance, the index trend for each species over the time series was estimated by fitting a linear regression model to the point estimates of annual abundance whose structure is (Zuur et al., 2007):

$$\hat{I}_{j,k,t} = \alpha_{j,k,t} + \beta_t t_i + \varepsilon_{i,j,k,t} \quad \text{(Equation 7)}$$

$$\varepsilon_{i,j,k,t} \sim N(0, \sigma^2)$$

Where $\hat{I}_{j,k,t}$ is the estimated annual abundance index for a given species and season in year, t_i, the population slope over time is β_t, the population intercept is $\alpha_{j,k,t}$, and $\varepsilon_{i,j,k,t}$ denotes the residuals which are assumed to be normally distributed around 0, with a standard deviation σ^2.

The bias of survey estimates (e.g., catch rates or trends in catch rates) between survey effort scenarios was quantified via the mean relative error (MRE) and mean absolute error (MAE) over

the most recent five years, (T; generally, 2016-2021), while the mean absolute relative error (MARE) over the most recent five years in the time series was used to quantify the precision:

$$MRE_{j,k} = \frac{1}{T}\sum_{t=1}^{T}\frac{\hat{I}_{j,k,t}^{P} - \hat{I}_{j,k,t}^{SQ}}{\hat{I}_{j,k,t}^{SQ}} \quad \text{(Equation 8)}$$

$$MAE_{j,k} = \frac{1}{T}\sum_{t=1}^{T}\left|\hat{I}_{j,k,t}^{P} - \hat{I}_{j,k,t}^{SQ}\right|; \text{ and} \quad \text{(Equation 9)}$$

$$MARE_{j,k} = \frac{1}{T}\sum_{t=1}^{T}\frac{\left|\hat{I}_{j,k,t}^{P} - \hat{I}_{j,k,t}^{SQ}\right|}{\hat{I}_{j,k,t}^{SQ}} \quad \text{(Equation 10)}$$

where $\hat{I}_{j,k,t}^{P}$ represents the annual abundance index in the preclusion scenario, and $\hat{I}_{j,k,t}^{SQ}$ represents the annual abundance index in the status quo survey.

MRE and MARE were also used to calculate the bias and precision, respectively, of the wind-precluded survey effort population trend estimates when compared to the trends estimated by the status quo survey effort scenario, as well as the differences between the survey's precision under the two effort scenarios.

Furthermore, I expanded this analysis further for summer flounder and Atlantic mackerel by (1) comparing the changes to trend estimates when survey effort is precluded due to wind to those when a similar magnitude of survey effort is reduced at random throughout the survey footprint due to unforeseen circumstances such as vessel maintenance needs or logistical constraints (hereafter "general survey effort reduction"); and (2) calculating the change in perceived trend when the preclusion of the survey within wind areas occurred systematically over time.

2.1.2.1 Comparisons to general survey effort reduction impacts

To compare wind-precluded impacts to general survey effort reduction impacts, I used bootstrap resampling to create independent and distinct seasonal data sets representing a status quo survey effort and a reduced survey effort. 1,000 bootstrapped datasets were generated for the status quo survey effort scenario by sampling with replacement the seasonal time series for the same number of observations that comprised the status quo survey effort datasets. Each new status quo

dataset was reduced twice: first by removing the wind-area tows (e.g., those simulated to be in wind areas) to recreate the wind-precluded survey effort, and second by randomly removing the same number of observations that constituted the wind-precluded survey effort scenario for a given species. More specifically, wind-area tows constituted an average of ten (10) percent of the total survey data for summer flounder in each season and five (5) percent of the total survey data for Atlantic mackerel in the spring. Thus, three types of datasets were generated: (1) status quo, where the historical expanded dataset was randomly resampled to generate a new dataset with the same number of tows; (2) wind-precluded effort, where the bootstrapped datasets under status quo had the wind-area tows removed; and (3) general effort reduction, where the bootstrapped datasets were randomly reduced to generate a new dataset with only 90 percent of survey tows for summer flounder or 95 percent of survey tows for Atlantic mackerel, emulating a 10- and 5-percent removal of survey tows respectively. Each dataset was then used to calculate annual abundance indices and estimates of the population trend according to Equation 3 through Equation 7. Using the distribution of the bootstrap estimates of trend, I identified the proportion of estimates that were larger than the observed wind-precluded estimate of trend from the original data to quantify the difference between a general survey effort reduction impact and a wind-precluded survey effort impact:

$$p = \frac{n_{\beta_{b,j,k}}}{N_{\beta_{b,j,k}}} \qquad \text{(Equation 11)}$$

Where $n_{\beta_{b,j,k}}$ is the total number of occurrences where the bootstrap estimates of trend were greater than the observed wind-precluded survey effort population trend and $N_{\beta_{b,j,k}}$ is the total number of bootstrap estimates.

2.1.2.2 Systematic changes in trend over time

To calculate the change in perceived trend when the survey is precluded from wind areas systematically over time, I first calculated the annual abundance indices and the change in indices over time under a status quo survey effort assumption for the full time series. Next, I calculated the annual abundance index in the most recent year of the seasonal dataset under a wind-precluded survey effort assumption but calculated the annual abundance index for the

remaining previous years in the time series under a status quo survey effort assumption. This iteration resulted in one year of a wind-precluded abundance index, and *T-1* years of a status quo abundance index, where *T-1* is the remaining total number of years in the data set. I then repeated this process such that an additional annual index was calculated under a wind-precluded survey effort assumption and one less annual abundance index was calculated under a status quo survey effort assumption with each repetition, until the last iteration calculated indices under a wind-precluded survey effort assumption for all the years in the time series (i.e. the same datasets analyzed in Section 2.1.2). Additionally, with each iteration, the population trend over the full time series was estimated as above.

2.2 A simulation study of potential impacts on indices of abundance

The second phase employed species distribution modeling and simulation testing to understand wind preclusion impacts on abundance indices including for survey data simulated under assumed changes in fish density. This second phase then helped evaluate possible effects on abundance indices when there are both changes in species productivity and reductions in survey effort due to the presence of wind turbines.

Species distribution models are an increasingly prevalent set of tools that can incorporate spatial and temporal non-stationarity to understand changes in species geographic distribution and density (Anderson et al., 2022; Barnett et al., 2021; Elith et al., 2010; Elith & Leathwick, 2009; Johnson et al., 2019; Ward et al., 2022). Here I used species distribution models to characterize changes in the seasonal fish density observed by the NEFSC bottom trawl survey over the time series for the purposes of simulating data sets for future years under alternative sampling strategies and scenarios for fish population change. More specifically, I fit geostatistical generalized linear mixed effects models (GLMMs) to the fall and spring survey data for summer flounder and spring survey data for Atlantic mackerel given a set of environmental covariates. From the GLMMs, I simulated future survey time series data sets under scenarios of change in sampling effort and fish density in areas of offshore wind energy development.

2.2.1 Species distribution models

Spatiotemporal GLMMs were developed using the R package "sdmTMB" (version 0.5.0.9; (Anderson et al., 2022)), which employs Template Model Builder (TMB) to perform integrated nested Laplace approximations (INLA) and provides a user-friendly extension of generalized linear models for interpretation. A model was fit for each case study species, and estimated seasonal biomass catch rates and regression coefficients for depth, year, wind energy area as fixed effects:

$$E[y_{s,t}] = \mu_{s,t}$$

$$\mu_{s,t} = f^{-1}(f(\beta_{j,k,depth} DEPTH_i) + \beta_t YEAR_i + \beta_{wind} AREA_i + \omega_{i,s} + \epsilon_{i,s,t}) \quad \text{(Equation 12)}$$

where the expected survey catch rate, $E[y_{s,t}]$, for each species, at a point in space, *s*, and year, *t*, is equal to a mean, $\mu_{s,t}$, determined by the inverse link f^{-1} and a linear predictor. The linear predictor in this study was defined where $DEPTH_i$, $YEAR_i$, and $AREA_i$ are elements of the design matrix and represented the main effects for a given observation *i*; $\beta_{j,depth}$, β_t, and β_{wind} are the corresponding effects on catch rate for each main effect; $\omega_{i,s}$ is the spatial random effect on catch rate that is constant over time; and $\epsilon_{i,s,t}$ is the spatiotemporal random effect on catch rate that varies over time. The values for $YEAR_i$ and $AREA_i$ were either 1 or 0 depending on whether an observation is in that given year or wind area. The spatial ($\omega_{i,s}$) and spatiotemporal random effects ($\epsilon_{i,s,t}$), were modeled via the stochastic partial differential equation (SPDE) approximation to Gaussian Markov spatial random fields and spatiotemporal random fields:

$$\omega_{i,s} \sim \text{MVN}(0, \Sigma_\omega),$$

$$\epsilon_{i,s,t} \sim \text{MVN}(0, \Sigma_\epsilon) \quad \text{(Equation 13)}$$

where the annual spatiotemporal random fields were assumed to be independent and identically distributed.

Separate fall and spring models for summer flounder were fit to survey catch rates assuming a Tweedie probability distribution for the observation model:

$$y_{s,t} \sim \text{Tweedie}(\mu_{s,t}, \text{p}, \phi) \quad \text{(Equation 14)}$$

where, p, represents the power parameter and ϕ represents the dispersion parameter. The fall models were evaluated across a triangular mesh with 723 knots or vertices, while the spring models were evaluated across 684 knots, using the default assumptions in the make_mesh() function in sdmTMB (Anderson et al., 2022). In total, I fit twelve (12) model configurations for each season which varied in whether to include spatial and spatiotemporal fields, a categorical variable indicating whether tows took place inside and/or outside a wind area, and if a depth effect was modeled through a penalized spline or a second-degree orthogonal polynomial (Table 6).

The models for Atlantic mackerel were fit to survey observations from the spring assuming either a Tweedie probability distribution according to Equation 12 or a Poisson-link delta gamma probability distribution (hereafter "delta gamma"). Both the Tweedie and the delta gamma observation families are adept at handling positive continuous data with zeroes which is characteristic of the NEFSC survey data (Barnett et al., 2021; Commander et al., 2022; Thorson, 2018; Ward et al., 2022). The difference with the delta gamma models, however, is that the process is split into two components, a probability of encounter (hereafter "presence-absence") component and a positive catch rate component. The presence-absence component, $p_{i,s,t}$, is derived by:

$$p_{i,s,t} = 1 - exp(\text{-}N_{i,s,t}) \quad \text{(Equation 15)}$$

where $N_{i,s,t}$ is the predicted density of individuals or groups at sample, i, given by a linear predictor with the same structure as Equation 10 and is distributed according to (Thorson, 2018):

$$P_{i,s,t} \sim \text{Bernoulli}(p_{i,s,t}) \quad \text{(Equation 16)}$$

The predicted density and probability of encounter is then used to derive the positive catch rate component, $r_{i,s,t}$, such that

$$c_{i,s,t} = \frac{N_{i,s,t}}{p_{i,s,t}} \times b_{i,s,t} \quad \text{(Equation 17)}$$

where $b_{i,s,t}$ is the predicted biomass per group of individuals also given by a linear predictor with the same structure as Equation 10 but distributed according to:

$$C_{i,s,t} \sim \text{Gamma}(\phi, \frac{c_{i,s,t}}{\phi}) \quad \text{(Equation 18)}$$

where ϕ represents the shape of the distribution (Thorson, 2018). Applying the two distribution families, a total of sixty-nine (69) models were fit to Atlantic mackerel spring survey data which varied in whether to include spatial and spatiotemporal fields, a categorical variable indicating whether tows took place inside and/or outside a wind area, and the habitat relationship assumption associated with the observed biomass at a given average depth. Preliminary model selection identified better fits to biomass catch rates that were limited to average depths at less than 200 meters and estimated as a function of a fourth-order polynomial depth relationship, independent year effects, and spatial and spatiotemporal random effects. Of the 69 models fit, only four (4) models were chosen as potential candidates for further evaluation. These models varied in the distribution families and the estimation of the range parameter, or the distance at which two observations were no longer correlated. More specifically, one model with a Tweedie distribution estimated independent spatial and spatiotemporal ranges, and three models with the delta gamma distribution were fit by varying which component, presence-absence and/or positive catch rate, estimated independent or shared ranges. Table 13 includes the list of candidate model configurations evaluated for Atlantic mackerel.

Model Selection

Models were compared using Akaike's information criterion (AIC, Akaike 1974) which measures the goodness of fit (Barnett et al., 2021), and a cross-validation approach to quantify the predictive accuracy of each model according to a cross-validation test error rate, and the total

log-likelihood of each model (Anderson et al., 2022). Additional model diagnostics included inspecting residuals, such as Empirical Bayes, approximate posterior samples assuming a multivariate normal distribution, Markov Chain Monte Carlo (MCMC) samples, and simulation-based Dharma, as well as visualizing marginal and conditional effects of model predictors, and post-model predictive checking of abundance indices following a similar process to a posterior predictive check (Conn et al., 2018). For the posterior predictive check, new survey data and random effects were simulated at the same locations and in the same time period used to fit the model. Annual abundance indices were derived under the same status quo and wind-driven preclusion survey effort scenarios as for section 2.1.2 and summarized across years by estimating the population trend over time, invoking the same process and equations as described above in section 2.1.2. I repeated this process for 1,000 iterations and contrasted the distribution of the estimated average biomass catch rates, proportions of zeroes, annual abundance indices, and population trends from the simulated data to the best estimates from the originally fitted model. Equation 11 from section 2.1.2 was employed to contrast the distribution to the fitted population trend such that $n_{\beta_{b,j,k}}$ are the simulated population trends.

2.2.2 Scenarios of changing spatial distributions

The fitted models then served to simulate data to analyze the effect of changes in fish density and the preclusion of survey effort within wind areas on survey data, annual abundance indices, and estimates of the population trend. Five-year datasets of survey stations were produced by randomly selecting with replacement five years from the historical survey period and thereby the previously surveyed locations for a selected year which served as assumed locations of future survey efforts. New survey biomass catch rates were then simulated at these assumed future tow locations based on the estimated spatial random fields from the same locations used in the model fit, the estimated year effects from the respective resampled year of the time series, the estimated depth effects, and new spatiotemporal random fields that were generated by the simulation. Biomass catch rates were simulated under three scenarios of wind-driven fish density assumptions (hereafter "productivity scenarios"): (1) *baseline density* where the effect of wind areas on expected survey catch rate was unchanged from the effect predicted by the fitted model, (2) *enhanced density* where the effect of wind areas on simulated survey catch rates was doubled

from the baseline effect assuming that fish density would increase within wind areas once in place, and (3) *reduced density* where the effect of wind areas on simulated observations of biomass was halved from the baseline effect assuming that fish density would decrease within wind areas. In practice, this was implemented by adjusting the linear predictor for wind-area tow locations accordingly. Once survey data were simulated under each productivity scenario, annual abundance indices and estimates of the simulated population trends were calculated and compared under the survey effort scenarios, status quo or full survey effort, and wind-precluded survey effort. This was conducted over 1,000 iterations to represent 1,000 instances of different populations and five years of a randomly stratified survey. The performance of survey effort scenarios was calculated using the same MRE, MAE, and MARE calculations as discussed in Section 2.1.2 above.

3 RESULTS

3.1 An empirical analysis of potential impacts on survey data

3.1.1 Impacts on sample sizes

Analysis of the spatial overlap of actively sampled survey strata with proposed wind areas showed that inshore strata in the mid-Atlantic will have the highest overlap measured by the percent of stratum overlapped by wind areas, directly off the coast of southern New Jersey, south-eastern Maryland, and southern Massachusetts (Figure 2).

Over the time series, 8,102 survey tows caught 488 species. No species was caught in all 8,102 survey tows. Silver hake had the highest capture frequency, occurring in 77% (n = 6,244) of the tows over the total survey area across the time series. Survey tows in planned and leased wind areas ('wind-area tows') accounted for 5% (n = 431) of the total tows across the full survey spatial footprint over the time series. Alternatively, wind-area tows accounted for 18% of the total tows when the sampling frame was restricted to only strata that are overlapped by wind areas (n = 2,337). Survey tows within strata that overlap with wind areas (n = 2,337) account for 29% of the total tows over the full survey footprint.

Of the 8,102 tows, there were two wind-area tows that caught the only observations of silverstripe halfbeak and frigate mackerel. Thus, 100% of the tows over the time series for each of these two species occurred in wind areas (Figure 3b). The same wind-area tow that caught frigate mackerel was also the only tow that caught silver hatchetfish in strata overlapped by wind (Figure 3a). However, that wind-area tow was one of a total 11 tows (9%) that caught silver hatchetfish throughout the survey area (Figure 3b). There were an additional 7 wind-area tows that each caught the only observation of 7 other species in strata overlapped by wind (Figure 3a). Each wind-area tow that caught the given species constituted 100% of the total tows in those strata, but anywhere from 4% to 50% of the total tows that occurred over the survey footprint (Figure 3b).

Out of the 488 species caught by the survey, 323 were not caught in any wind-area tows (Figure 3b) and 156 were caught across all 431 wind-area tows that occurred in strata overlapped by

wind areas (Figure 3a). Of the 156 species, a single fish was caught from 26 species within wind areas. Those single fish from a wind area made up 0.02% to 4% of the total number of fish caught for that species across the survey area. Longfin squid was caught the most in wind areas in terms of the numbers of fish (n = 177,518) totaling 7% of the total numbers of squid caught across the survey area and the time series. Spiny dogfish were caught the most in wind areas in terms of biomass (n = 55,968.3 kg) totaling 6% of its total biomass caught across the survey area and time series. Blotched swimming crab was caught the least in wind areas in terms of biomass (n = 0.001 kg) totaling 0.08% of its total biomass caught across the survey area and times series.

3.1.1.1 SSEEP Workshop Species

The eleven (11) species prioritized in the stakeholder workshops were caught in up to 20% of the wind-area tows that occurred in strata overlapped by wind energy areas and constituted up to 35% of the total number of fish caught in those areas (Figure 4). Compared to those 11 species, butterfish and silver hake were caught in a lower percentage of tows occurring in potential wind areas with 15% (n = 200 and n = 240) of the total tows that occurred in survey strata overlapped by wind areas (Figure 4). Biomass from those tows constituted 15% (2,569 kg), and 7% (2,116 kg), respectively, of the total biomass caught in the strata overlapped by wind areas (Figure 4). That is equivalent to 15% (n = 81,361), and 9% (n = 47,950), respectively, of the total numbers of fish caught (Figure 4).

The skate complex, on the other hand, was caught in 20% (n = 411) of the tows from strata that overlap with wind areas, catching a total of 44,541 kg of skates and 83,141 individual skates (Figure 4). Although the skate complex was caught in the largest proportion of tows in strata overlapped by wind areas (Figure 4), those tows did not catch the largest proportion of biomass or numbers of fish that would be precluded by wind areas. Rather, wind-area tows caught a higher proportion of Atlantic herring and yellowtail flounder in terms of biomass and numbers of fish than they did of the skate complex. Wind-area tows caught 37% (n = 85,083) of the total number of yellowtail flounder and 28% (n = 4,214.5 kg) of its total biomass caught in overlapped strata, while also catching 34% (n = 1,354) of the total number of Atlantic herring and 35% (n = 456.9 kg) of its total biomass caught in overlapped strata (Figure 4).

For the stakeholder identified species, up to 10% of positive tows for each species occurred in wind areas, accounting for up to 13% of the total catch of those species (both by weight and by numbers) across the full survey footprint (Figure 5). Of the total survey tows, winter flounder, silver hake, Atlantic mackerel, and Atlantic herring were caught in 4% of the tows that occurred in wind areas (Figure 5). However, these tows only represented 2% (n = 307.7 kg) of the total survey biomass and 1% (n = 721) of the total number of winter flounder over the full survey area and time series (Figure 5). These observations of biomass and numbers of fish were the second lowest over the 11 species, ahead of silver hake which was caught in tows that made up 1% (n = 2,115.9 kg) of the total biomass and 2% (n = 47,950) of the total numbers of fish that occurred throughout the survey footprint, within wind areas (Figure 5).

3.1.1.1.1 Summer flounder

Summer flounder was caught in the highest percentage of tows located in wind areas of the 11 species and across tows that occurred in strata overlapped by wind (Figure 4a) as well as the total survey area (Figure 5a). The positive tows in strata overlapped by wind represented the third highest percentage of biomass and the fourth highest percentage of total number of fish observed in wind areas (Figure 4b and Figure 4c). From 2009-2021, 20% of survey tows (n = 256) in wind-overlapped strata that caught summer flounder were in wind areas (Figure 4a). These wind-area tows constituted 25% of the total biomass (n = 1,685.9 kg) and 24% of the total number of summer flounder (n = 2,321) caught in survey strata overlapped by wind (Figure 4b and Figure 4c).

Summer flounder was caught in 30% (n = 2,461) of the total survey tows, catching a total of 13,350 kg or 17,689 fish. Of those tows, 10% (n = 256) were in wind areas, the highest proportion of the 11 key species. (Figure 5a). These wind-area tows corresponded to 13% of total weight and numbers of fish caught by the survey, again the highest proportions for the 11 species (Figure 5b and Figure 5c).

3.1.1.1.2 Atlantic mackerel

Of the eleven species, Atlantic mackerel had the fifth lowest percentage of total biomass and total number of fish caught in tows located in wind areas out of the tows that occurred in survey strata proposed for overlap (Figure 4b and Figure 4c). Atlantic mackerel was also caught in the lowest proportion of total survey tows that occurred in survey strata overlapped by wind areas (14%; n = 76; Figure 4a) across the eleven species within the time series. Biomass and the number of Atlantic mackerel in these tows constituted 15% of the total biomass (n = 1,103 kg) and the total number of Atlantic mackerel (n = 11,206) caught by survey tows in strata overlapped by wind (Figure 4b and Figure 4c).

Atlantic mackerel was caught in 24% (n = 1,902) of the total survey tows between 2009 and 2021. Of those tows, only 4% (n = 76) were in wind areas, the second lowest proportion of total survey tows throughout the survey area compared to the other key species (Figure 5a). It was also found to be the third lowest in terms of percent of total biomass (3%; n = 1,102.8 kg) and sixth lowest (5%; n = 11,206) in terms of percent of total numbers of fish caught throughout the survey area that occurred in wind areas (Figure 5b and Figure 5c.).

3.1.2 Impacts on indices of abundance

A total of 278 species were caught in 3 or more strata within a given year. Of those 278 species, 255 were caught in 3 or more strata within a given year during the fall survey, and 201 were caught in 3 or more strata within a given year during the spring survey. The fall survey observed 189 species in 3 or more strata in at least 3 survey years, and the spring survey observed 151 species in 3 or more strata in at least 3 survey years. Of these, 149 species were observed in the fall survey in at least one stratum overlapping with wind areas, and 113 species in the spring survey (Table 1). Stratified random mean annual abundance indices were calculated for each of the 149 species caught by the fall survey, and the 113 species caught by the spring survey under the two survey effort scenarios, status quo and wind preclusion (Table 2, Appendix A).

Precluding the fall survey from wind areas had the largest impact on the annual abundance indices and the precision of the survey when estimating roughtail stingray with a 60% relative

difference between indices (Table 2 and Figure 7a) and a MARE in CVs of 40% (Table 2 and Figure 8a); it also had the second largest impact in estimating the population trends for roughtail stingray (MAE = 0.94; Table 2 and Figure 9a). Five percent of the total tows that caught roughtail stingray overlapped wind areas but caught roughly 30% of the total biomass caught throughout the survey (7,325.4 kg). On average, wind-area tows caught 16 kg of roughtail stingray compared to tows occurring outside wind areas which caught a nominal average of 1.5 kg of roughtail stingray. Furthermore, the fall survey had higher catch rates of roughtail stingray within wind areas in the most recent five years of the times series. Specifically in 2016, 2018, and 2021, wind catch rates constituted 93%, 81%, and 63% of the total biomass caught in those years, respectively. In 2019, on the other hand, roughtail stingray was exclusively caught in areas outside of wind areas and was the highest recorded annual catch of roughtail stingray biomass during the time series (1,040 kg), though comparatively was still less than the total biomass caught in wind areas between 2016, 2018 and 2021 (1,742.36 kg). The removal of these large observations in wind catches in turn results in large differences in the survey precision and estimates of their population trend. For instance, the average CV of the fall survey under wind preclusion was 0.70 compared to the status quo CV of 0.59 (Table 2), which represented a 40% difference and therefore more imprecise survey for roughtail stingray. Population trends were also less accurate when estimated under the reduced survey effort (MAE = 0.94; Table 2 and Figure 9a) meaning that the slope estimate under wind preclusion was less than those under status quo, and the confidence intervals around the estimates were wider and thus more variable under wind preclusion.

Precluding the spring survey from wind areas had the largest impact on the annual abundance indices when estimating smallmouth flounder (MARE = 50%; Table 2 and Figure 7b), on the precision of the survey when estimating horseshoe crab (MARE = 30%; Table 2 and Figure 8b), and on estimating population trends of smooth dogfish (MAE = 3.27; Table 2 and Figure 9b). Catch rates of smallmouth flounder were higher in earlier years of the time series, and at stations outside of wind areas. Of the total tows, 5% occurred in wind areas and caught 7% of the total smallmouth flounder biomass throughout the time series (7.4 kg). Differences in abundance indices were calculated for smallmouth flounder based on abundance estimates from 2009 to

2012 and 2015 due to a lack of observations in the more recent years of the time series (e.g. 2016 to 2021) and were consistent across that timeframe. Between 2016 and 2021, estimates of annual abundance indices for striped bass were most impacted by wind preclusion of the spring survey (MARE = 38%; Table 2 and Figure 7b), with consistent differences over the five-year period. The spring survey rarely caught the species that were highlighted as having the highest impacts across abundance indices and coefficients of variation in Table 2, apart from striped bass, clearnose skate, and smooth dogfish. For example, the spring survey on average caught 0.71 kg of bluefish across the time series, but catch rates were highly variable (SD = 4.4 kg). As a result, the survey CV for catches of bluefish is high under status quo survey effort conditions (CV = 0.64; Table 2). When survey effort was precluded in wind areas, the survey CV increased to 0.74; because catch rates were variable over time, the CV was also variable over time. Both fall and spring surveys experienced an increase in CVs across the majority of species caught in Table 2 when effort was precluded from wind areas. Thus, precluding survey effort generated further imprecision for some species caught by each of the seasonal surveys.

There were marked differences across annual abundance indices, survey precision, and population estimates for a number of species when the seasonal surveys are precluded from wind areas (Table 2). However, annual abundance indices were unimpacted or minimally impacted for less than 60% of the species (approximately 85 species; Figure 7) caught by the seasonal surveys. Survey precision was unimpacted or minimally impacted for less than 80% of the species caught by the seasonal surveys (approximately 90 species; Figure 8). Population estimates were unimpacted of minimally impacted for less than 35% of the species caught by the seasonal surveys (approximately 40 species; Figure 9).

3.1.2.1 SSEEP Workshop Species

Preclusion of the fall survey from wind areas would have the greatest impact on the estimates of annual abundance indices for black sea bass (MARE = 23%) and the least impact on estimates of annual abundance indices for Atlantic mackerel (MARE = 0%; Table 3). Compared to all other species, impacts to abundance indices for black sea bass were above average (94th percentile) along with impacts to abundance indices for summer flounder (86th percentile), butterfish (70th

percentile), and the skate complex (56th percentile; Figure 7). All other stakeholder species were below the 50th percentile including Atlantic mackerel which represented the 28th percentile in terms of impacts to estimates of abundance across all species (Figure 7).

Precision estimates of the fall survey for black sea bass indices were lower on average during the most recent 5 years when the survey was precluded from wind areas, signaling that estimates of black sea bass abundance were more certain under wind-precluded effort (Table 3). Furthermore, these differences between precision estimates under the effort scenarios were the largest across the stakeholder species (MARE = 20%; Table 3) and represent the 96th percentile of impacts across all the species caught by the fall survey (Figure 8). Precision estimates of the fall survey were on average unchanged under the survey effort scenarios for yellowtail flounder, silver hake, Atlantic herring, and Atlantic mackerel (Table 3) and thus were the least impacted by wind preclusion when compared to the other stakeholder species. Precision estimates for winter flounder were also not notably different on average (MARE = 2%; Table 3). However, these differences were above average when compared to all the species caught by the fall survey (57th percentile; Figure 8). Yellowtail flounder, silver hake, Atlantic herring, and Atlantic mackerel, on the other hand, were below the average distribution of differences, representing the 46th, 42nd, 34th, and 29th percentiles, respectively (Figure 8).

Population trends of spiny dogfish were most affect by the preclusion of the fall (MAE = 0.68; Table 3), both across stakeholder species, and all species caught by the fall survey (99th percentile; Figure 9). Population trends for Atlantic mackerel, on the other hand, were again the least impacted by the preclusion of the fall survey (MAE = 0; Table 3), and this was the only stakeholder species below the average distribution of population trend impacts for all the species that were caught by the fall survey (26th percentile; Figure 9). The 10 other stakeholder species were above the 50th percentile of the cumulative distribution of impacts to population trends by precluding the fall survey (Figure 9).

While the preclusion of the fall survey had minimal impacts on abundance estimates, survey precision, and population trends for Atlantic mackerel, the preclusion of the spring survey from wind areas had the greatest impact on the estimates of annual abundance for Atlantic mackerel

(MARE = 8%) and some of the larger effects on estimated population trends (MAE = 0.1; Table 3). Differences between survey effort indices for Atlantic mackerel represented the 82nd percentile across all species caught by the spring survey (Figure 7). Of the 11 stakeholder species, estimates of annual abundance for silver hake and yellowtail flounder were mostly unchanged by wind preclusion of the spring survey (MARE = 0% and MARE = 0%; Table 3) and were below the average cumulative distribution of impacts across spring survey species, representing the 44th and 43rd percentile, respectively (Figure 7).

Silver hake and yellowtail flounder were also the least impacted stakeholder species in terms of survey precision estimates (MARE = 0% and MARE = 0%; Table 3). However, yellowtail flounder was the only stakeholder species below the 50th percentile of the cumulative distribution of impacts to survey precision across the species caught by the spring survey. All other stakeholder species were above the 50th percentile, and silver hake represented the average impact (Figure 8). Estimates of survey precision and population trends for spiny dogfish were the most impacted by precluded survey effort. On average, the CVs for spiny dogfish increased when the survey was precluded from wind areas suggesting greater uncertainty in annual abundance indices from the spring survey (Table 3).

Population trends for spiny dogfish were more negative when the survey was precluded and represented the 99th percentile of impacts to population trends across spring survey species (Figure 9). Population trend estimates of longfin squid were the least impacted across the stakeholder species by preclusion of the spring survey; though impacts to these estimates were still a part of the upper 75th quantile of the distribution of all species impacts.

3.1.2.1.1 Summer flounder

The spatial distribution of summer flounder catches varied by season (Figure 11), but the amount of tows occurring in wind areas was consistent over time between the two seasonal surveys (Figure 12).

Fall estimates of the annual abundance per tow were lower when survey effort was precluded from wind areas (Figure 12). This was especially true in 2009, 2011, 2013, and 2016. These

differences were driven by higher and more variable catch rates in wind areas, on average 9.01 ± 22.1 kg/tow, than those in the surrounding outside areas, 2.6 ± 5.7 kg/tow on average. These catch rates notably occurred at the northern end of their range, off the coast of New York and Massachusetts in these years. For spring, estimates were both lower (5 of 12 years) and higher (6 of 12 years) when wind-area tows were precluded than under the status quo (Figure 13b). The difference between a status quo survey effort and a wind-precluded survey effort was larger in the fall than in the spring. A reduction in survey effort due to wind in the fall resulted in a MARE between annual abundance indices of 14% whereas the spring had a 4% MARE (Table 5). Of the 164 species initially evaluated in terms of impacts to annual abundance indices, 80% had a lower MARE in the fall and 66% had a lower MARE in the spring compared to summer flounder (Figure 7).

CVs of annual estimates were similar between the two effort scenarios, except for CVs in the fall of 2009, 2011, 2013, and 2016 (Figure 13a). As noted above, the differences in these years were driven by the higher and more variable catch rates within areas, such that removing these years resulted in a 30% reduction in nominal average catch rates within wind areas but had little effect on the nominal average catch rates in surrounding outside areas. Differences in the survey CVs were similar to the differences in annual abundance indices in each season, with a 15% MARE and a 6% MARE in the fall and spring, respectively (Table 5). The MARE in survey CVs for summer flounder was in the upper third quantile of the distribution over species for each season, such that 89% of species had lower MARE in CVs from the fall survey between the two survey effort scenarios and 80% of species had lower MARE in CVs from the spring survey (Figure 8).

The linear regression slope estimate represents the average change in abundance index over time and can be used as an estimate of population trend. A decreasing trend was estimated for both seasons and effort scenario (Table 4), however under the wind-precluded survey effort the trend was slightly less negative than trends estimated under status quo effort (Table 4). Estimates of changes in population trend also had a larger MAE between the two survey effort scenarios in the fall (MAE = 0.05) than in the spring (MAE = 0.01; Table 5). These errors represented the 83rd and 80th percentiles of the distribution in errors across species between estimates of

population trend under the survey effort scenarios for the fall and spring survey, respectively (Figure 9).

3.1.2.1.1.1 Comparisons of general survey effort reduction

The fall and spring estimates of population trend under wind-precluded survey effort (slope = -0.10 and -0.04 respectively; Table 4) were compared to 1,000 estimates of population trend under three survey effort scenarios: (1) status quo, (2) wind-preclusion, and (3) general survey effort reduction using bootstrap resampling methods according to section 2.1.2.1 (Figure 14a-c). Estimates in trend for summer flounder in the fall under the status quo effort and the general survey effort reduction scenarios were different than the observed wind-precluded estimate in trend (Figure 14a and Figure 14c). The observed wind-precluded estimate in trend occurs at the upper bounds of the percentile intervals of both distributions and represents the 93rd percentile of the status quo distribution and the 92nd percentile of the general survey effort reduction distribution (Figure 14a and Figure 14c). Conversely, when comparing the observed estimate in trend for the wind-precluded survey to the bootstrap resampled estimates under wind preclusion, the observed estimate resulted in some minor differences but ultimately represented the 83rd percentile of the distribution, such that 17% of the bootstrap estimates were greater than the observed value (Figure 14b). Thus, the effect of removing wind-area tows in the fall on population trend estimates under a wind preclusion scenario is different than the effect of removing survey tows due to some other effort reduction mechanism.

Bootstrapped estimates of spring population trends, on the other hand, were not different from the observed wind-precluded population trend estimate under any of the three scenarios, status quo, wind preclusion or general survey effort reduction (Figure 14d-f). The observed estimate represented the 65th percentile, 61st percentile, and 64th percentile across the status quo, wind-preclusion, and general survey effort reduction scenarios, respectively (Figure 14d-f).

3.1.2.1.1.2 Systematic changes in trend over time

Estimating summer flounder population trends when the period of years with wind-preclusion changed also showed larger changes to trends in the fall than in the spring. The latter

experienced minimal changes to the estimated trends as the number of years that the survey is precluded from wind areas was increased (Figure 15b). The most notable change occurred in the ninth time step (Figure 15b), or when 2011 was added to the suite of years in which the survey was precluded from wind areas (Figure 13b). The spring survey in 2011 conducted the highest number of tows that overlapped wind areas throughout the time series (n = 23; Figure 12b), followed by 2016, which had the same number of tows. However, between those two years, the 2011 survey observed twice the biomass and three times the number of fish than the 2016 survey. Catch rates in the wind areas during the 2011 spring survey were higher than the catch rates in the wind areas during the 2016 and had a larger negative effect on the annual abundance index and the survey CV when it was precluded from the survey (Figure 13b). In other words, the abundance index and CV was lower in 2011 when the wind-area tows were removed because wind area catch rates were larger than the outside area catch rates. Comparing these estimates to the abundance index and CV in 2016 which was slightly higher when the wind-area tows are removed, indicated lower wind area catch rates than outside area catch rates during that survey year. Furthermore, the difference between the annual abundance index estimates under the two scenarios in 2011 was larger than the difference between the indices in the years succeeding, regardless of the direction of change (Figure 13b).

The fall trends became more negative as more years from the survey were precluded from wind areas until the time series became extremely short (Figure 15a). The notable change for this survey occurred in the seventh time step, or when 2013 was added to the length of a wind-precluded survey time series (Figure 15a). Contrary to the spring survey, this survey year was influential because the status quo abundance index was higher than the succeeding years prior to the survey being precluded and because the wind-precluded index was of the same magnitude as the succeeding years when it is added to the wind preclusion time series, not because the difference between survey effort indices was larger than the years succeeding. Thus, the estimates of trend are driven by the higher earlier years of the status quo index when the 2014 to 2021 surveys operate under wind-precluded effort, and then driven again by more stabilizing years of wind-precluded abundance indices when 2009 to 2013 is added to the time series (Figure 15a). In general, the perceived change in trend over time depended on the length of the

time series that was precluded to survey effort in wind areas and how much survey effort overlaps wind areas across years until the time series become extremely short (Figure 15a).

3.1.2.1.2 Atlantic mackerel

Annual abundance indices of Atlantic mackerel were only calculated across the full survey area using the spring survey data from 2009 to 2021 (Figure 16). Catch rates of Atlantic mackerel were much more variable over the spatial frame than summer flounder, with high observations of Atlantic mackerel occurring both in inshore and offshore areas (Figure 17 and Figure 20). Very few high catch rates of Atlantic mackerel biomass occurred in wind areas (Figure 17), and the number of tows that were located within wind areas were much lower (n = 209) than the number of tows that occurred outside the wind areas (n = 3,839; Figure 18), constituting 5% of the tows that occurred throughout the time series. While in contrast to the proportion of wind-area tows that observed summer flounder, on a whole Atlantic mackerel was encountered more frequently in the spring survey than summer flounder.

Estimates of annual abundance indices under the wind-preclusion scenario were more often unchanged from estimates under the status quo scenario, except for the indices in 2010, 2011, and 2017, when the wind-precluded abundance index point estimates were lower than the status quo abundance index (Figure 19). There were two years when the wind-precluded abundance index was higher than the status quo index, 2016 and 2018 (Figure 19). The MARE between the status quo abundance indices and the wind-precluded indices was 7% (Table 5), which represents the 80^{th} percentile of distribution of errors across the full suite of species (Figure 7).

The CV estimates in each year under a wind-precluded survey effort were unchanged when compared to the CV estimates in each year under a status quo survey effort (Figure 19). Further, the MARE between survey CVs between efforts was 3% signaling little impact to precision of the survey when it was precluded from wind areas (Table 5). Though small, the impacts to survey CVs for Atlantic mackerel represent the upper third quantile of the distribution of impacts across the species that were caught in the survey, such that across the 113 species caught by the spring survey, 71% of the survey CVs were less impacted by wind-precluded survey effort than survey efforts that caught Atlantic mackerel (Figure 8).

Atlantic mackerel was found to have a slightly declining, almost zero, trend (slope = -0.04) in population over time under a status quo survey effort scenario and a slightly increasing, almost zero, trend (slope = 0.01) in population over time under a wind-precluded survey effort scenario (Table 4). MAE for the change in trend when the survey is precluded from wind areas is 5%, which is a larger MAE than 93% of the 113 species analyzed, including spring trends of summer flounder (Figure 9).

3.1.2.1.2.1 Comparisons of general survey effort reduction

The spring estimate of population trend under wind-precluded survey effort (slope = -0.01; Table 4) for Atlantic mackerel was compared to 1,000 estimates of population trends under three survey effort scenarios: (1) status quo, (2) wind-preclusion, and (3) general survey effort reduction The observed estimate of trend under a wind preclusion scenario for Atlantic mackerel was not different from those trends estimated under a general survey effort reduction (Figure 20c). Even more so, the observed wind-precluded estimate represented the same percentile of the distribution of estimates under a general survey effort reduction as the distribution of estimates under a status quo survey effort (60%; Figure 20a and Figure 20c). Notably, though, the variability in the estimates across the three scenarios was wide, ranging from -2 to 2, with some slope estimates reaching as high as 4 (Figure 20). While the effect of wind-precluded survey effort in the spring on Atlantic mackerel population trend estimates was similar to some other general survey effort reduction. This is in part due to the high variability across catch rates in the observed data used to generate the bootstrap distributions. Less variable catch rates and more precise population trend estimates under either scenario would be needed to resolve a difference between efforts.

3.1.2.1.2.2 Systematic changes in trend over time

Estimates of spring Atlantic mackerel population trends were mostly unchanged as the number of years the survey was precluded increased and had high variability due to the variation in catch rates between years (Figure 21).

3.2 A simulation study of potential impacts on indices of abundance

3.2.1 Species distribution modeling and diagnostics

3.2.1.1 Summer flounder

The most parsimonious GLMM for summer flounder fall survey catch rates included a second-order polynomial relationship with depth, independent year effects, spatial and spatiotemporal random fields (model 10; Table 6). The final fall model had the lowest AIC and highest deviance explained of the candidate models (Table 7). Though model 12 (Table 7), can explain the data as well as model 10, it is a more complex model and is penalized as such with a higher AIC. The optimal spring survey GLMM estimated catch rates of summer flounder as a function of a second-order polynomial relationship with depth, year effects, a categorical wind area effect, spatial and spatiotemporal random fields (model 12; Table 6). The final spring model had the lowest AIC and most deviance explained of the candidate models (Table 7), indicating this more complex model better explains spring survey catch rates of summer flounder.

Residuals were returned with 10 samples from a single MCMC chain for both models. The QQplot of the MCMC-resampled residuals for the fall model is summed over the 10 samples and indicates some deviation from the assumed distribution around the lower tail of the distribution (Figure 22a). Of the 10 samples returned, only two resulted in a distribution about the theoretical quantiles; the remaining 8 produced underestimation to some degree (Appendix A). The greatest values of predicted biomass were underestimated in link space (Figure 23a). Residuals from the spring model, on the other hand, did not deviate much from the theoretical quantile distribution (Figure 22b) and were evenly distributed about 0 when compared to the fitted values in link space (Figure 23b).

There is some uncertainty around the depth covariate in both the fall and spring models with the largest uncertainties around the peak expected biomass (Table 8, Figure 24). The fall model expected biomass catch rates to peak around 0.7 kg at around 38 meters of depth but could vary as high as 2.1 kg (Figure 24a). The spring model predicted the largest biomass catch rates of 1.3 kg between 133 and 145 meters but could reach as high as 3.4 kg (Figure 24b). The fall model

predicted higher values of biomass catch rates around 40 meters, but the maximum catch rates plateaued at differing values each year (Figure 25a). The highest peak biomass catch rate was predicted around 0.7 kg in 2009, while the lowest peak biomass catch rate was predicted around 0.3 kg in 2015 (Figure 25a). The spring model predicted biomass catch rates peaking at 146 meters but also varied each year. The highest peak biomass catch rate at this depth was 2.4 kg in 2016 while the lowest was 1.1 kg in 2015 (Figure 25b). Similarly, at this depth, the spring model expected the marginal effect of wind areas to have higher biomass catch rates than in outside areas, 1.70 kg with 95% confidence intervals (CI)[0.59, 4.91] and 1.3 kg with 95% CI [0.5, 3.4], respectively (Figure 26). The spring model predicted a similar marginal effect for the year and area predictors where the larger biomass catch rates were within wind areas, though 2016 was predicted to have the highest biomass catch rates in both areas (Figure 27). Furthermore, when evaluating the estimated wind area parameter (Table 8), there was a more positive effect expected for catch rates within those areas in turn resulting in higher observed biomass within wind areas (Figure 26b).

Fixed effects from the fall model predicted a strong relationship with the inshore areas of the continental shelf (Figure 28a). This spatial influence is reinforced by the predictions of the spatial random effects, noted by the greater amount of constant biological or oceanographic influence along these same areas in Figure 29a. Predictions of the spatiotemporal fields from the fall model in Figure 30a demonstrate the expected patchiness over space; though in recent years, and in years later in the time series (Appendix A), there tended to be large areas in the northern portion of the fall summer flounder spatial range that recurringly expected high biomass indicating there might be a potential biological or oceanographic covariate not explicitly captured in terms of fixed effects influencing catch rates in those years (Figure 30a). In general, the fall model estimated biomass catch rates to be fairly dispersed with a φ parameter of 1.5 but correlated within a range of 94 km (Table 8), and expected higher catch rates along the inshore areas in the fall to be driven by the fixed effects and spatial random effects (Figure 31).

The spring model estimated a continuous and strong relationship along the entire length of the offshore areas of the continental shelf both in terms of the fixed effects and the spatial random effects (Figure 28b and Figure 29b). The predictions of the spatiotemporal random fields also

detected some persistent connections with the offshore areas, especially in earlier years of the time series (Figure 30b and Appendix A). The spring model expected more dispersed observations of biomass with a φ parameter of 1.7 but that catch rates were more similar within a range of 112 km (Table 8).

Posterior checks of predictive performance show that nominal averages of fall biomass catch rates (3 kg/tow) did not correspond across the simulations (quantile = 0%; Figure 32a and Table 9); though the fall model was better at generating representative biomass catch rates in some years over others (Figure 33a and Table 9). The observed average biomass catch rate corresponded to approximately the interquartile range of the simulated distribution in five out of the eleven years (Table 9). All other years in the time series were overestimated with more than 80% of the distribution above the observed mean biomass catch rate (Table 9). Conversely, the distribution of simulated average proportion of zeroes was below the observed proportion of zeroes, indicating that the fall model is underinflated (Figure 34a and Table 10). When broken out by yearly proportions, simulated distributions in six out of twelve years were below the overall average proportion (proportion = 0.51). However, there were four years when the observed yearly average proportion was above the overall average, three of which corresponded to the central tendency of the simulated yearly distribution (Figure 35a). In other words, the observed proportion corresponded to the 76^{th}, 48^{th}, and 68^{th} percentile of the simulated distribution of proportions in 2015, 2016, and 2018, respectively (Figure 35a and Table 10). Moreover, the simulated distribution in 2019 was centered about the overall average proportion (proportion = 0.51), but the observed proportion of zeroes in that year (proportion = 0.47) only corresponded to the 6^{th} percentile of the distribution. Thus, while generally underinflated, the model was able to adequately capture the proportion of zeroes in some years.

The fall model was much better at estimating seasonal annual abundance indices, and more so for the wind-precluded index than the status-quo index (Figure 36a, Figure 36b, and Table 11). Under the wind-precluded survey effort scenario, the model performed well estimating 9 out of the 12 years in the time series, with the lowest performance occurring for 2012 and the best performance occurring for 2011 based on the quantile that the observed abundance index represents of the simulated distribution (Table 11). Further still, the model performed relatively

well when estimating the population trends under both survey effort scenarios, where the observed population trend represented the 50th percentile under simulated status quo survey effort and the 73rd percentile under the wind-precluded survey effort (Figure 37 and Table 12).

The observed average spring biomass catch rate corresponded to the extreme 10% of the simulated distribution of averages from the spring model indicating that the model was overestimating average biomass catch rates (Figure 32b and Table 9). When examined by year, observed averages in seven out of the twelve years drove the overall average biomass catch rate (Figure 33b). Out of those seven, the model was able to simulate average biomass catch rates in four years that closely corresponded to the observed average biomass catch rate, 2009 (quantile = 63%), 2011 (quantile = 38%), 2013 (quantile = 53%), and 2018 (quantile = 48%) respectively (Table 9). On the other hand, the model was also able to simulate average proportions of zeroes that corresponded with the observed proportion of zeroes from the data (proportion = 0.41). Furthermore, the observed proportion only corresponded to the extreme 4th percentile of the simulated distribution (Figure 34b and Table 10). When broken down by yearly proportions, the observed proportions corresponded to the extreme 30th percentiles in eight out of the twelve years (Figure 35b and Table 10).

The observed annual abundance index under both the status quo survey effort scenario and the wind-precluded survey effort scenario were well represented by the simulated distribution in the six years for each scenario (Figure 36c, Figure 36d, and Table 11). The model performed poorly in the remaining six years of the time series (Figure 36c and Figure 36d), where the observed abundance index under both scenarios corresponded to the most extreme 15% of the distribution of the simulated means (Table 11). Lastly, the spring model performed relatively well at generating distributions of trends in either scenario, such that the observed trend corresponded to the 65th percentile of the status quo survey effort distribution and the 80th percentile of the wind-precluded survey effort scenario (Figure 37 and Table 12).

3.2.1.2 Atlantic mackerel

The most parsimonious model for Atlantic mackerel spring survey catch rates included a fourth-order polynomial relationship with depth, independent year effects, spatial and spatiotemporal

random effects, and assumed a Delta Gamma observation distribution with a Poisson link (model 5; Table 13). This model had the lowest AIC out of the candidate delta gamma models and had the same amount of deviance explained as model 4 (Table 14). However, Model 4 had a higher AIC most likely due to the added complexity of spatial random fields estimation in the positive catch rate component, which was omitted from model 5's positive catch rate component. Additionally, a deeper inspection of the three delta gamma models that converged found that the positive catch rate component was over-parameterized when spatial random effects were included in the estimation, thereby selecting model 5 as the more optimal model.

According to the QQplots, the presence-absence component of the model indicated a successful fit (Figure 38). However, the positive catch rate component did not fit the tails of the distribution well (Figure 39). The comparison of fitted biomass values to the MVN residuals resulted in similar findings, where the residuals were more normally distributed in the presence-absence component but deviated at the lower and upper ends of biomass in the positive catch rate component (Figure 40 and Figure 41). Based on the analysis conducted on the impacts on sample size (Section 2.1.1), the spring survey of Atlantic mackerel observed a wide range of biomass that was variable over the time series which could contribute to the overestimation within the model; on average, positive catch rates from the survey observed 15 ± 82 kg of Atlantic mackerel with a median of 0.7 kg, and a single maximum observation of 1,894 kg. This is further supported by the QQplot of the simulated Dharma residuals where the middle of the distribution does not conform to the assumed distribution, suggesting an influence from the positive catch rate component (Figure 42). Therefore, while the presence-absence component of the model was able to adequately reflect the data, the positive catch rate component was not.

The model predicted higher values of biomass catch rates around 66 meters, though the value of which was different in each year (Table 15, Figure 43). The largest peak biomass catch rate was predicted at 0.5 kg in 2016, and the lowest peak biomass catch rate at 60 meters was predicted in 2009 at 0.2 kg (Figure 43).

Model predictions of the main effects found a strong relationship with depth throughout Georges Bank the mid-Atlantic, and the inshore areas of the Gulf of Maine (Figure 44). The strongest

relationships were found at depths ranging from 55 meters to 110 meters, while the weakest relationships were found at depths greater than 110 meters within the Gulf of Maine. The model found a similar relationship through the mid-Atlantic in terms of estimated spatial random effects, but it also expected consistent spatial deviations within the Gulf of Maine (Figure 45) indicating there are other spatially latent covariates affecting the biomass catch rates of Atlantic mackerel that were not explicitly accounted for through the fixed effects. The spatiotemporal random fields generally expected a patchy distribution throughout space and time (Figure 46). However, in recent years, the model estimated a consistent positive deviation in the spatiotemporal random field off the coast of Cape Cod (Figure 46).

The presence-absence component estimated a large spatial range (161 ± 46 km) and a low spatial standard deviation (1.4±0.3) indicating that a pair of present or absent observations are more correlated over a wider space (Table 15). More specifically, these estimates correspond with the spatial correlation of the survey observations rather than the behavior of the species, in that over time the survey observations over large distances in space are very similar and that the survey would need to travel farther 161 km before two observations are different (Figure 45). The spatiotemporal range for this component was estimated as 99 ± 12 km and the spatiotemporal standard deviation was estimated as 1.5 ± 0.1 (Table 15). Thus, observations of presence or absence are more correlated and more similar over space.

The spatial random fields were omitted from the positive catch rate component and thus only a spatiotemporal range and standard deviation were estimated from the gamma observation model. The spatiotemporal range was estimated at 27 ± 6 km and the standard deviation was estimated at 2.1 ± 0.3 (Table 15). However, the phi parameter was relatively low ($\varphi = 0.83$; Table 15). While observations had a tighter distribution, the values of biomass catch rates were expected to change quicker over space, and over a larger magnitude of change. Ultimately, the spatiotemporal fields from the gamma model component were the driving force behind predictions of biomass catch rates as evidenced by Figure 47, where areas of higher expected catch rates corresponded with areas estimated to have positive deviations in the spatiotemporal fields.

The post-model predictive check was used to further assess the model's performance. In general, the model was unable to generate representative distributions of average biomass catch rates or proportions of zeroes. Simulated average biomass catch rates were greater than the observed average catch rate (5.1 kg/tow; Figure 48). There were only two years, 2012 and 2019, where the simulated catch rates moderately represented the observed biomass catch rates in those years (Figure 49 and Table 16). Simulated proportions of zeroes were less than the observed proportion of zeroes (proportion = 0.67), both across years and between years (Figure 50, Figure 51, and Table 17).

The model was slightly better at simulating estimates of annual abundance indices, and more specifically indices under status quo survey effort with seven years where the distributions corresponded well to the observed respective index (Figure 52 and Table 18). Under wind-precluded survey effort, the model was able to simulate representative distributions of indices in six years. Furthermore, between years, the model was able to simulate representative distributions under status quo effort as well as those under wind-precluded survey effort in the same three years (Table 18). Lastly, the model performed much better at simulating population trends than nominal average catch rates, proportions of zeroes, or annual abundance indices. Across simulations, the observed population trend by status quo survey effort was represented by 65% of the distribution while the population trend estimated under wind-precluded survey effort was represented by 80% of the distribution (Figure 53 and Table 19). Therefore, the model is much better at generating population trends and abundance indices across years within the bounds of the observed uncertainty but ultimately was unable to adequately represent survey catch rates.

3.2.2 Scenarios of changing spatial distributions

3.2.2.1 Summer flounder

Simulations of the fall survey under a baseline, or unchanged, fish density from what was estimated by the seasonal model, generated similar estimates of annual abundance of summer flounder regardless of the survey effort (status quo or wind-precluded effort; Figure 54a and Figure 55). However, when changes in fish density from the baseline were simulated in response to wind areas, simulated estimates of annual abundance indices were different when survey effort was precluded from the

wind areas compared to estimates calculated based on status quo survey effort. Under scenarios of enhanced fish density, simulated estimates of annual abundance were lower when survey effort was precluded from wind areas (Figure 54b and Figure 55a), mirroring the findings from Section 3.1.2.1.1. Whereas, under reduced fish density scenarios, estimates of annual abundance were higher under wind-precluded survey effort as a result of lower catch rates within wind areas compared to catch rates outside of wind areas (Figure 54c and Figure 55a). Notably, the distribution of estimates of abundance when survey effort was precluded under the reduced fish density scenario was similar to the distribution of estimates of abundance based on status quo effort under the baseline fish density (Figure 55a).

Across all scenarios, the preclusion of the fall survey resulted in biased stock abundance indices for summer flounder (Figure 56a). The bias between indices under enhanced and reduced fish densities was almost twice the bias between indices under baseline fish densities, with the greatest bias occurring when the survey was precluded from surveying wind areas with enhanced fish densities overall (Figure 56a). The bias between survey effort scenarios also resulted larger MARE in the estimates of abundance under the enhanced fish density scenarios when compared to the baseline and reduced fish density scenarios for fall populations of summer flounder (Figure 57a). While the bias between indices under reduced fish density was also greater when the fall survey was precluded compared to under baseline fish densities; the differences were only about 10% (Figure 57a).

CVs across all simulations and fish density scenarios were about 20% higher when wind areas were precluded from fall survey effort (Figure 58a). In other words, the fall survey was less precise in estimating the relative abundance of summer flounder when wind areas were precluded from survey effort.

Distributions of population trend estimates were similar across survey effort and fish density scenarios (Figure 59a). The only minor difference occurred under the status quo survey effort scenario with enhanced fish density where the distribution of population trends was wider at the tails (Figure 59a). Regardless of their similarity in distribution, there were marked differences between trends estimated under enhanced fish densities and reduced fish densities inside wind

areas (Figure 60a). The distribution of differences was greatest when fish density was enhanced within wind areas indicating that population trends estimated based on status quo survey effort were more different that estimates based on wind-precluded effort, especially when compared to the differences in estimates under baseline fish density (Figure 60a). The distribution of differences when fish density was reduced in wind areas, on the other hand, was lower than either cases where fish density was enhanced or under baseline fish densities. Thus, wind-precluded population trend estimates were closer to trends estimated under status quo survey effort when fish density was reduced compared to the estimates between survey effort scenarios when fish density was enhanced or unchanged from the baseline.

Simulations of the spring survey and baseline fish densities resulted in minor differences between annual abundance indices calculated from status quo and wind-precluded survey effort, such that the wind-precluded estimates were lower than status quo estimates in each year and across simulations (Figure 54d and Figure 55b). Similarly, wind-precluded abundance indices were lower than the status quo abundance indices under the enhanced fish density scenario (Figure 54e and Figure 55b). However, wind-precluded abundance indices were higher than the status quo abundance indices under the reduced fish density scenario (Figure 54f and Figure 55b).

These differences translated to biased annual abundance indices for summer flounder when the spring survey was precluded from wind energy areas across all fish density scenarios. The greatest bias occurred when the survey was precluded from surveying wind areas with enhanced fish densities in terms of magnitude, which was double the bias quantified under the baseline scenario (Figure 56b). Further, these differences between survey effort scenarios resulted in higher MARE in the estimates of abundance when compared to the baseline fish density for spring populations of summer flounder (Figure 57b).

Under reduced fish densities, bias between annual abundance indices was also greater than the bias between indices under baseline fish densities, though to a lesser degree than the difference in bias when comparing enhanced fish densities and baseline fish densities (Figure 56b). As a result, MARE in the estimates of abundance under reduced fish densities were lower than the

MARE in estimates of abundance under baseline fish density (Figure 57b). This differs from the findings for the fall survey under reduced summer flounder densities due to the positive effect of wind areas on biomass catch rates estimated by the optimal spring model (Table 8). Simulating reduced fish densities in wind areas effectively removed the effect of wind areas on biomass catch rates thereby equalizing catch rates regardless of the area in which they occurred and lessening the difference between survey effort estimates when compared to baseline estimates of fish density in wind areas (Figure 57b).

Across all simulations and fish density scenarios, the CV of survey estimates when wind was precluded was higher than the CV of survey estimates under status quo survey effort (Figure 58b). Thus, the spring survey was also less precise in estimating a stocks relative abundance when survey effort was precluded from wind areas.

Similar to the findings for the fall survey under the fish density scenarios, distributions of spring population trend estimates were similar across survey effort and fish density scenarios (Figure 59b). Furthermore, differences between survey effort population trends were greater under enhanced fish densities and lowest under reduced fish densities across simulations when compared to baseline fish density (Figure 60b).

At a minimum, under baseline fish densities, estimates of annual abundance and population trends would be biased and less precise when either fall or spring survey is precluded from wind energy areas. This effect is exacerbated when the surveys are precluded from wind energy areas and in scenarios where fish density increases within these areas after installation. For the fall survey, there was also an increased effect on estimates on annual abundance indices when fish densities declined within wind areas after installation. While the spring survey, on the other hand, demonstrated a decreased effect on estimates of annual abundance indices when the survey was precluded and fish densities were reduced from baseline levels, such that the preclusion of the spring survey had a greater effect on estimates of abundance in scenarios of unchanged fish density than it did on estimates of abundance in scenarios where fish density declined in wind areas. Similarly, the preclusion of the fall and spring surveys had a smaller effect on estimates of

population trends of summer flounder when fish density was reduced within wind areas than when fish density was unchanged from baseline levels.

3.2.2.2 Atlantic mackerel

Simulations of the spring survey under baseline Atlantic mackerel densities generated estimates of annual abundance that were similar each year and across simulations regardless of the survey effort, status quo or wind-precluded (Figure 61a and Figure 62). Simulated estimates of annual abundance were lower when the survey was precluded from wind areas when enhanced Atlantic mackerel densities were simulated compared to estimates calculated based on status quo survey effort (Figure 61b and Figure 62). Under reduced Atlantic mackerel densities, simulated estimates of annual abundance were slightly higher when the survey was precluded than those calculated at the status quo survey effort (Figure 61c and Figure 62).

These differences translated to biased annual abundance indices for Atlantic mackerel (Figure 63). Mean relative differences between annual abundance indices under survey effort scenarios deviated further from zero than the differences at baseline fish densities under both enhanced and reduced fish density scenarios (Figure 63). The greatest deviation occurred under enhanced fish densities, indicating that annual abundance indices under enhanced fish density scenarios were more biased than either indices calculated in the baseline or reduced fish density scenario (Figure 63). This was further reinforced by the higher MARE values under enhanced fish density when compared to baseline or reduced fish density errors (Figure 64).

When fish densities in wind areas were reduced and the survey was precluded, bias was also higher than the bias quantified under baseline fish densities (Figure 63). However, when translated to MARE, the differences between indices were slightly lower compared to a baseline fish density scenario (Figure 64). Lower MARE under reduced fish density are most likely a result of the high variability between catch rates used to fit the model (Section 3.1.2.1.2) and the lack of relationship found by the model between wind areas and expected catch rates (Table 15). Thus, manipulating catch rates under a reduced fish density assumption forced catch rates to be more similar to each other across areas thereby resulting in lower differences between indices

when effort was or was not precluded (Figure 64). In either survey effort or fish density scenarios, survey precision estimates were unchanged across simulations (Figure 65).

Distributions of population trend estimates were similar across survey effort and fish density scenarios (Figure 66). Though, there were notable differences between survey effort trends estimated under enhanced and reduced fish densities (Figure 67). The distribution of differences was greatest when fish density was enhanced within wind areas, indicating that population trends estimated based on status quo survey effort were more different that estimates based on wind-precluded effort, while the distribution of differences when fish density was reduced in wind areas was lower than either cases where fish density was enhanced or unchanged (Figure 67). More specifically, wind-precluded population trends estimated under reduced fish densities were closer to trends estimated based on status quo survey effort compared to the estimates between survey effort scenarios when fish density was enhanced or unchanged from the baseline.

The preclusion of wind energy areas to the spring survey would have a greater effect on estimates of Atlantic mackerel annual abundance indices and population trends under a scenario where fish density increases within these areas after installation. Whereas the reduction of fish and the preclusion of the survey in these areas would result in a smaller effect to that seen if fish density was unchanged from existing conditions due to the high variability in catch rates throughout the spatial footprint.

4 DISCUSSION

It is expected that the installation of large-scale offshore wind areas will preclude fishery-independent surveys along the eastern coast. Even though current protocols for the NEFSC bottom trawl survey dictate the reallocation of pre-selected tows in the case of untrawlable areas, here I set out to illustrate the impacts to stock abundance indices if the full reallocation of lost survey tows would not be possible.

In this study, I aimed to address three main research questions: (1) what would the effect on previous annual abundance indices have been if wind areas prevented bottom trawl survey effort, (2) can species distribution models be used to analyze potential impacts of offshore wind areas on survey operations and changes in abundance, and (3) how do the impacts to abundance indices as a result of wind-precluded survey effort change when there are changes in species productivity and fish density due to the presence of wind turbines. To address these questions, I assumed that the understanding of proposed and leased wind energy areas as of June 2022 were in place and precluding survey efforts at the start of the bottom trawl survey times series (e.g., 2009).

An empirical analysis of potential impacts on survey data

Using an empirical analysis approach, I evaluated the magnitude of loss and its propagation into annual abundance indices by removing observations of catch rates that were identified as having occurred within wind energy areas tows (e.g., “wind-area tows”; Section 2.1.1). My findings show that under such a worst-case scenario, sample sizes, annual abundance indices or the precision of their estimates (CVs) will be impacted. Specifically, the loss of species biomass and numbers will vary in magnitude ranging anywhere from 0% to 100% depending on the frequency in which the survey catches a given species. On one hand, sample sizes for over 65% of the species caught by the survey will be unimpacted by its preclusion. On the other hand, 32% of the species caught by the survey will be impacted, with the largest effects on sample sizes occurring where survey catch ratios (wind catch rates to total survey catch rates) are the largest. These impacts then propagated into estimates of annual abundance indices, population trend, and survey precision, such that some species included in Table 2 that were found to have the greatest

differences between estimates, were also found to suffer the most losses in terms of percentages of tows, biomass, and numbers of fish removed when the survey was precluded. In other words, the largest impacts of wind preclusion to sample sizes were seen for species that were less available to the survey throughout the area but were caught in larger proportions within wind areas when they were encountered.

However, the survey was not designed for these rare or uncommon species. The survey efficiency quickly deteriorates with respect to sampling these species, and many of them are only recorded at the family or genus level (i.e., spider crab uncl or entropus uncl in Table 2). Thus, evaluating at the species level can make results variable and uncertain. Further iterations of this work could perform the empirical analysis at the taxa level rather than the species level to derive more certain estimates of impacts in the context of rare or uncommon species. Conversely, ongoing analyses or applications could consider either foregoing evaluating impacts on this group of species by either including additional spatial and temporal constraints on the data or exclude observations and catch rates of species that occur at the tails of the catch rate distribution.

One approach considered in this study included focusing the empirical evaluation on the commercially important species for which the survey is principally designed. Input from stakeholders during two Survey Simulation Experimentation and Evaluation Project (SSEEP) workshops formed the basis of this list of species of interest. The analysis found that sample sizes throughout the survey area for the majority of stakeholder-selected species were less impacted by wind-precluded survey effort. The minimal spatial overlap within wind areas and the high rate in which the survey encounters these species outside of potential wind areas was identified as the main driver behind these smaller impacts. Similar findings occurred when impacts were evaluated in terms of estimates of annual abundance indices, survey precision, and population trends. However, impacts to estimates of population trend amongst skates, Atlantic herring, Atlantic mackerel, butterfish, spiny dogfish, and yellowtail flounder were the greatest for these species when comparing across the stakeholder-selected species as well as across the total group of species encountered by the survey (Table 2 and Table 3).

There was further invested interest to evaluate the empirical analysis and the other research questions in the context of two stakeholder-selected species: summer flounder and Atlantic mackerel, both of which represent classic definitions of species that are well-sampled and poorly sampled by the survey, respectively. As illustrated above, wind preclusion will impact all the species caught by the multispecies survey. By focusing a more applied evaluation of impacts on summer flounder, a demersal fish distributed contiguously across the continental shelf, and Atlantic mackerel, a schooling, pelagic fish with a patchier and more variable distribution, results can be more readily translated to other species that fit within these definitions.

Empirical analyses found that the propagation of lower sample sizes of summer flounder resulted in lower estimates of annual abundance indices and population trend and increased estimated uncertainty. This was most notable for estimates derived from the fall survey where historically there have been higher catch rates within potential wind areas. Higher catch rates within potential wind areas are due to the increased availability of summer flounder to the survey when they are inshore and in their preferred habitat. Similar impacts occurred when the spring survey was precluded from wind areas, but to a lesser extent as the seasonal offshore distribution of summer flounder will have minimal overlap with areas proposed for installation and development.

Catch rates of Atlantic mackerel have historically been variable over the time series and over space, in turn creating high interannual variability in estimates of abundance and population trends (NEFSC 2021). As such, with status quo survey effort, the spring survey has been imprecise when sampling Atlantic mackerel populations (e.g., high average CV in Table 5). This high variability in catch rates and survey imprecision is expected to precipitate through to impacts on sample sizes, estimates of annual abundance, and estimates of population trends for Atlantic mackerel when the spring survey is precluded from wind areas. That is, high variability and imprecision will persist with reduced survey effort, but on average, estimates will effectively be unimpacted.

Species distribution modeling

The historical data for summer flounder and Atlantic mackerel were used to fit geostatistical GLMMs to evaluate potential impacts of offshore wind areas to survey operations, changes in abundance, and hypothetical scenarios of changing spatial fish density distributions. A motivating factor to experimenting with species distribution models was their ability to account for spatial and temporal non-stationarity (or spatial and temporal changes over time) to understand changes in a species geographic distribution and density (Elith & Leathwick, 2009; Elith et al., 2010; Johnson et al., 2019; Barnett et al., 2021; Anderson et al., 2022; Ward et al., 2022). Between the two species, three separate models were fit: a spatiotemporal Tweedie observation model for summer flounder in the fall, a spatiotemporal Tweedie observation model for summer flounder in the spring, and a spatiotemporal Delta Gamma with a poisson link observation model for Atlantic mackerel in the spring.

Only the Tweedie model for summer flounder in the spring was able to adequately fit the data and generate representative catch rate data based on new spatiotemporal random fields. The fall summer flounder model and spring Atlantic mackerel models were able to generate representative estimates of annual abundance indices and populations trends but ultimately had issues with their fit and simulating raw catch rates of biomass. Three of the main problems with the models included residual heteroscedasticity, overdispersion, and the inflating (or lack thereof) of zeroes within the two models.

The fall model for summer flounder and the gamma component of the delta gamma model for Atlantic mackerel both showed indications of residual heteroscedasticity and overdispersion that was not accounted for through the estimation of the spatial or spatiotemporal random fields (Appendix Figure A48-Figure A49 and Figure A59-Figure A60). For summer flounder, this could be the result of some additional habitat relationship that should be included as a predictor of biomass, especially given the fact that summer flounder has distinct migration patterns, spending early spring to late fall inside estuaries and moving offshore to spawn (Buchheister & Latour, 2011). The same could be said with respect to the Atlantic mackerel model especially given that the gamma component, which represents the encounter rate of the observations,

showed unequal scatter across its residuals and predictors (Figure 40-Figure 41; Appendix Figure A59-Figure A60).

While there were some issues with residual scattering and data fitting, this does not inherently indicate that the models were unusable. Fortunately, the models were able to emulate plausible scenarios for annual abundance indices and population trends, which were more adequately representative when compared to real estimates from the observed data. At a minimum, the models fit on this study were deemed worthy to meet the objectives and support the use of geostatistical GLMMs to identify impacts on estimates of abundance and population trends.

Should other objectives be pursued when applying this framework, additional model exploration and parameterization will be needed to resolve the residual and diagnostic issues. Additional parameterizations could consider incorporating predictors of bottom temperature, which has been included in previous summer flounder modeling efforts (Perretti & Thorson, 2019), and predictors of sea surface temperature and salinity, which has been included in research evaluating distributions of spawning Atlantic mackerel (Mbaye et al., 2020). Additional model explorations could also investigate alternative error distributions, particularly for Atlantic mackerel.

Scenarios of changing spatial distributions

The simulation study assumed a change in fish density in response to the presence of offshore wind turbines to emulate hypothesized artificial reef effects or avoidance effects (Mavraki et al., 2021; Reubens, Braeckman, et al., 2013; Reubens, Vandendriessche, et al., 2013) and how that might propagate changes in estimates for abundance and population trends. Across the two case study species and both seasonal surveys, increases in fish density and the preclusion of the survey within these areas will result in the greatest differences to estimates of annual abundance indices and population trends. The preclusion of the survey will result in varied impacts on estimates of annual abundance indices and population trends when fish density was reduced depending on the season in which it is conducted. For instance, when the fall survey was precluded, estimates for summer flounder annual abundance indices would be more biased and less precise than the baseline state but would not be as impacted when compared to an enhanced

state. The preclusion of the spring survey, on the other hand, would result in estimates of annual abundance indices for summer flounder and Atlantic mackerel that are less biased and more precise than in the baseline state. It is likely that in this scenario, there would not be a difference in catch rates within wind areas and outside wind areas; therefore, wind areas and reduced survey efforts in response would be the least impactful. Population trends for both species and in both seasons would be mostly unchanged by the preclusion of the respective survey and changes in fish density, while the survey's precision would be higher and less precise when there are reductions in survey effort independent of the changes in fish density.

An empirical study at BIWF concluded that increases in abundance at an area of potential effect when compared to a reference site were due to a regional artificial reef effect (Gervelis et al., 2023) potentially indicating support for the attraction hypothesis. The attraction hypothesis proposes that increases in fish density are a result of immigration from the surrounding environment rather than an increase in productivity. The assumptions made in the simulation study assumed a local increase or decrease in fish density at a given wind area rather than a global increase in fish abundance and at previously sampled locations. In doing so, I hypothesized that for species like summer flounder that are already observed to have high catch rates within proposed wind areas, the attraction to offshore wind turbines will result in a greater impact on the estimates of abundance when the survey is precluded and the need to mitigate that impact to appropriately track abundance changes. This could also be true for species like Atlantic mackerel where their observations are not as consistent in the survey. Conversely, this response may not be as strong if fish have an aversion to wind areas and instead avoid these areas, in which case the difference in the estimates of abundance when the survey is precluded would be smaller (Figure 57 and Figure 64).

The simulation study only looked at potential impacts for a period of five years. Some artificial reef studies have shown that although there were increases in abundance at a younger four-year old artificial reef compared to a natural reef or no reef at all, there was a higher abundance and overall diversity at a 41-year old reef indicating that productive environments have the potential to become more productive over time (Harrison & Rousseau, 2020). Furthermore, similar work by Yalcin et al. (2023) found that geostatistical GLMMs such as the ones employed in this study

could mitigate the effects of survey reduction. However, GLMMs may not always be able to account for the population processes as they change and particularly after an area has already been excluded, and at some level the accuracy of them degrades substantially (Yalcin et al., 2023). Thus, future iterations of this work could apply the treatments over time and for longer durations to identify how the impacts might change with time, if there would be a maximum threshold at which point impacts to the abundance index are no longer accrued, and at what point within that accrual are the species distribution models unable to make up for the loss. Beyond this, future directions could also consider using the impacted estimates of abundance concluded from this study or using impacts reassessed at the stock unit resolution as inputs into a stock assessment and management strategy evaluation to evaluate how their performance compares to an unimpacted input. Currently, there are two projects evaluating the impact of wind preclusion on annual abundance indices as inputs for stock assessments. Sun et al. (*in prep)* found that abundance index bias had limited impacts on model-based stock assessments, while index-based methods were much more sensitive to these changes. Similarly, the Northeast Fisheries Science center is assessing the impacts on index-based assessments when inputs are derived based on wind-precluded survey effort; preliminary findings indicate that the impact is dependent on a species distribution relative to the wind energy areas and relative to the proportion of stock biomass encountered by the survey in the wind energy areas (Cacciapaglia et al., *in prep*).

Fishery-independent surveys have proven to be an imperative tool in the fisheries management toolbox to track species distributions and changes through a standardized design, even if it is at the expense of less resolute data when compared to fishery dependent data such as CPUE. In this study I identified potential differences in stock abundance indices when the federal Northeast bottom trawl survey is precluded from operating inside wind energy areas. Many of these species and stocks that are federally managed depend on average biomass catch rates, estimates of abundance, and changes in population trends to derive their management advice, whether empirically or analytically. More specifically, biased and imprecise inputs would elicit the need for more precautionary management to account for management uncertainty and protect against overfishing in pursuit of complying with the National Standard Guidelines in the Magnuson-Stevens Fishery Conservation and Management Act.

As such, it is imperative that those differences can be mitigated. At a minimum, existing protocols for the bottom trawl survey should be maintained and upheld, which allow for the reallocation of lost effort within the same sampling unit (Politis et al., 2014). However, this study demonstrated the impact when large portions of survey strata or whole survey strata are lost from the sampling frame due to the inability to sample within wind energy areas. It further showed the impact when that loss is coupled with changing species distributions. Should the current understanding of species distributions and dynamics remain the same, then it is possible that reallocating lost effort will be enough to mitigate impacts of wind preclusion. If, however, the changes in species distribution and dynamics simulated in this study are realized, then additional sampling efforts will need to supplement the reallocated survey to appropriately estimate relative annual abundances and population trends. These efforts could include sampling within the wind energy areas and operating according to the same objectives, and temporal and seasonal scales as the federal scientific survey; though a smaller vessel may be warranted to safely transit between the turbines as well as calibration factors to relate relative abundances between the differing vessels. Another option with regards to sampling could implement video sampling protocols and co-locating the gear on the wind turbine structures; though this alternative would lose the important biological sampling data that also feeds into federal stock assessments.

Other initiatives and research through the Federal Survey Mitigation Implementation Strategy for the Northeast Region (Hare et al., 2022), in addition to the Survey Experimentation and Evaluation Project (SSEEP), aim to analyze how the reallocation of effort, supplemental sampling strategies, and alternative survey designs can mitigate the findings herein. For instance, the NEFSC has drafted a survey mitigation plan that is currently under reviewed which details the evaluation of the existing stratification and station allocation design and its performance to potentially adapt the survey's design to something more spatially-balanced. The plan also considers including perimeter sampling around smaller wind energy areas to try to capture those higher abundances that would be precluded from survey effort through the immigration and emigration of fish between wind energy areas.

As the marine use environment is becoming more inundated, spatial management of resources becomes more imperative, as do standardized and consistent fishery-independent surveys that

can meet management objectives and track changes in the distribution and abundance of resources. Offshore wind development is at the forefront of many marine spatial use conflicts with fisheries, with expected impacts to an additional eleven federal fisheries surveys on the eastern coast and various others within the Gulf of Mexico and along the northwest coast, regions which are in the beginning stages of development planning.

This study found an important connection between the magnitude of spatial overlap of wind energy areas and bottom trawl survey strata, and the temporal overlap between a species distribution and their availability to a given seasonal survey. For example, impacts to estimates of annual abundance indices for summer flounder were greater when the fall survey was precluded from wind energy areas than when the spring survey was precluded. The proposed wind energy areas overlap with the inshore strata of the survey where historically summer flounder has been more available to the fall survey whereas in the spring, summer flounder is more available to the survey along the outer continental shelf which does not align with proposed wind energy area overlap. As the spatial conflict between wind energy areas and the survey sampling footprint grows larger with the expansion into the Gulf of Maine (https://www.boem.gov/Gulf-of-Maine) and the installation of floating wind turbine structures, it is expected that some of the impacts identified in this study would grow alongside those updated understandings. For instance, the estimates of population trend for spiny dogfish were identified as having some of the largest impacts when compared against all the species encountered by the survey, and against other stakeholder-selected species. These estimates were assessed on a spatial sampling frame where upwards of 75% of the total biomass caught by the survey over the time series occurred in the Gulf of Maine strata. As such, an updated analysis that includes proposed wind energy areas within the Gulf of Maine could further exacerbate the impacts identified in this study due to an increased loss in sample sizes for spiny dogfish.

Nonetheless, the underlying framework of this study has been developed in such a way such that the analysis can be supplied with any updated understandings of proposed wind energy areas or proposed structures and can be applied in the context of any of the other eleven federal surveys and species of interest. Further still, because this research uses the spatial footprint of wind energy areas to reflect an area of impact, there is the potential to extend this framework into

other spatial impact analysis applications such as the impacts of scientific survey preclusion or fishery preclusion due to aquaculture or oil and gas development.

Finally, further work needs to be conducted with regards to impacts from longstanding changes to survey design and sampling on these federal surveys but also considering the added complexities of tracking species distributions in the face of climate change (Nye et al., 2009). Existing research thus far has performed well in identifying distribution shifts, but the work is still ongoing to incorporate this information into species stock assessments, with stock assessors starting to discuss how to define spatial stock structures, break conventional stock assessment structures, and incorporate ecosystem-based fisheries management (EBFM), which is still in the realm of innovation. My work aims to contribute a novel approach using time series analysis and species distribution modeling to identify potential disruptions, to work towards designing a more flexible fishery-independent survey, and in advancement of analyses that consider the full management cycle from data collection to analysis and assessment inputs, to reference points and total allowable catch advice.

5 CONCLUSIONS

The reduction in survey effort in the presence of offshore wind is expected to be most impactful for species that had larger differences in catch rates within wind energy areas compared to catch rates outside wind energy areas. With respect to the case study species, the historical analysis suggests greater impacts on estimates of summer flounder than Atlantic mackerel, and greater impacts still when those estimates were derived based on the fall survey. Additionally, changes to data products derived for summer flounder due to wind preclusion of the fall survey were different than changes due to general reduction in survey effort. Data products derived for Atlantic mackerel or summer flounder from the spring survey were robust to changes in survey effort on average regardless of the driver in reductions of survey effort.

Species distribution modeling was able to assist in meeting the objectives of this study and contribute to the evaluation of potential impacts of wind preclusion. With further model refinement, impact analysis can be another useful application of SDMs, and particularly geostatistical GLMMs.

Wind preclusion will result in more biased and imprecise stock abundance indices with a reduction in survey efforts. This would be especially true under assumptions of increased fish density changes within wind areas and the theorized reef effect is actualized.

The findings in this study reinforce the call to mitigate anticipated disruptions in survey effort and conserve the integrity of federal scientific survey data. Without the mitigation, resulting biased and imprecise inputs from reduced sample sizes and the failure to account for uncertainty from reduced survey effort could lead to more precautionary management or more conservative decisions for measures that protect against overfishing.

6 REFERENCES

Anderson, S. C., English, P. A., Gale, K. S. P., Haggarty, D. R., Robb, C. K., Rubidge, E. M., & Thompson, P. L. (2024). Impacts on population indices if scientific surveys are excluded from marine protected areas. *ICES Journal of Marine Science*, fsae009. https://doi.org/10.1093/icesjms/fsae009

Anderson, S. C., Ward, E. J., English, P. A., & Barnett, L. A. K. (2022). *sdmTMB: An R package for fast, flexible, and user-friendly generalized linear mixed effects models with spatial and spatiotemporal random fields* (p. 2022.03.24.485545). bioRxiv. https://doi.org/10.1101/2022.03.24.485545

Barnett, L. A. K., Ward, E. J., & Anderson, S. C. (2021). Improving estimates of species distribution change by incorporating local trends. *Ecography*, *44*(3), 427–439. https://doi.org/10.1111/ecog.05176

Bell, R. J., Hare, J. A., Manderson, J. P., & Richardson, D. E. (2014). Externally driven changes in the abundance of summer and winter flounder. *ICES Journal of Marine Science*, *71*(9), 2416–2428. https://doi.org/10.1093/icesjms/fsu069

Bell, R. J., Richardson, D. E., Hare, J. A., Lynch, P. D., & Fratantoni, P. S. (2015). Disentangling the effects of climate, abundance, and size on the distribution of marine fish: An example based on four stocks from the Northeast US shelf. *ICES Journal of Marine Science*, *72*(5), 1311–1322. https://doi.org/10.1093/icesjms/fsu217

Bergström, L., Kautsky, L., Malm, T., Rosenberg, R., Wahlberg, M., Åstrand Capetillo, N., & Wilhelmsson, D. (2014). Effects of offshore wind farms on marine wildlife—A generalized impact assessment. *Environmental Research Letters*, *9*(3), 034012. https://doi.org/10.1088/1748-9326/9/3/034012

Berkenhagen, J., Döring, R., Fock, H. O., Kloppmann, M. H. F., Pedersen, S. A., & Schulze, T. (2010). Decision bias in marine spatial planning of offshore wind farms: Problems of singular versus cumulative assessments of economic impacts on fisheries. *Marine Policy*, *34*(3), 733–736. https://doi.org/10.1016/j.marpol.2009.12.004

Blanchard, J. L., Maxwell, D. L., & Jennings, S. (2008). Power of monitoring surveys to detect abundance trends in depleted populations: The effects of density-dependent habitat use, patchiness, and climate change. *ICES Journal of Marine Science*, *65*(1), 111–120.

BOEM. *State Activities*. Retrieved June 29, 2023, from https://www.boem.gov/renewable-energy/state-activities

BOEM. (2019). *National Environmental Policy Act Documentation for Impact-Producing Factors in the Offshore Wind Cumulative Impacts Scenario on the North Atlantic Continental Shelf.* US Dept. of the Interior, Bureau of Ocean Energy Management, Office of Renewable Energy Programs, Sterling, VA. OCS Study 2019- 036. https://www.boem.gov/sites/default/files/environmental-stewardship/Environmental-Studies/Renewable-Energy/IPFs-in-the-Offshore-Wind-Cumulative-Impacts-Scenario-on-the-N-OCS.pdf

BOEM. (2023). *Renewable Energy GIS Data*. Retrieved June 30, 2023, from https://www.boem.gov/renewable-energy/mapping-and-data/renewable-energy-gis-data

BOEM. (2021). *Vineyard Wind 1 Offshore Wind Energy Project Final Environmental Impact Statement Volume I*. Retrieved September 2, 2025, from https://www.boem.gov/sites/default/files/documents/renewable-energy/state-activities/Vineyard-Wind-1-FEIS-Volume-1.pdf

Buchheister, A., & Latour, R. J. (2011). Trophic ecology of summer flounder in lower Chesapeake Bay inferred from stomach content and stable Isotope analyses. *Transactions of the American Fisheries Society*, *140*(5), 1240–1254. https://doi.org/10.1080/00028487.2011.618364

Caracappa, J., Gaichas, S., Beet, A., Beltz, B., DePiper, G., Hyde, K., Large, S., & Weisberg, S. (2025). State of the Ecosystem 2025: New England. https://doi.org/10.25923/zr75-a788

Coates, D. A., Kapasakali, D.-A., Vincx, M., & Vanaverbeke, J. (2016). Short-term effects of fishery exclusion in offshore wind farms on macrofaunal communities in the Belgian part of the North Sea. *Fisheries Research*, *179*, 131–138. https://doi.org/10.1016/j.fishres.2016.02.019

Cochran, W. G. (1977). *Sampling techniques*. John Wiley & Sons.

Commander, C. J. C., Barnett, L. A. K., Ward, E. J., Anderson, S. C., & Essington, T. E. (2022). The shadow model: How and why small choices in spatially explicit species distribution models affect predictions. *PeerJ*, *10*, e12783. https://doi.org/10.7717/peerj.12783

Conn, P. B., Johnson, D. S., Williams, P. J., Melin, S. R., & Hooten, M. B. (2018). A guide to Bayesian model checking for ecologists. *Ecological Monographs*, *88*(4), 526–542. https://doi.org/10.1002/ecm.1314

Dennis, D., Plagányi, É., Van Putten, I., Hutton, T., & Pascoe, S. (2015). Cost benefit of fishery-independent surveys: Are they worth the money? *Marine Policy*, *58*, 108–115. https://doi.org/10.1016/j.marpol.2015.04.016

Ducharme-Barth, N. D., Grüss, A., Vincent, M. T., Kiyofuji, H., Aoki, Y., Pilling, G., Hampton, J., & Thorson, J. T. (2022). Impacts of fisheries-dependent spatial sampling patterns on catch-per-unit-effort standardization: A simulation study and fishery application. *Fisheries Research*, *246*, 106169. https://doi.org/10.1016/j.fishres.2021.106169

Elith, J., Kearney, M., & Phillips, S. (2010). The art of modelling range-shifting species. *Methods in Ecology and Evolution*, *1*(4), 330–342. https://doi.org/10.1111/j.2041-210X.2010.00036.x

Elith, J., & Leathwick, J. R. (2009). Species Distribution Models: Ecological Explanation and Prediction Across Space and Time. *Annual Review of Ecology, Evolution, and Systematics*, *40*(1), 677–697. https://doi.org/10.1146/annurev.ecolsys.110308.120159

Gaichas, S., Caracappa, J., Beet, A., Beltz, B., DePiper, G., Hyde, K., Large, S., & Weisberg, S. (2025). State of the Ecosystem 2025: Mid-Atlantic. https://doi.org/10.25923/23nx-qf59

Gervelis, B., Wilber, D. H., Brown, L., & Carey, D. A. (2023). The Role of Fishery-Independent Bottom Trawl Surveys in Providing Regional and Temporal Context to Offshore Wind

Farm Monitoring Studies. *Marine and Coastal Fisheries*, *15*(1), e10231. https://doi.org/10.1002/mcf2.10231

Gill, A. B., Degraer, S., Lipsky, A., Mavraki, N., Methratta, E., & Brabant, R. (2020). Setting the context for offshore wind development effects on fish and fisheries. *Oceanography*, *33*(4), 118–127.

Godo, O. (1994). Factors affecting the reliability of groundfish abundance estimates from bottom trawl surveys. In A. Ferno & S. Olsen (Eds.), *Marine Fish Behavior in Capture and Abundance Estimation* (pp.166-200). Fishing News Books.

Guyant, M., Miller, A., Roman, C., O'Keefe, C., Lipsky, A., Politis, P., Ford, K., & Fay, G. (2022a). *Survey Simulation Experimentation and Evaluation Project Stakeholder Workshop #1 Report*. https://drive.google.com/file/d/1-qUwAlE-P-iXT3lCk0fFDXeulTCR5I1Q/view?usp=sharing

Guyant, M., Miller, A., Roman, C., O'Keefe, C., Lipsky, A., Politis, P., Ford, K., & Fay, G. (2022b). *Survey Simulation Experimentation and Evaluation Project Stakeholder Workshop #2 Report*. https://drive.google.com/file/d/13yO5g9niezIN4kzaNGesiOA9eDdStrb1/view?usp=drive_link

Guyant, M., Miller, A., Roman, C., O'Keefe, C., Lipsky, A., Politis, P., Ford, K., & Fay, G. (2023). *Survey Simulation Experimentation and Evaluation Project Participatory design*

workshops to develop a spatial observation simulator to evaluate changes to marine fishery ecosystem monitoring surveys: Final Report.

Haggett, C., ten Brink, T., Russell, A., Roach, M., Firestone, J., Dalton, T., & McCay, B. (2020). Offshore Wind Projects and Fisheries: Conflict and Engagement in the United Kingdom and the United States. *Oceanography*, *33*(4), 38–47. https://doi.org/10.5670/oceanog.2020.404

Hare, J., Blythe, B., Ford, K., Godfrey-McKee, S., Hooker, B., Jensen, B., Lipsky, A., Nachman, C., Pfeiffer, L., & Rasser, M. (2022). *NOAA Fisheries and BOEM Federal Survey Mitigation Implementation Strategy-Northeast US Region*. https://doi.org/10.25923/jqse-x746

Harley, S., Myers, R., & Dunn, A. (2001). Is Catch-per-Unit-Effort Proportional to Abundance. *Canadian Journal of Fisheries and Aquatic Sciences*, *58*, 1760–1772. https://doi.org/10.1139/cjfas-58-9-1760

Harrison, S., & Rousseau, M. (2020). Comparison of Artificial and Natural Reef Productivity in Nantucket Sound, MA, USA. *Estuaries and Coasts*, *43*(8), 2092–2105. https://doi.org/10.1007/s12237-020-00749-6

Henderson, M. E., Mills, K. E., Thomas, A. C., Pershing, A. J., & Nye, J. A. (2017). Effects of spring onset and summer duration on fish species distribution and biomass along the Northeast United States continental shelf. *Reviews in Fish Biology and Fisheries*, *27*(2), 411–424. https://doi.org/10.1007/s11160-017-9487-9

Hilborn, R., & Walters, C. J. (1992). *Quantitative fisheries stock assessment: Choice, dynamics and uncertainty*. Routledge, Chapman & Hall, Inc.

Hjellvik, V., Godø, O. R., & Tjøstheim, D. (2002). Diurnal variation in bottom trawl survey catches: Does it pay to adjust? *Canadian Journal of Fisheries and Aquatic Sciences*, *59*(1), 33–48. https://doi.org/10.1139/f01-193

Hyun, S.-Y., & Seo, Y. I. (2018). The systematic sampling for inferring the survey indices of Korean groundfish stocks. *Fisheries and Aquatic Sciences*, *21*(1), 24. https://doi.org/10.1186/s41240-018-0102-3

ICES. (2020). *Workshop on unavoidable survey effort reduction (WKUSER)* [Report]. ICES Scientific Reports. https://doi.org/10.17895/ices.pub.7453

ICES. (2023). *Workshop on Unavoidable Survey Effort Reduction 2 (WKUSER2)* [Report]. ICES Scientific Reports. https://doi.org/10.17895/ices.pub.22086845.v1

Inger, R., Attrill, M. J., Bearhop, S., Broderick, A. C., James Grecian, W., Hodgson, D. J., Mills, C., Sheehan, E., Votier, S. C., Witt, M. J., & Godley, B. J. (2009). Marine renewable energy: Potential benefits to biodiversity? An urgent call for research. *Journal of Applied Ecology*, *46*(6), 1145–1153. https://doi.org/10.1111/j.1365-2664.2009.01697.x

Johnson, K. F., Thorson, J. T., & Punt, A. E. (2019). Investigating the value of including depth during spatiotemporal index standardization. *Fisheries Research*, *216*, 126–137. https://doi.org/10.1016/j.fishres.2019.04.004

Kleisner, K. M., Fogarty, M. J., McGee, S., Hare, J. A., Moret, S., Perretti, C. T., & Saba, V. S. (2017). Marine species distribution shifts on the U.S. Northeast Continental Shelf under continued ocean warming. *Progress in Oceanography*, *153*, 24–36. https://doi.org/10.1016/j.pocean.2017.04.001

Kotwicki, S., Ianelli, J. N., & Punt, A. E. (2014). Correcting density-dependent effects in abundance estimates from bottom-trawl surveys. *ICES Journal of Marine Science*, *71*(5), 1107–1116. https://doi.org/10.1093/icesjms/fst208

Kotwicki, S., & Ono, K. (2019). The effect of random and density-dependent variation in sampling efficiency on variance of abundance estimates from fishery surveys. *Fish and Fisheries*, *20*(4), 760–774. https://doi.org/10.1111/faf.12375

Large, S. I., Fay, G., Friedland, K. D., & Link, J. S. (2013). Defining trends and thresholds in responses of ecological indicators to fishing and environmental pressures. *ICES Journal of Marine Science*, *70*(4), 755–767. https://doi.org/10.1093/icesjms/fst067

Lipsky, A., Moura, S., Kenney, A., & Bellavance, R. (2016). *Addressing Interactions between Fisheries and Offshore Wind Development: The Block Island Wind Farm*. MarXiv. https://doi.org/10.31230/osf.io/3jpxn

Liu, Y., Chen, Y., & Cheng, J. (2009). A comparative study of optimization methods and conventional methods for sampling design in fishery-independent surveys. *ICES Journal of Marine Science*, *66*(9), 1873–1882. https://doi.org/10.1093/icesjms/fsp157

Liu, Y., Chen, Y., Cheng, J., & Lu, J. (2011). An adaptive sampling method based on optimized sampling design for fishery-independent surveys with comparisons with conventional designs. *Fisheries Science*, *77*, 467–478. https://doi.org/10.1007/s12562-011-0355-6

Magnusson, A., Punt, A. E., & Hilborn, R. (2013). Measuring uncertainty in fisheries stock assessment: The delta method, bootstrap, and MCMC. *Fish and Fisheries*, *14*(3), 325–342. https://doi.org/10.1111/j.1467-2979.2012.00473.x

Maunder, M. N., & Punt, A. E. (2004). Standardizing catch and effort data: A review of recent approaches. *Fisheries Research*, *70*(2), 141–159. https://doi.org/10.1016/j.fishres.2004.08.002

Mavraki, N., Degraer, S., & Vanaverbeke, J. (2021). Offshore wind farms and the attraction–production hypothesis: Insights from a combination of stomach content and stable isotope analyses. *Hydrobiologia*, *848*(7), 1639–1657. https://doi.org/10.1007/s10750-021-04553-6

Mbaye, B., Doniol-Valcroze, T., Brosset, P., Castonguay, M., Van Beveren, E., Smith, A., Lehoux, C., Brickman, D., Wang, Z., & Plourde, S. (2020). Modelling Atlantic mackerel spawning habitat suitability and its future distribution in the north-west Atlantic. *Fisheries Oceanography*, *29*(1), 84–99. https://doi.org/10.1111/fog.12456

McMahan, M. D., Sherwood, G. D., & Grabowski, J. H. (2020). Geographic Variation in Life-History Traits of Black Sea Bass (Centropristis striata) During a Rapid Range Expansion.

Frontiers in Marine Science, *7*. https://www.frontiersin.org/articles/10.3389/fmars.2020.567758

McManus, M. C., Hare, J. A., Richardson, D. E., & Collie, J. S. (2018). Tracking shifts in Atlantic mackerel (Scomber scombrus) larval habitat suitability on the Northeast U.S. Continental Shelf. *Fisheries Oceanography*, *27*(1), 49–62. https://doi.org/10.1111/fog.12233

Methratta, E. T., Hawkins, A., Hooker, B. R., Lipsky, A., & Hare, J. A. (2020). Offshore Wind Development in the Northeast US Shelf Large Marine Ecosystem. *Oceanography*, *33*(4), 12.

Miller, T. J., Das, C., Politis, P. J., Miller, A. S., Lucey, S. M., Legault, C. M., Brown, R. W., & Rago, P. J. (2010). *Estimation of Albatross IV to Henry B. Bigelow calibration factors*. https://repository.library.noaa.gov/view/noaa/3726

NEFSC. (2019). *66th Northeast Regional Stock Assessment Workshop (66th SAW) Assessment Report* (Northeast Fish Sci Cent Ref Doc. 19-08; p. 1170). US Deptartment of Commerce. http://www.nefsc.noaa.gov/ publications/

NEFSC. (2021). *Draft 2021 Management Track Assessment Report: Northwest Atlantic mackerel*.

NEFSC. (2023a). *Draft 2023 Management Track Assessment Report: Summer flounder*.

Nichol, D. G., Kotwicki, S., Wilderbuer, T. K., Lauth, R. R., & Ianelli, J. N. (2019). Availability of yellowfin sole Limanda aspera to the eastern Bering Sea trawl survey and its effect on estimates of survey biomass. *Fisheries Research*, *211*, 319–330.

Nye, J., Link, J., Hare, J., & Overholtz, W. (2009). Changing spatial distribution of fish stocks in relation to climate and population size on the Northeast United States continental shelf. *Marine Ecology Progress Series*, *393*, 111–129. https://doi.org/10.3354/meps08220

Overholtz, W. J., Hare, J. A., & Keith, C. M. (2011). Impacts of Interannual Environmental Forcing and Climate Change on the Distribution of Atlantic Mackerel on the U.S. Northeast Continental Shelf. *Marine and Coastal Fisheries*, *3*(1), 219–232. https://doi.org/10.1080/19425120.2011.578485

Oyafuso, Z. S., Barnett, L. A. K., Siple, M. C., Cooper, D. W., & Kotwicki, S. (2023). Evaluating potential changes to the US Chukchi Sea bottom trawl survey design via simulation testing. *Frontiers in Marine Science*, *10*. https://www.frontiersin.org/articles/10.3389/fmars.2023.1214526

Oyafuso, Z. S., Barnett, L. A., & Kotwicki, S. (2021). Incorporating spatiotemporal variability in multispecies survey design optimization addresses trade-offs in uncertainty. *ICES Journal of Marine Science*, *78*(4), 1288–1300.

Pauly, D., Hilborn, R., & Branch, T. A. (2013). Fisheries: Does catch reflect abundance? *Nature*, *494*(7437), Article 7437. https://doi.org/10.1038/494303a

Pennington, M., & Strømme, T. (1998). Surveys as a research tool for managing dynamic stocks. *Fisheries Research*, *37*(1), 97–106. https://doi.org/10.1016/S0165-7836(98)00129-5

Perretti, C. T., & Thorson, J. T. (2019). Spatio-temporal dynamics of summer flounder (Paralichthys dentatus) on the Northeast US shelf. *Fisheries Research*, *215*, 62–68. https://doi.org/10.1016/j.fishres.2019.03.006

Politis, P. J., Galbraith, J. K., Kostovick, P., & Brown, R. W. (2014). *Northeast Fisheries Science Center bottom trawl survey protocols for the NOAA Ship Henry B. Bigelow.* https://doi.org/10.7289/V5C53HVS

Rago, P. J. (2005). 12. Fishery independent sampling: Survey techniques and data analyses. *Management Techniques for Elasmobranch Fisheries*, 201.

Reubens, J. T., Braeckman, U., Vanaverbeke, J., Van Colen, C., Degraer, S., & Vincx, M. (2013). Aggregation at windmill artificial reefs: CPUE of Atlantic cod (Gadus morhua) and pouting (Trisopterus luscus) at different habitats in the Belgian part of the North Sea. *Fisheries Research*, *139*, 28–34. https://doi.org/10.1016/j.fishres.2012.10.011

Reubens, J. T., Vandendriessche, S., Zenner, A. N., Degraer, S., & Vincx, M. (2013). Offshore wind farms as productive sites or ecological traps for gadoid fishes? – Impact on growth, condition index and diet composition. *Marine Environmental Research*, *90*, 66–74. https://doi.org/10.1016/j.marenvres.2013.05.013

Rhodes, J. R., & Jonzén, N. (2011). Monitoring temporal trends in spatially structured populations: How should sampling effort be allocated between space and time? *Ecography*, *34*(6), 1040–1048.

Schupp, M. F., Kafas, A., Buck, B. H., Krause, G., Onyango, V., Stelzenmüller, V., Davies, I., & Scott, B. E. (2021). Fishing within offshore wind farms in the North Sea: Stakeholder perspectives for multi-use from Scotland and Germany. *Journal of Environmental Management*, *279*, 111762. https://doi.org/10.1016/j.jenvman.2020.111762

Simmonds, E. (1996). Which are better, random or systematic acoustic surveys? A simulation using North Sea herring as an example. *ICES Journal of Marine Science*, *53*(1), 39–50. https://doi.org/10.1006/jmsc.1996.0004

Sosebee, K. A., & Cadrin, S. X. (2006). *A historical perspective on the abundance and biomass of northeast demersal complex stocks from NMFS and Massachusetts inshore bottom trawl surveys, 1963-2002*.

Thorson, J. T. (2018). Three problems with the conventional delta-model for biomass sampling data, and a computationally efficient alternative. *Canadian Journal of Fisheries and Aquatic Sciences*, *75*(9), 1369–1382. https://doi.org/10.1139/cjfas-2017-0266

Thorson, J. T., & Barnett, L. A. K. (2017). Comparing estimates of abundance trends and distribution shifts using single- and multispecies models of fishes and biogenic habitat. *ICES Journal of Marine Science*, *74*(5), 1311–1321. https://doi.org/10.1093/icesjms/fsw193

Thorson, J. T., & Ward, E. J. (2014). Accounting for vessel effects when standardizing catch rates from cooperative surveys. *Fisheries Research*, *155*, 168–176. https://doi.org/10.1016/j.fishres.2014.02.036

Von Szalay, P. G., Kotwicki, S., Barnett, L. A. K., Rugolo, L. J., & Ono, K. (2023). Reducing uncertainty in survey abundance estimates by considering alternative designs and estimators: A case study with 3 species in the Gulf of Alaska. *Fishery Bulletin*, *121*(1–2), 50–66. https://doi.org/10.7755/FB.121.1-2.5

von Szalay, P. G., & Somerton, D. A. (2005). The effect of net spread on the capture efficiency of a demersal survey trawl used in the eastern Bering Sea. *Fisheries Research*, *74*(1–3), 86–95. https://doi.org/10.1016/j.fishres.2005.04.007

Ward, E. J., Barnett, L. A. K., Anderson, S. C., Commander, C. J. C., & Essington, T. E. (2022). Incorporating non-stationary spatial variability into dynamic species distribution models. *ICES Journal of Marine Science*, *79*(9), 2422–2429. https://doi.org/10.1093/icesjms/fsac179

Wilber, D., Brown, L., Griffin, M., DeCelles, G., & Carey, D. (2022). Offshore wind farm effects on flounder and gadid dietary habits and condition on the northeastern US coast. *Marine Ecology Progress Series*, *683*, 123–138. https://doi.org/10.3354/meps13957

Xu, B., Chongliang, Z., Xue, Y., Ren, Y., & Chen, Y. (2015). Optimization of sampling effort for a fishery-independent survey with multiple goals. *Environmental Monitoring and Assessment*, *187*, 4483. https://doi.org/10.1007/s10661-015-4483-9

Yalcin, S., Anderson, S. C., Regular, P. M., & English, P. A. (2023). Exploring the limits of spatiotemporal and design-based index standardization under reduced survey coverage. *ICES Journal of Marine Science*, fsad155. https://doi.org/10.1093/icesjms/fsad155

Yu, H., Jiao, Y., Su, Z., & Reid, K. (2012). Performance comparison of traditional sampling designs and adaptive sampling designs for fishery-independent surveys: A simulation study. *Fisheries Research*, *113*(1), 173–181. https://doi.org/10.1016/j.fishres.2011.10.009

Zhao, J., Cao, J., Tian, S., Chen, Y., & Zhang, S. (2018). Evaluating Sampling Designs for Demersal Fish Communities. *Sustainability*, *10*(8), Article 8. https://doi.org/10.3390/su10082585

Zimmermann, F., & Enberg, K. (2017). Can less be more? Effects of reduced frequency of surveys and stock assessments. *ICES Journal of Marine Science*, *74*(1), 56–68. https://doi.org/10.1093/icesjms/fsw134

Zuur, A. F., Ieno, E. N., & Smith, G. M. (2007). *Analysing ecological data* (Vol. 680). Springer.

TABLES

Table 1. Number of species by criteria

Criteria	**Total number of species**	**Number in the fall**	**Number in the spring**
1	Occurs in 3 or more strata within a given year		
	278	255	201
2	Observed in 3 or more strata for at least 3 years		
	199	189	151
3	Observed in at least one strata that is proposed for overlap by offshore wind		
	164	149	113

Table 2. Summary of performance metrics comparing the differences between survey effort scenarios. For each criteria species the following information is given: the mean absolute relative differences between abundance indices; the average coefficients of variation for each scenario (status quo and wind-precluded) and the mean absolute relative difference between the two scenarios; and the trend estimate under status quo survey effort and the mean absolute difference between the two survey effort scenarios. The species with the greatest differences between status quo and preclusion based on the quantiles of the distribution are highlighted in green (darker green = upper quantile, light green = lower quantile).

	Abundance Indices	*CV*			*Trend Estimates*	
	Mean Absolute Relative Difference	With Wind Included	With Wind Precluded	**Mean Absolute Relative Difference**	With Wind Included	**Mean Absolute Difference**
Fall						
All skates	4.07%	0.19	0.20	15.29%	-3.24	5.33×10^{-1}
Atlantic croaker	13.05%	0.44	0.47	9.06%	-7.76×10^{-1}	4.47×10^{-1}
Black sea bass	22.77%	0.34	0.31	20.01%	1.89×10^{-1}	8.71×10^{-2}
Bluntnose stingray	29.85%	0.71	0.66	11.65%	1.65	5.20×10^{-1}
Bullnose ray	32.48%	0.45	0.49	11.69%	-6.18×10^{-1}	1.57
Coarsehand lady crab	15.39%	0.39	0.45	17.65%	4.01×10^{-2}	2.56×10^{-3}
Horseshoe crab	35.63%	0.46	0.48	15.56%	1.12	2.96×10^{-1}
Little skate	6.40%	0.17	0.17	20.14%	-1.45	2.29×10^{-1}

cont. on next page

Table 2 cont.

	Abundance Indices	*CV*			*Trend Estimates*	
	Mean Absolute Relative Difference	With Wind Included	With Wind Precluded	**Mean Absolute Relative Difference**	With Wind Included	**Mean Absolute Difference**
Fall						
Northern searobin	28.65%	0.28	0.26	13.33%	1.25	1.04×10^{-1}
Rough scad	31.15%	0.46	0.50	6.87%	-1.34×10^{-1}	1.73×10^{-3}
Roughtail stingray	57.99%	0.59	0.70	39.85%	1.28	9.44×10^{-1}
Round herring	15.54%	0.59	0.63	6.45%	-7.93×10^{-1}	3.23×10^{-1}
Scup	9.15%	0.30	0.39	36.45%	1.36×10^{-1}	7.36×10^{-2}
Sea scallop	12.19%	0.33	0.35	8.43%	-3.56×10^{-1}	4.38×10^{-1}
Shrimp (pink,brown,white)	23.69%	0.65	0.65	1.22%	-4.86×10^{-2}	3.22×10^{-2}
Smallmouth flounder	28.87%	0.70	0.69	19.79%	-3.55×10^{-3}	2.61×10^{-3}
Spider crab uncl	11.43%	0.42	0.51	22.93%	-4.96×10^{-4}	6.31×10^{-4}
Spiny butterfly ray	35.06%	0.45	0.55	25.13%	2.40×10^{-1}	1.08×10^{-1}
Spiny dogfish	0.97%	0.29	0.31	3.59%	-1.09×10^{-1}	6.85×10^{-1}

cont. on next page

Table 2 cont.

	Abundance Indices	*CV*			*Trend Estimates*	
	Mean Absolute Relative Difference	With Wind Included	With Wind Precluded	**Mean Absolute Relative Difference**	With Wind Included	**Mean Absolute Difference**
Fall						
Spotted hake	15.20%	0.20	0.24	18.81%	5.89×10^{-2}	3.05×10^{-2}
Windowpane	10.36%	0.20	0.24	19.74%	-9.14×10^{-2}	5.38×10^{-3}
Yellowtail flounder	0.46%	0.29	0.29	0.50%	-1.16	2.56×10^{-1}
Spring						
All skates	2.74%	0.13	0.14	5.67%	-2.94	5.57×10^{-2}
Atlantic herring	5.30%	0.31	0.31	1.21%	-1.45	2.84×10^{-1}
Atlantic mackerel	8.58%	0.45	0.45	2.89%	-1.02×10^{-1}	9.69×10^{-2}
Atlantic seasnail	25.26%	0.60	0.62	3.18%	-1.30×10^{-4}	4.29×10^{-5}
Atlantic silverside	34.05%	0.46	0.46	18.62%	-4.57×10^{-4}	4.11×10^{-5}
Atlantic surfclam	18.62%	0.85	0.92	12.88%	-3.18×10^{-3}	1.32×10^{-5}
Bluefish	20.24%	0.64	0.74	15.98%	-6.03×10^{-3}	3.33×10^{-3}
Bobtail uncl	18.58%	0.25	0.30	19.15%	-9.89×10^{-4}	2.04×10^{-5}
Butterfish	6.36%	0.32	0.30	4.62%	3.40×10^{-1}	5.59×10^{-2}

cont. on next page

Table 2 cont.

	Abundance Indices	*CV*			*Trend Estimates*	
	Mean Absolute Relative Difference	With Wind Included	With Wind Precluded	**Mean Absolute Relative Difference**	With Wind Included	**Mean Absolute Difference**
Spring						
Clearnose skate	13.46%	0.17	0.18	23.78%	-6.99×10^{-1}	1.51×10^{-1}
Coarsehand lady crab	19.19%	0.36	0.43	17.86%	2.30×10^{-3}	2.75×10^{-4}
Etropus uncl	5.71%	0.23	0.24	21.96%	9.06×10^{-5}	3.67×10^{-4}
Horseshoe crab	9.49%	0.23	0.29	30.17%	1.28×10^{-1}	3.25×10^{-2}
Lady crab	23.99%	0.42	0.52	25.38%	3.89×10^{-3}	1.14×10^{-3}
Little skate	7.58%	0.13	0.14	10.45%	-2.02	4.76×10^{-2}
Smallmouth flounder	50.31%	0.59	0.67	20.45%	-3.86×10^{-3}	4.16×10^{-4}
Smooth dogfish	21.19%	0.52	0.57	12.53%	5.80	3.27
Spider crab uncl	28.42%	0.74	0.77	12.13%	-2.66×10^{-4}	6.46×10^{-5}
Spiny dogfish	4.89%	0.16	0.17	9.86%	-6.65	1.99
Striped bass	37.59%	0.67	0.74	14.65%	-2.26	8.38 × 10^-1

Table 3. Summary of performance metrics comparing the differences between survey effort scenarios. For each stakeholder-identified species the following information is given: the mean absolute relative differences between abundance indices; the average coefficients of variation for each scenario (status quo and wind-precluded) and the mean absolute relative difference between the two scenarios; and the trend estimate under status quo survey effort and the mean absolute difference between the two survey effort scenarios.

	Abundance Indices	*CV*			*Trend Estimates*	
	Mean Absolute Relative Difference	Status quo survey effort	Wind-precluded survey effort	**Mean Absolute Relative Difference**	Status quo survey effort	**Mean Absolute Difference**
Fall						
All skates	2.63%	0.19	0.20	15.29%	-3.24	0.53
Atlantic herring	0.07%	0.33	0.33	0.06%	-0.63	0.00
Atlantic mackerel	0.00%	0.55	0.55	0.00%	4.00	0.00
Black sea bass	20.94%	0.34	0.31	20.01%	0.19	0.09
Butterfish	4.97%	0.25	0.25	3.29%	0.06	0.06
Longfin squid	0.84%	0.09	0.10	13.04%	0.53	0.00
Silver hake	1.80%	0.12	0.12	0.36%	1.61	0.05
Spiny dogfish	1.34%	0.29	0.31	3.59%	-10.85	0.68
Summer flounder	15.44%	0.19	0.22	15.89%	-0.20	0.06

cont. on next page

Table 3 cont.

	Abundance Indices	*CV*			*Trend Estimates*	
	Mean Absolute Relative Difference	Status quo survey effort	Wind-precluded survey effort	**Mean Absolute Relative Difference**	Status quo survey effort	**Mean Absolute Difference**
Fall						
Winter flounder	1.43%	0.25	0.25	1.50%	-0.64	0.04
Yellowtail flounder	0.46%	0.29	0.29	0.50%	-1.16	0.26
Spring						
All skates	2.74%	0.13	0.14	5.67%	-2.94	0.06
Atlantic herring	5.30%	0.31	0.31	1.21%	-1.45	0.28
Atlantic mackerel	8.58%	0.45	0.45	2.89%	-0.10	0.10
Black sea bass	3.66%	0.53	0.54	2.98%	0.34	0.03
Butterfish	6.36%	0.32	0.30	4.62%	0.34	0.06
Longfin squid	6.94%	0.17	0.17	1.37%	0.20	0.01
Silver hake	0.21%	0.11	0.11	0.18%	1.22	0.02
Spiny dogfish	4.89%	0.16	0.17	9.86%	-6.65	1.99
Summer flounder	2.42%	0.17	0.18	5.84%	-0.06	0.01
Winter flounder	2.91%	0.26	0.26	1.96%	-0.15	0.03
Yellowtail flounder	0.07%	0.25	0.25	0.05%	-0.69	0.01

Table 4. Estimates of population trends, and their respective lower and upper confidence intervals (CI), under each survey effort scenario for fall and spring summer flounder populations and spring populations for Atlantic mackerel.

	Fall			*Spring*		
	Estimate	**Lower CI**	**Upper CI**	**Estimate**	**Lower CI**	**Upper CI**
Summer flounder						
With Wind Included	-0.15	-0.26	-0.04	-0.05	-0.16	0.07
With Wind Precluded	-0.10	-0.19	-0.02	-0.04	-0.15	0.08
Atlantic mackerel						
With Wind Included	---	---	---	-0.04	-0.69	0.61
With Wind Precluded	---	---	---	0.01	-0.65	0.67

Table 5. Summary of performance metrics comparing the differences between survey effort scenarios. For summer flounder and Atlantic mackerel, the following information is given: the mean absolute relative differences between abundance indices; the average coefficients of variation for each scenario (status quo and wind-precluded) and the mean absolute relative difference between the two scenarios; and the trend estimate under status quo survey effort and the mean absolute difference between the two survey effort scenarios.

	Annual Abundance Indices	*CV*			*Trend Estimates*	
	Mean Absolute Relative Difference	Status quo survey effort	Wind-precluded survey effort	**Mean Absolute Relative Difference**	Status quo survey effort	**Mean Absolute Difference**
Fall						
Summer flounder	14%	0.188	0.211	15%	-0.147	0.045
Spring						
Summer flounder	4%	0.164	0.173	6%	-0.048	0.008
Atlantic mackerel	7%	0.428	0.433	2%	-0.041	0.052

Table 6. Configurations used to fit fall and spring models predicting summer flounder biomass catch rates.

Models	Predictors	Spatial	Spatiotemporal	Time	Family
m1	Depth (spline) Year	Off	Off	-	Tweedie
m2	Depth (second-order polynomial) Year	Off	Off	-	Tweedie
m3	Depth (spline) Year Area	Off	Off	-	Tweedie
m4	Depth (second-order polynomial) Year Area	Off	Off	-	Tweedie
m5	Depth (spline) Year	On	Off	-	Tweedie
m6	Depth (second-order polynomial) Year	On	Off	-	Tweedie
m7	Depth (spline) Year Area	On	Off	-	Tweedie
m8	Depth (second-order polynomial) Year Area	On	Off	-	Tweedie
m9	Depth (spline) Year	On	IID	Year	Tweedie
m10	Depth (second-order polynomial) Year	On	IID	Year	Tweedie

cont. on next page

Table 6 cont.

Models	Predictors	Spatial	Spatiotemporal	Time	Family
m11	Depth (spline) Year Area	On	IID	Year	Tweedie
m12	Depth (second-order polynomial) Year Area	On	IID	Year	Tweedie

Table 7. Diagnostic quantities for the fall and spring models fit for summer flounder. For each of the models, the following information is given: Akaike's Information Criterion (AIC), percent deviance explained, the total log-likelihood, the mean squared error across the folds of each cross-validation, and the model convergence. The optimal model in each season is highlighted in red.

Models	**AIC**	**Deviance Explained**	**Sum log likelihood**	**Mean Squared Error**	**Convergence**
Fall					
m1	7,442.52	94.48%	-3,748.01	56.31	True
m2	7,446.88	94.53%	-3,770.55	56.93	True
m3	7,424.88	94.23%	-3,733.14	55.83	True
m4	7,425.62	94.24%	-3,737.39	55.38	True
m5	6,330.89	80.26%	-3,299.06	38.33	True
m6	6,323.95	80.17%	-3,277.81	38.55	True
m7	6,330.41	80.23%	-3,272.14	39.92	True
m8	6,323.60	80.14%	-3,294.04	40.33	True
m9	6,193.75	78.48%	-4,172.68	67.44	True
m10	6,187.25	78.40%	-4,188.35	56.84	True
m11	6,195.49	78.48%	-4,141.33	55.67	True
m12	6,189.04	78.40%	-4,116.86	54.56	True

cont. on next page

Table 7 cont.

Models	AIC	Deviance Explained	Sum log likelihood	Mean Squared Error	Convergence
Spring					
m1	9,186.74	92.27%	-4,601.46	47.07	True
m2	9,190.69	92.31%	-4,604.67	45.22	True
m3	9,184.48	92.23%	-4,593.76	46.14	True
m4	9,187.94	92.26%	-4,606.39	45.84	True
m5	8,672.89	87.05%	-4,327.68	39.80	True
m6	8,666.36	86.98%	-4,342.23	39.28	True
m7	8,672.28	87.02%	-4,320.11	37.75	True
m8	8,665.47	86.95%	-4,346.33	40.85	False
m9	8,420.82	84.49%	-4,635.97	44.44	True
m10	8,409.22	84.37%	-4,636.02	44.06	True
m11	8,419.56	84.46%	-4,794.72	45.81	True
m12	8,407.41	84.33%	-4,666.95	45.28	True

Table 8. Main and random effect parameter estimates, and the respective standard error, from the chosen optimal fall model (m10) and spring model (m12) for summer flounder.

	Fall		*Spring*	
Term	**Estimate**	**Standard Error**	**Estimate**	**Standard Error**
Main effect parameters				
Depth	-52.50	9.63	5.22	5.02
Depth	-30.76	5.33	-41.72	3.99
Year: 2009	-1.27	0.51	-1.02	0.48
Year: 2010	-1.69	0.51	-1.15	0.48
Year: 2011	-1.65	0.52	-0.92	0.48
Year: 2012	-1.34	0.50	-0.53	0.47
Year: 2013	-1.79	0.52	-0.68	0.47
Year: 2014	-1.27	0.51	-0.89	0.50
Year: 2015	-2.08	0.53	-1.17	0.48
Year: 2016	-1.80	0.51	-0.36	0.46
Year: 2017	-	-	-1.06	0.47
Year: 2018	-1.96	0.52	-0.99	0.48
Year: 2019	-1.83	0.51	-0.88	0.47
Year: 2021	-2.04	0.51	-1.13	0.50
Area: Wind	-	-	0.31	0.16
Random effect parameters				
Range	94.47	11.53	111.54	16.50
Phi	1.54	0.08	1.72	0.08
Spatial standard deviation (ω)	1.75	0.17	1.34	0.16
Spatiotemporal standard deviation (ϵ)	1.04	0.09	1.02	0.07
Tweedie power parameter	1.34	0.01	1.40	0.01

Table 9. The nominal mean biomass catch rate generated by the optimal seasonal models in each year, and the quantile of the distribution that corresponds to the observed average biomass catch rate in each year for summer flounder. The average biomass catch rate across years generated in each season and the quantile of the distribution that corresponds to the observed average biomass catch rate across years for summer flounder is provided at the bottom of the table.

	Fall		*Spring*	
Year	**Average Biomass (kg/tow)**	**Quantile**	**Average Biomass (kg/tow)**	**Quantile**
2009	3.19	0.42	2.79	0.63
2010	2.36	0.04	4.03	0.78
2011	4.39	0.75	4.26	0.38
2012	3.67	0.07	3.21	0.19
2013	3.61	0.14	3.51	0.53
2014	3.35	0.33	3.42	0.77
2015	3.56	0.05	3.12	0.93
2016	2.55	0.02	2.36	0.04
2017	---	---	2.17	0.15
2018	2.22	0.31	2.99	0.48
2019	2.19	0.86	3.29	0.10
2021	1.88	0.64	2.64	0.00
Overall	3.00	0.01	3.16	0.10

Table 10. The proportion of zeroes generated by the optimal seasonal models in each year, and the quantile of the distribution that corresponds to the observed proportion of zeroes in each year for summer flounder. The overall proportion of zeroes generated in each season and the quantile of the distribution that corresponds to the overall proportion of zeroes for summer flounder is provided at the bottom of the table.

	Fall		*Spring*	
Year	**Average Proportion of Zeroes**	**Quantile**	**Average Proportion of Zeroes**	**Quantile**
2009	0.48	0.56	0.42	0.51
2010	0.49	0.51	0.44	0.84
2011	0.49	0.47	0.45	0.91
2012	0.45	0.83	0.36	0.80
2013	0.56	1.00	0.38	0.72
2014	0.47	0.91	0.40	0.84
2015	0.57	0.76	0.44	0.41
2016	0.52	0.48	0.35	0.81
2017	---	---	0.41	0.41
2018	0.55	0.68	0.42	0.48
2019	0.47	0.06	0.37	0.32
2021	0.58	0.97	0.43	1.00
Overall	0.51	0.95	0.41	0.96

Table 11. The annual stratified mean biomass generated by the optimal seasonal models in each year, and the quantile of the distribution that corresponds to the observed annual abundance index for summer flounder.

Year	*Status quo survey effort*		*Wind-precluded survey effort*	
	Stratified Mean (kg/tow)	**Quantile**	**Stratified Mean (kg/tow)**	**Quantile**
Fall				
2009	3.53	0.88	2.59	0.55
2010	2.25	0.11	2.11	0.22
2011	4.22	0.73	3.05	0.50
2012	3.06	0.12	3.05	0.18
2013	2.66	0.24	1.92	0.12
2014	3.38	0.39	3.15	0.34
2015	2.55	0.35	2.17	0.21
2016	2.96	0.07	2.00	0.04
2017	---	---	---	---
2018	1.95	0.16	1.77	0.42
2019	1.69	0.59	1.59	0.51
2021	1.78	0.90	1.60	0.79
Spring				
2009	3.05	0.54	3.25	0.79
2010	3.96	0.64	3.85	0.56
2011	4.08	0.11	3.71	0.09
2012	4.33	0.31	4.49	0.40
2013	3.79	0.38	3.91	0.41
2014	3.23	0.34	3.28	0.37
2015	3.96	0.98	3.57	0.91
2016	2.85	0.10	2.99	0.22
2017	2.18	0.12	2.21	0.12
2018	4.07	0.78	4.42	0.81
2019	3.78	0.18	3.69	0.22
2021	3.11	0.03	3.17	0.08

Table 12. The estimates of population trend generated by the optimal seasonal models, and the quantile of the distribution that corresponds to the observed estimate of population trend for summer flounder.

	Fall		*Spring*	
	Population Trend Estimate	**Quantile**	**Population Trend Estimate**	**Quantile**
Status quo survey effort	-0.15	0.50	-0.05	0.19
Wind-precluded survey effort	-0.10	0.73	-0.04	0.21

Table 13. Configurations used to fit spring models predicting Atlantic mackerel biomass catch rates.

Models	Predictors	Family	Spatial	Spatiotemporal	Time	Shared range
Delta gamma						
m1	Depth (fourth-order polynomial) Year	Binomial (*Component 1*)	On	IID	Year	Yes
		Gamma (*Component 2*)	On	IID	Year	Yes
m2	Depth (fourth-order polynomial) Year	Binomial (*Component 1*)	On	IID	Year	No
		Gamma (*Component 2*)	On	IID	Year	No
m3	Depth (fourth-order polynomial) Year	Binomial (*Component 1*)	On	IID	Year	Yes
		Gamma (*Component 2*)	On	IID	Year	No
m4	Depth (fourth-order polynomial) Year	Binomial (*Component 1*)	On	IID	Year	No
		Gamma (*Component 2*)	On	IID	Year	Yes
m5	Depth (fourth-order polynomial) Year	Binomial (*Component 1*)	On	IID	Year	No
		Gamma (*Component 2*)	-	IID	Year	-

cont. on next page

Table 13 cont.

Models	Predictors	Family	Spatial	Spatiotemporal	Time	Shared range
Tweedie						
m6	Depth (fourth-order polynomial) Year	Tweedie	On	IID	Year	Yes
m7	Depth (fourth-order polynomial) Year	Tweedie	On	IID	Year	No

Table 14. Diagnostic quantities for the final set of spring models fit for Atlantic mackerel. For each model, the following information is given: Akaike's Information Criterion (AIC), percent deviance explained, the total log-likelihood, the mean squared error across the folds of each cross-validation, the model convergence and the cross-validation convergence. The optimal model is highlighted in red.

Models	AIC	Deviance Explained	Sum log likelihood	Mean Squared Error	Model Convergence	Cross Validation Convergence
Delta Gamma						
m1	8,802.19	82.31%	-8,286.17	2,330.05	True	True
m2	8,803.62	82.29%	-8,690.88	2,311.10	False	False
m3	8,804.19	82.31%	-8,441.83	2,310.69	False	False
m4	8,801.62	82.29%	-8,092.74	2,324.47	True	True
m5	8,799.62	82.29%	-8,305.95	2,216.04	True	True
Tweedie						
m6	8,930.46	83.28%	-11,711.63	2,501.87	True	True
m7	8,912.83	83.10%	-	-	True	-

Table 15. Main and random effect parameter estimates, and their respective standard errors, for each of the model components (binomial and gamma) of the chosen optimal spring model (m5) for Atlantic mackerel.

	Binomial Component		*Gamma Component*	
Term	**Estimate**	**Standard Error**	**Estimate**	**Standard Error**
Main effect parameters				
Depth	-4.13	6.68	-15.01	4.16
Depth	-7.24	4.55	-16.39	4.02
Depth	8.32	3.62	5.03	3.69
Depth	-8.70	3.00	6.34	3.43
Year: 2009	-2.08	0.54	-0.39	0.30
Year: 2010	-1.98	0.53	-0.18	0.26
Year: 2011	-2.14	0.54	0.23	0.28
Year: 2012	-1.55	0.53	-0.30	0.26
Year: 2013	-1.44	0.52	-0.17	0.23
Year: 2014	-2.33	0.55	-0.14	0.28
Year: 2015	-2.06	0.53	-0.01	0.26
Year: 2016	-1.35	0.52	-0.10	0.23
Year: 2017	-2.01	0.53	0.27	0.26
Year: 2018	-1.75	0.54	0.06	0.28
Year: 2019	-1.66	0.53	-0.34	0.25
Year: 2021	-2.18	0.54	0.03	0.27
Random effect parameters				
Spatial range	161.20	46.01	-	-
Spatiotemporal range	99.71	11.89	27.37	5.71
Spatial standard deviation (ω)	1.44	0.26	-	-
Spatiotemporal standard deviation (ϵ)	1.48	0.10	2.10	0.26
Dispersion	-	-	0.83	0.04

Table 16. The nominal mean biomass catch rate generated by the optimal spring model in each year, and the quantile of the distribution that corresponds to the observed average biomass catch rate in each year for Atlantic mackerel. The overall average biomass catch rate across years generated by the spring model and the quantile of the distribution that corresponds to the observed average catch rate across years for Atlantic mackerel is provided at the bottom of the table.

Year	Average Biomass (kg/tow)	Quantile
2009	6.58	0.01
2010	4.79	0.00
2011	5.34	0.09
2012	4.34	0.26
2013	5.41	0.02
2014	0.58	0.00
2015	10.49	0.03
2016	2.58	0.09
2017	6.82	0.01
2018	2.18	0.06
2019	4.08	0.30
2021	5.76	0.00
Overall	5.06	0.00

Table 17. The average proportion of zeroes generated by the optimal spring model in each year, and the quantile of the distribution that corresponds to the observed proportion of zero in each year for Atlantic mackerel. The average proportion of zeroes across years generated by the spring model and the quantile of the distribution that corresponds to that observed average proportion of zeroes across years for Atlantic mackerel is provided at the bottom of the table.

Year	Average Proportion of Zeroes	Quantile
2009	0.70	1.00
2010	0.69	1.00
2011	0.71	1.00
2012	0.61	1.00
2013	0.60	1.00
2014	0.76	1.00
2015	0.71	1.00
2016	0.57	0.99
2017	0.67	1.00
2018	0.68	1.00
2019	0.62	1.00
2021	0.71	1.00
Overall	0.67	1.00

Table 18. The annual stratified mean biomass generated by the optimal spring model in each year and each survey effort, and the quantile of the distribution that corresponds to the observed annual abundance index under the respective survey effort for Atlantic mackerel.

	Status Quo Survey Effort		*Wind-Precluded Survey Effort*	
Year	**Stratified Mean (kg/tow)**	**Quantile**	**Stratified Mean (kg/tow)**	**Quantile**
2009	9.50	0.50	9.80	0.57
2010	4.38	0.00	3.37	0.00
2011	6.88	0.48	5.88	0.23
2012	3.31	0.06	3.32	0.08
2013	2.82	0.00	2.70	0.00
2014	0.62	0.01	0.65	0.01
2015	16.68	0.72	16.90	0.77
2016	3.51	0.67	4.03	0.86
2017	9.59	0.21	8.08	0.06
2018	3.72	0.64	4.11	0.76
2019	4.41	0.39	4.36	0.40
2021	7.76	0.11	8.60	0.23

Table 19. The estimates of population trend generated by the optimal seasonal models, and the quantile of the distribution that corresponds to the observed estimate of population trend for Atlantic mackerel.

	Population Trend Estimate	Quantile
Status quo survey effort	0.04	0.65
Wind-precluded survey effort	0.10	0.80

FIGURES

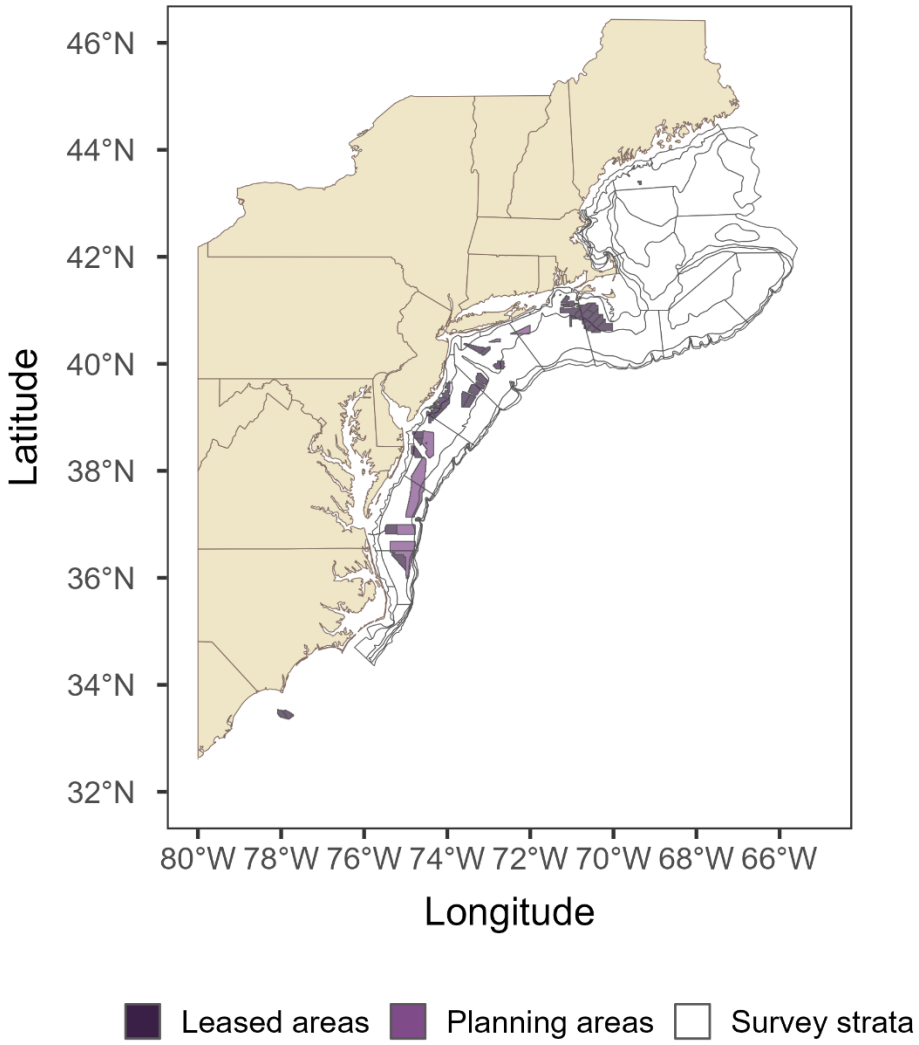

Figure 1. A map of the actively sampled NEFSC bottom trawl survey strata (white polygons) overlapped by leased wind areas (dark purple), and the planned wind areas (purple).

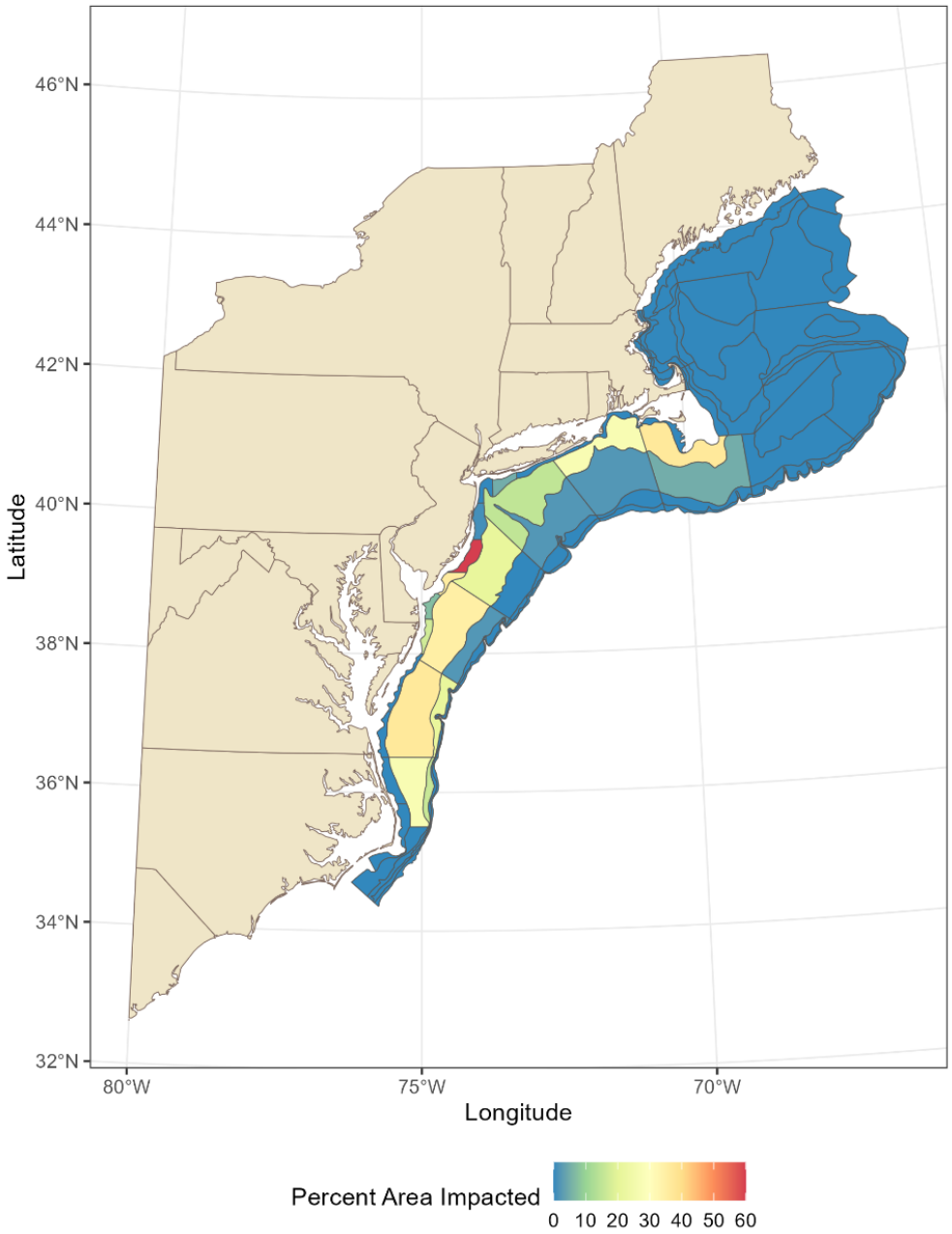

Figure 2. A map of the actively sampled NEFSC bottom trawl survey strata and the percentage of area impacted and subject to survey preclusion by offshore wind area overlap.

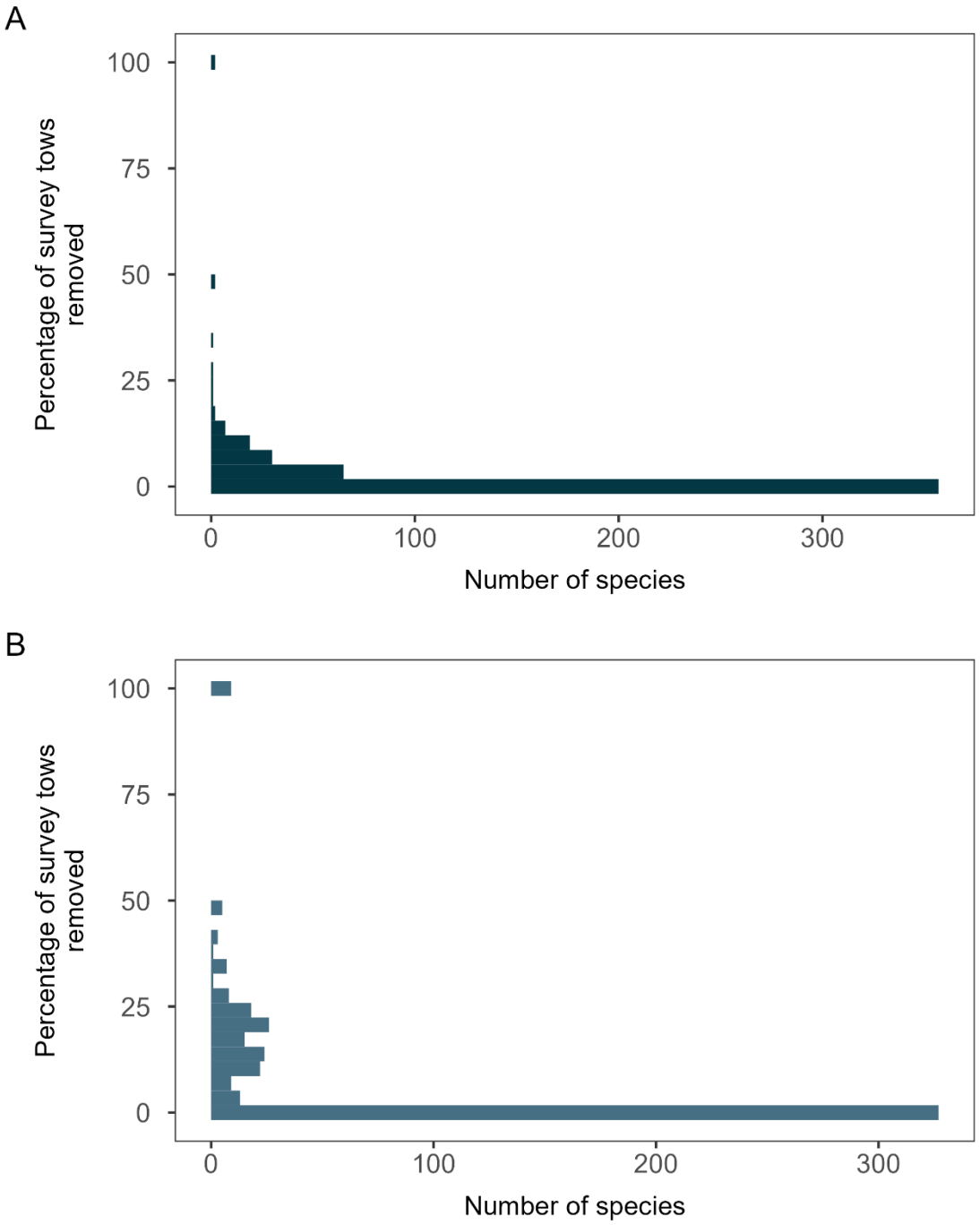

Figure 3. The percentage of (A) tows conducted in strata proposed for overlap by wind and (B) tows conducted over the full survey area that would be removed from positive survey observations due to wind-precluded effort.

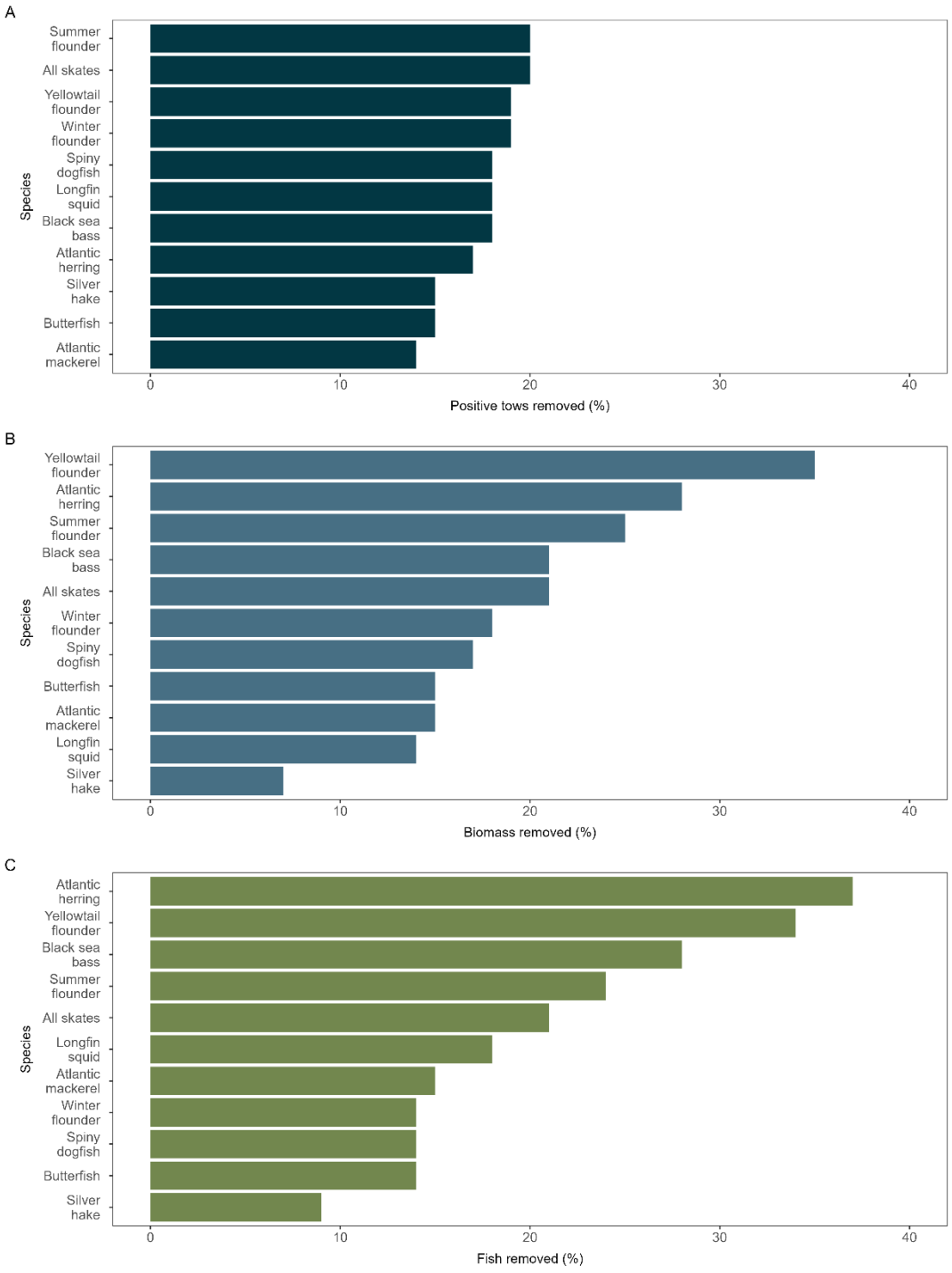

Figure 4. The percentage of (A) tows, (B) total biomass, and (C) total number of fish observed in strata that are proposed for overlap by wind that would be removed from positive survey observations due to wind-precluded effort for a set of stakeholder-identified species.

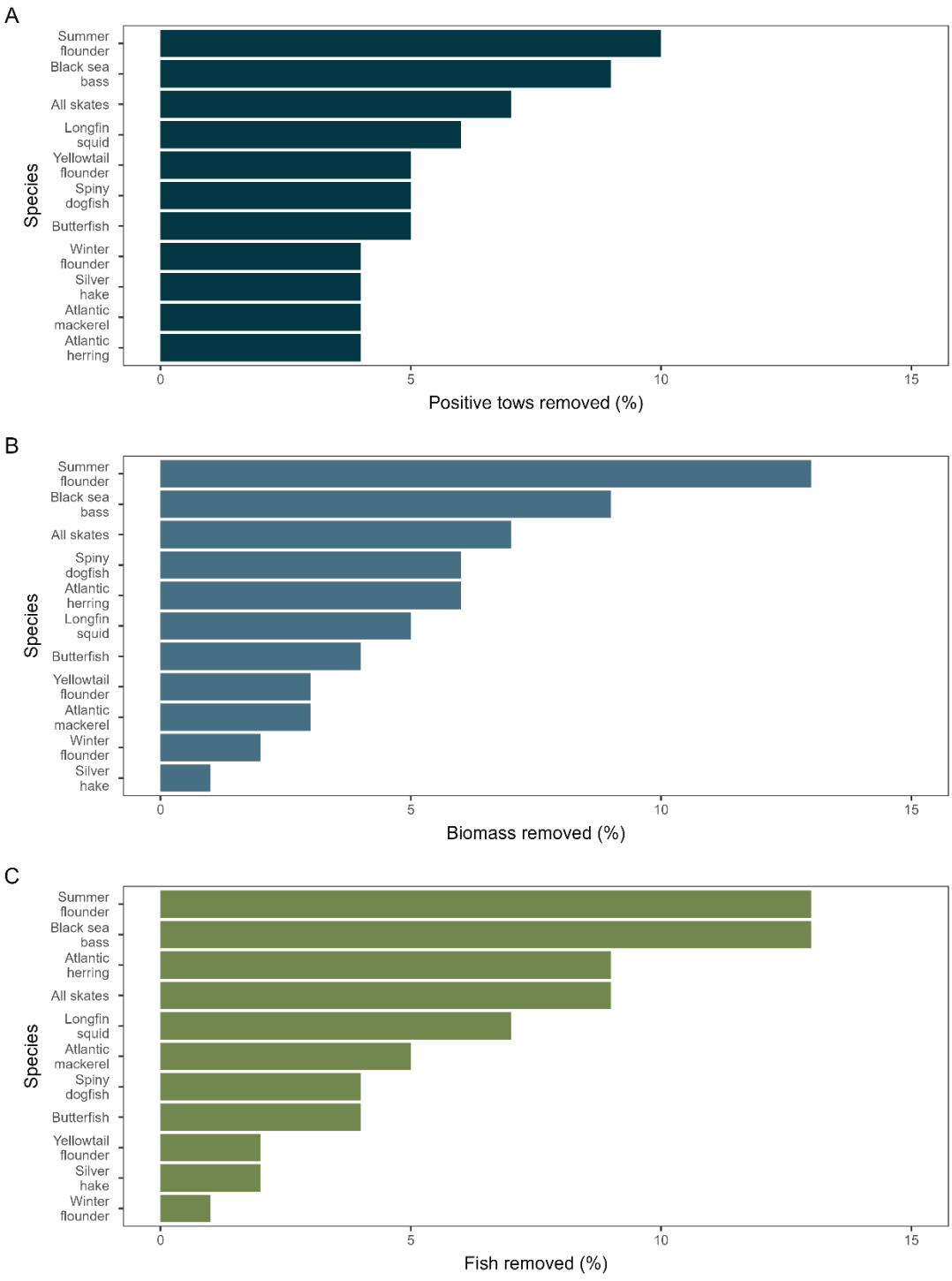

Figure 5. The percentage of (A) tows, (B) total biomass, and (C) total number of fish observed over the full survey area that would be removed from positive survey observations due to wind-precluded effort for a set of stakeholder-identified species.

Figure 6. The percentage of (A) tows, (B) total biomass, and (C) total number of fish observed over the full survey area that would be removed from positive survey observations due to wind-precluded effort for a set of stakeholder-identified species.

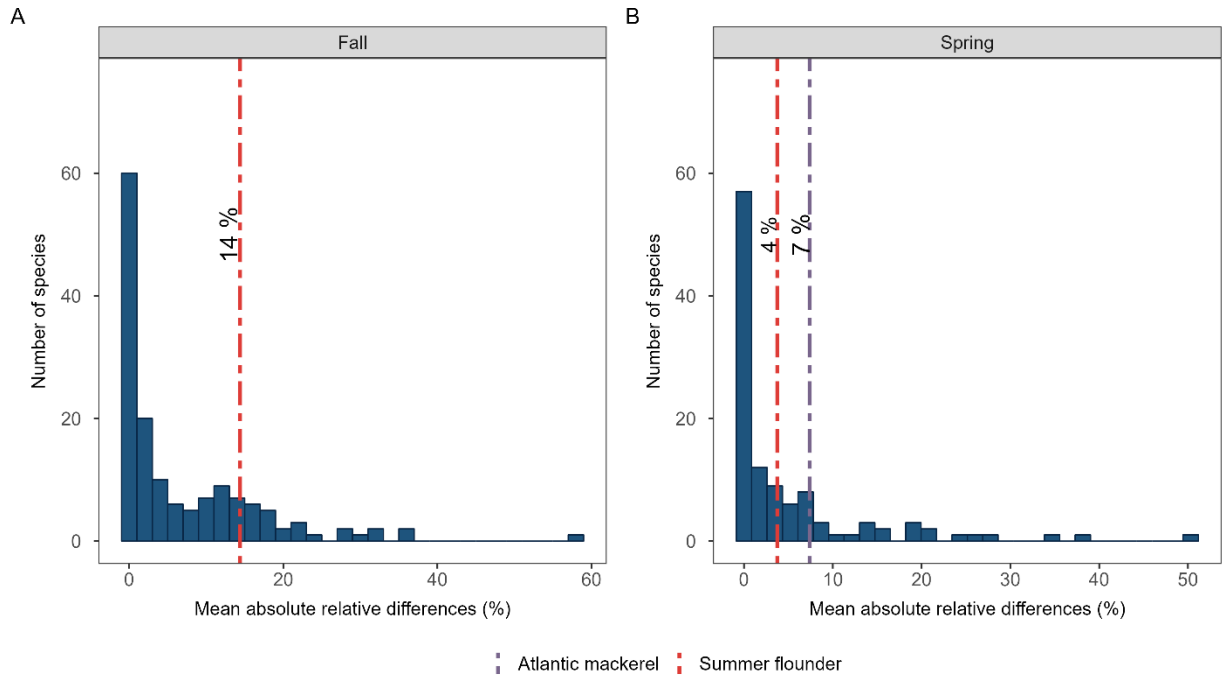

Figure 7. The distribution of mean absolute relative differences between survey effort scenarios for all species observed in the A) fall survey data and B) spring survey data (dark blue bars). The mean absolute relative differences between status quo and wind-precluded indices for summer flounder and Atlantic mackerel are denoted by the red and purple dotted lines, respectively.

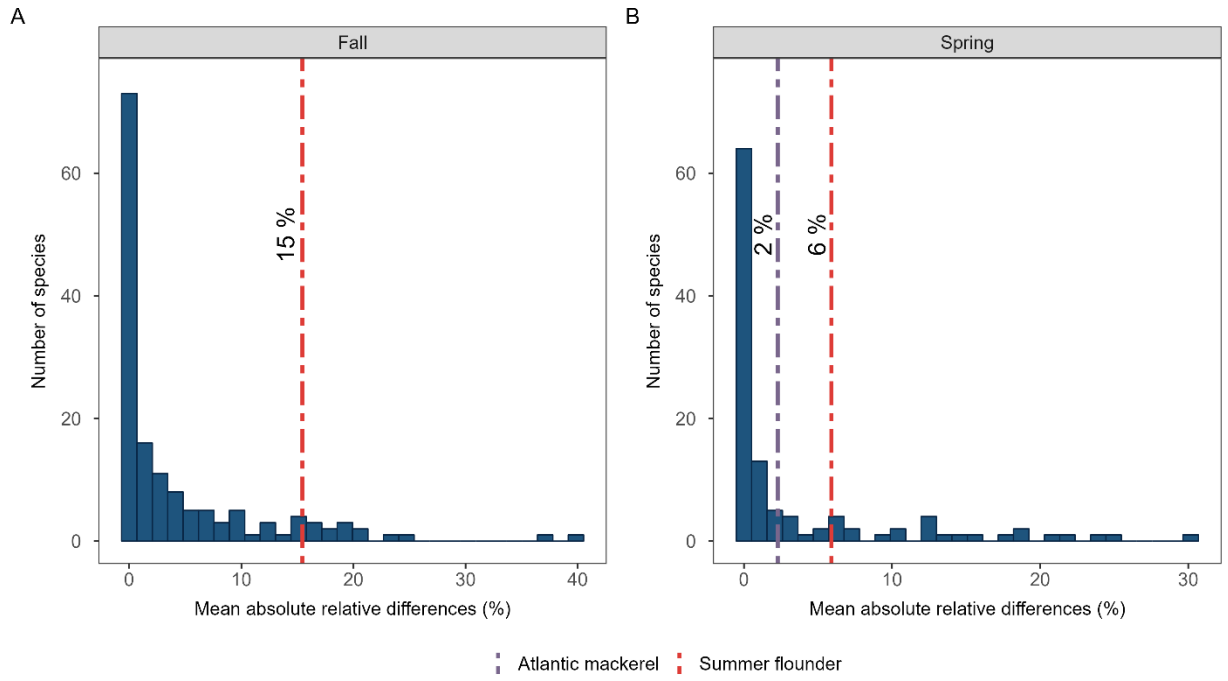

Figure 8. The distribution of mean absolute relative differences between survey effort scenarios for all species observed in the A) fall survey data and B) spring survey data (light blue bars). The mean absolute relative differences between status quo and wind-precluded CVs for summer flounder and Atlantic mackerel are denoted by the red and purple dotted lines, respectively.

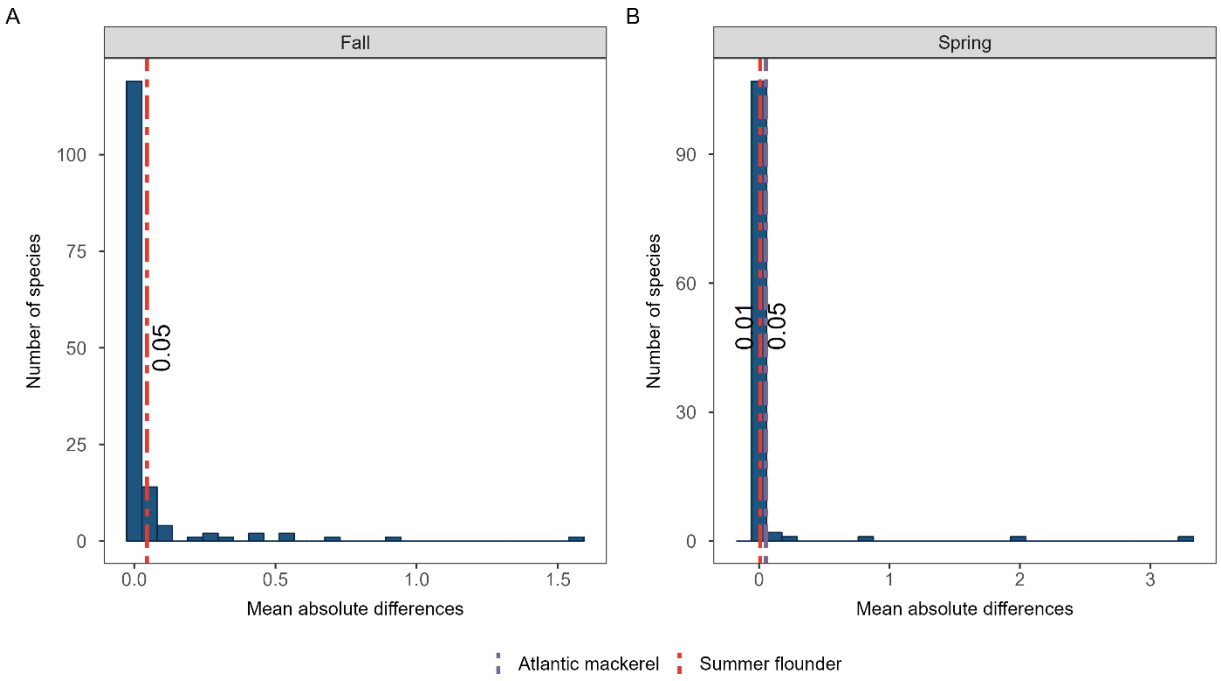

Figure 9. The distribution of mean absolute relative differences between survey effort scenarios for all species observed in the A) fall survey data and B) spring survey data (light blue bars). The mean absolute relative differences between status quo and wind-precluded population trends for summer flounder and Atlantic mackerel are denoted by the orange and dark blue dotted lines, respectively.

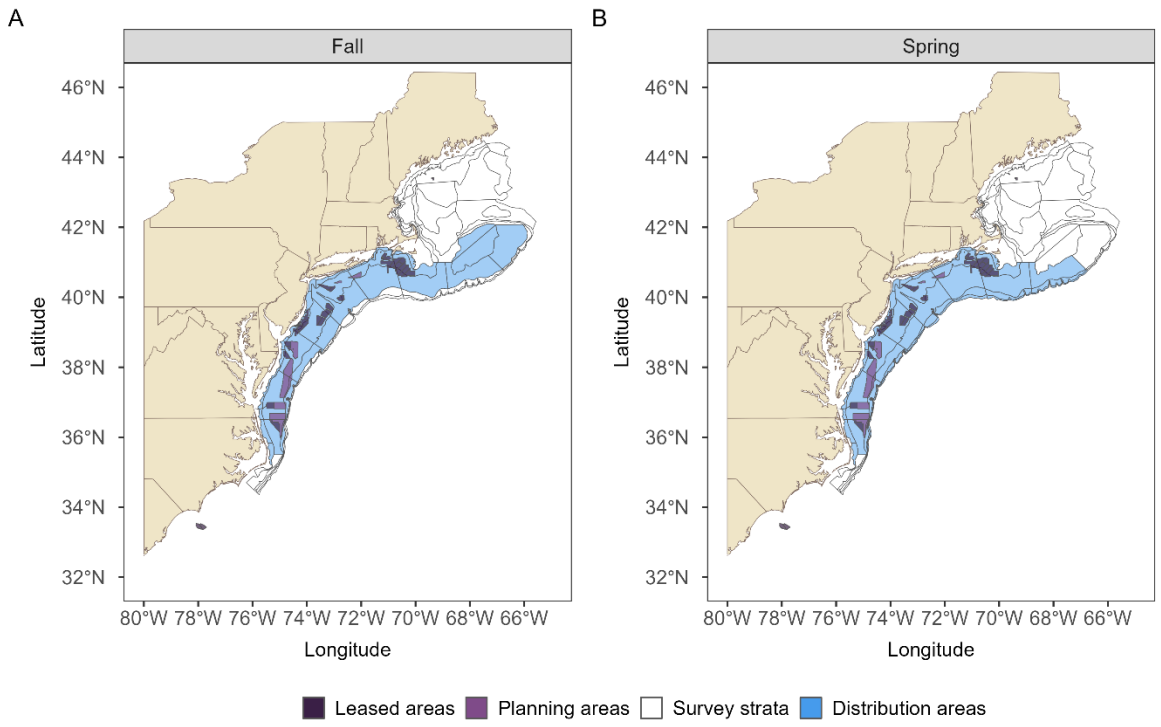

Figure 10. The A) fall and B) spring sampling frames for summer flounder (light blue) comprised of the 95% total cumulative biomass observed by the historical time series overlapped by the leased wind areas (dark purple), and the planned wind areas (light purple).

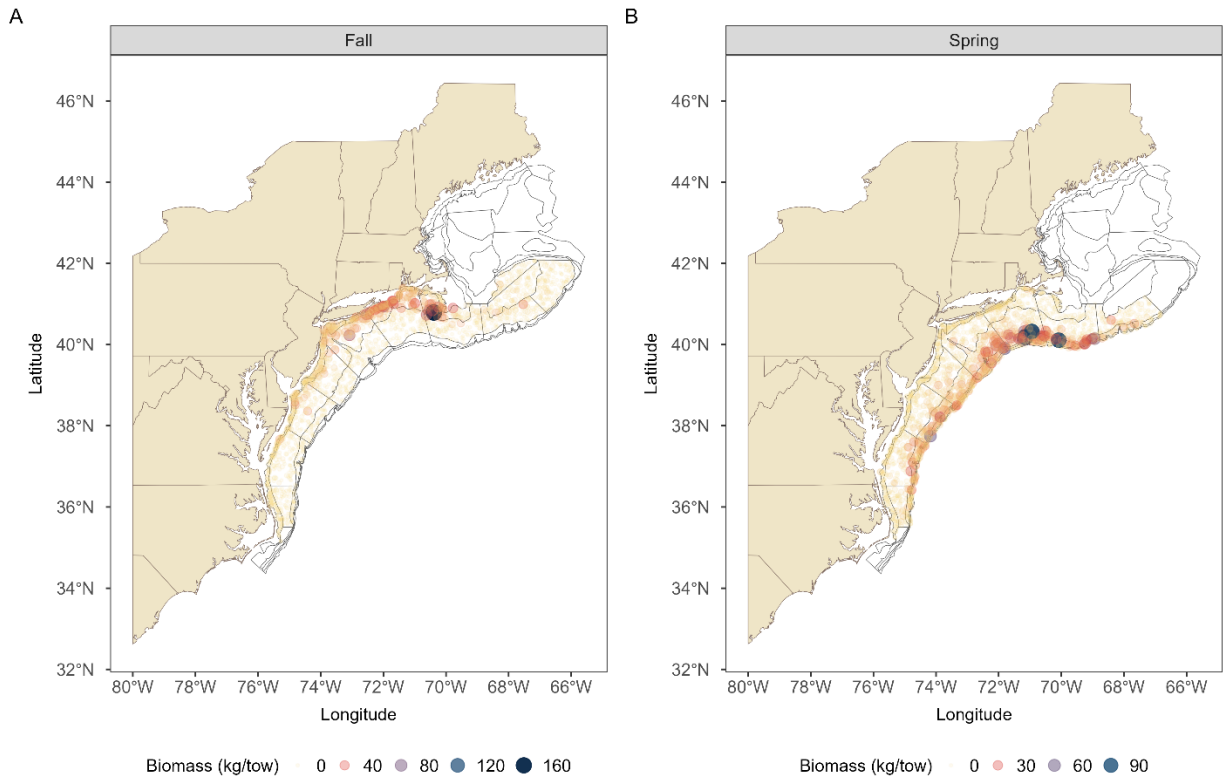

Figure 11. Summer flounder biomass observations based on whether the biomass was observed inside or outside of planned and leased wind energy areas.

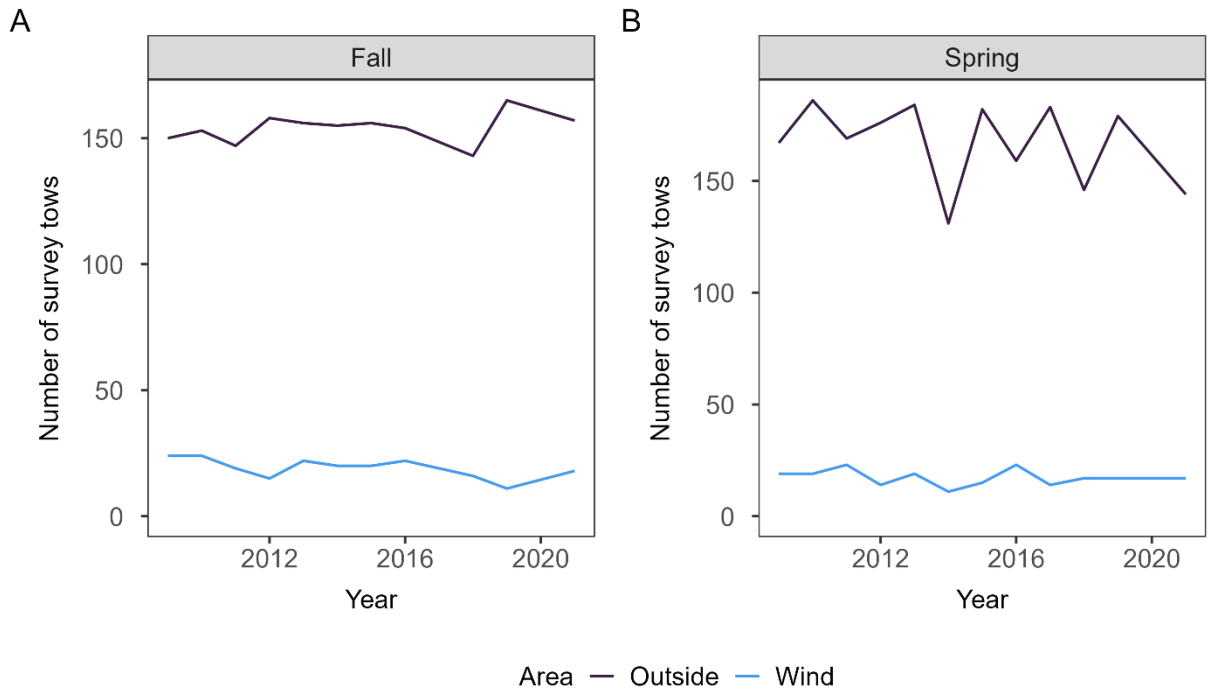

Figure 12. The number of survey tows that caught summer flounder that would have occurred inside and outside wind energy areas in each year during the A) fall survey and B) spring survey.

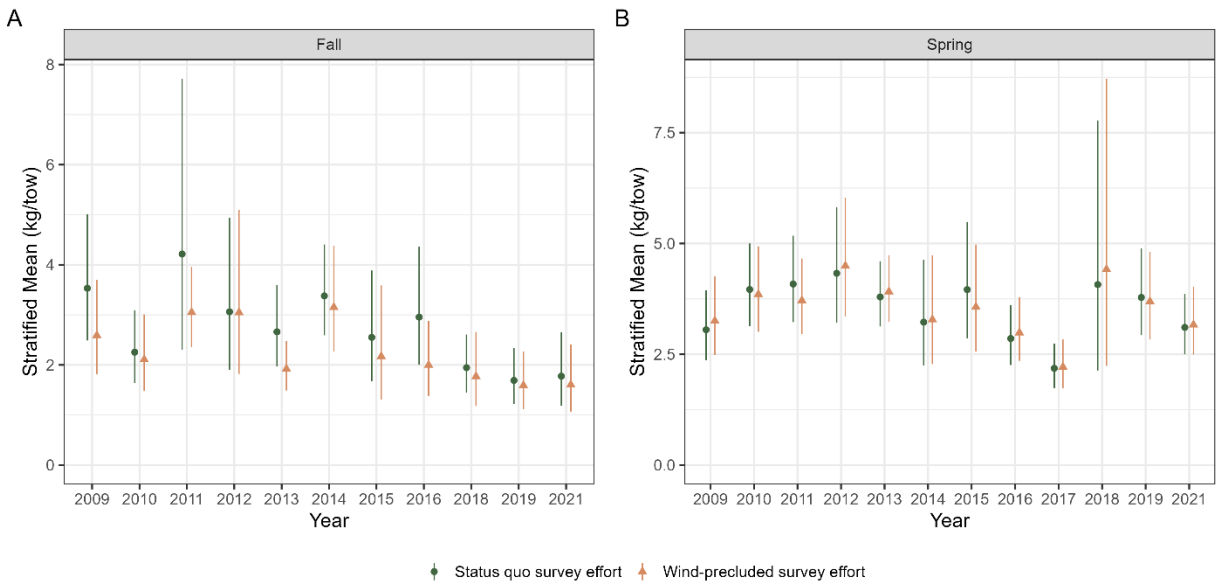

Figure 13. The seasonal annual abundance indices for summer flounder under a status quo survey effort assumption (green) and a wind-precluded survey effort assumption (orange). The bars on each of the points represent the standard error around the stratified mean.

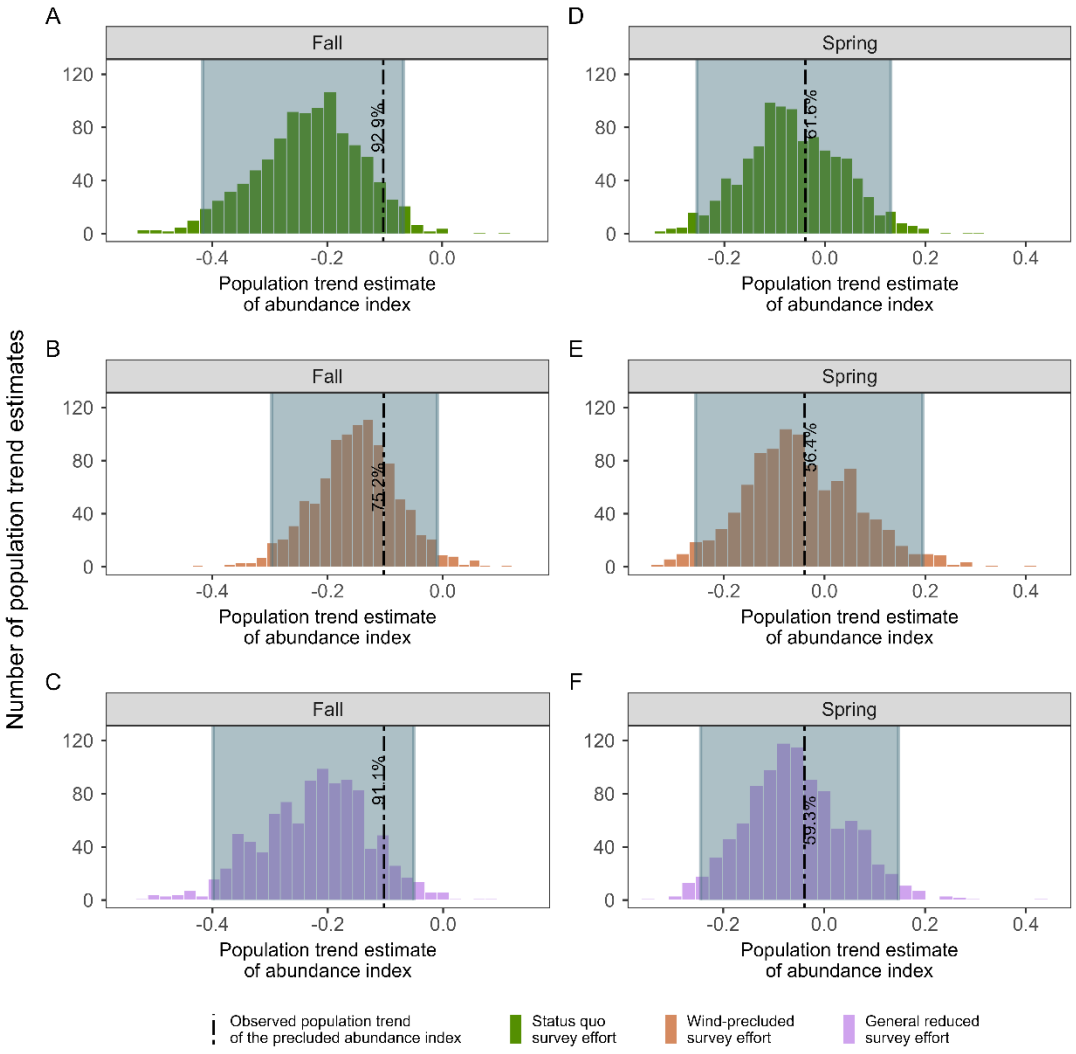

Figure 14. The distribution of estimated fall (left column) and spring (right column) population trends for summer flounder when the observed data is randomly resampled with replacement to emulate a status quo survey effort for each season (green), when wind-area tows are precluded from trend estimation (orange), and when the status quo effort data is randomly reduced by the same proportions as the potential wind-precluded effort to emulate a general reduction in survey effort (purple). The 95% confidence intervals of each distribution are represented by the dark blue shaded rectangle in each panel, and the estimated population trend from the observed data under the wind-precluded survey effort scenario is presented by the black dotted line and annotated with the representative quantile of the distribution.

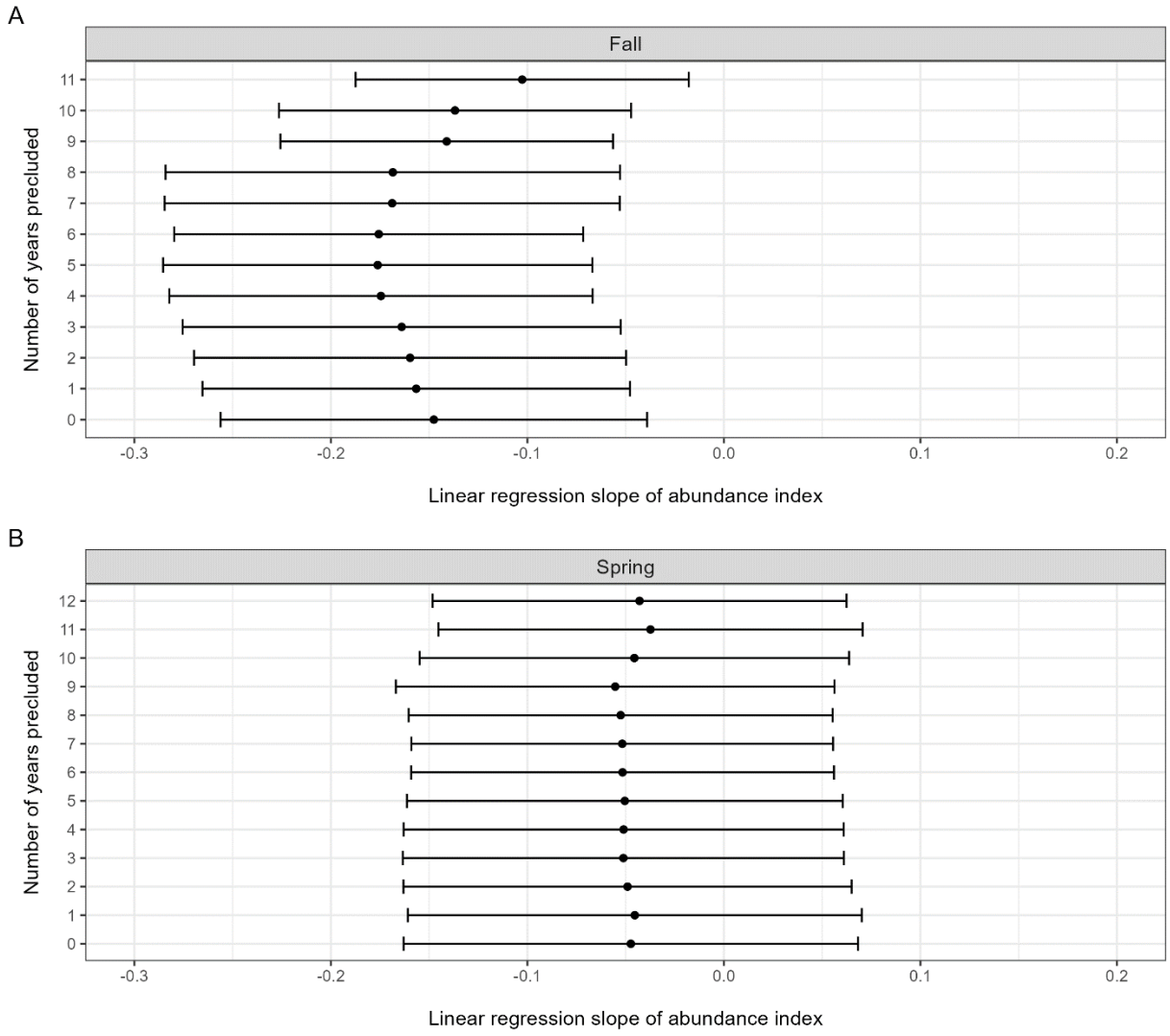

Figure 15. The change in estimates of population trend for summer flounder from the A) fall and B) spring survey as the number of years the survey is precluded from wind areas increases. The bars represent the 95% confidence intervals around the trend estimate.

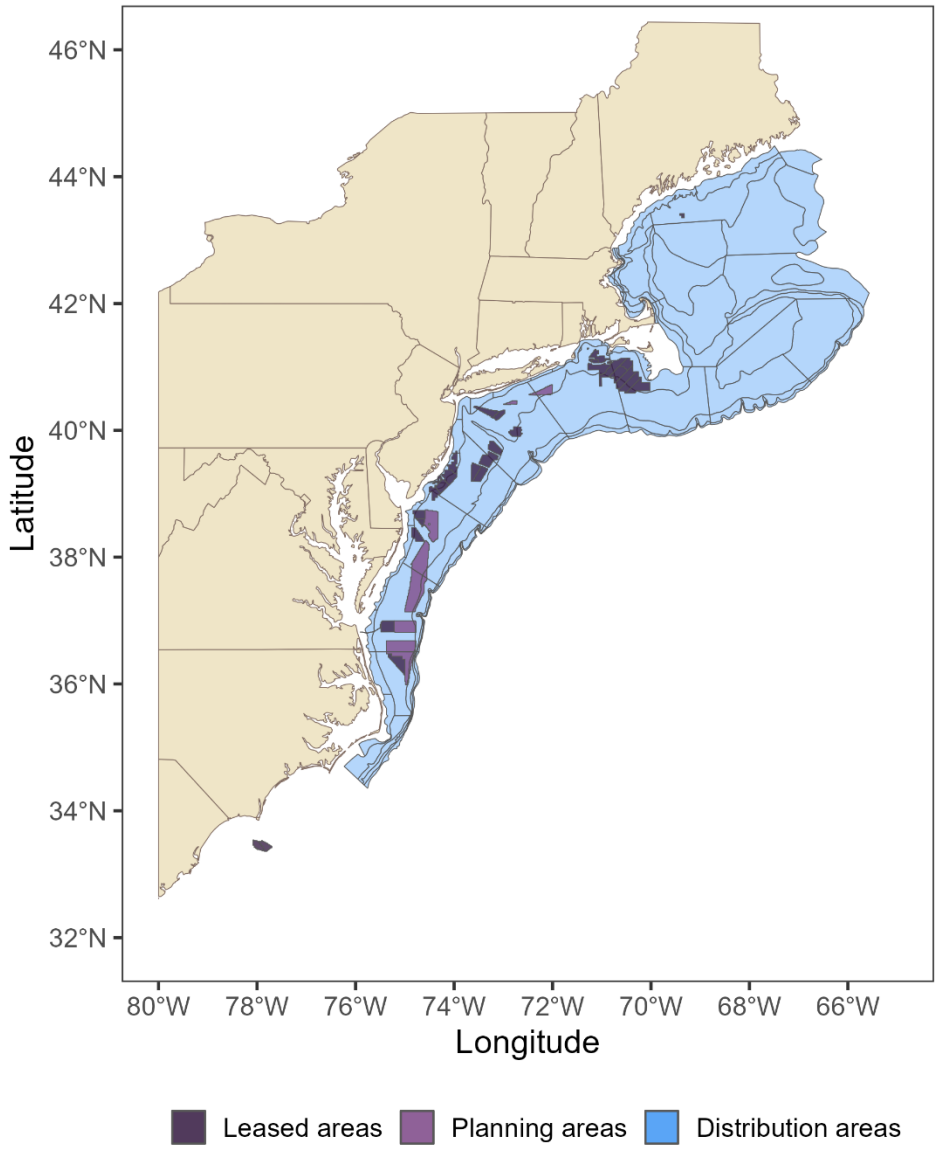

Figure 16. The seasonal sampling frame for Atlantic mackerel (light blue) overlapped by the leased wind areas (dark purple), and the planned wind areas (purple).

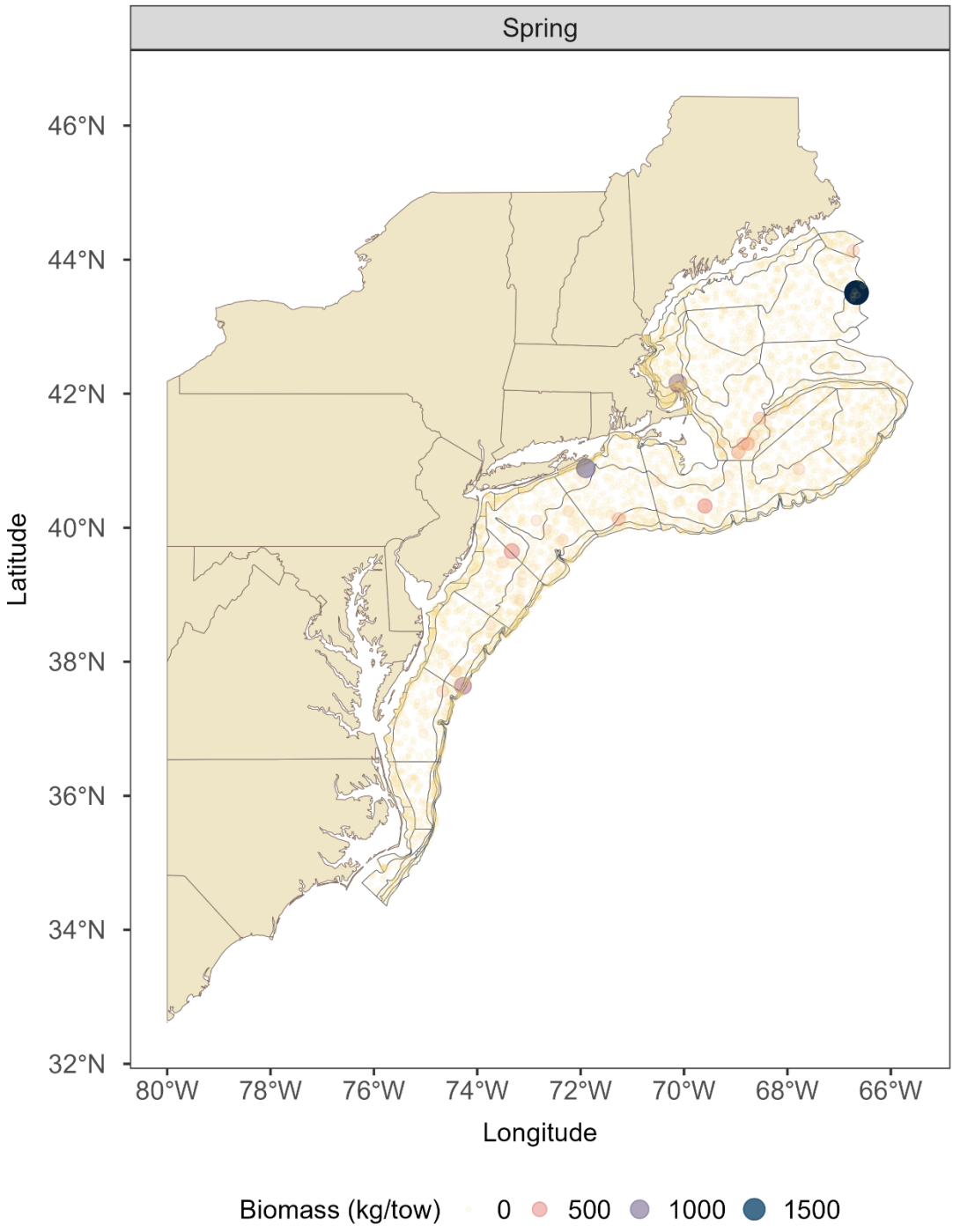

Figure 17. A map of spring Atlantic mackerel biomass observations based on whether the biomass was observed inside or outside of planned and leased wind energy areas.

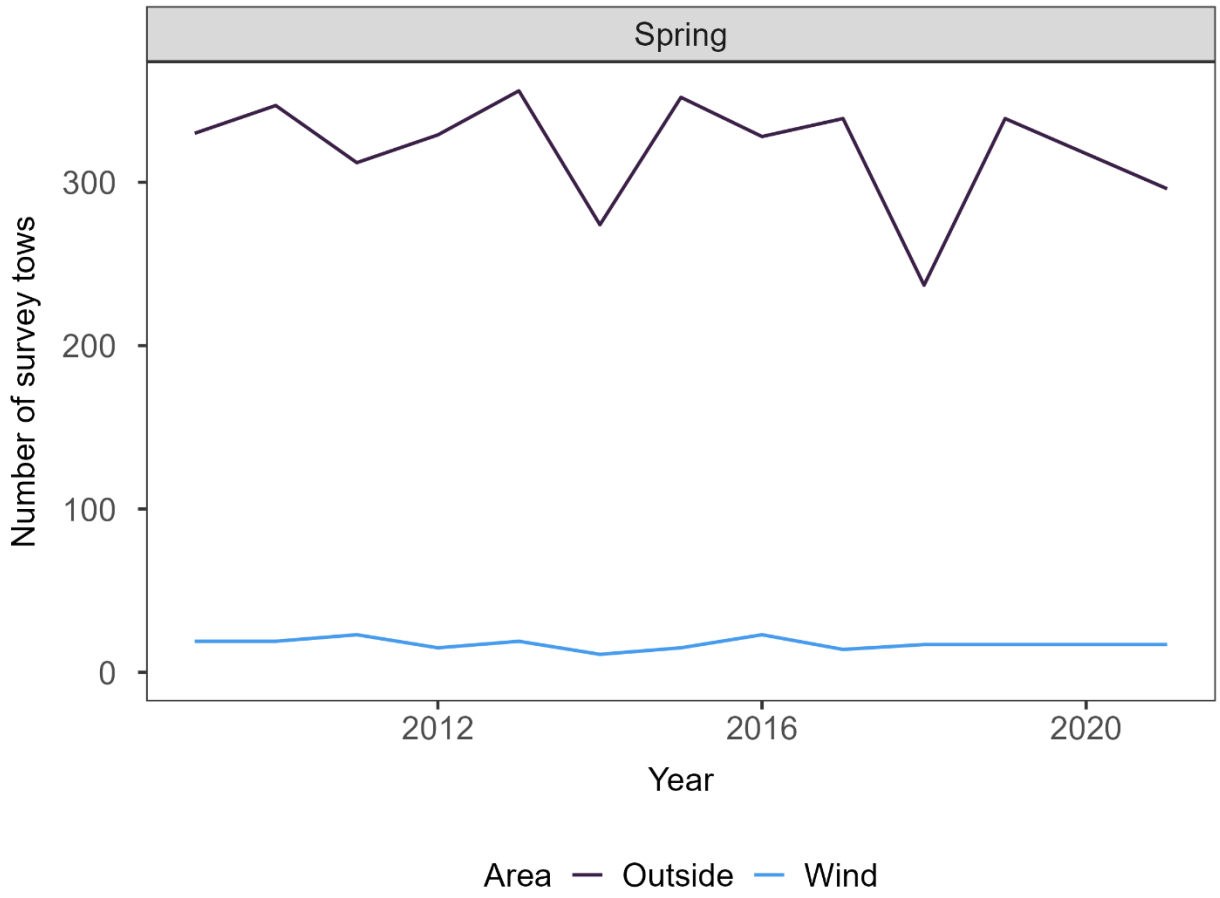

Figure 18. The number of survey tows that observed Atlantic mackerel that would have occurred inside and outside wind energy areas in each year.

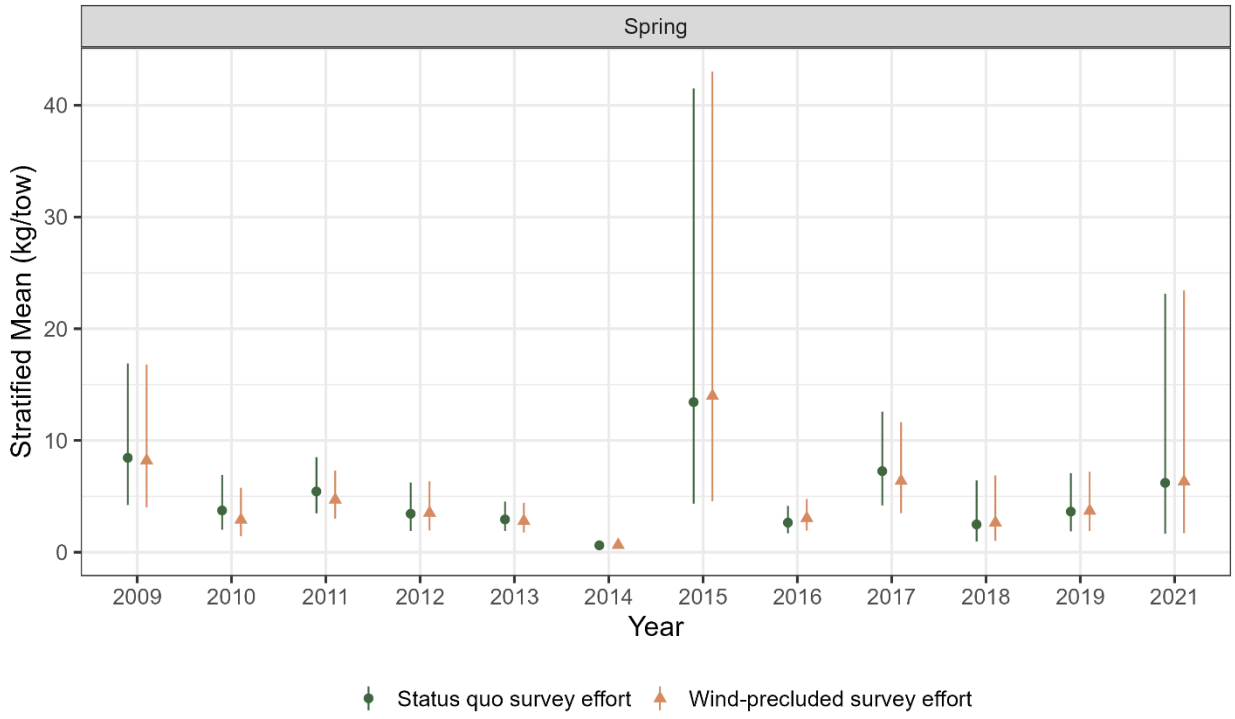

Figure 19. The spring annual abundance indices for Atlantic mackerel under a status quo survey effort assumption (green points) and a wind-precluded survey effort assumption (orange points). The bars on each of the points represent the standard error around the stratified mean.

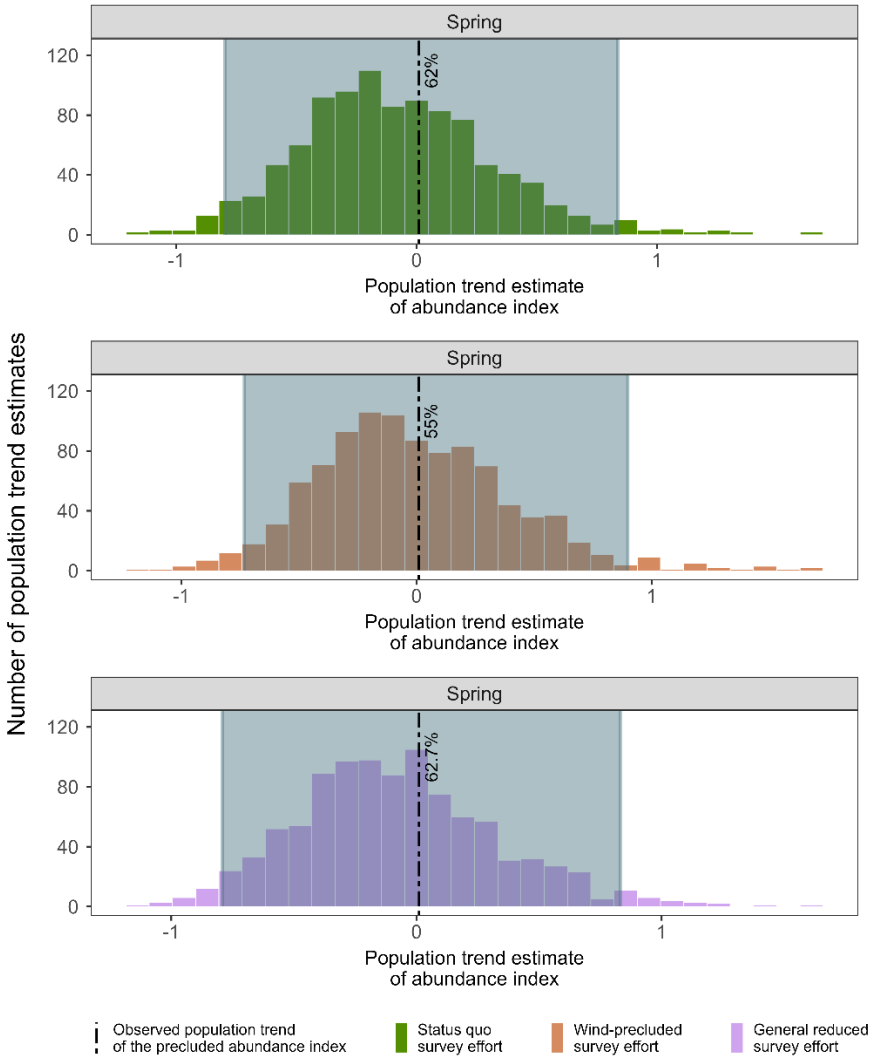

Figure 20. The distribution of estimated spring population trends for Atlantic mackerel when the observed data is randomly resampled with replacement to emulate a status quo survey effort (top panel), when wind-area tows are precluded from trend estimation (middle panel), and when the status quo effort data is randomly reduced by the same proportions as the potential wind-precluded effort to emulate a general reduction in survey effort (bottom panel). The 95% confidence intervals of each distribution are represented by the dark blue shaded rectangle in each panel, and the estimated population trend from the observed data under the wind-precluded survey effort scenario is presented by the black dotted line annotated with the representative quantile of the distribution.

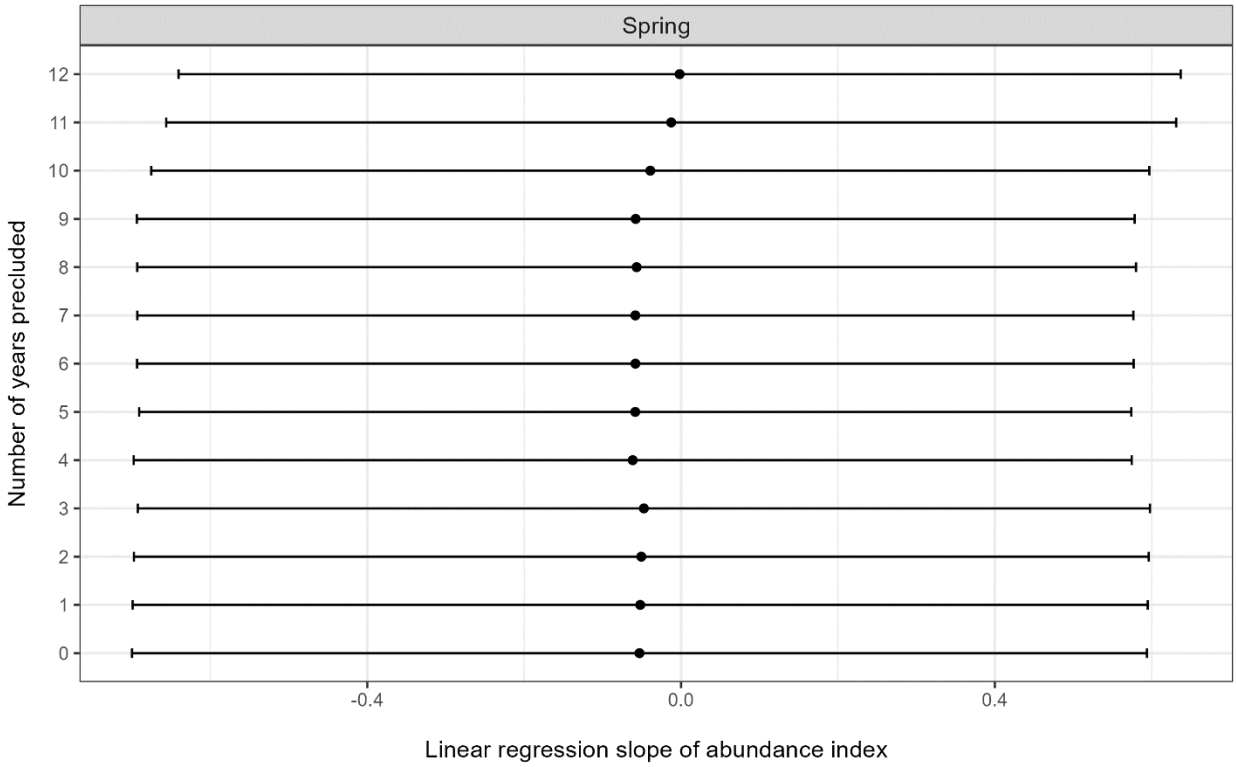

Figure 21. The change in estimates of population trend for Atlantic mackerel as the number of years the survey is precluded from wind areas increases. The bars represent the 95% confidence intervals around the trend estimate.

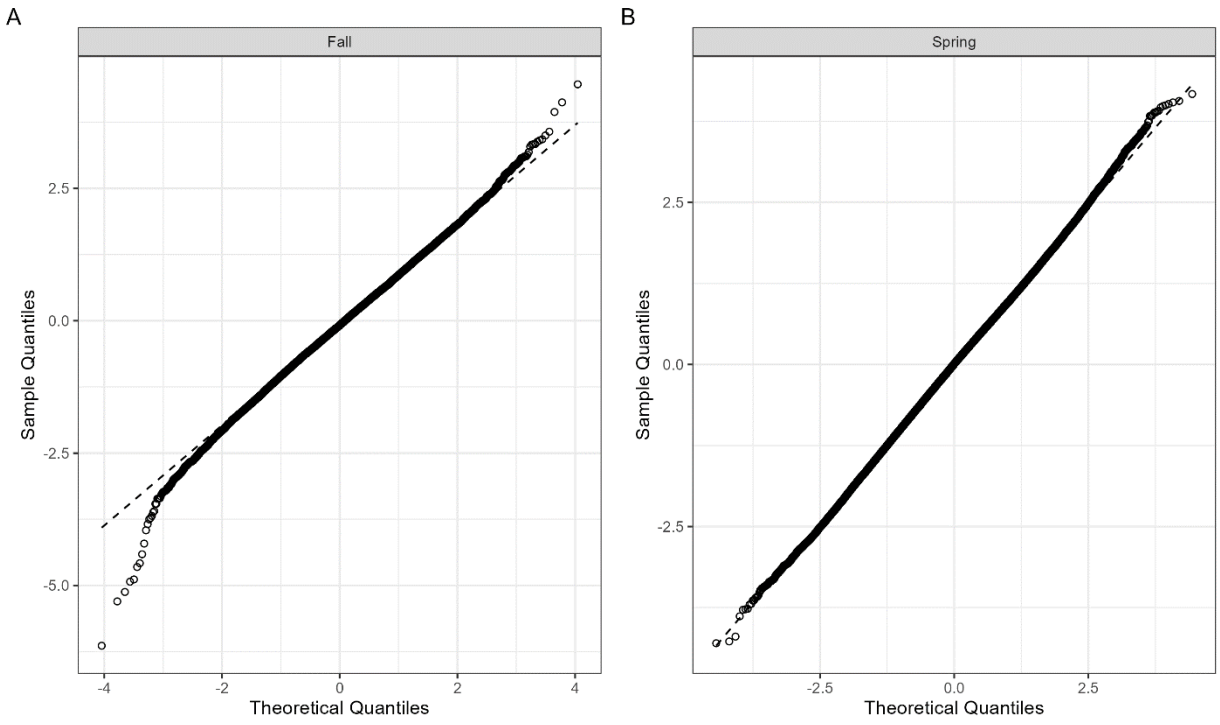

Figure 22. A quantile-quantile plot of observed quantiles of MCMC-resampled residuals compared to the theoretical quantiles of residuals from the models fit to A) fall summer flounder survey data, and B) spring summer flounder survey data.

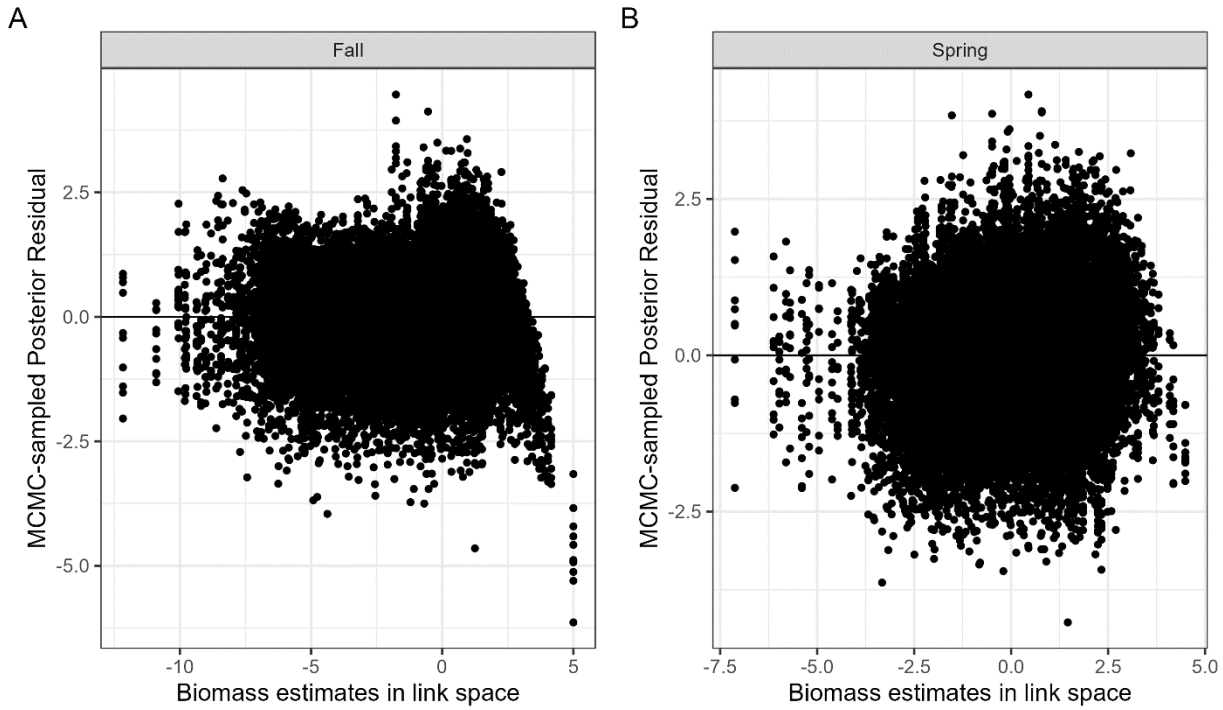

Figure 23. The distribution of MCMC-resampled residuals predicted over 10 simulations for summer flounder compared to the observed values of biomass in link space fit to A) fall summer flounder survey data, and B) spring summer flounder survey data.

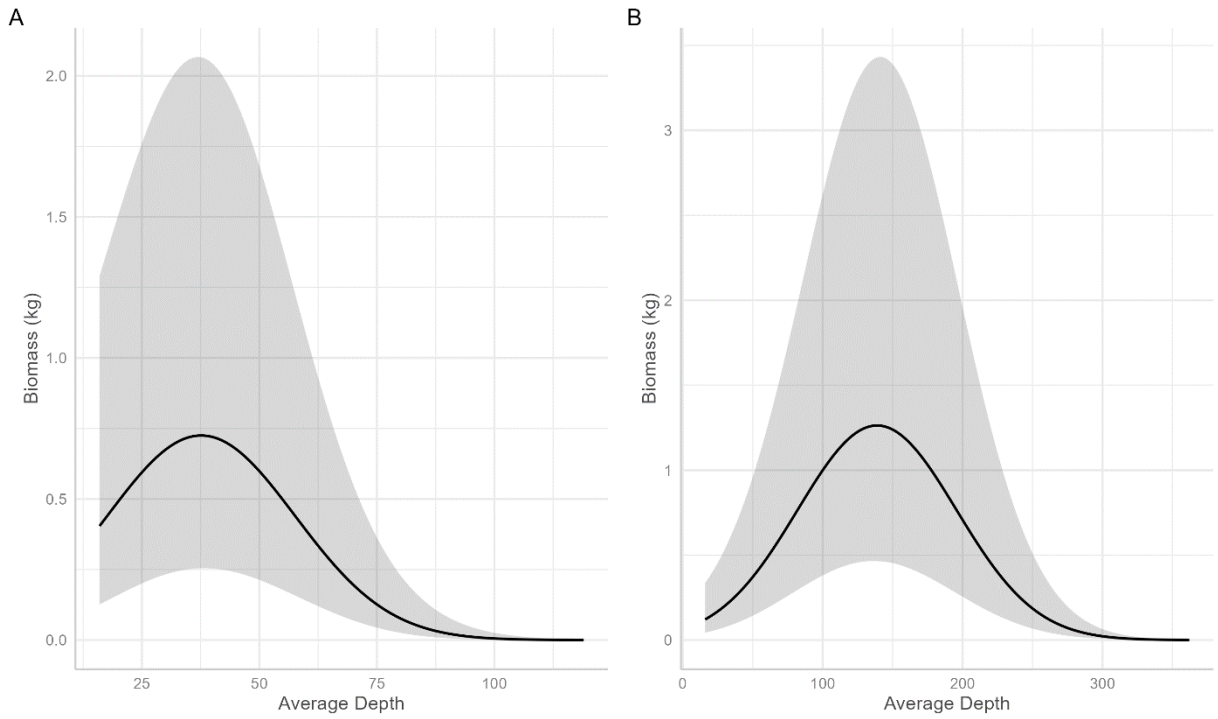

Figure 24. The marginal effect of depth on summer flounder biomass catch rates predicted by the A) fall summer flounder model, and B) spring summer flounder model. Gray shaded area represents the 95% confidence intervals around the predictions.

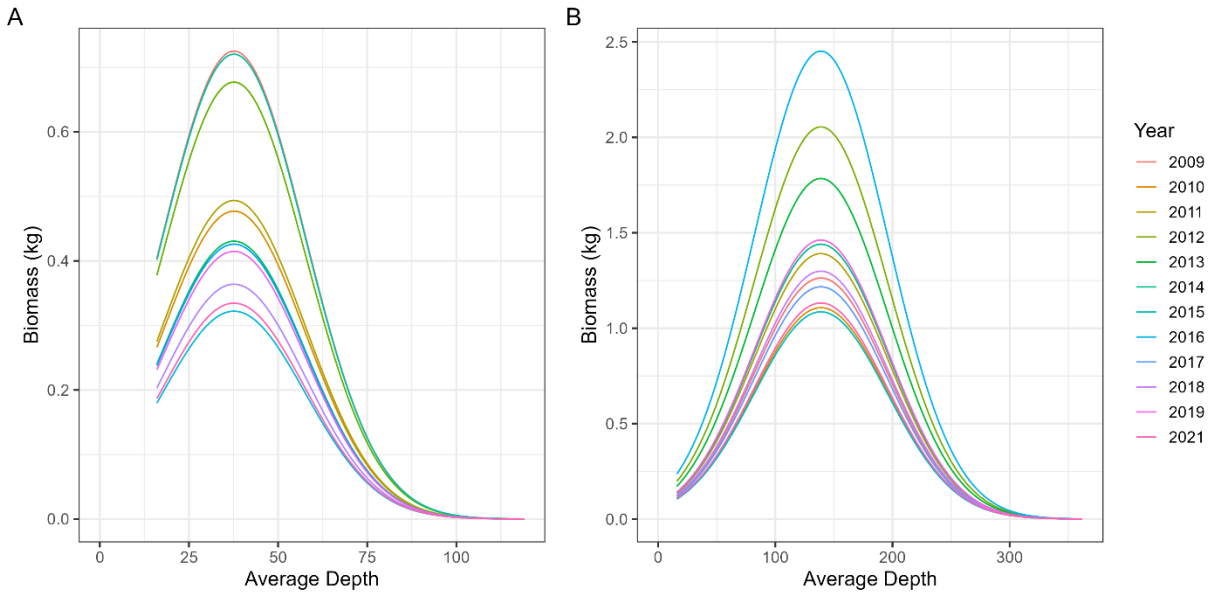

Figure 25. The marginal effect of depth and year on summer flounder biomass catch rates predicted by the A) fall summer flounder model, and B) spring summer flounder model.

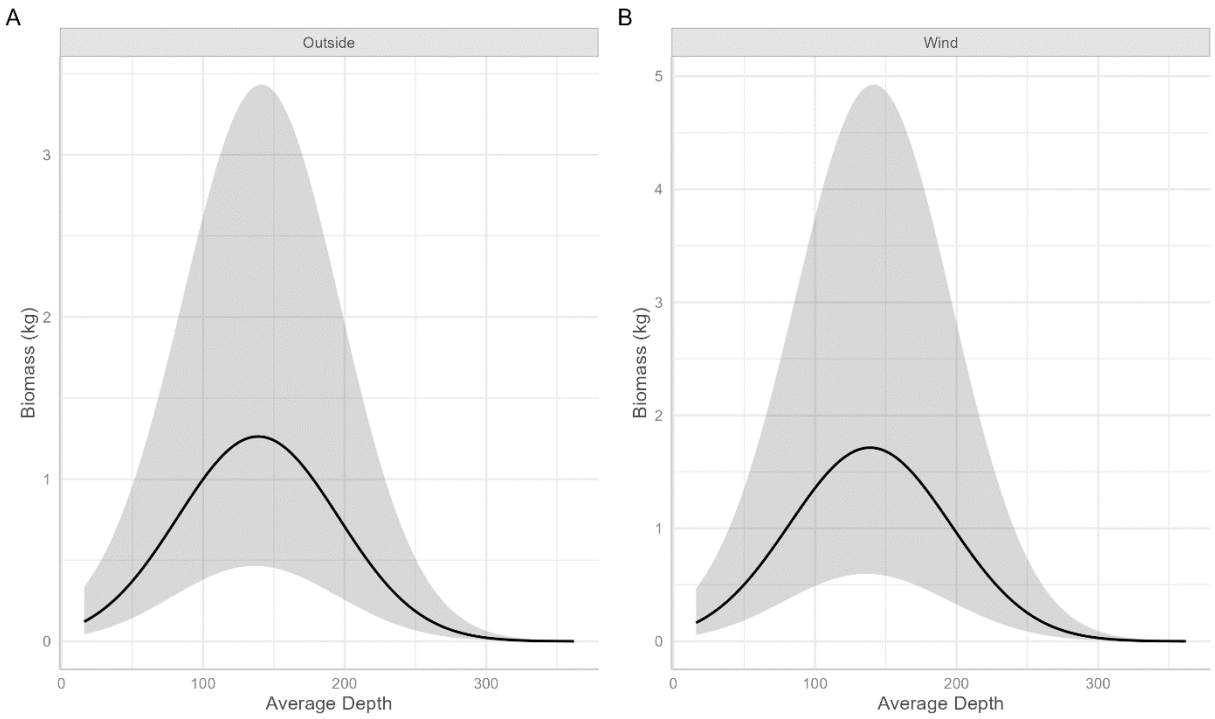

Figure 26. The marginal effect of depth and area on summer flounder biomass catch rates within areas A) outside wind areas and B) inside wind areas predicted by the spring model.

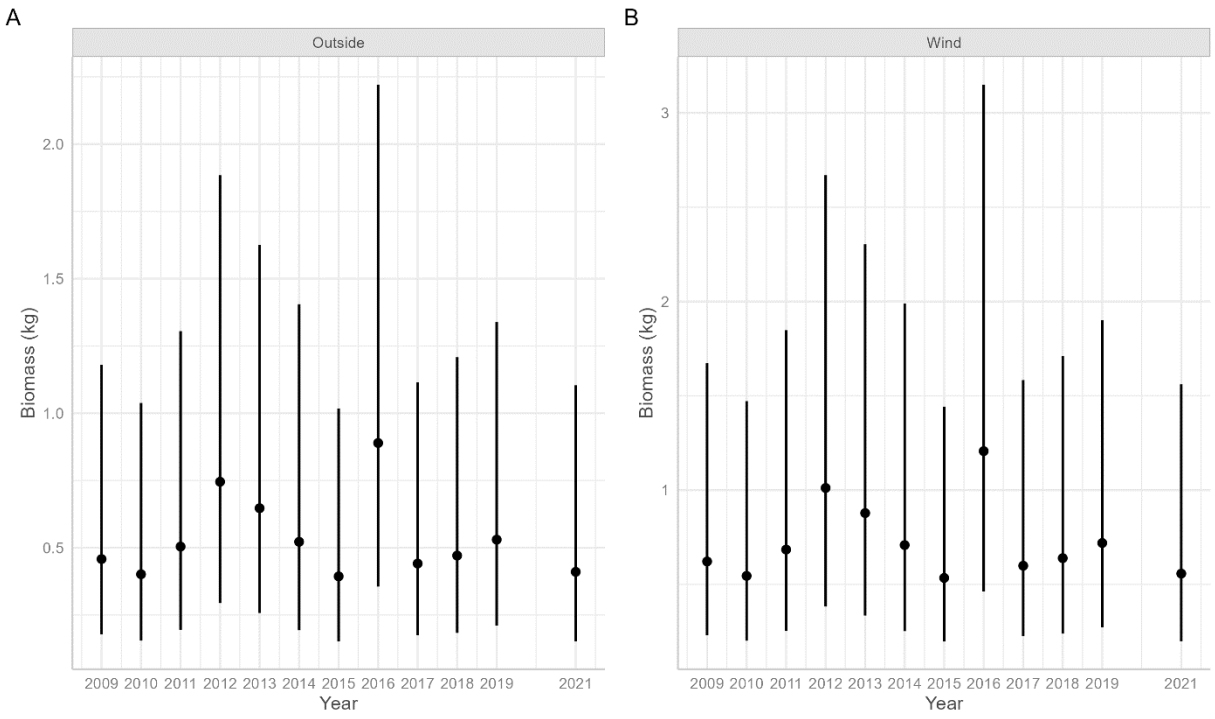

Figure 27. The marginal effect of year and area on summer flounder biomass catch rates within areas A) outside wind areas and B) inside wind areas predicted by the spring model.

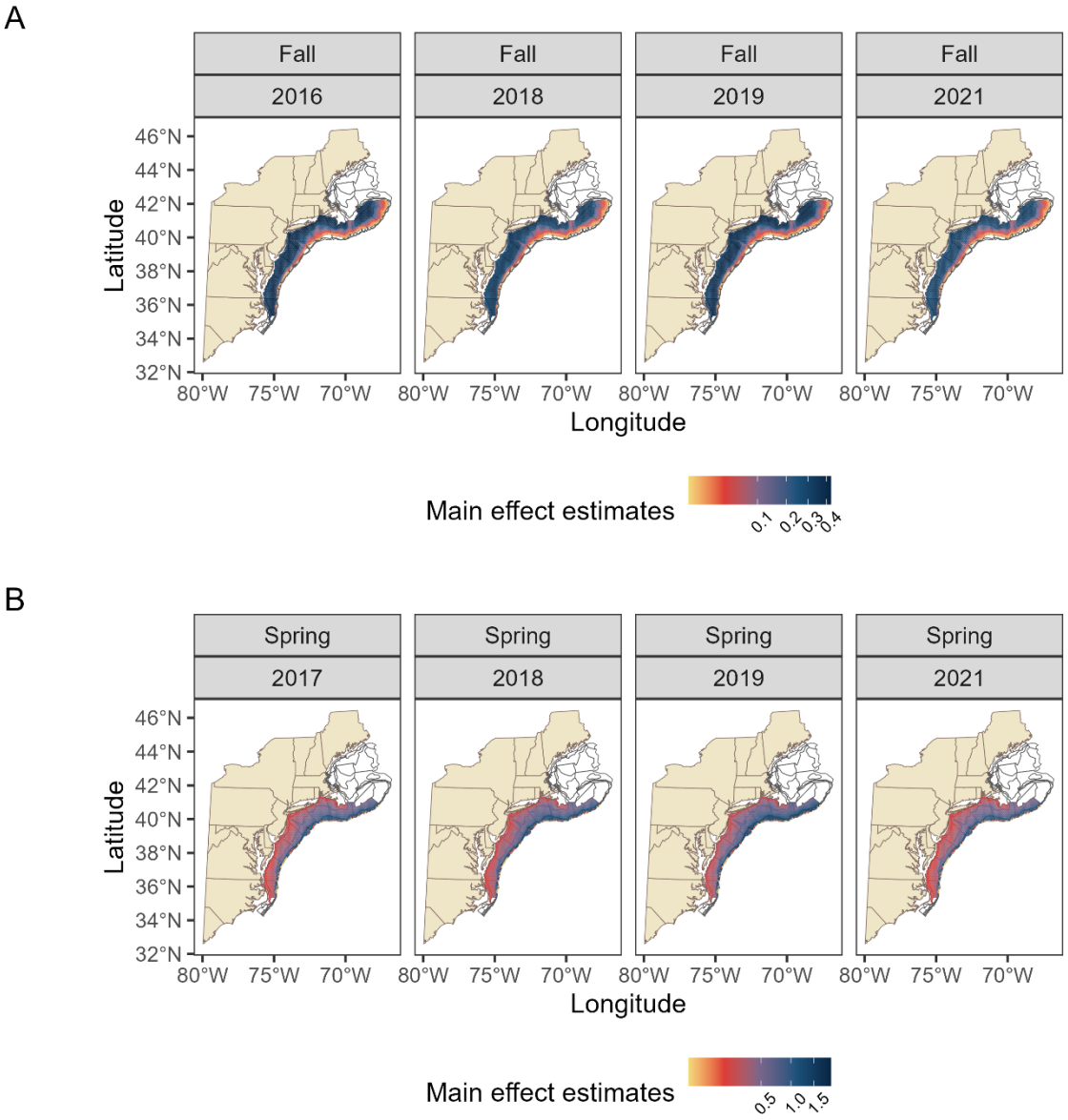

Figure 28. Fall (top four panels) and spring (bottom four panels) estimates of the fixed effects for the most recent four years of the time series from the respective models for summer flounder.

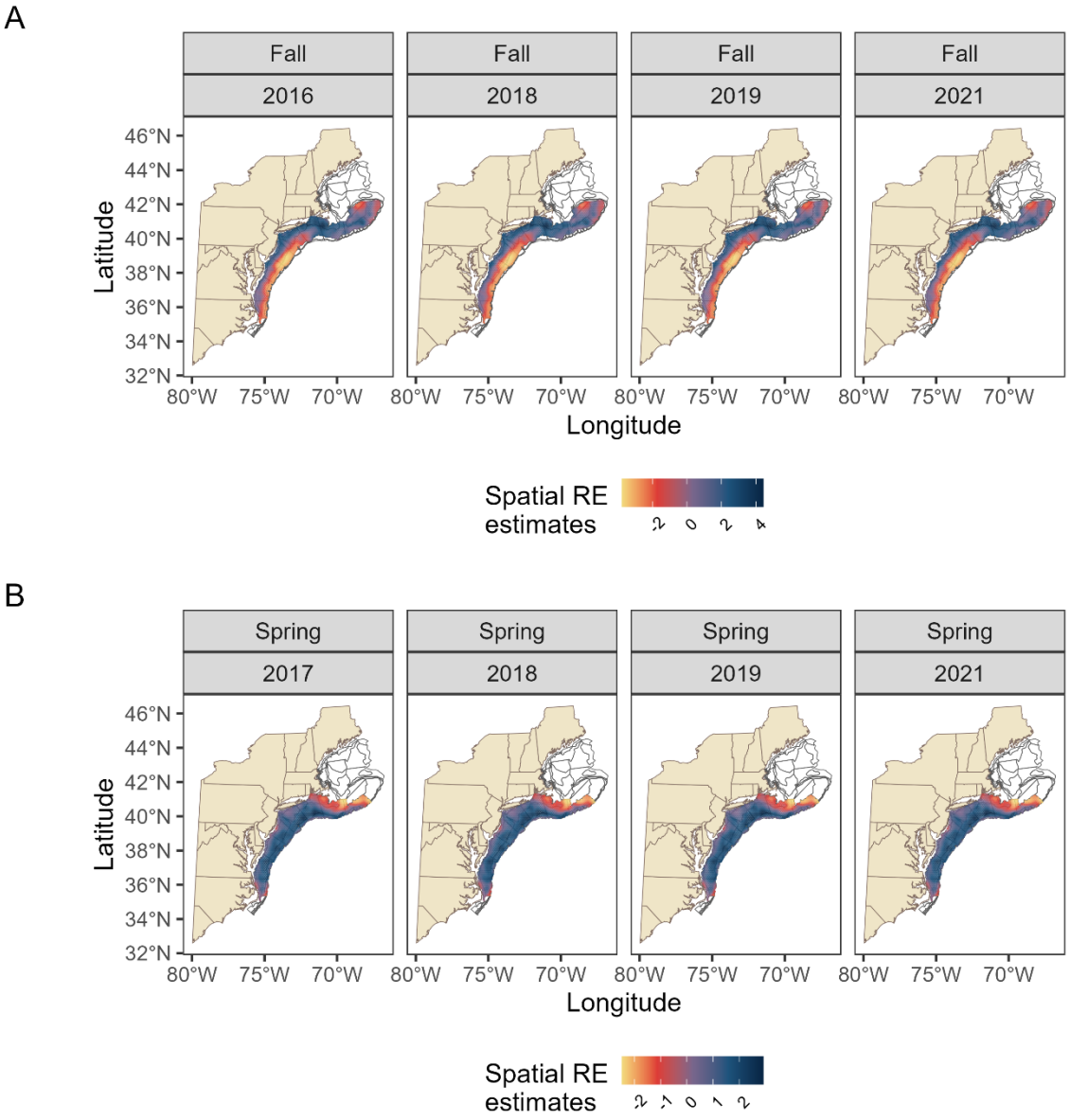

Figure 29. Fall (top four panels) and spring (bottom four panels) estimates of the spatial random effects from the respective models for summer flounder.

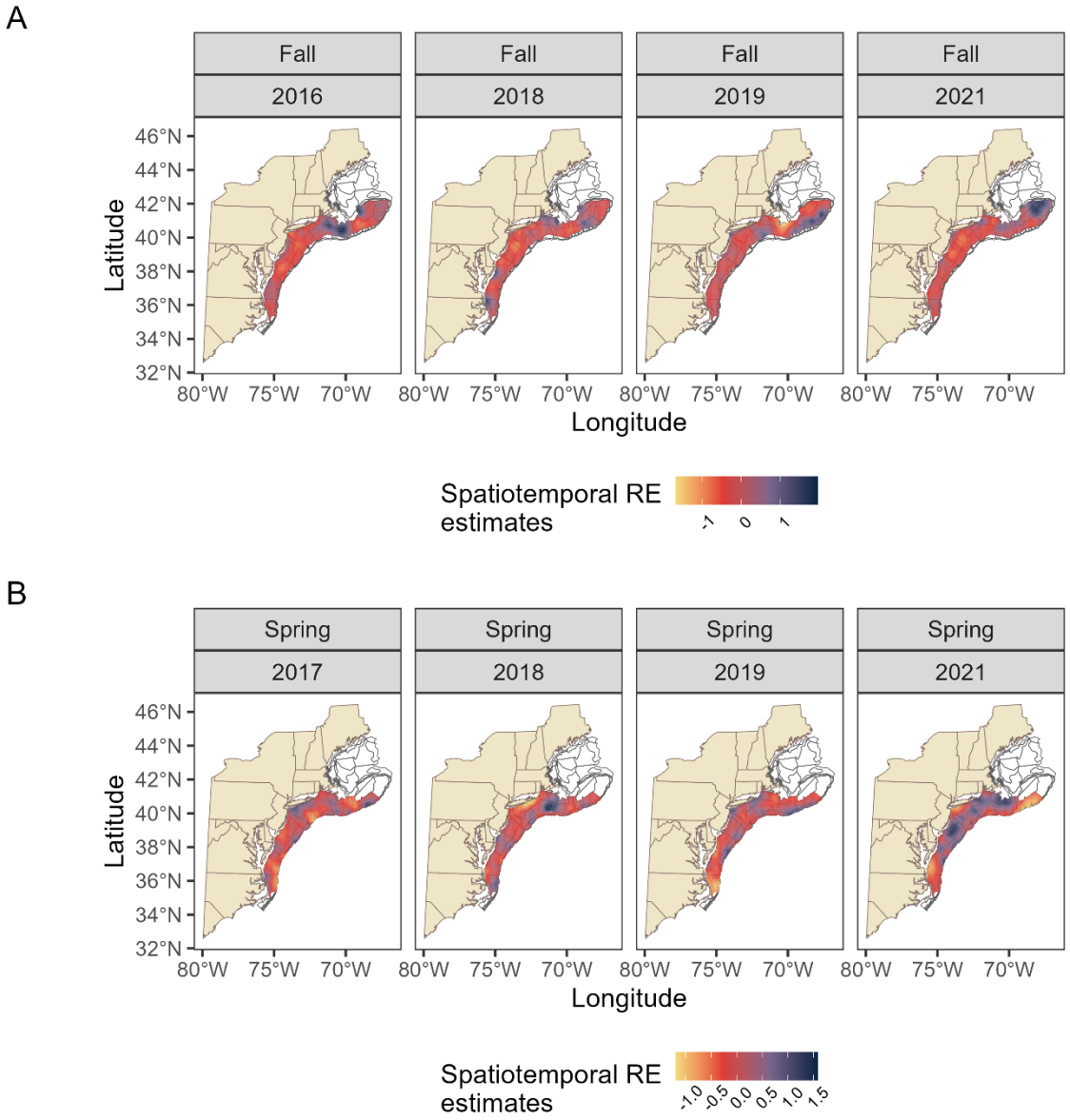

Figure 30. Fall (top four panels) and spring (bottom four panels) estimates of the spatiotemporal random effects for the most recent four years of the time series from the respective models for summer flounder.

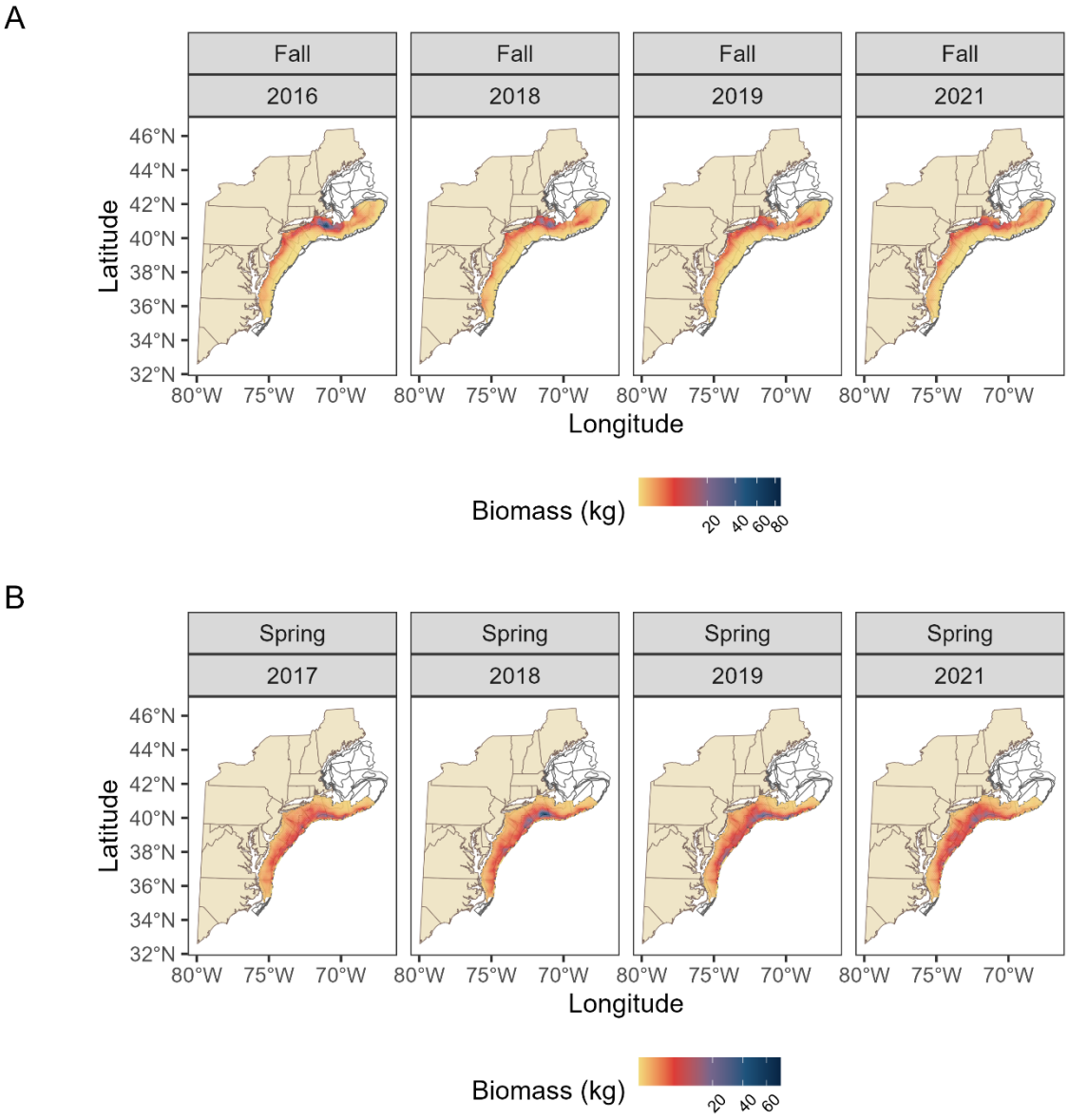

Figure 31. Fall (top four panels) and spring (bottom four panels) predictions of summer flounder biomass extrapolated from the model across the sampling frame and within respective survey strata.

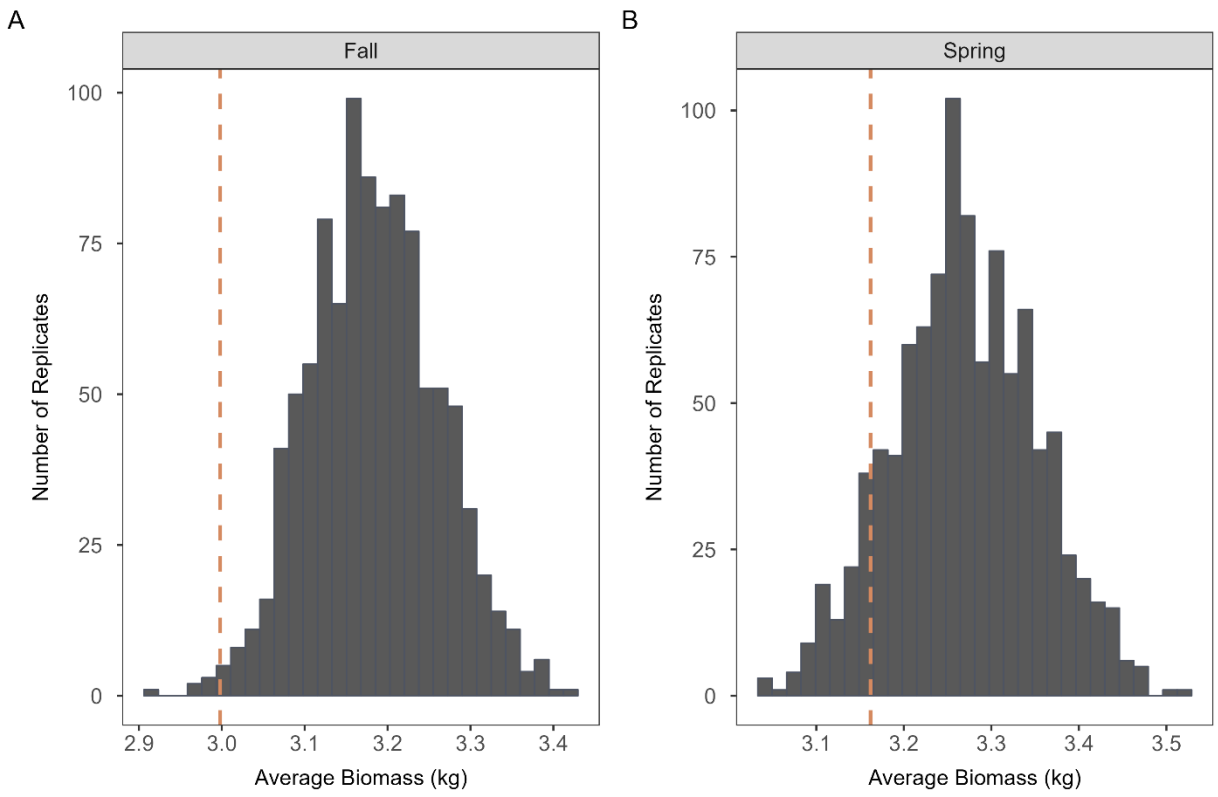

Figure 32. The distribution of simulated average biomass catch rates generated by the A) fall summer flounder model, and B) spring summer flounder model. The observed average survey biomass catch rate is represented by the orange dotted line.

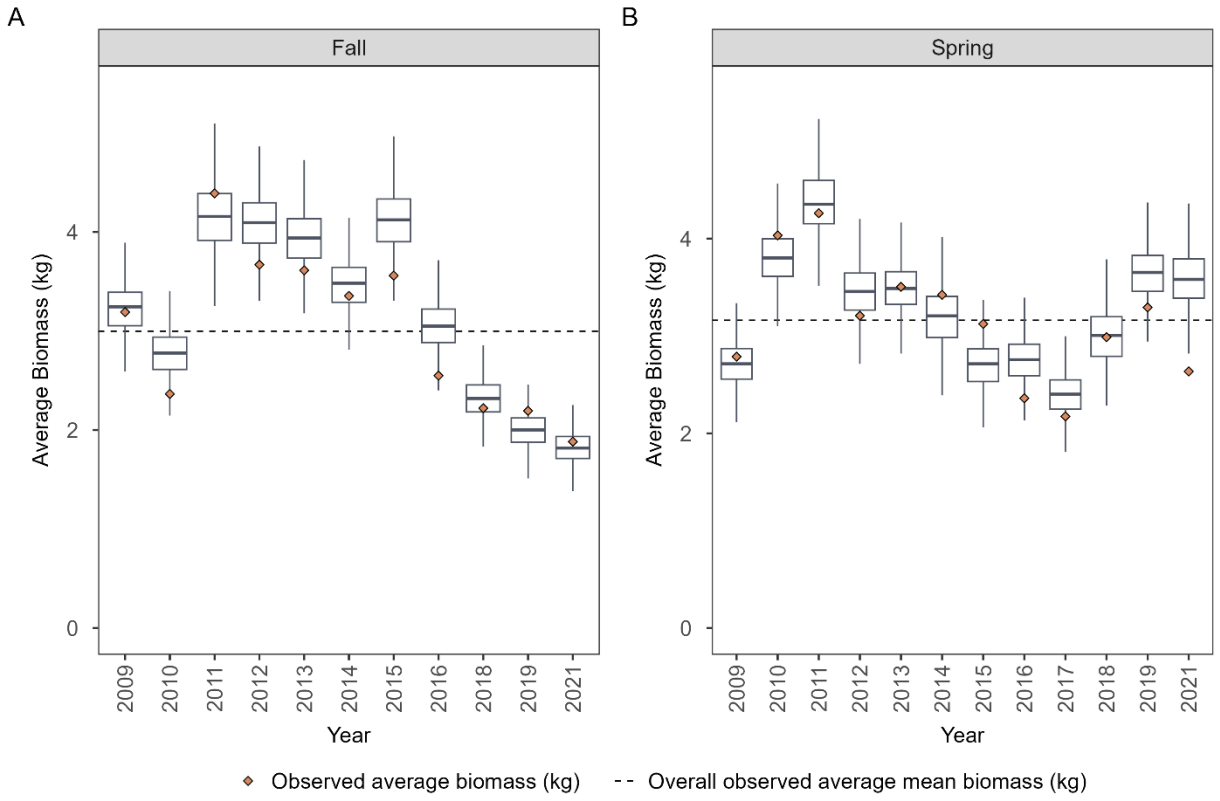

Figure 33. The distribution of simulated average biomass catch rates in each year generated by the A) fall summer flounder model, and B) spring summer flounder model. The observed average survey biomass catch rate in each year and season from the data is represented by the orange diamond. The annual nominal averages of biomass catch rates is represented by the black dotted line. The effect of outliers has been removed from the distribution.

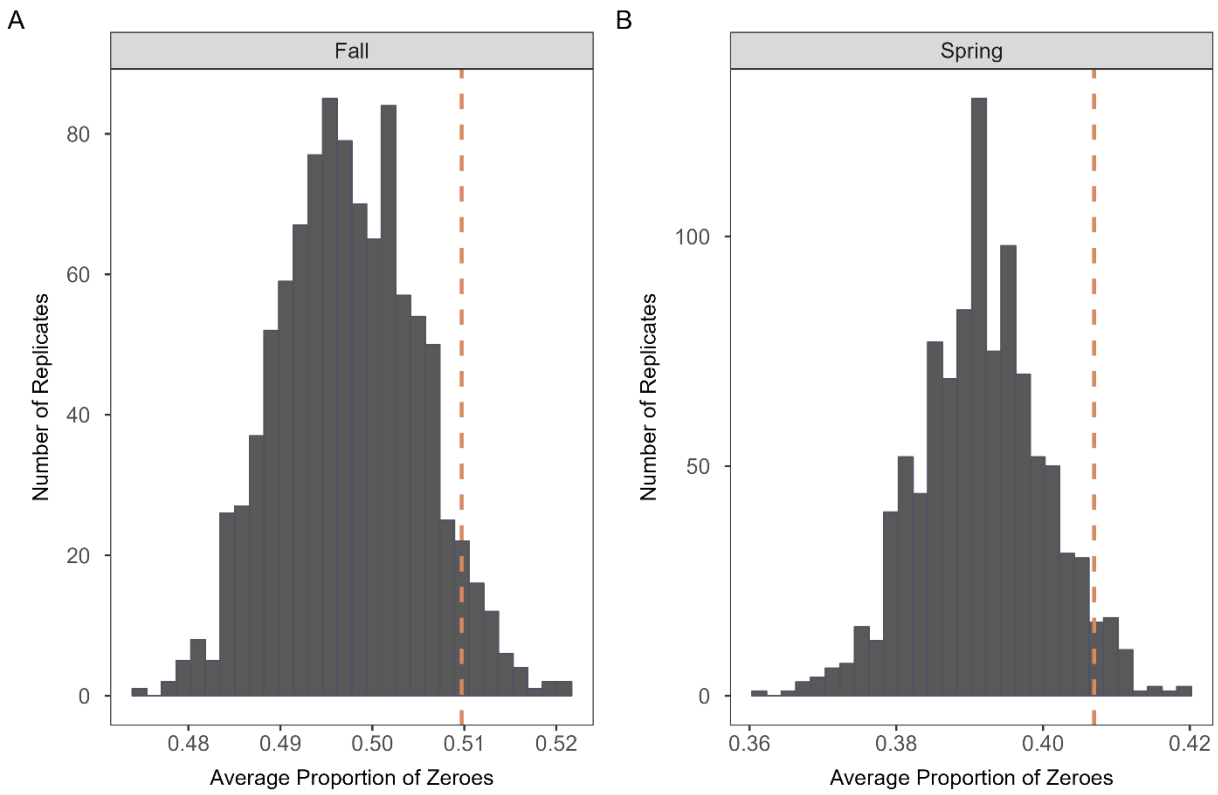

Figure 34. The distribution of simulated average proportion of zeroes generated by the A) fall summer flounder model, and B) spring summer flounder model. The observed average proportion of zeroes is represented by the orange dotted line.

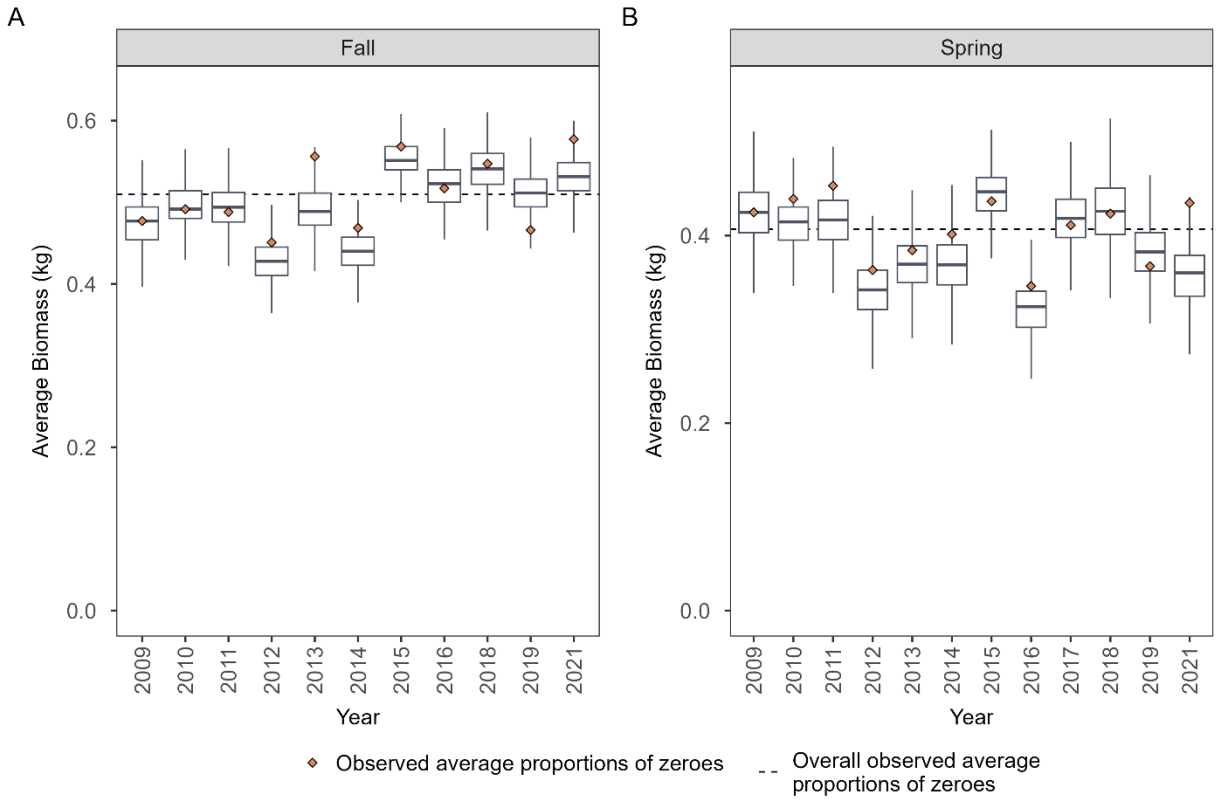

Figure 35. The distribution of simulated average proportions of zeroes in each year generated by the A) fall summer flounder model, and B) spring summer flounder model. The observed average proportion of zeroes in each year and season from the data is represented by the orange diamond. The overall observed average proportion of zeroes in each year is represented by the black dotted line. The effect of outliers has been removed from the distribution.

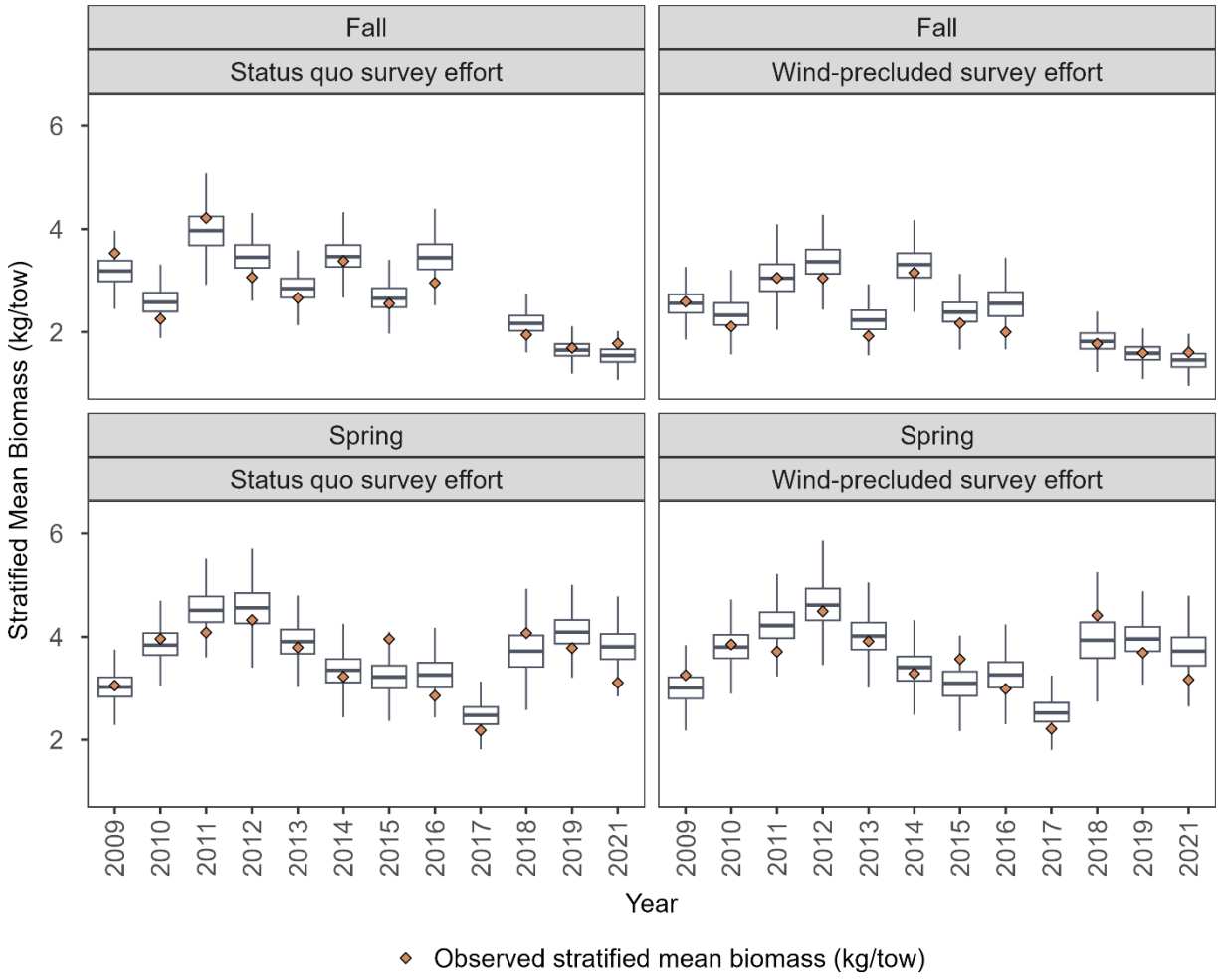

Figure 36. The distribution of simulated abundance indices in each year and under each survey effort scenario generated by the A) fall summer flounder model, and B) spring summer flounder model. The observed survey annual abundance indices in each year, season, and survey effort scenario from the data is represented by the orange diamond. The effect of outliers has been removed from the distribution.

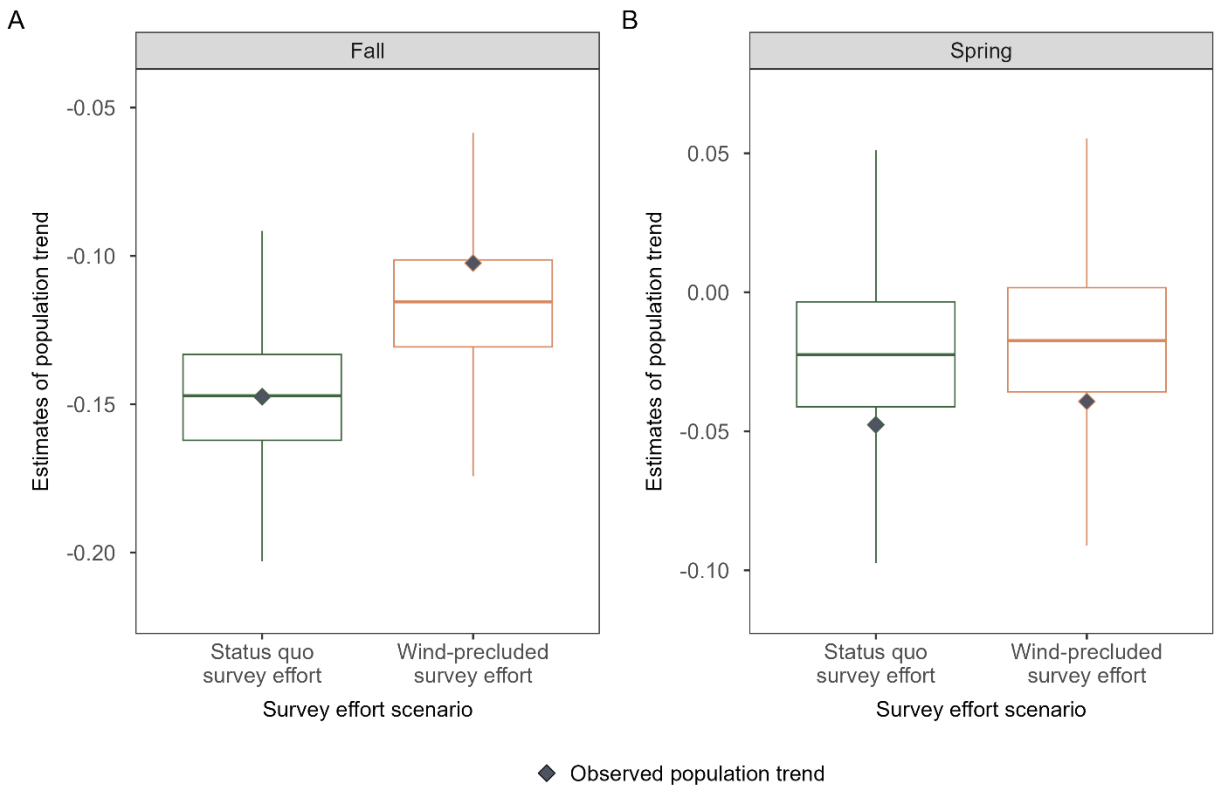

Figure 37. The distribution of estimates of population trend calculated with survey data simulated from A) the fall model fit for summer flounder and B) the spring model fit for summer flounder under status quo survey effort or under wind-precluded survey effort. The observed population trend by the survey under the respective survey effort scenarios and seasons are presented by the dark purple diamond, respectively. The effect of outliers has been removed from the distribution.

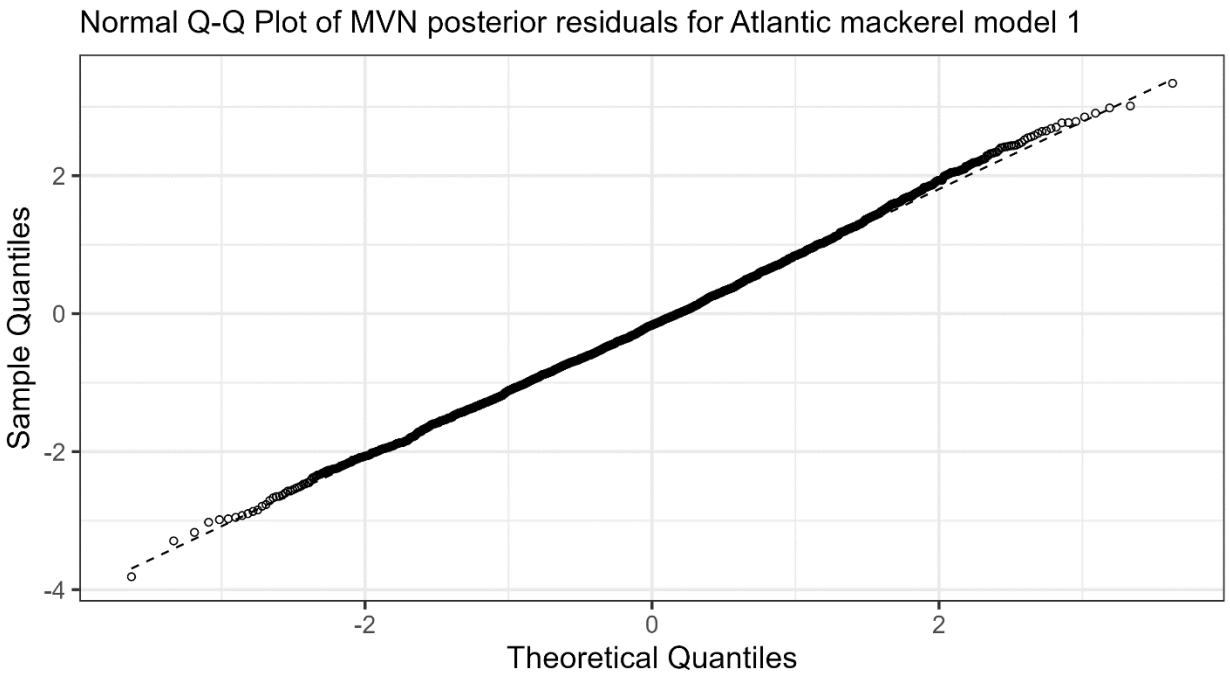

Figure 38. A quantile-quantile plot of observed quantiles of MVN residuals compared to the theoretical quantiles of residuals for the presence-absence component of the model fit to spring Atlantic mackerel survey data.

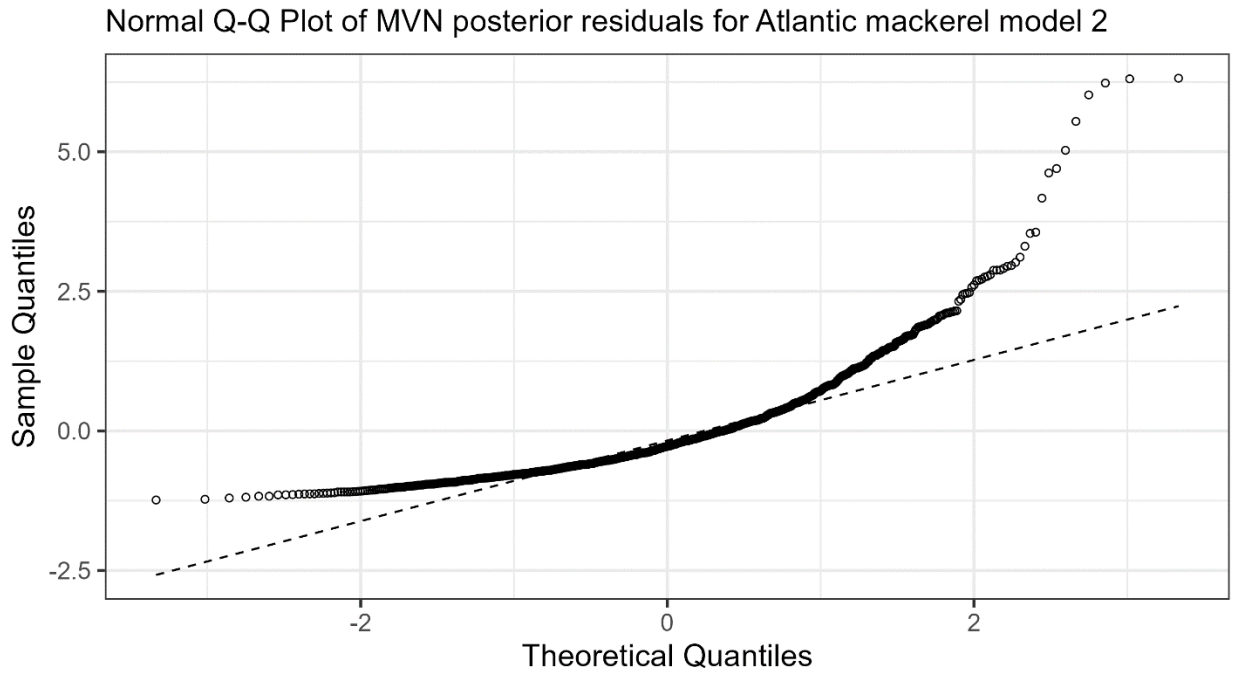

Figure 39. A quantile-quantile plot of observed quantiles of MVN residuals compared to the theoretical quantiles of residuals for the positive catch rate component of the model fit to spring Atlantic mackerel survey data.

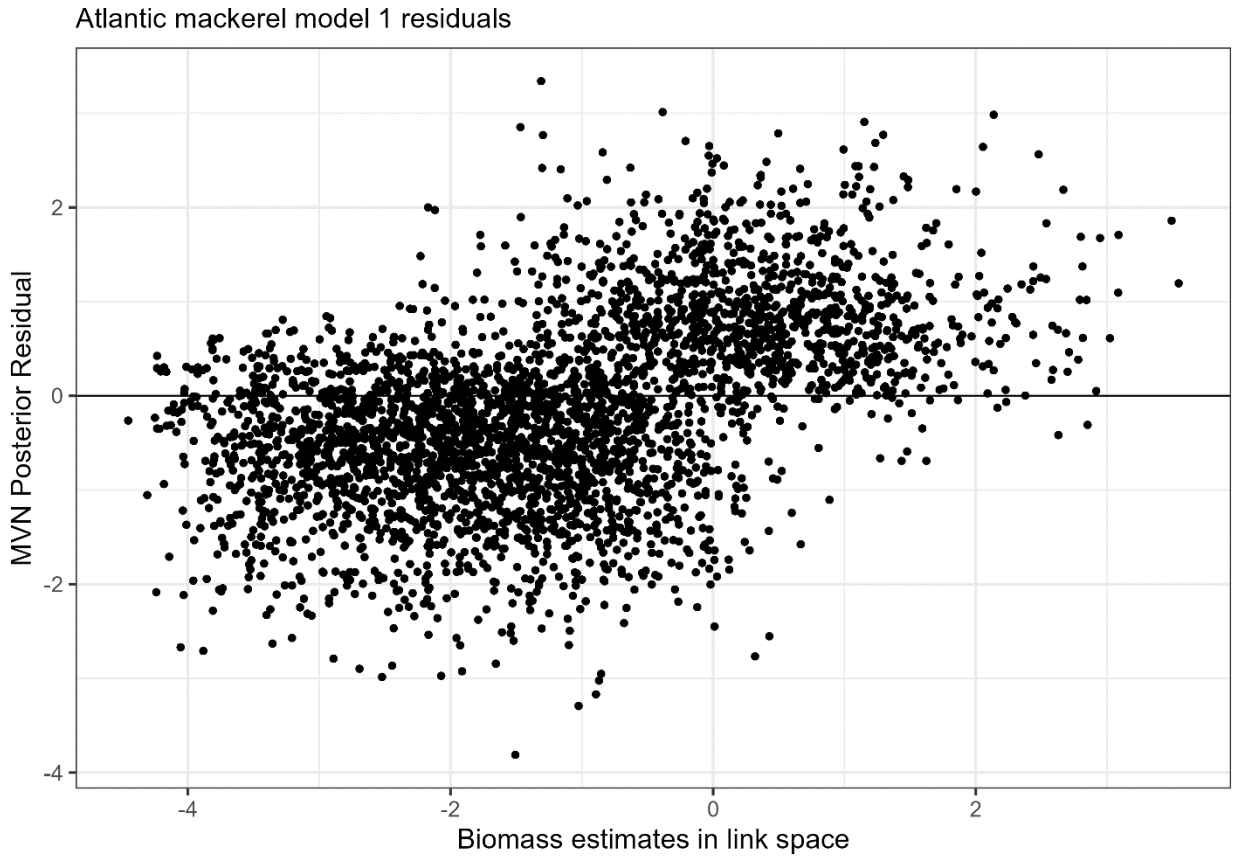

Figure 40. The distribution of MVN residuals predicted by the binomial (presence-absence) component of the spring model for Atlantic mackerel compared to the observed values of biomass in link space used to fit the model.

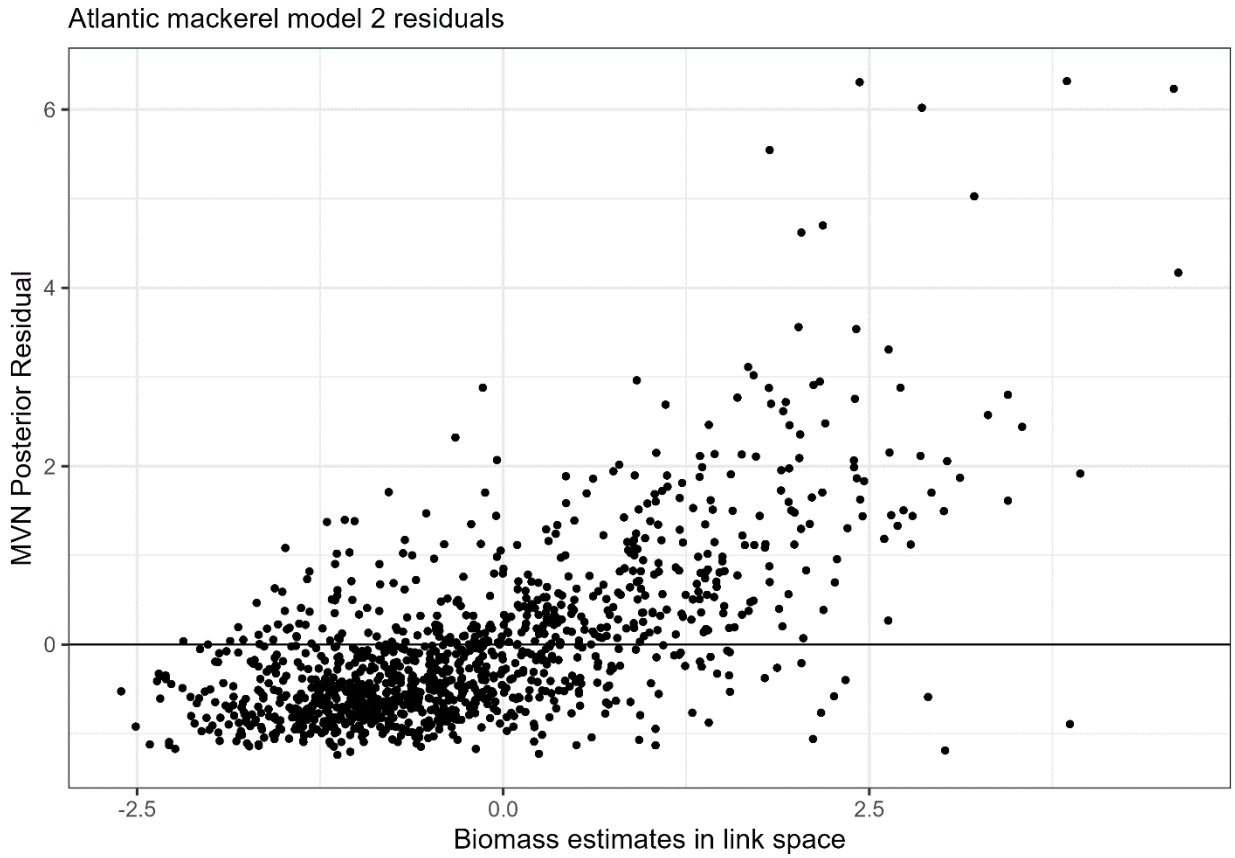

Figure 41. The distribution of MVN residuals predicted by the gamma (positive catch rate) component of the spring model for Atlantic mackerel compared to the observed values of biomass in link space used to fit the model.

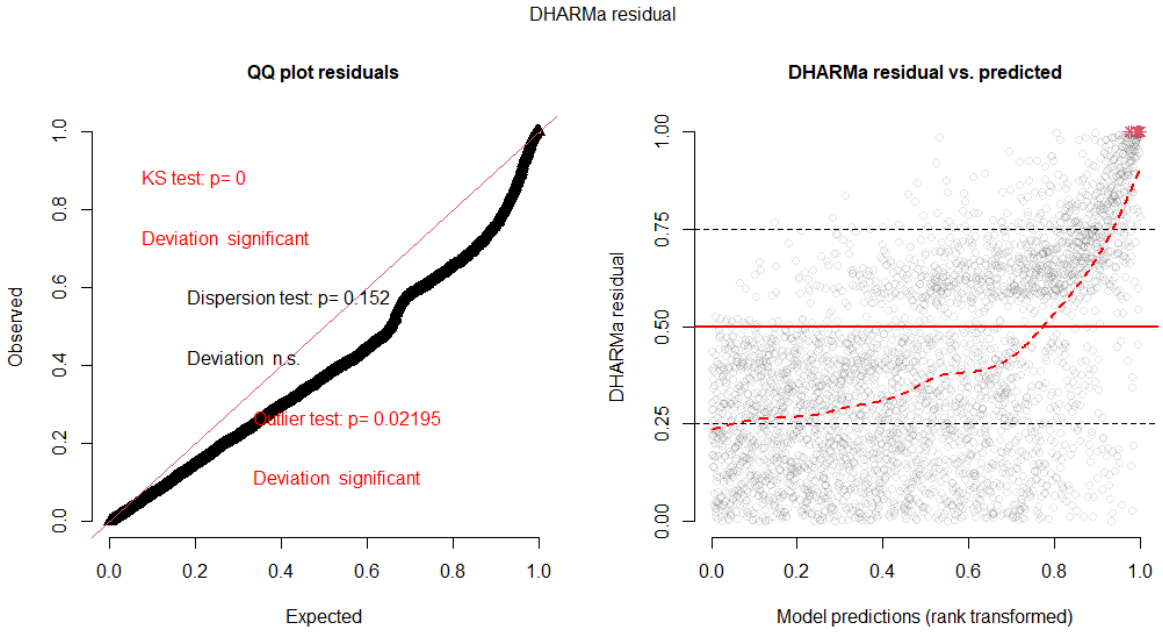

Figure 42. The quantile-quantile plot of DHARMa-simulated residuals (left plot) and the distribution of residuals plotted against the predicted values (right plot) from the optimal Atlantic mackerel model.

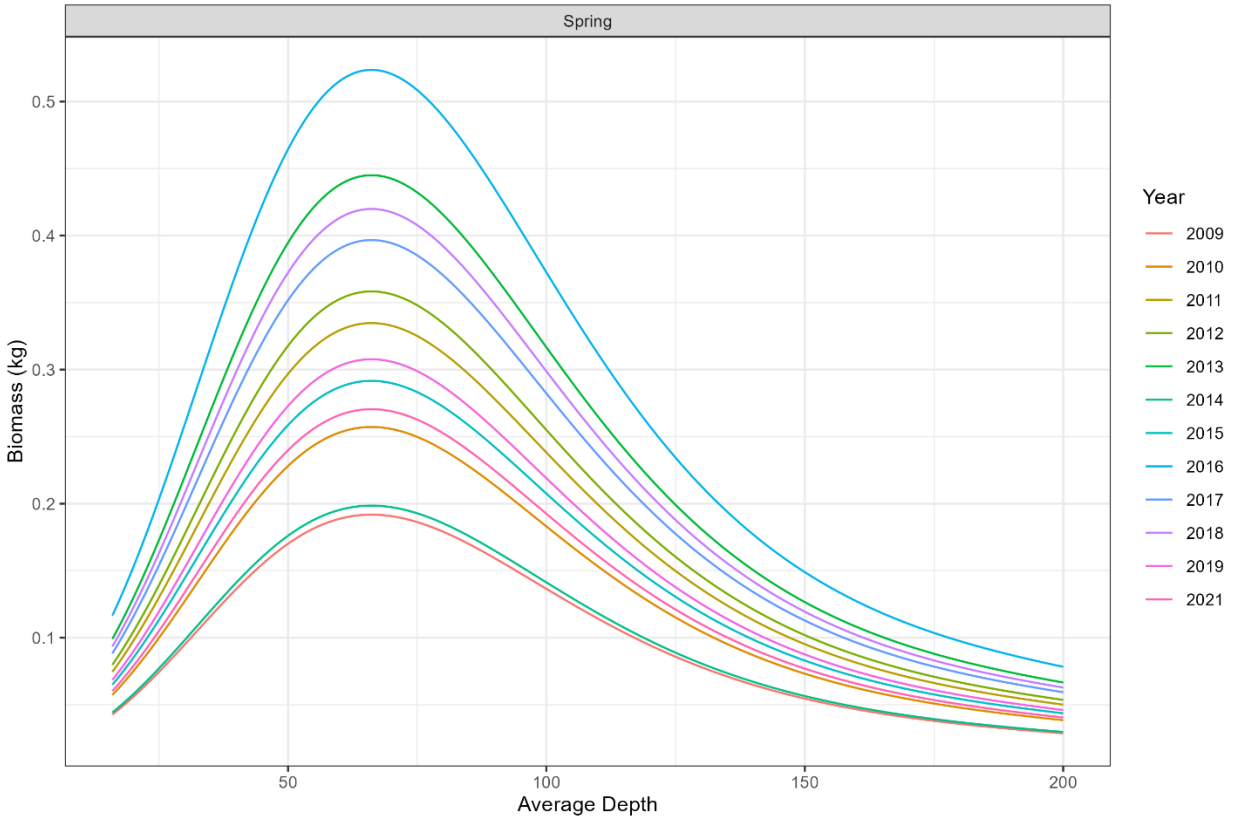

Figure 43. The marginal effect of depth and year on Atlantic mackerel biomass catch rates predicted by the spring combined Delta Gamma model (model 5;Table 14).

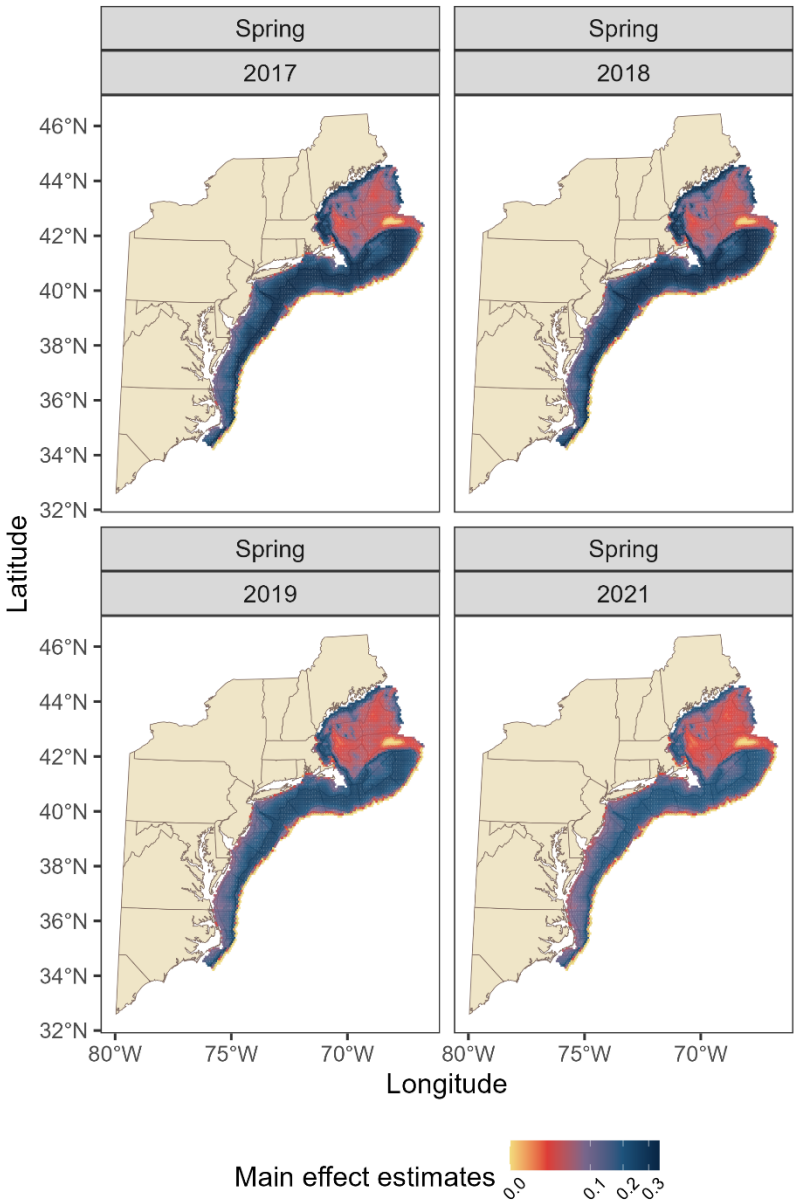

Figure 44. Spring estimates of the fixed effects for the most recent four years in the time series from the model for Atlantic mackerel.

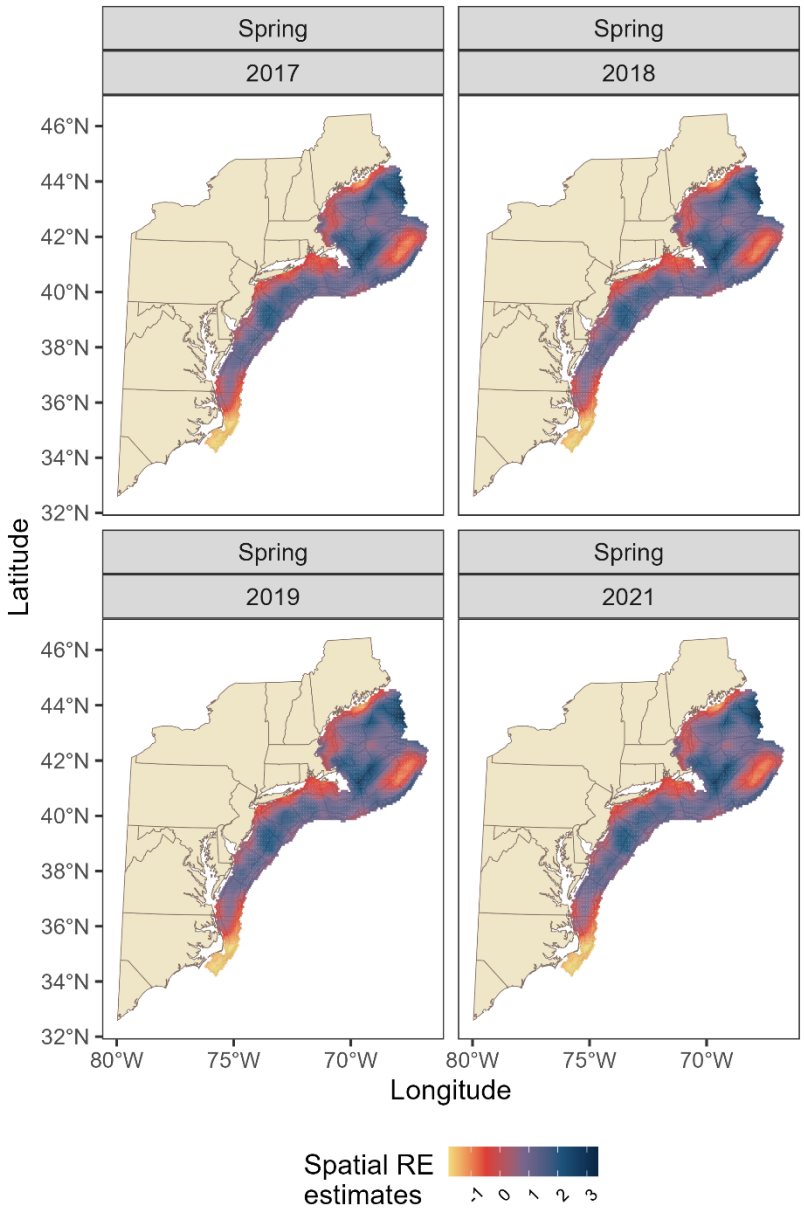

Figure 45. Spring estimates of the spatial random effects from the model for Atlantic mackerel.

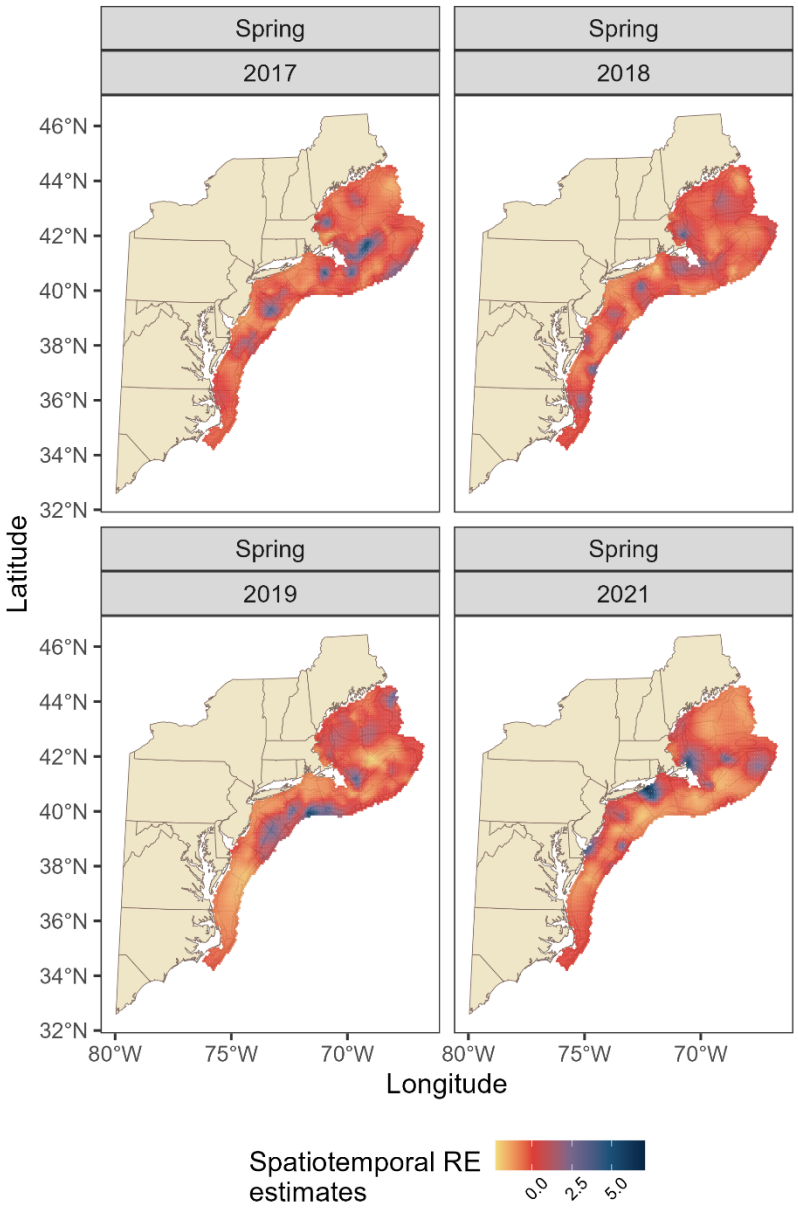

Figure 46. Spring estimates of the spatiotemporal random effects for the most recent four years in the time series from the model for Atlantic mackerel.

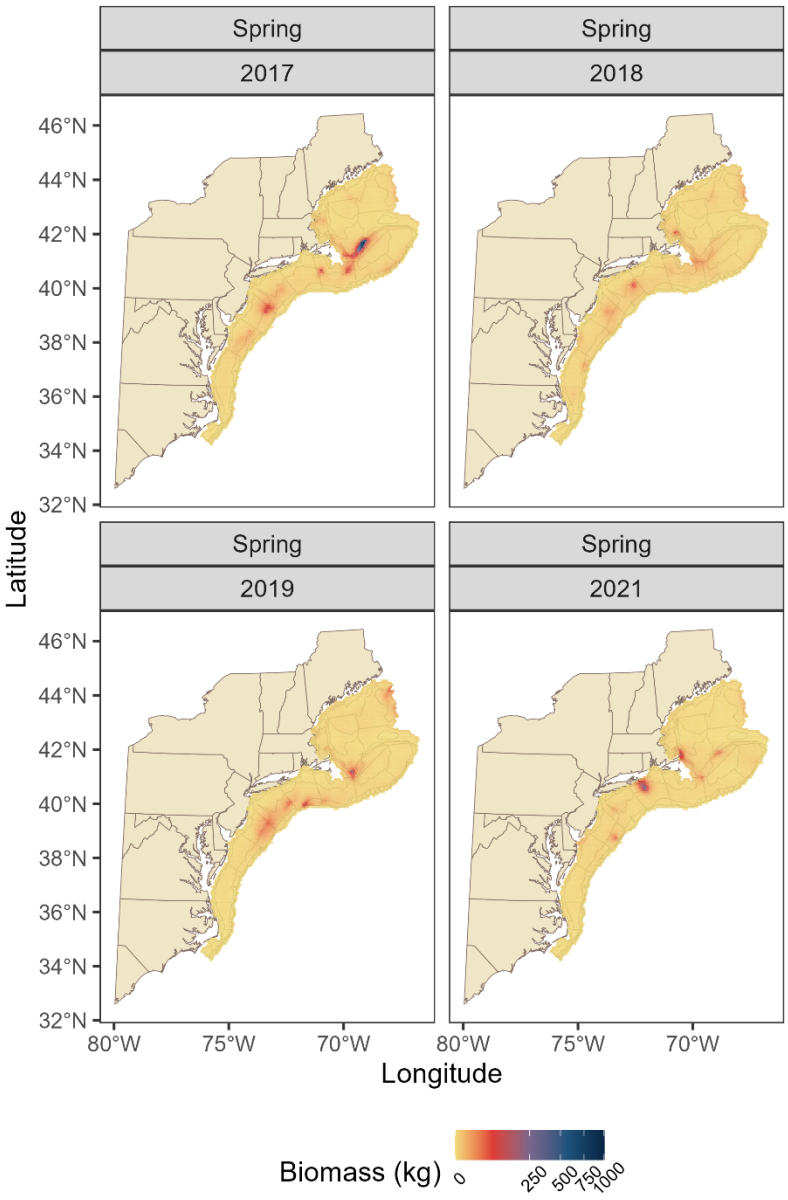

Figure 47. Spring predictions of Atlantic mackerel biomass extrapolated from the model across the sampling frame for the most recent four years in the time series.

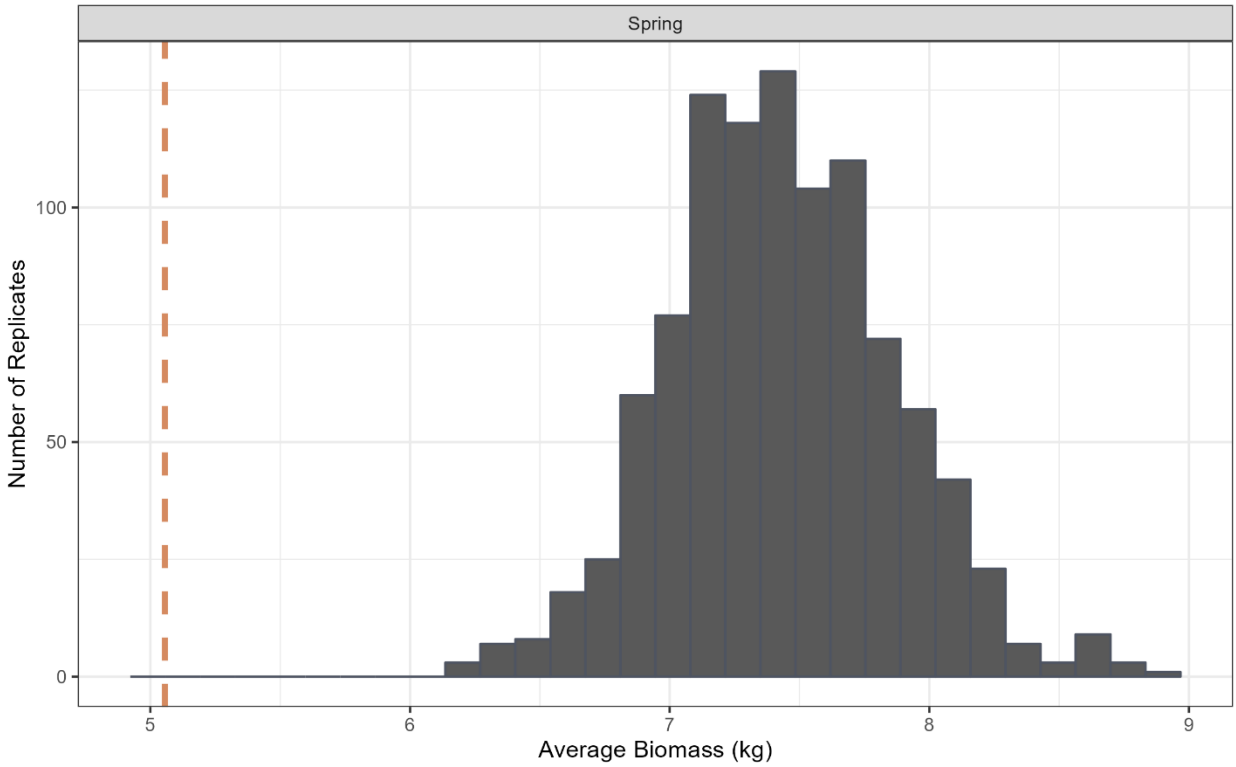

Figure 48. The distribution of simulated average biomass catch rates generated by the spring Atlantic mackerel model. The observed average survey biomass catch rate is represented by the orange dotted line.

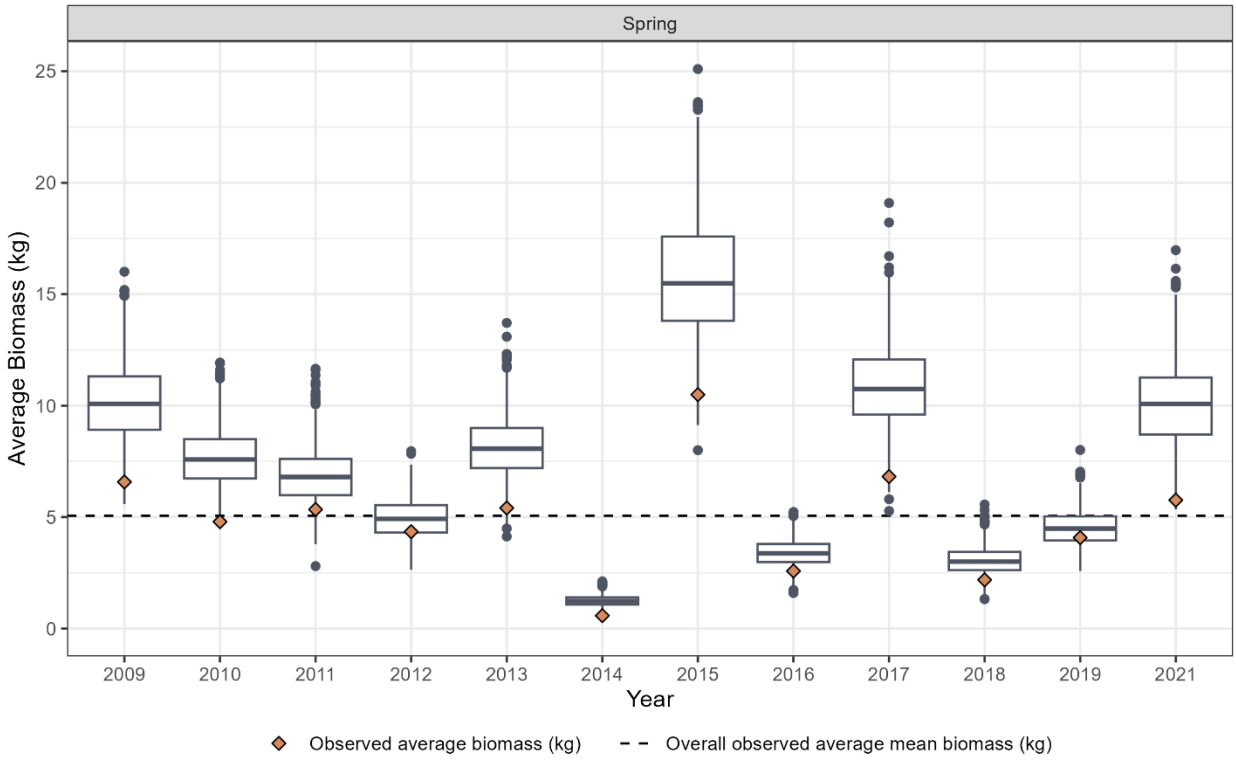

Figure 49. The distribution of simulated average biomass catch rates in each year generated by the optimal Atlantic mackerel model. The observed spring survey biomass catch rate in each year from the data is represented by the orange diamond. The overall nominal average of biomass catch rate is represented by the black dotted line. The effect of outliers has been removed from the distribution.

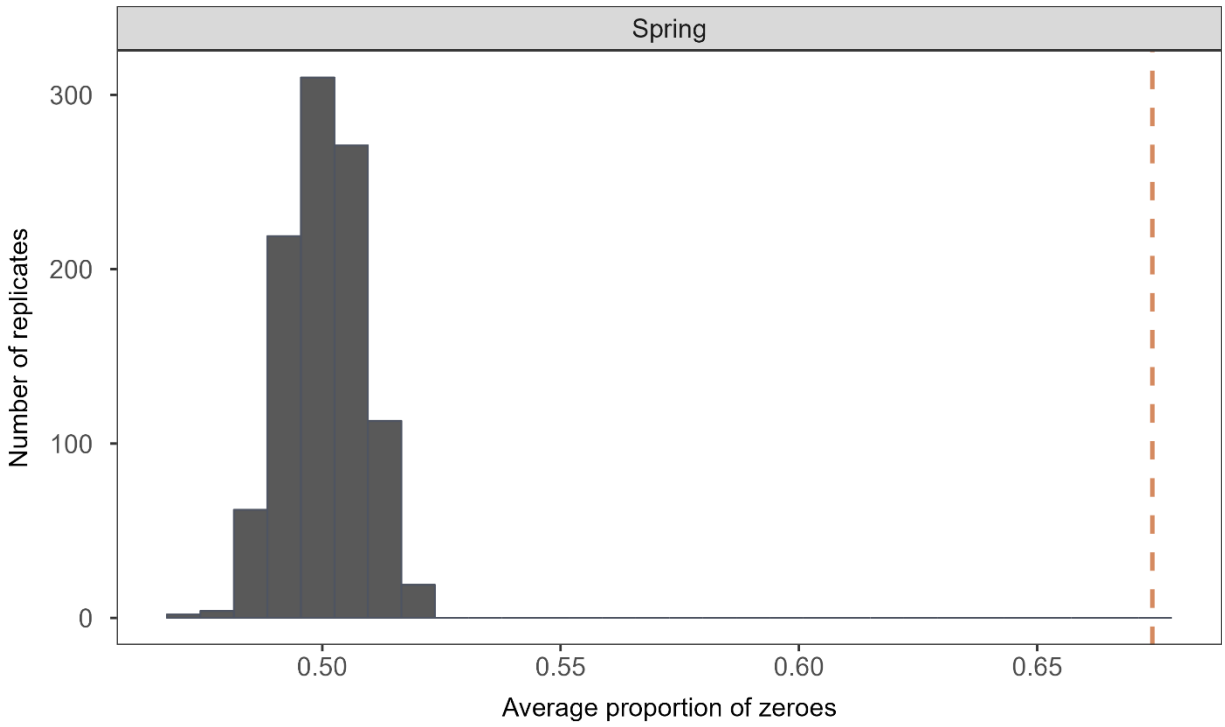

Figure 50. The distribution of simulated proportions of zeroes generated by the spring Atlantic mackerel model. The observed proportion of zeroes is represented by the orange dotted line.

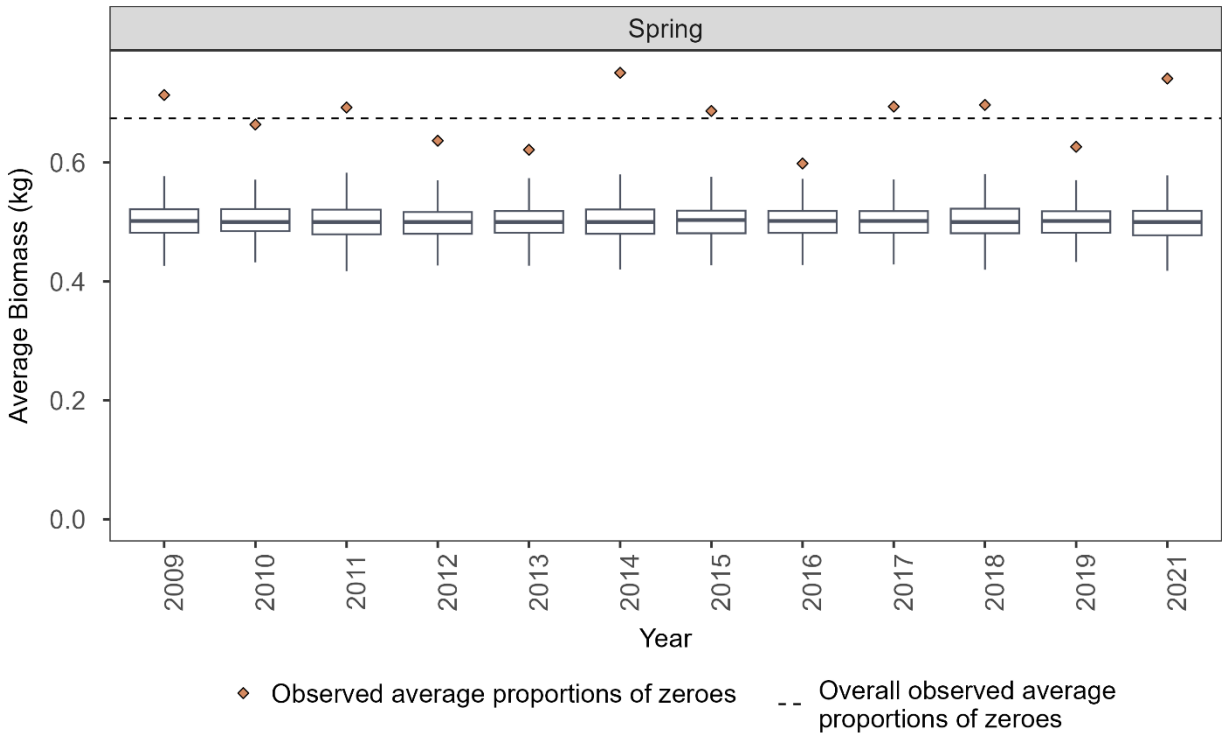

Figure 51. The distribution of simulated proportions of zeroes in each year generated by the optimal Atlantic mackerel model. The observed proportion of zeroes in each year from the data is represented by the orange diamond. The overall proportion of zeroes is represented by the black dotted line. The effect of outliers has been removed from the distribution.

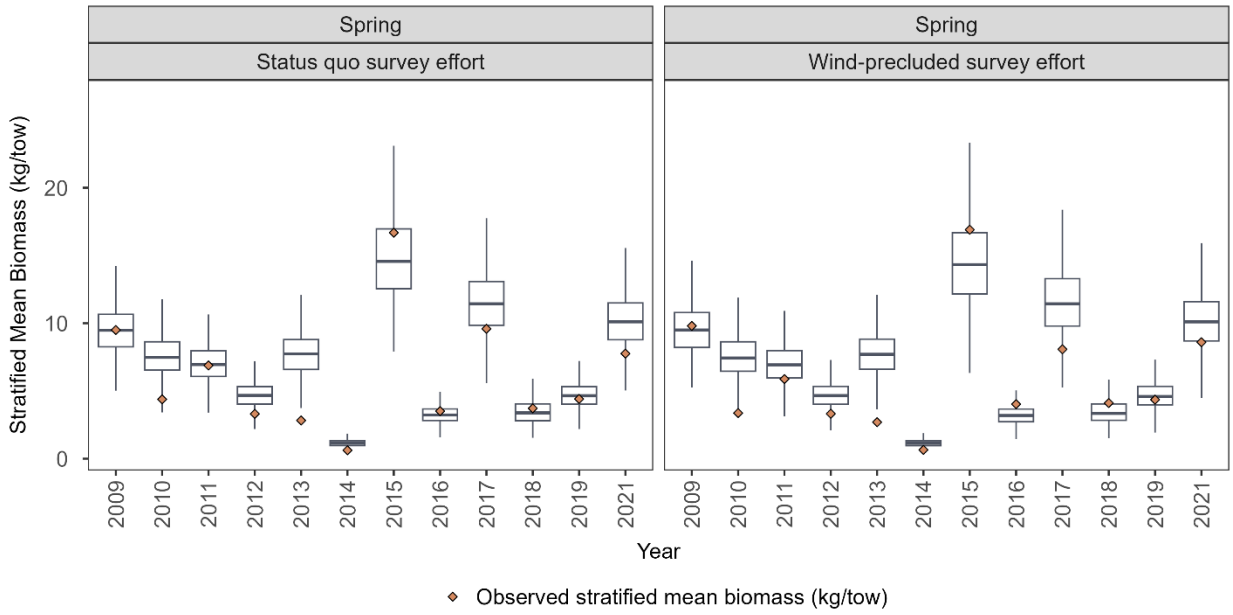

Figure 52. The distribution of simulated annual abundance indices in each year and under each survey effort scenario generated by the optimal Atlantic mackerel model. The observed spring annual abundance indices in each year from the data and under the respective survey effort scenario is represented by the orange diamond. The effect of outliers has been removed from the distribution.

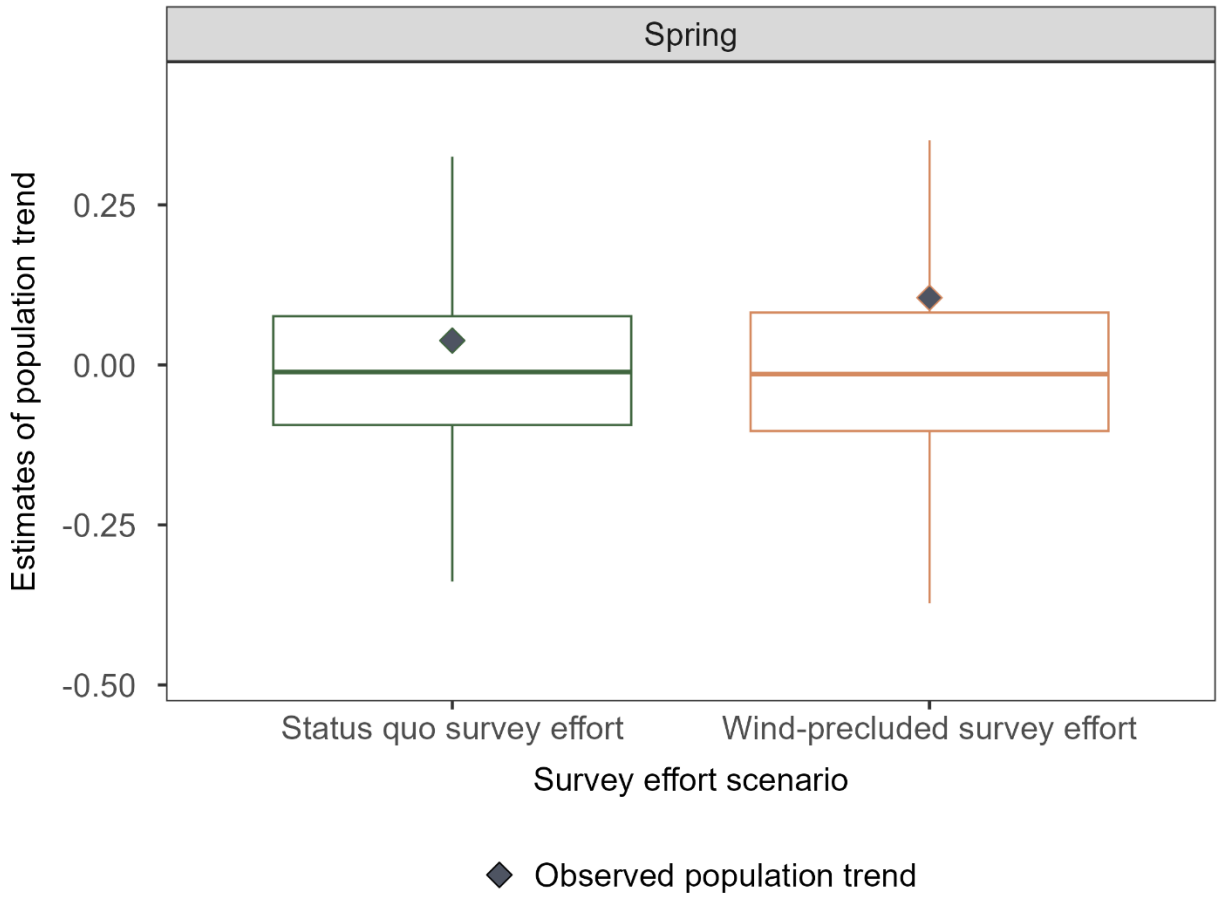

Figure 53. The distribution of estimates of population trend calculated with survey data simulated from the spring model fit for Atlantic mackerel under status quo survey effort (green boxplot) or under wind-precluded survey effort (orange boxplot). The observed population trend by the survey under the respective survey effort scenarios is presented by the dark purple diamond, respectively. The effect of outliers has been removed from the distribution.

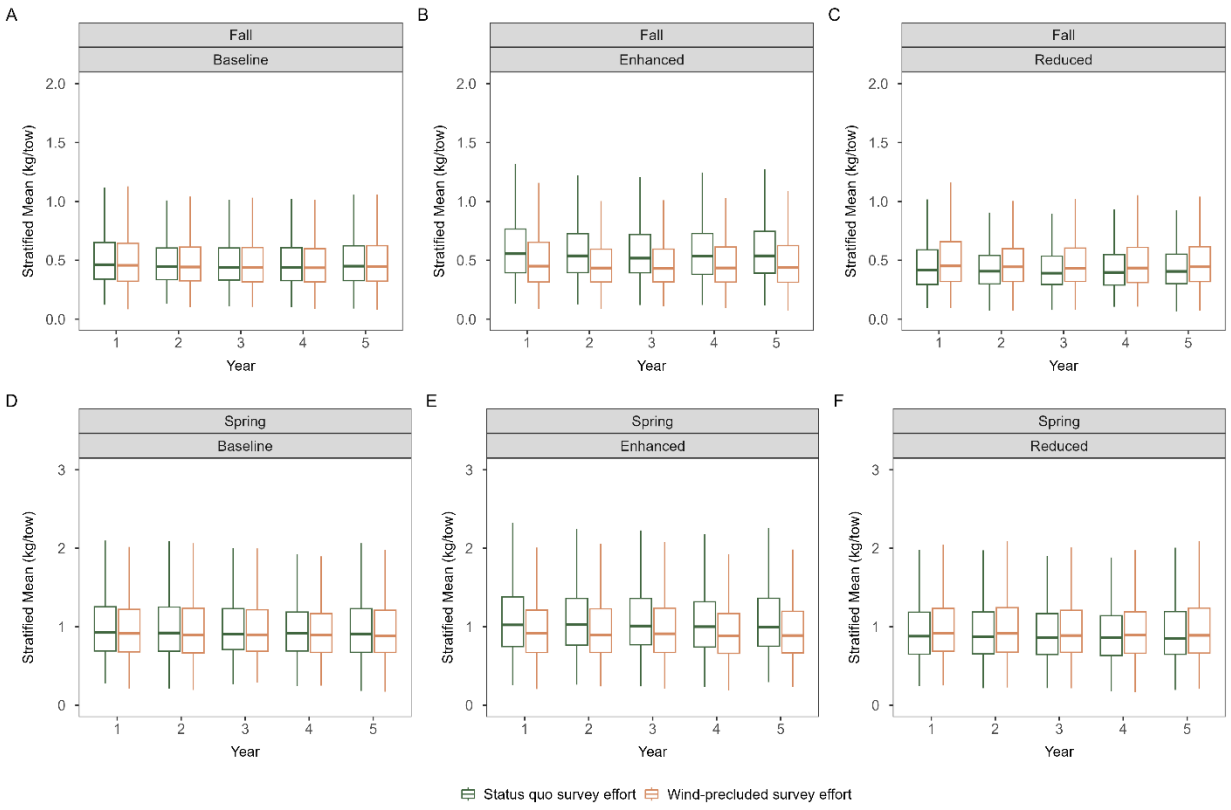

Figure 54. The distribution of simulated annual abundance indices in each year for A-C) fall summer flounder populations and D-F) spring summer flounder populations under status quo survey effort (green boxplots) and wind-precluded survey effort (orange boxplots) in each of the productivity treatments: baseline fish density (left panels), enhanced fish density (middle panels), and reduced fish density (right panels). The effect of outliers has been removed from the distribution.

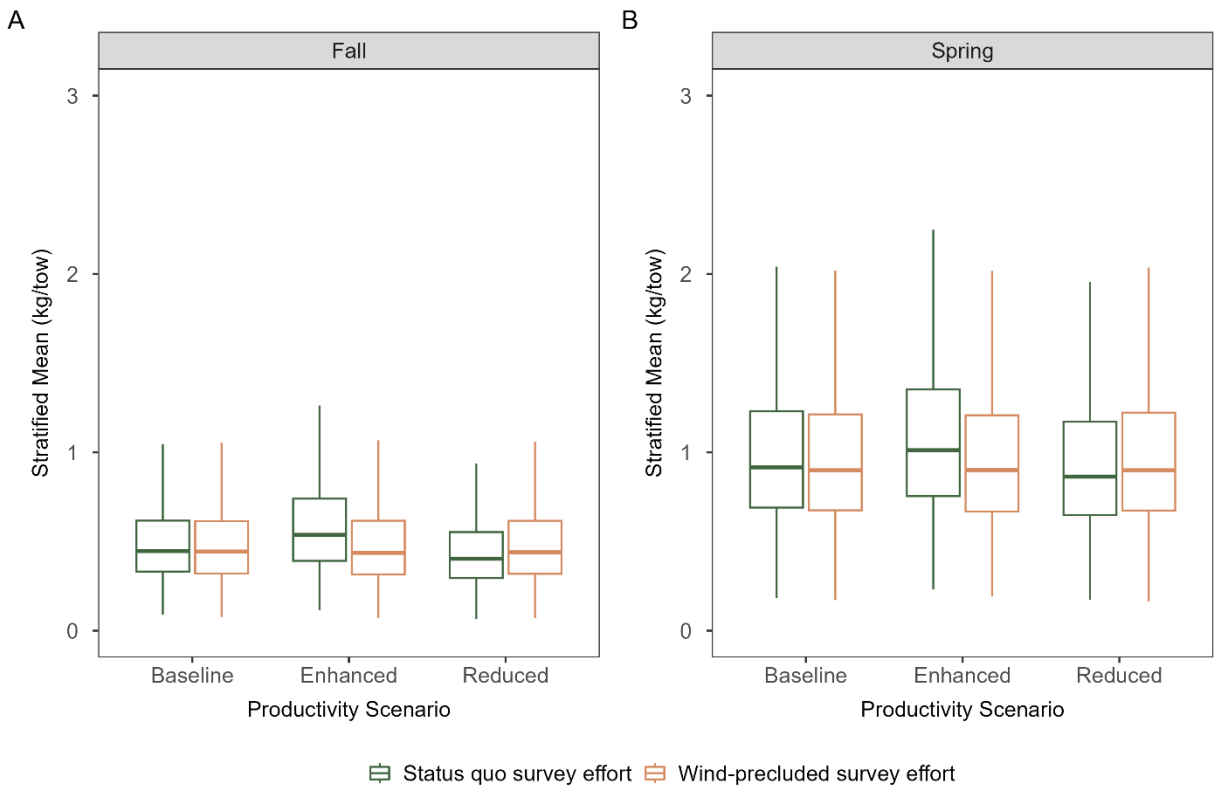

Figure 55. The distribution of annual abundance indices calculated for A) fall summer flounder populations and B) spring summer flounder populations under status quo survey effort (green boxplots) and wind-precluded survey effort (orange boxplots) over the simulated five-year time series across the productivity treatments: baseline, enhanced, and reduced fish density. The effect of outliers has been removed from the distribution.

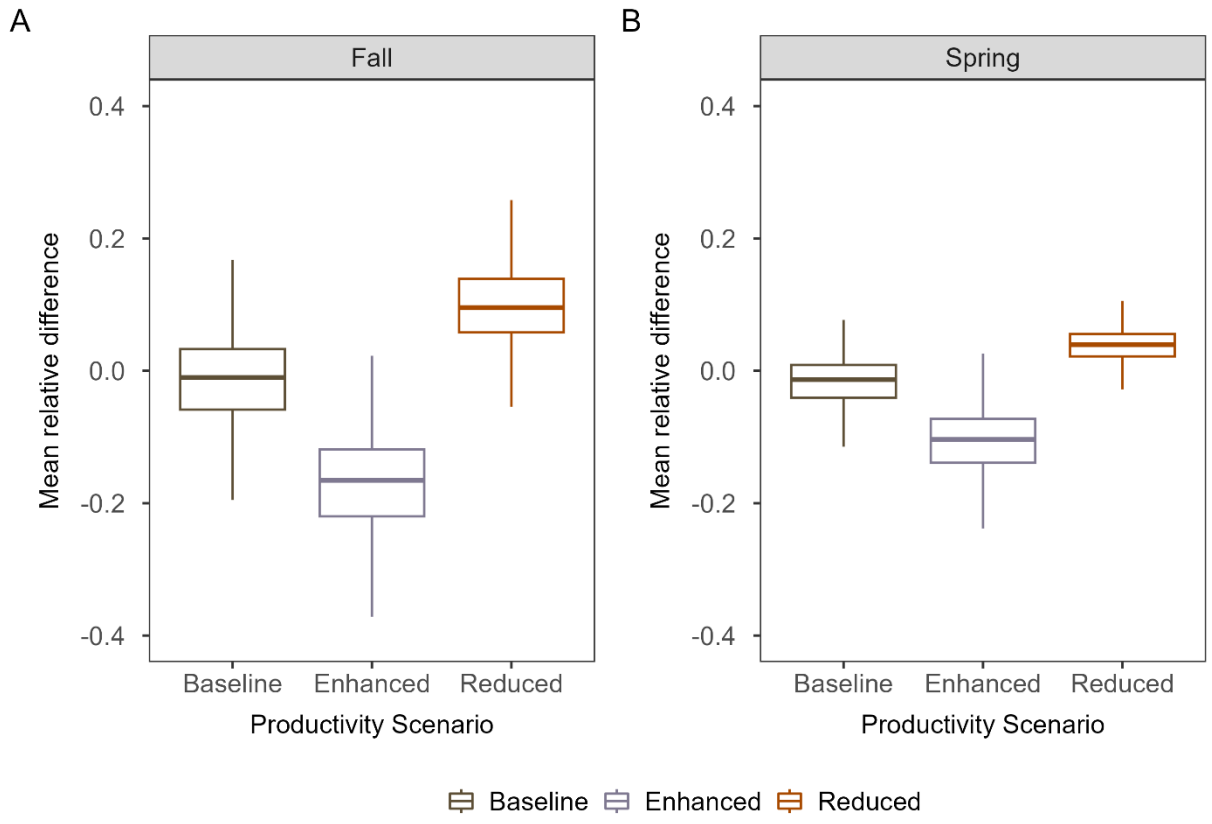

Figure 56. The distribution of relative differences between annual abundance indices calculated for A) fall summer flounder populations and B) spring summer flounder populations under status quo and wind-precluded survey effort averaged over the simulated five-year time series across the productivity treatments: baseline, enhanced, and reduced fish density. The effect of outliers has been removed from the distribution.

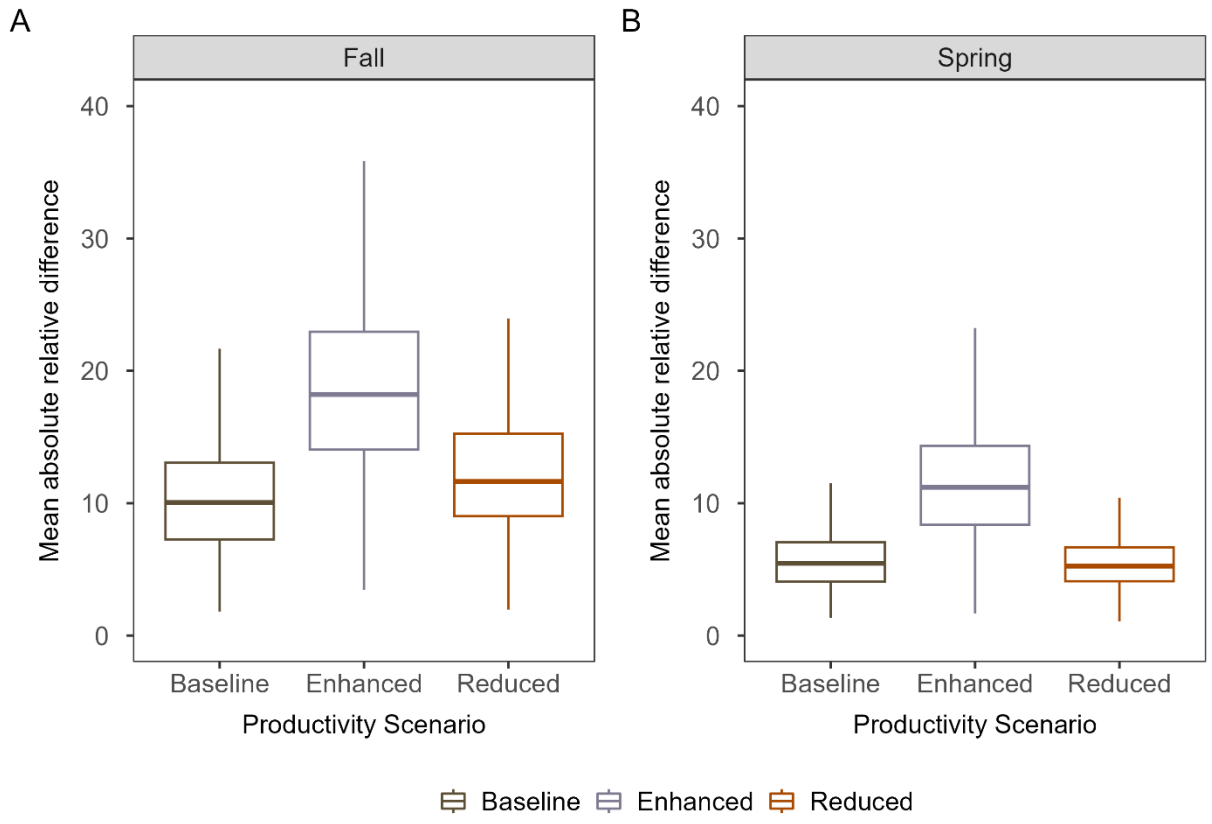

Figure 57. The distribution of absolute relative differences between annual abundance indices calculated for A) fall summer flounder populations and B) spring summer flounder populations under status quo and wind-precluded survey effort averaged over the simulated five-year time series across the productivity treatments: baseline, enhanced, and reduced fish density. The effect of outliers has been removed from the distribution.

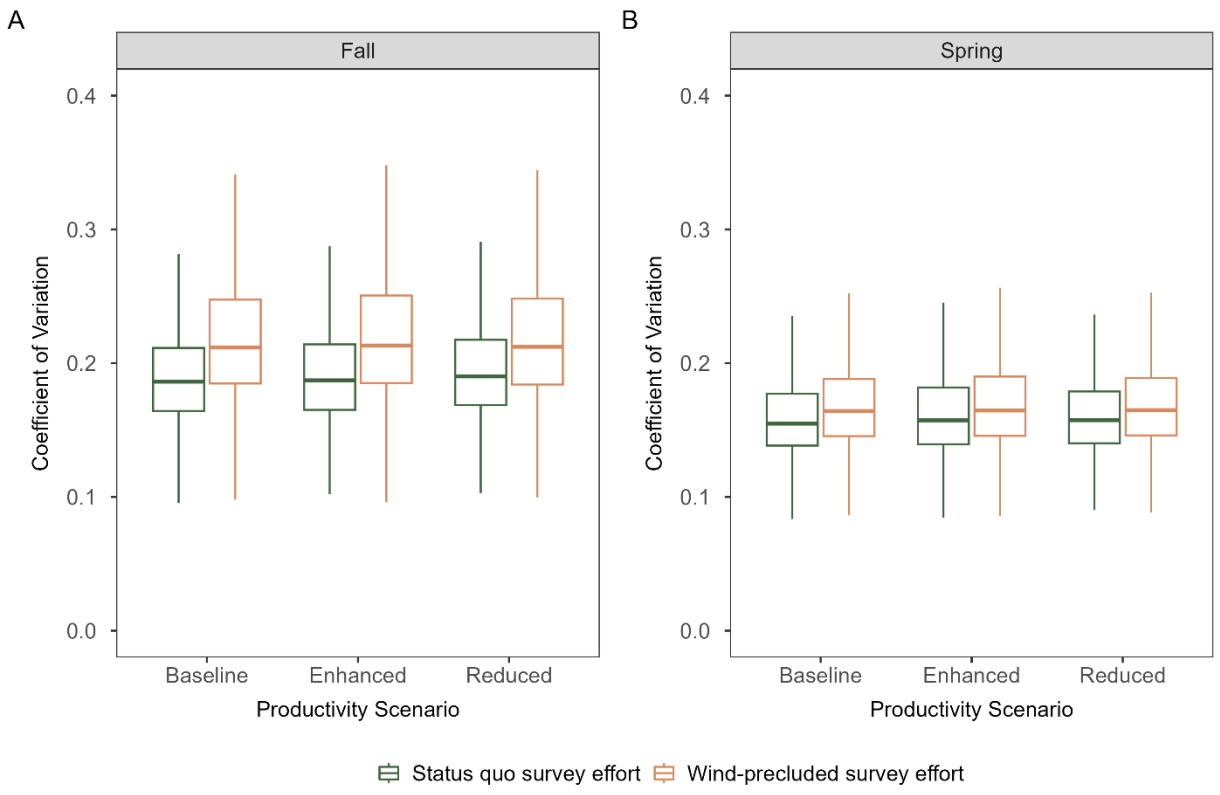

Figure 58. The distribution of coefficient of variations (CVs) of A) fall summer flounder abundance indices and B) spring summer flounder abundance indices calculated under status quo survey effort (green boxplots) and wind-precluded survey effort (orange boxplots) over the simulated five-year time series across the productivity treatments: baseline, enhanced, and reduced fish density. The effect of outliers has been removed from the distribution.

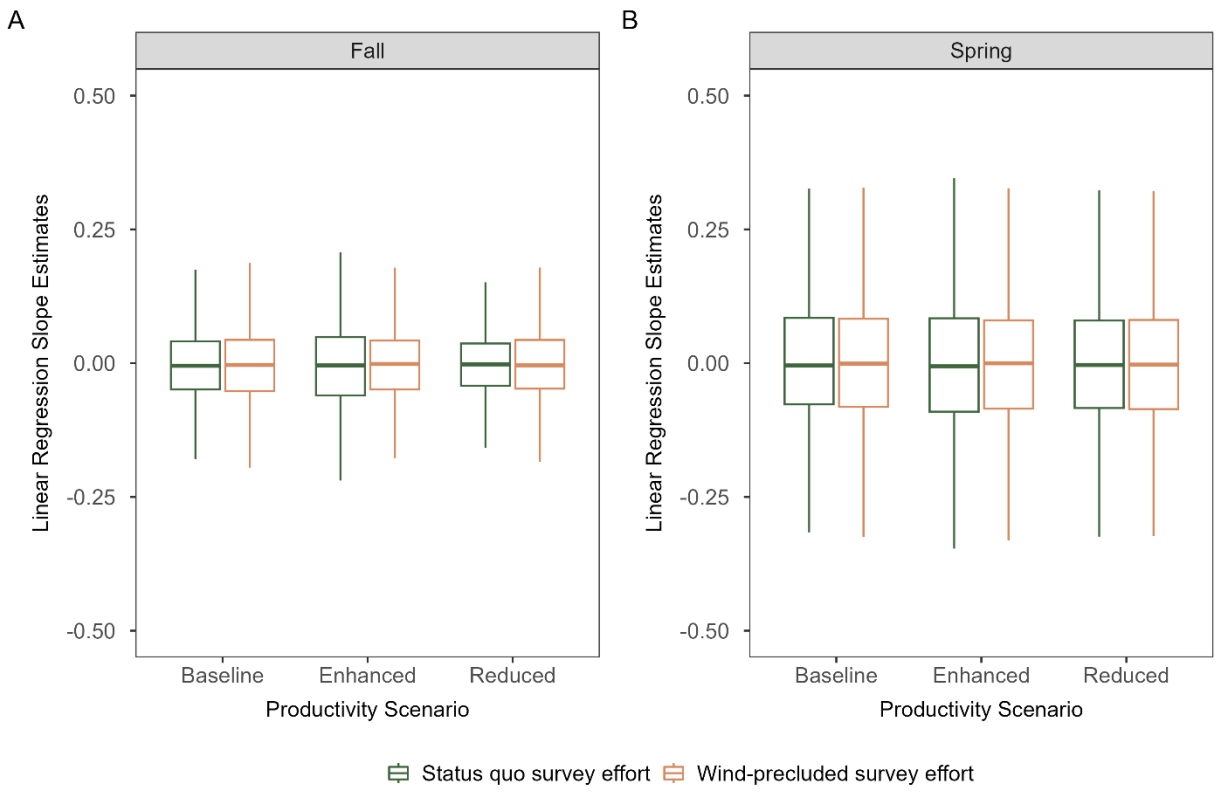

Figure 59. The distribution of changes in A) fall summer flounder population trends and B) spring summer flounder population trends calculated under status quo survey effort (green boxplots) and wind-precluded survey effort (orange boxplots) over the simulated five-year time series across the productivity treatments: baseline, enhanced, and reduced fish density. The effect of outliers has been removed from the distribution.

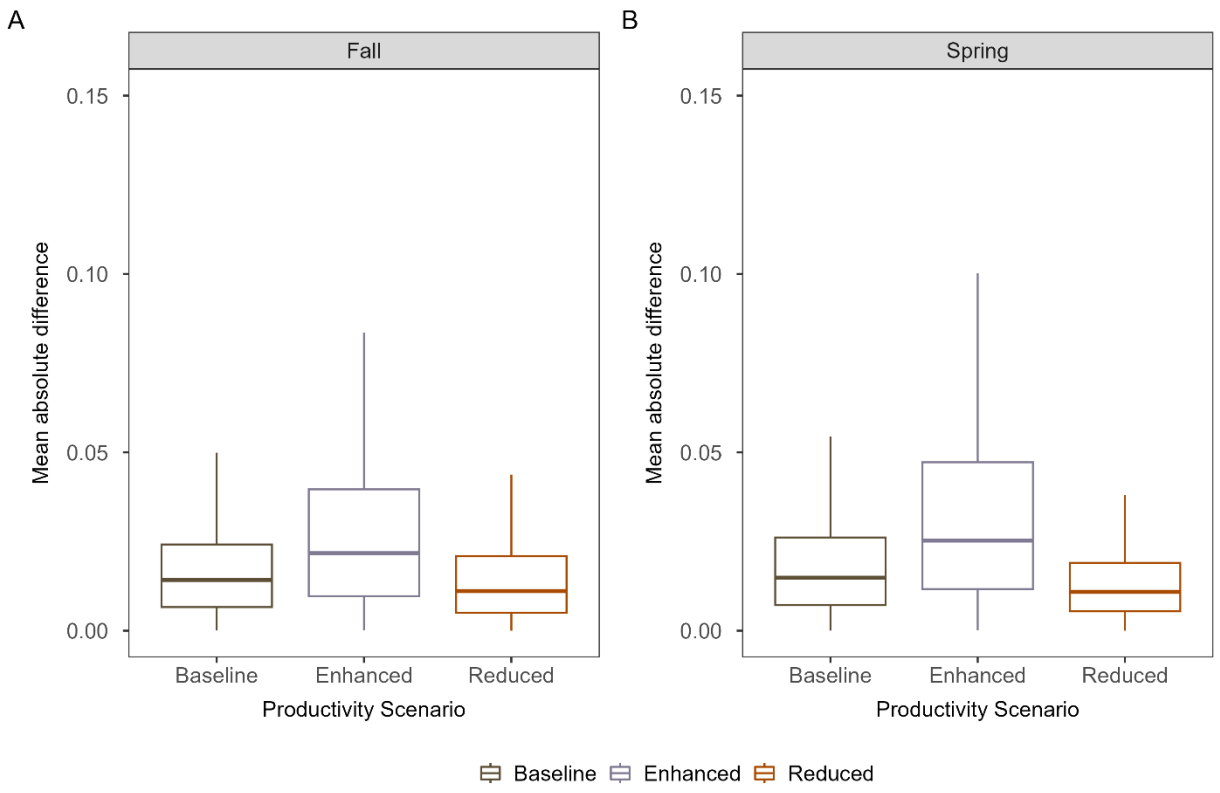

Figure 60. The distribution of absolute differences between A) fall summer flounder population trends and B) spring summer flounder population trends calculated under status quo survey effort and wind-precluded survey effort over the simulated five-year time series across the productivity treatments: baseline, enhanced, and reduced fish density. The effect of outliers has been removed from the distribution.

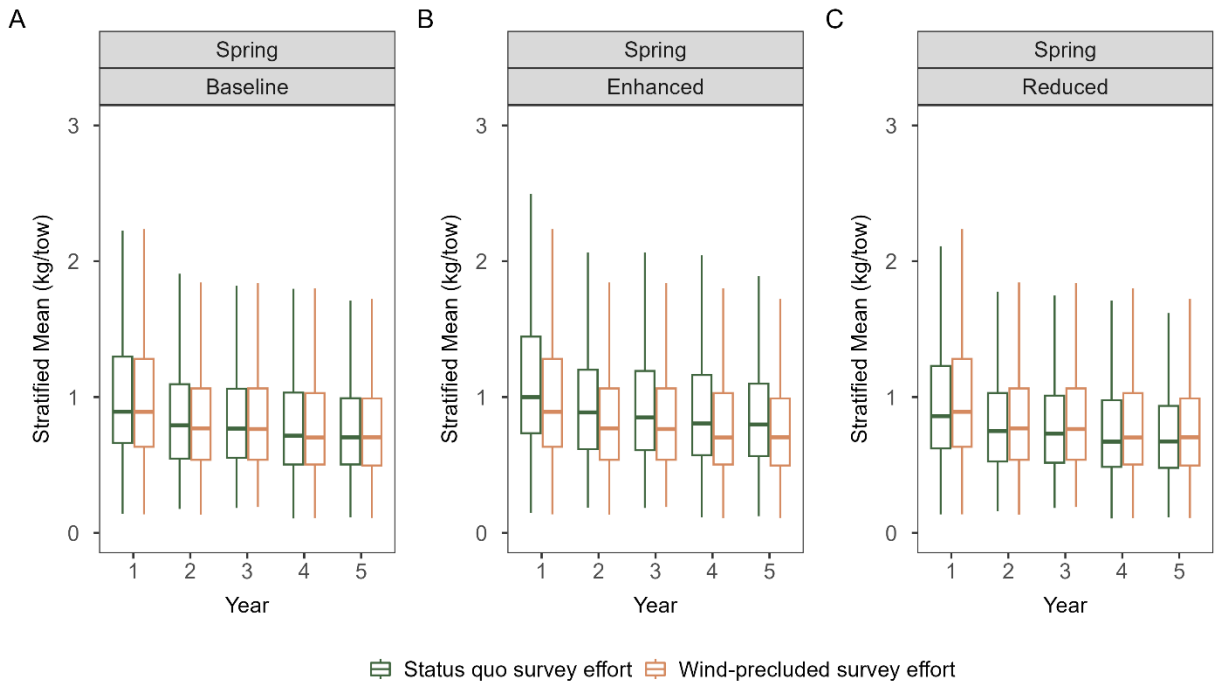

Figure 61. The distribution of simulated annual abundance indices in each year for spring Atlantic mackerel populations under status quo survey effort (green boxplots) and wind-precluded survey effort (orange boxplots) in each of the productivity treatments: A) baseline fish density, B) enhanced fish density, and C) reduced fish density. The effect of outliers has been removed from the distribution.

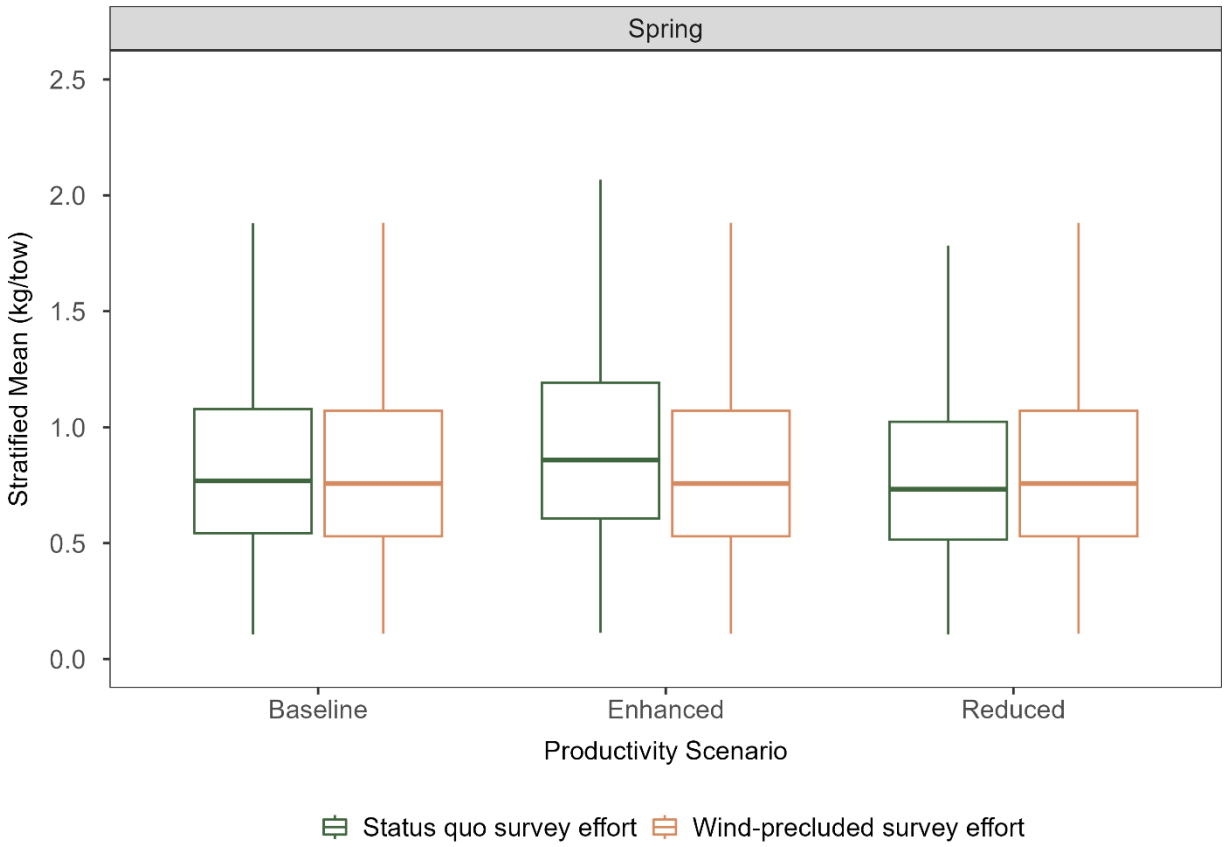

Figure 62. The distribution of Atlantic mackerel abundance indices calculated under status quo survey effort (green boxplots) and wind-precluded survey effort (orange boxplots) over the simulated five-year time series across the productivity treatments: baseline, enhanced, and reduced fish density. Y-axis has been modified to remove the effect of outliers on the distribution. The effect of outliers has been removed from the distribution.

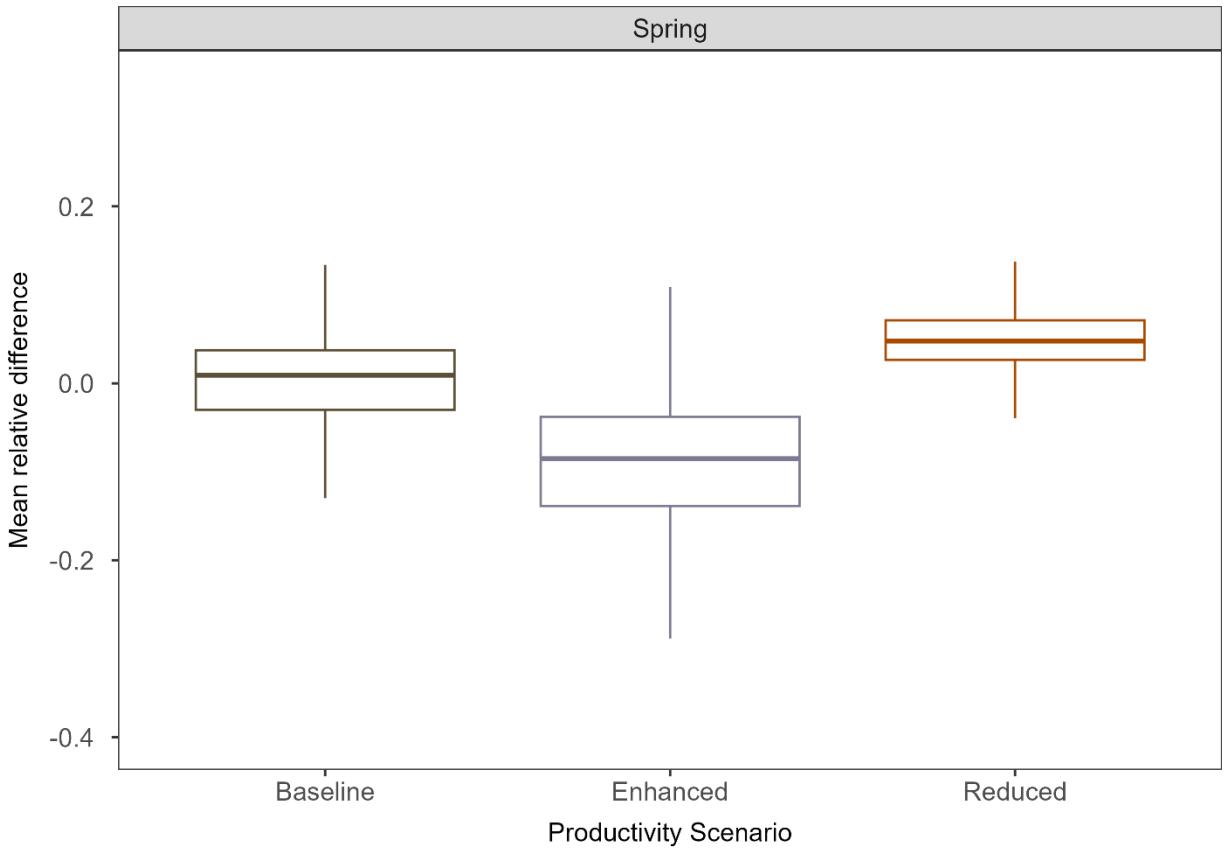

Figure 63. The distribution of relative differences between annual abundance indices calculated for spring Atlantic mackerel populations under status quo and wind-precluded survey effort averaged over the simulated five-year time series across the productivity treatments: baseline, enhanced, and reduced fish density. The effect of outliers has been removed from the distribution.

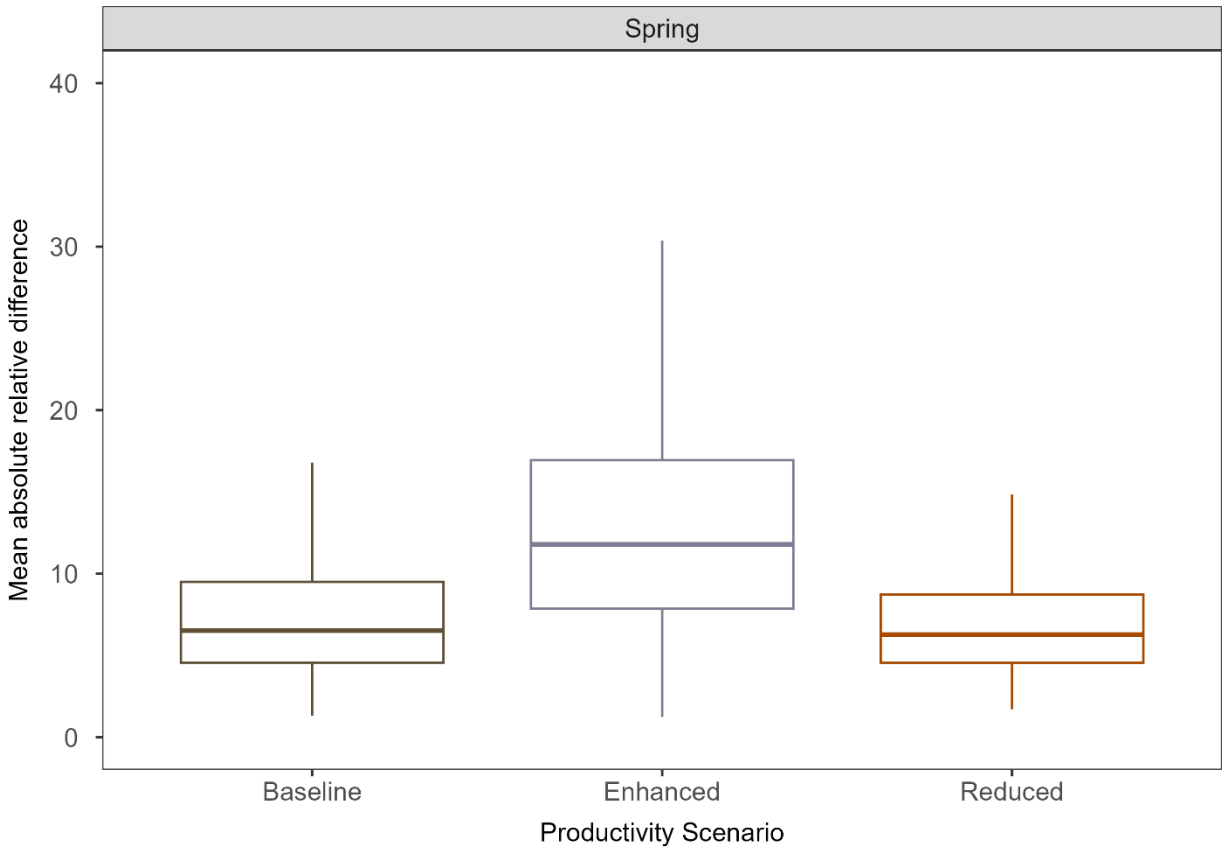

Figure 64. The distribution of absolute relative differences between annual abundance indices for Atlantic mackerel calculated under status quo and wind-precluded survey effort averaged over the simulated five-year time series across the productivity treatments: baseline, enhanced, and reduced fish density. The effect of outliers has been removed from the distribution.

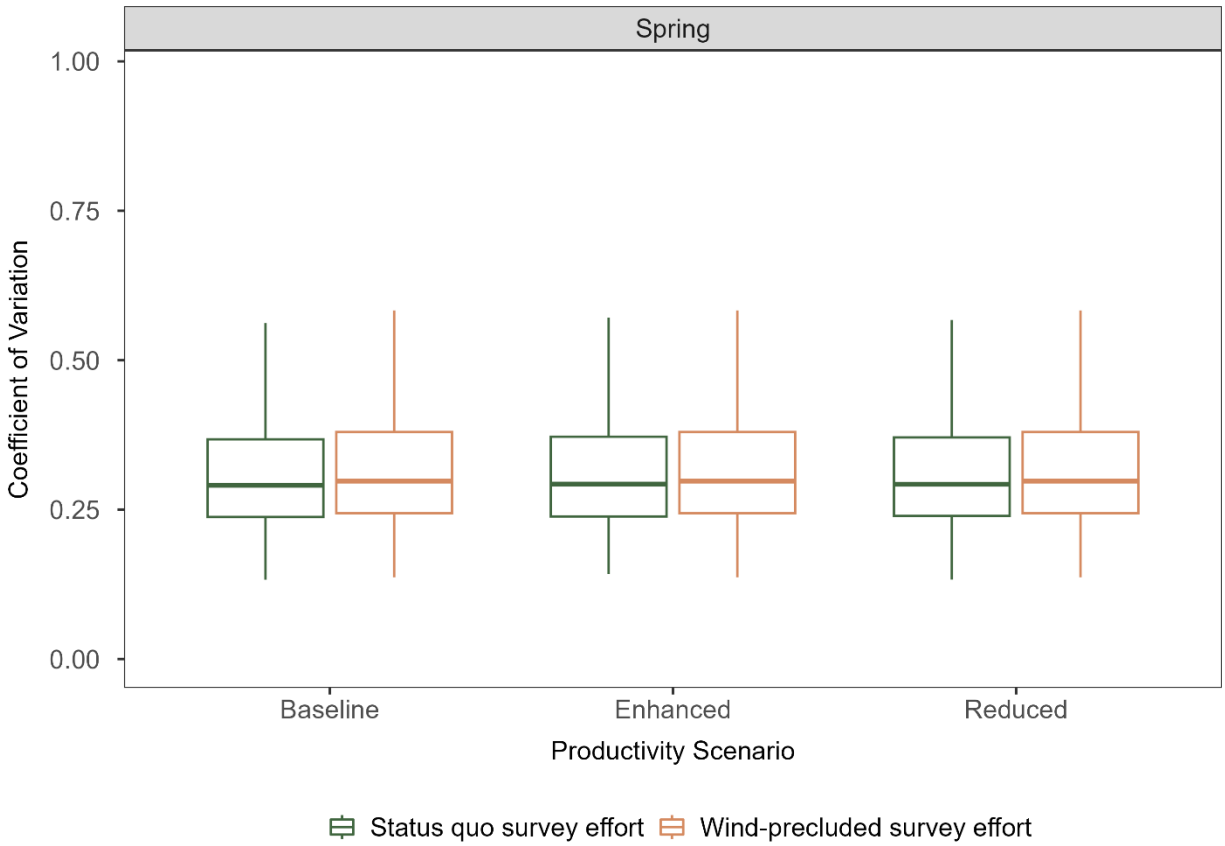

Figure 65. The distribution of coefficient of variations (CVs) of Atlantic mackerel abundance indices calculated under status quo survey effort (green boxplots) and wind-precluded survey effort (orange boxplots) over the simulated five-year time series across the productivity treatments: baseline, enhanced, and reduced fish density. The effect of outliers has been removed from the distribution.

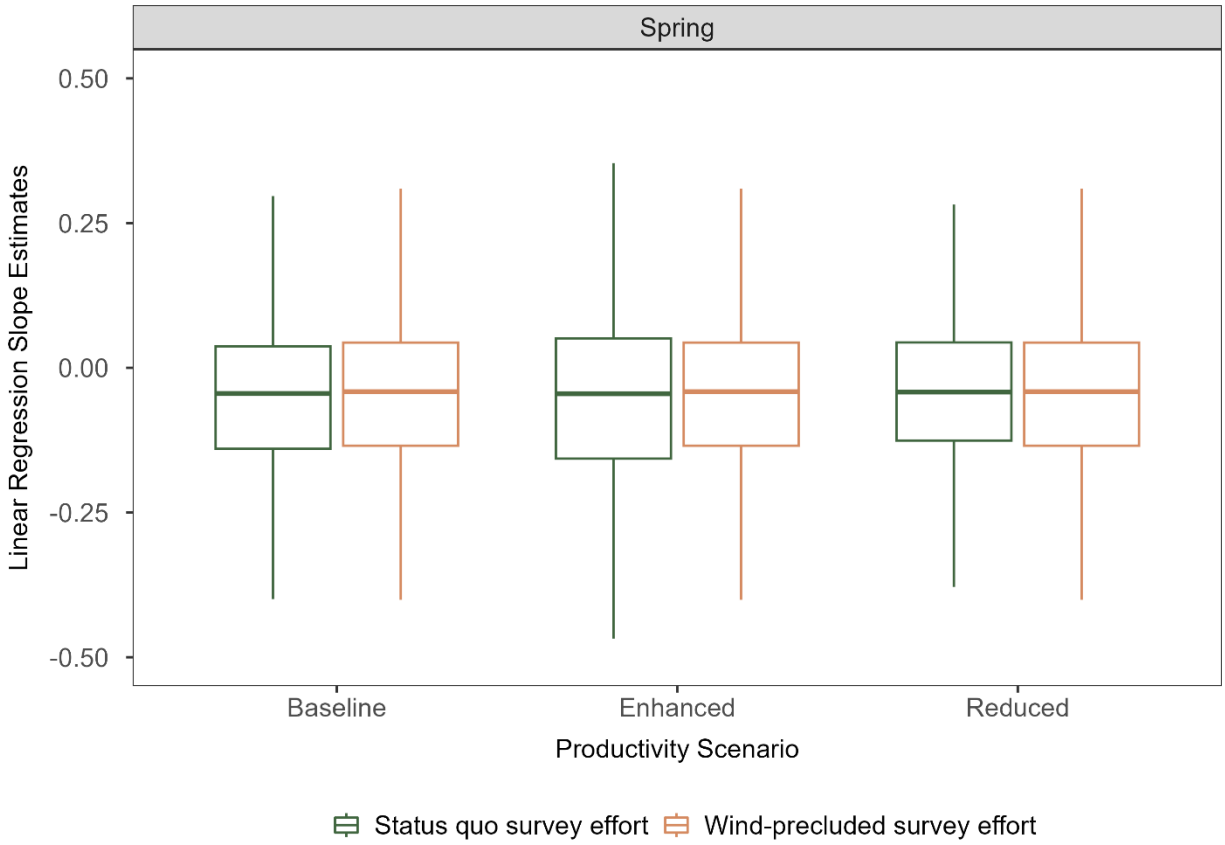

Figure 66. The distribution of changes in population trends for Atlantic mackerel calculated under status quo survey effort (green boxplots) and wind-precluded survey effort (orange boxplots) over the simulated five-year time series across the productivity treatments: baseline, enhanced, and reduced fish density. Y-axis has been modified to remove the effect of outliers on the distribution. The effect of outliers has been removed from the distribution.

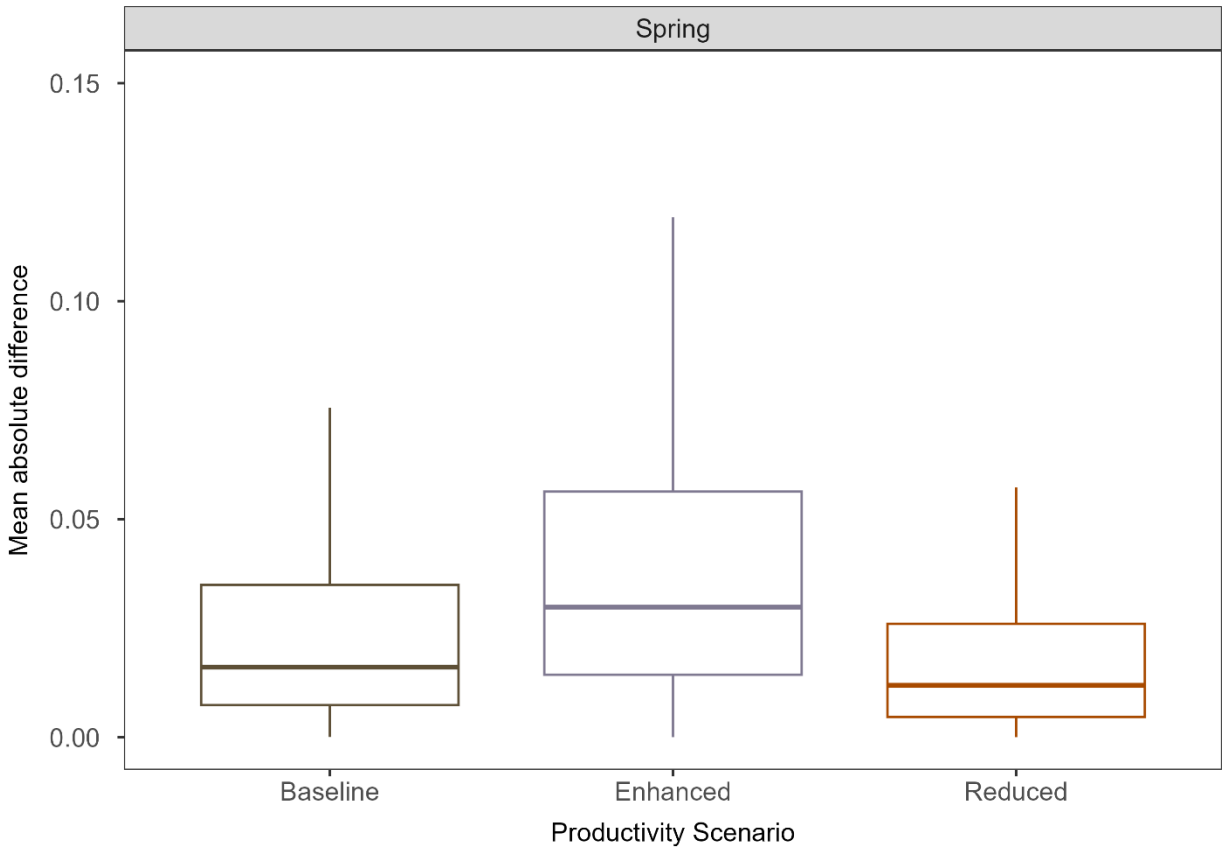

Figure 67. The distribution of absolute differences between population trends for Atlantic mackerel calculated under status quo and wind-precluded survey effort averaged over the simulated five-year time series across the productivity treatments: baseline, enhanced, and reduced fish density. Y-axis has been modified to remove the effect of outliers on the distribution. The effect of outliers has been removed from the distribution.

APPENDIX A: FIGURES

A1. Species with the highest observed differences between survey effort indices

Time series of annual abundance indices from the seasonal bottom trawl survey under a status quo survey effort assumption (green) and a wind-precluded survey effort assumption (orange) for each of the species identified as having the highest observed differences between effort scenarios in terms of annual abundance indices, coefficients of variation, and/or estimates of population trend (Table 2). The bars on each of the points represent the standard error around the stratified mean.

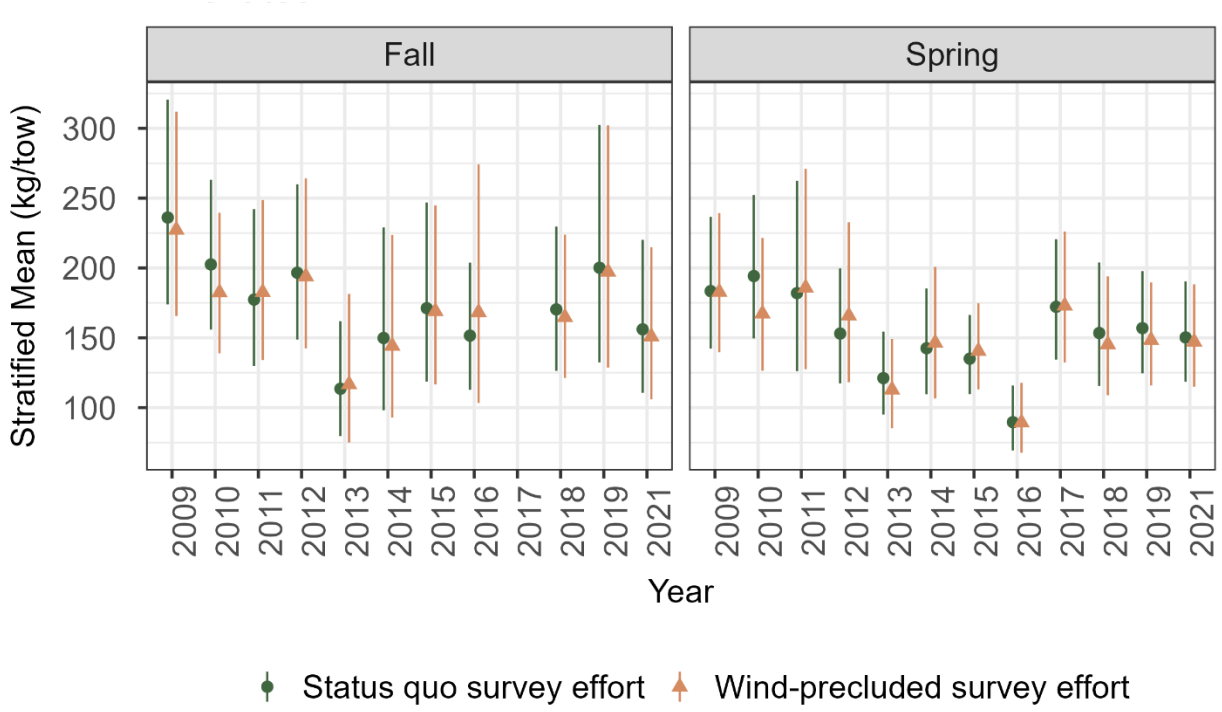

Figure A1. Fall and spring estimates of annual abundance for the skate complex.

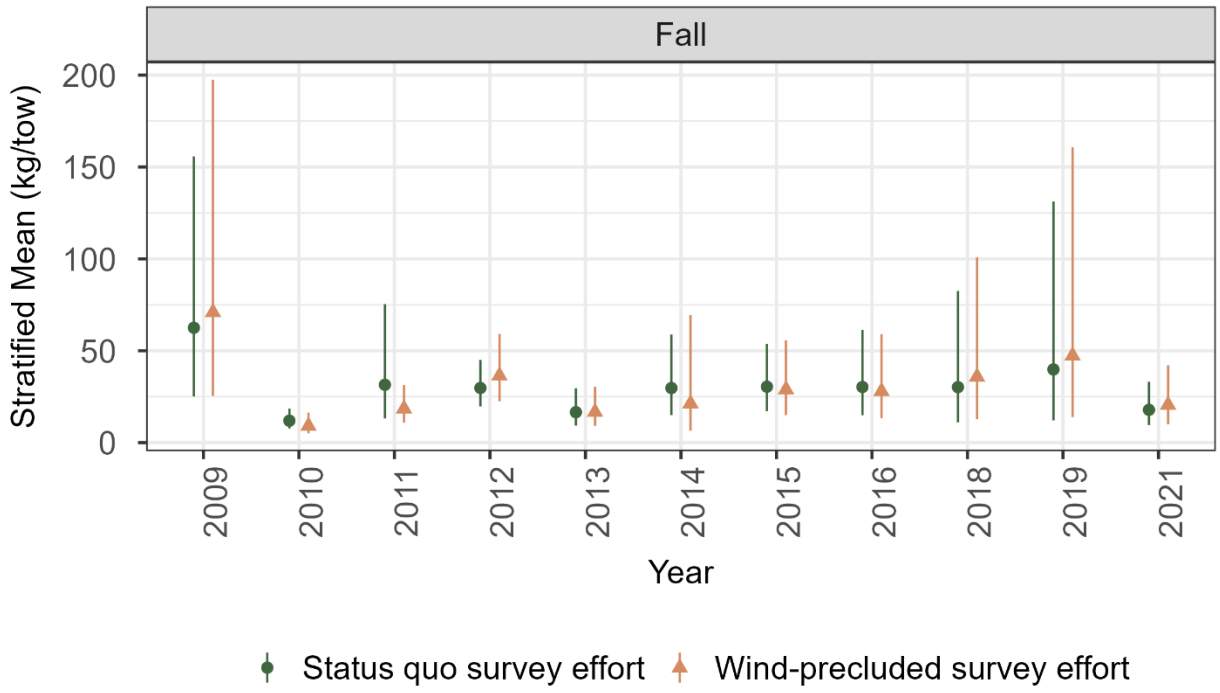

Figure A2. Fall estimates of annual abundance for Atlantic croaker.

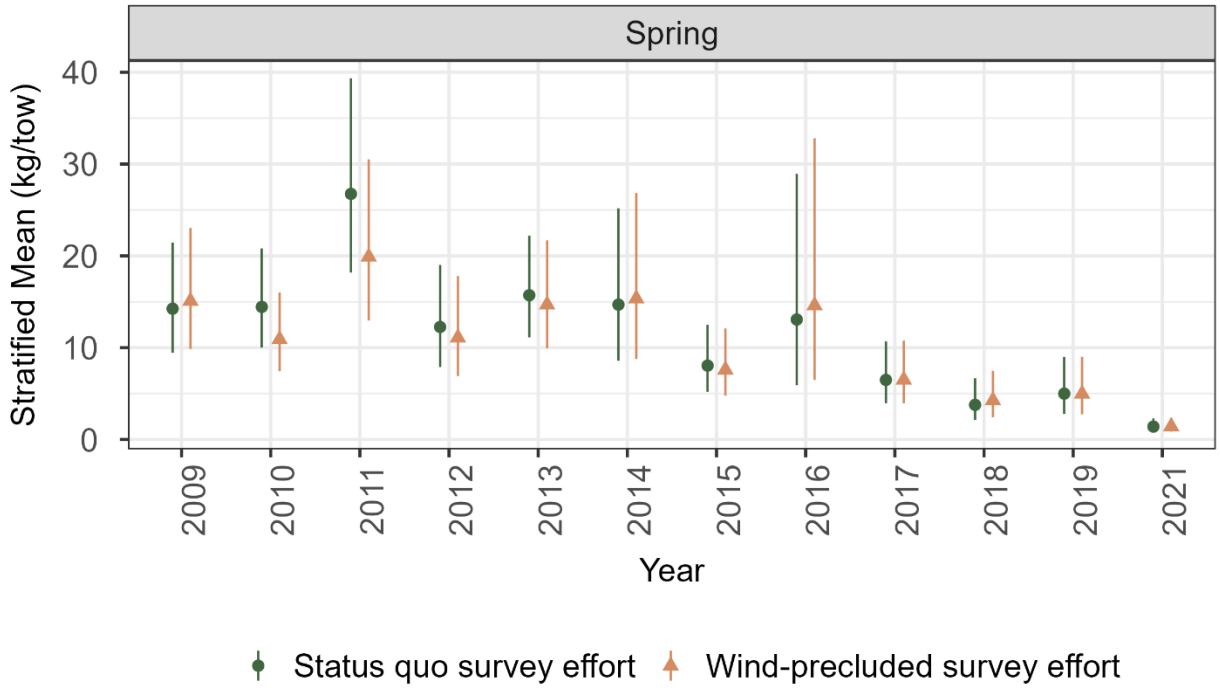

Figure A3. Spring estimates of annual abundance for Atlantic herring.

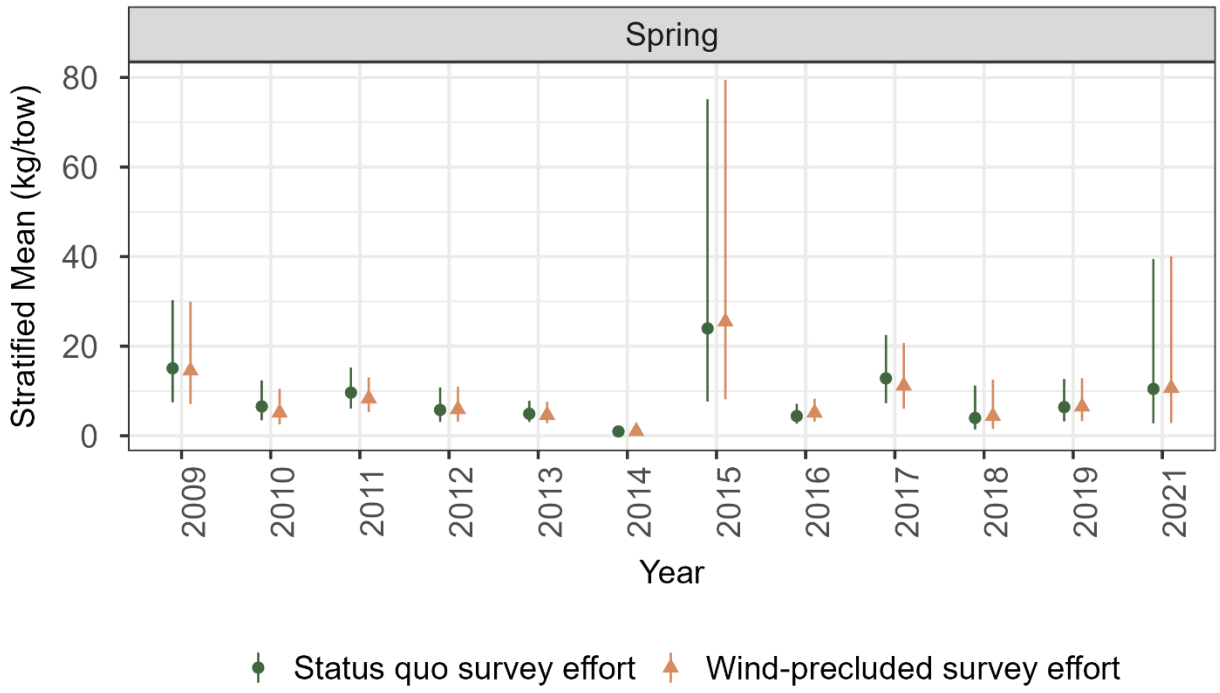

Figure A4. Spring estimates of annual abundance for Atlantic mackerel.

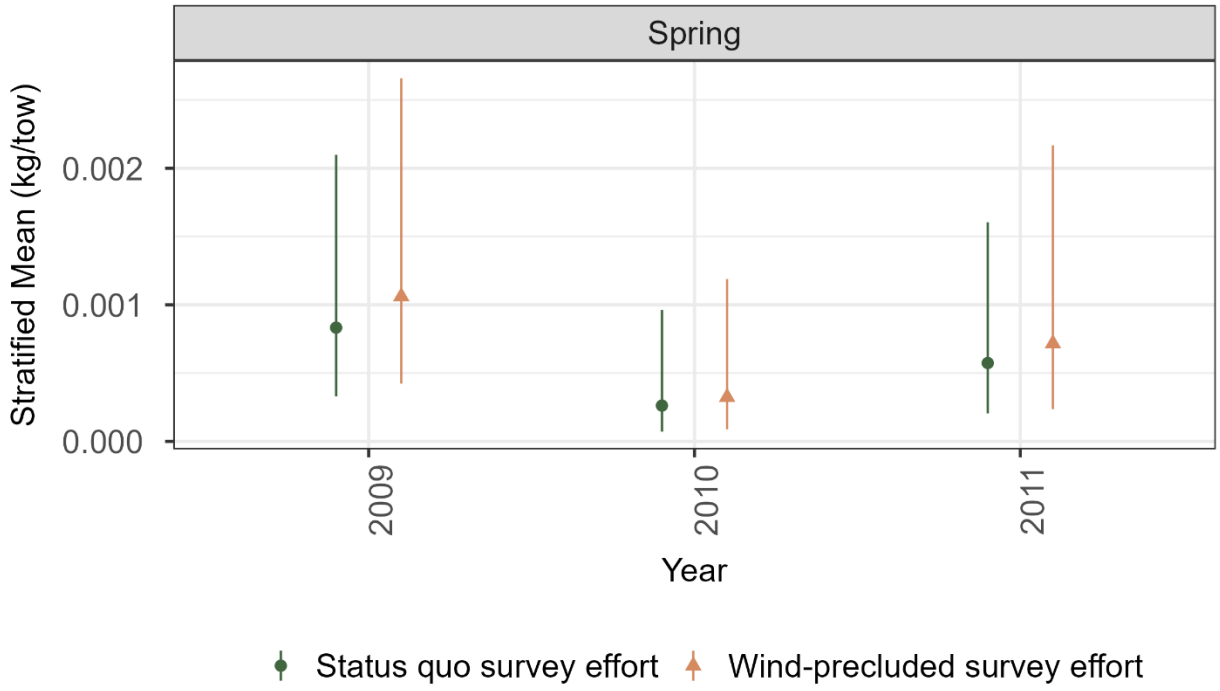

Figure A5. Spring estimates of annual abundance for Atlantic seasnail.

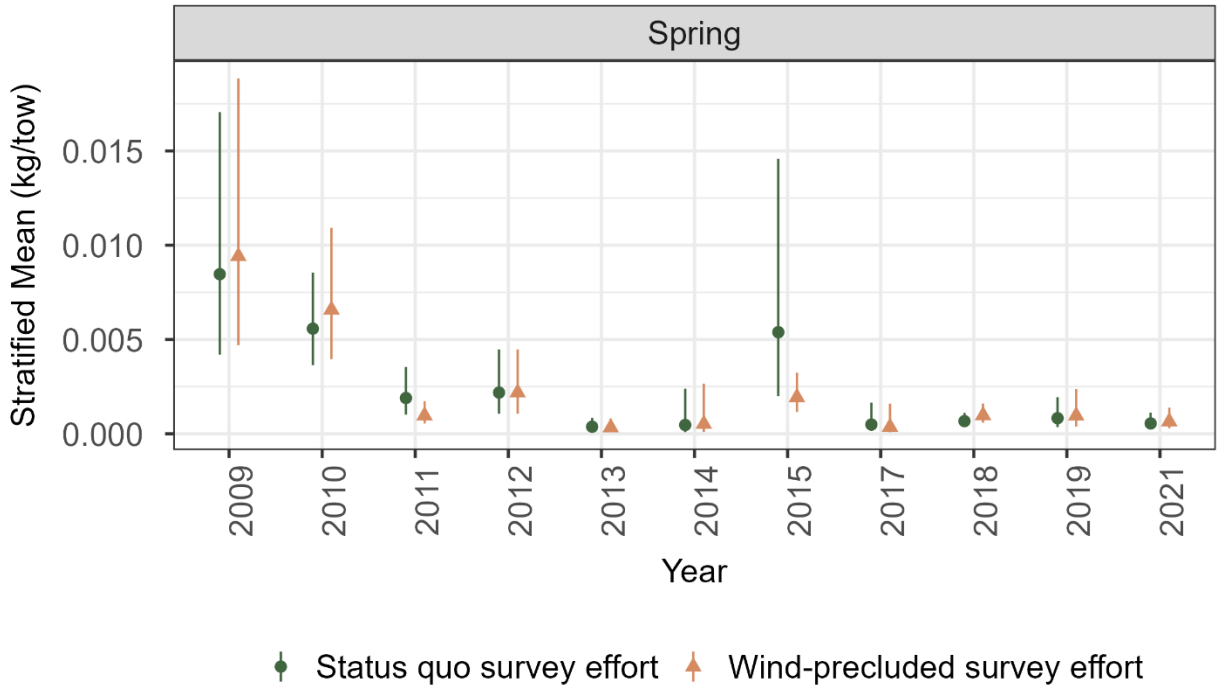

Figure A6. Spring estimates of annual abundance for Atlantic silverside.

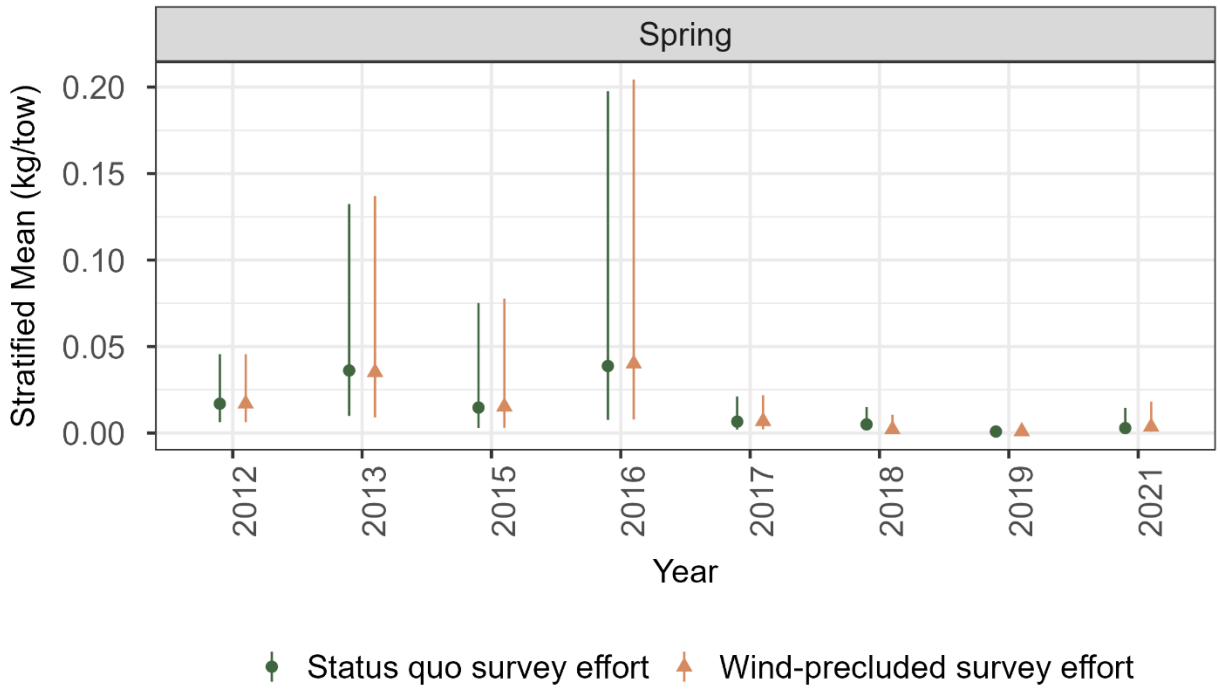

Figure A7. Spring estimates of annual abundance for Atlantic surfclam.

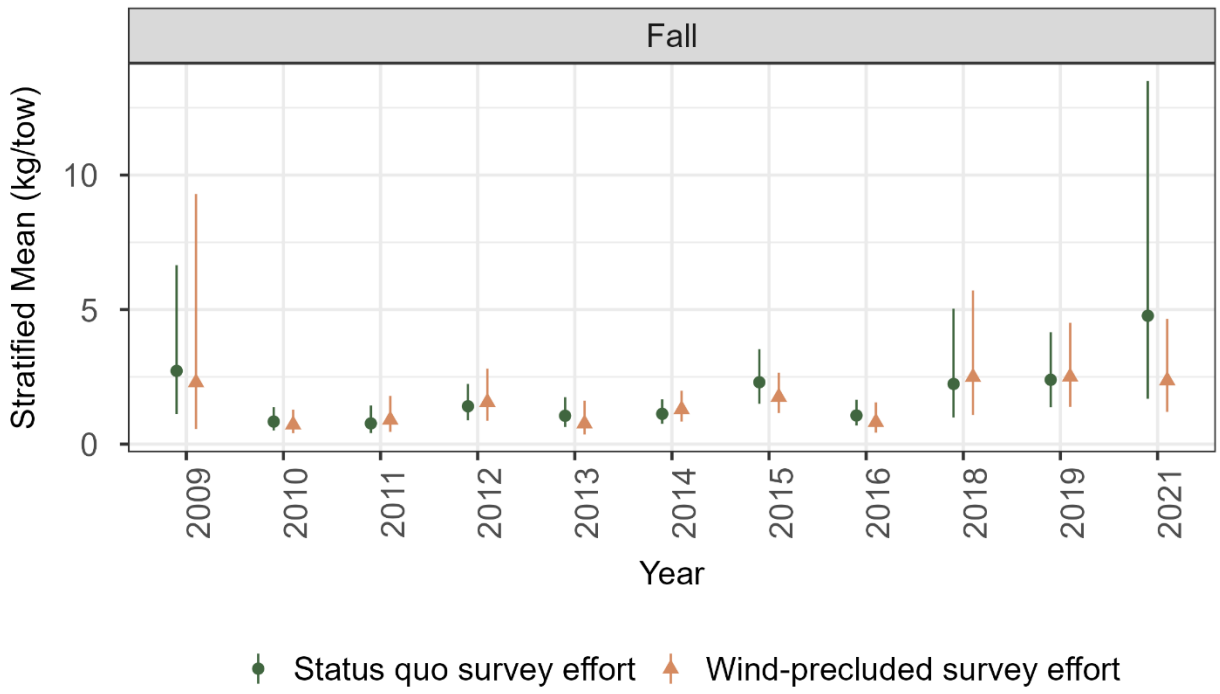

Figure A8. Fall estimates of annual abundance for black sea bass.

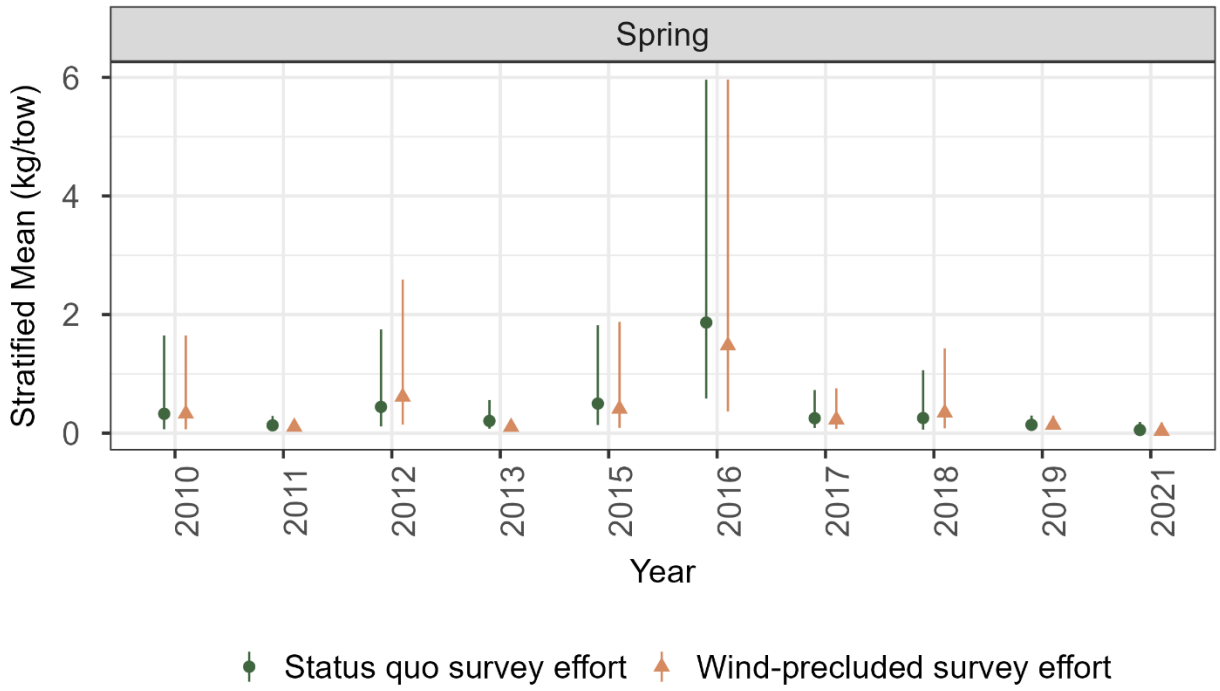

Figure A9. Spring estimates of annual abundance for bluefish.

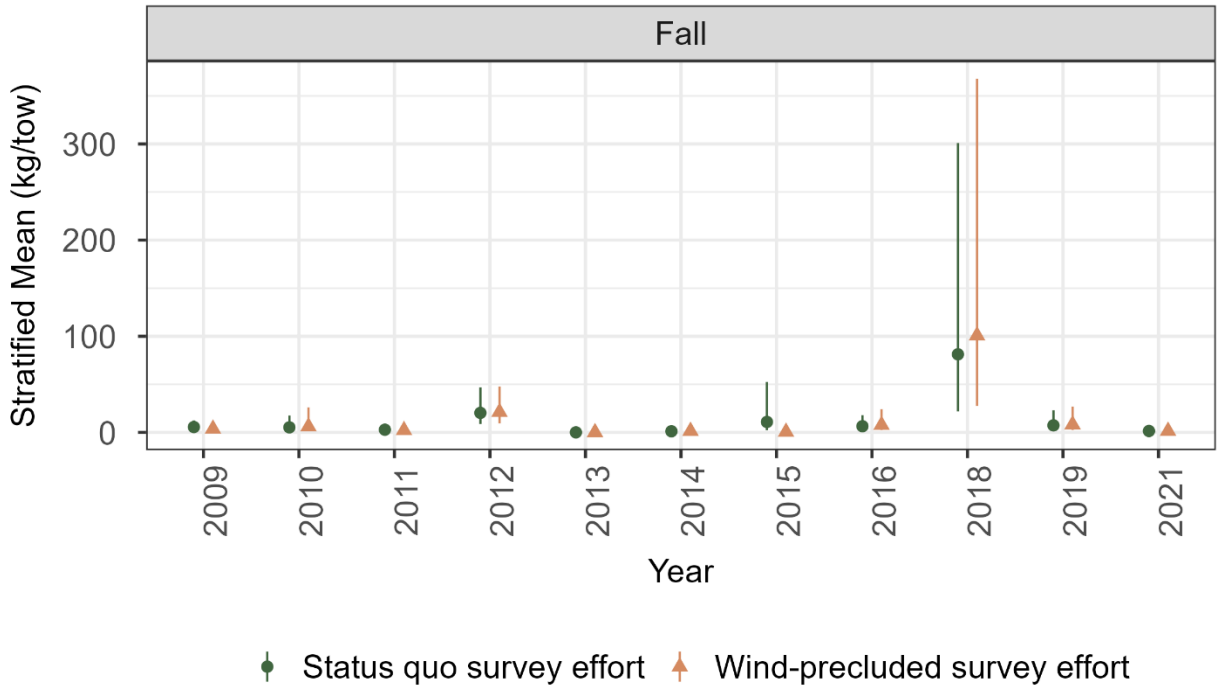

Figure A10. Fall estimates of annual abundance for bluntnose stingray.

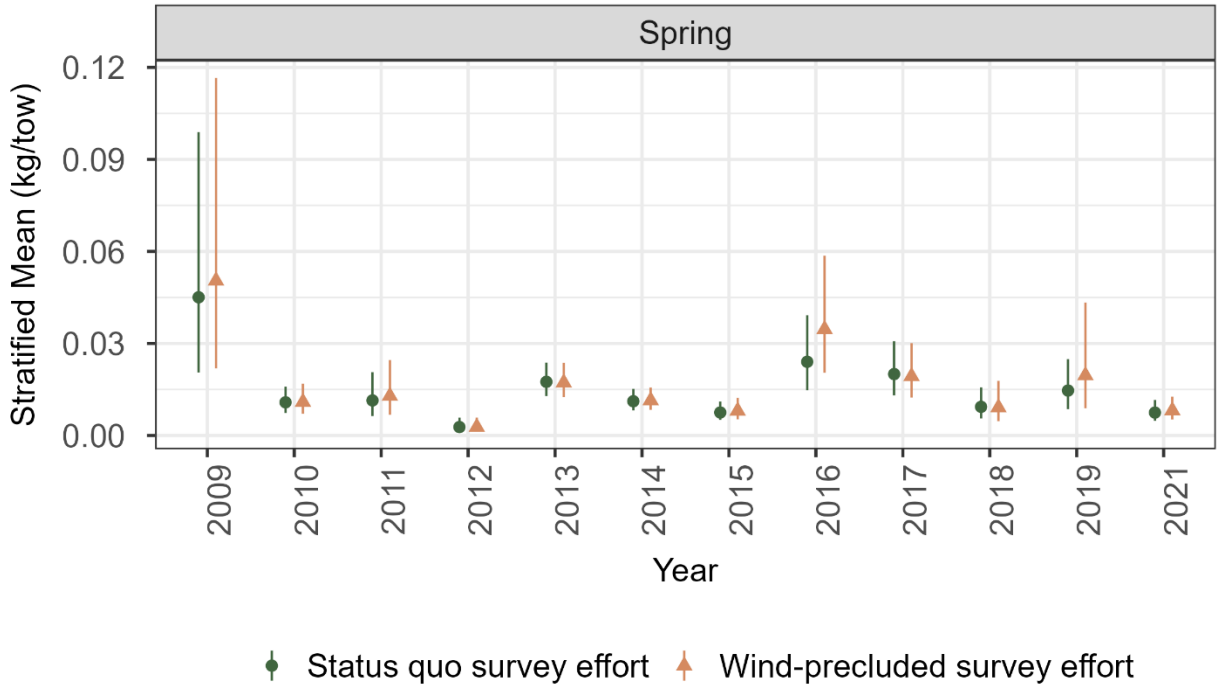

Figure A11. Spring estimates of annual abundance for unclassified bobtail species.

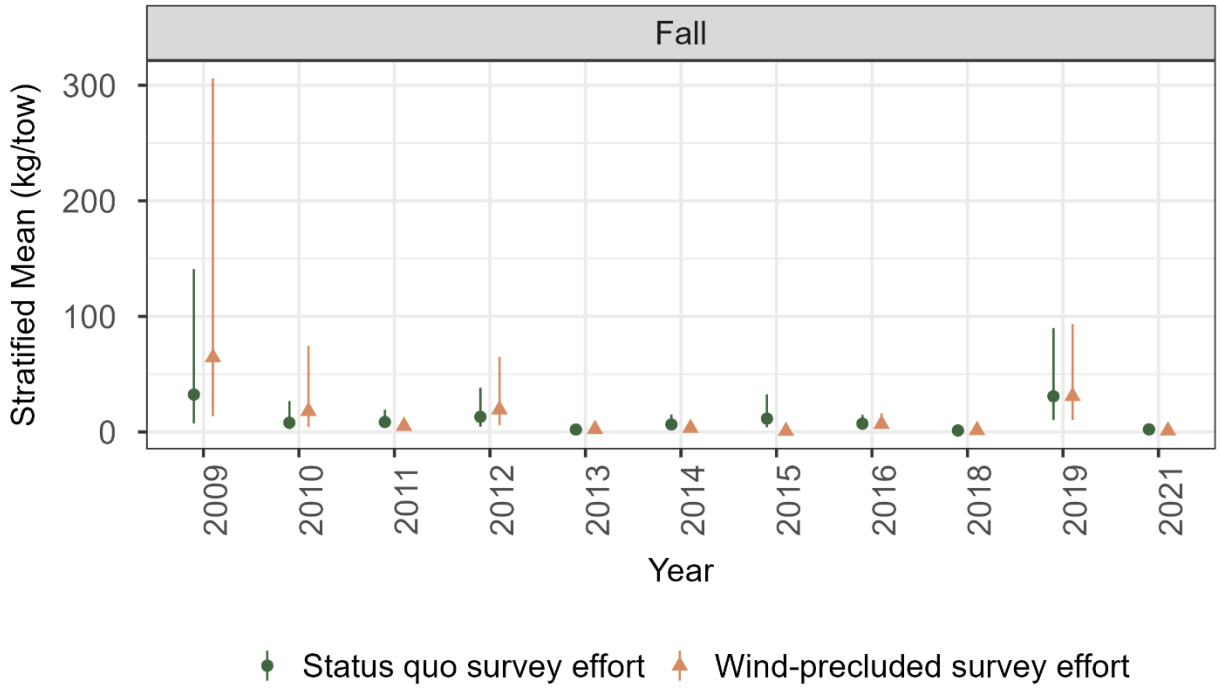

Figure A12. Fall estimates of annual abundance for bullnose ray.

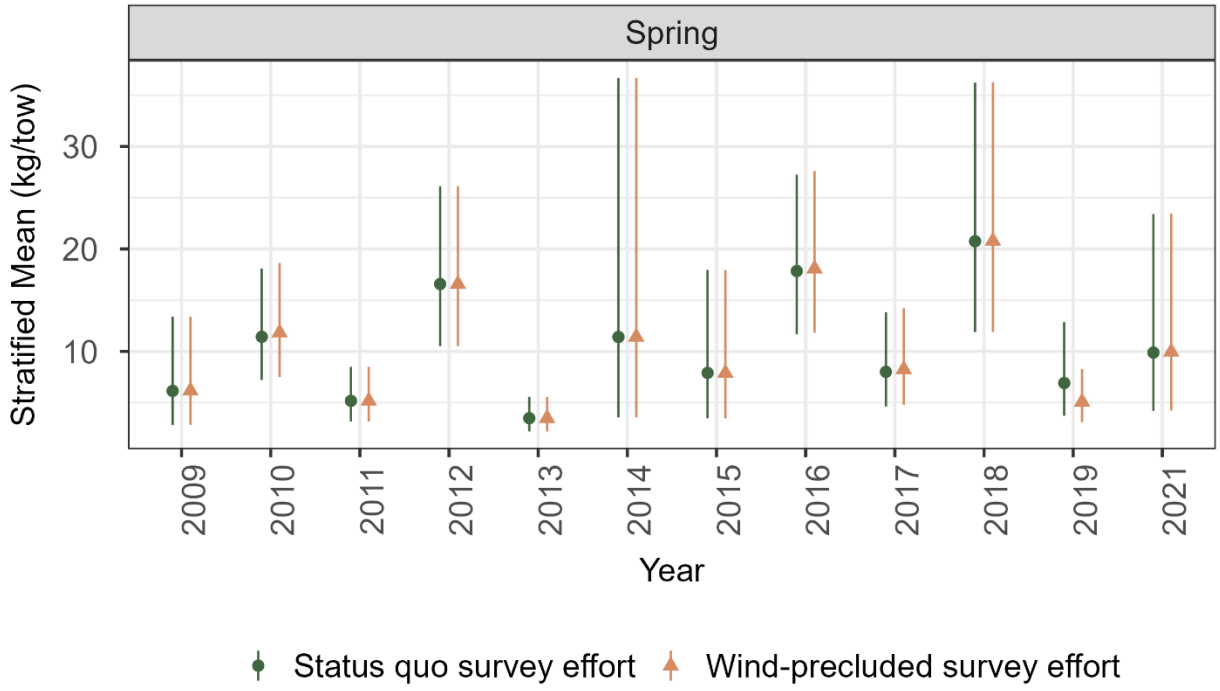

Figure A13. Spring estimates of annual abundance for butterfish.

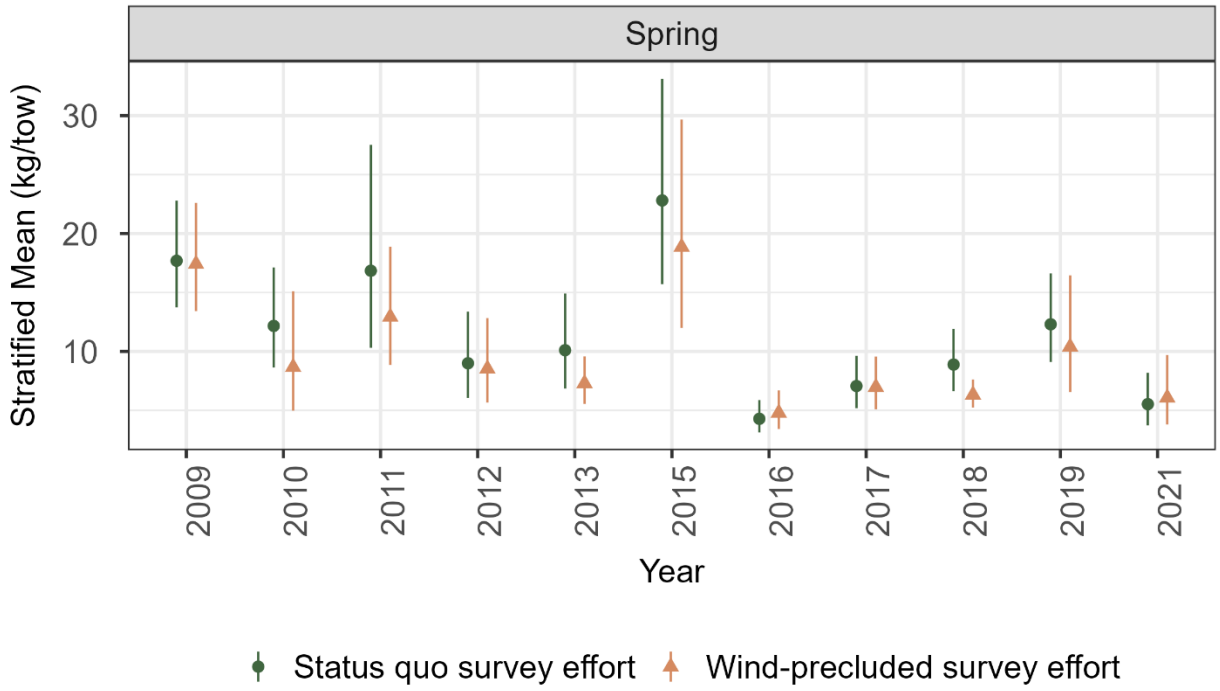

Figure A14. Spring estimates of annual abundance for clearnose skate.

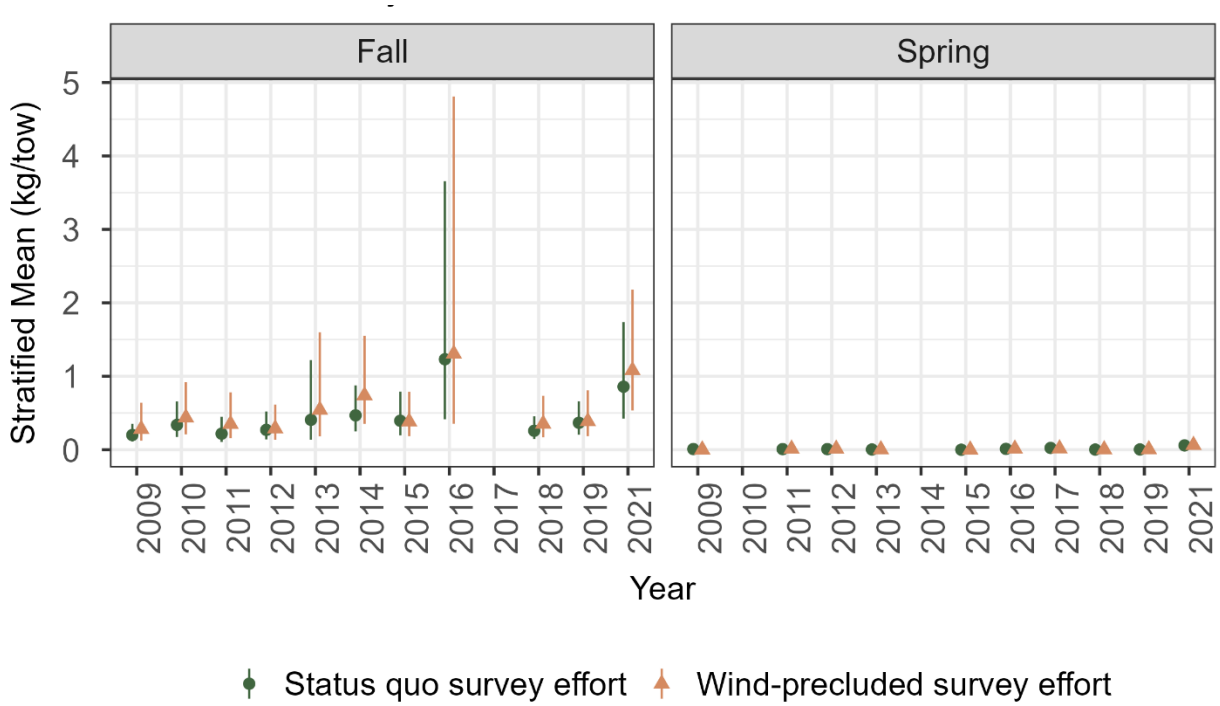

Figure A15. Fall and spring estimates of annual abundance for coarsehand lady crab.

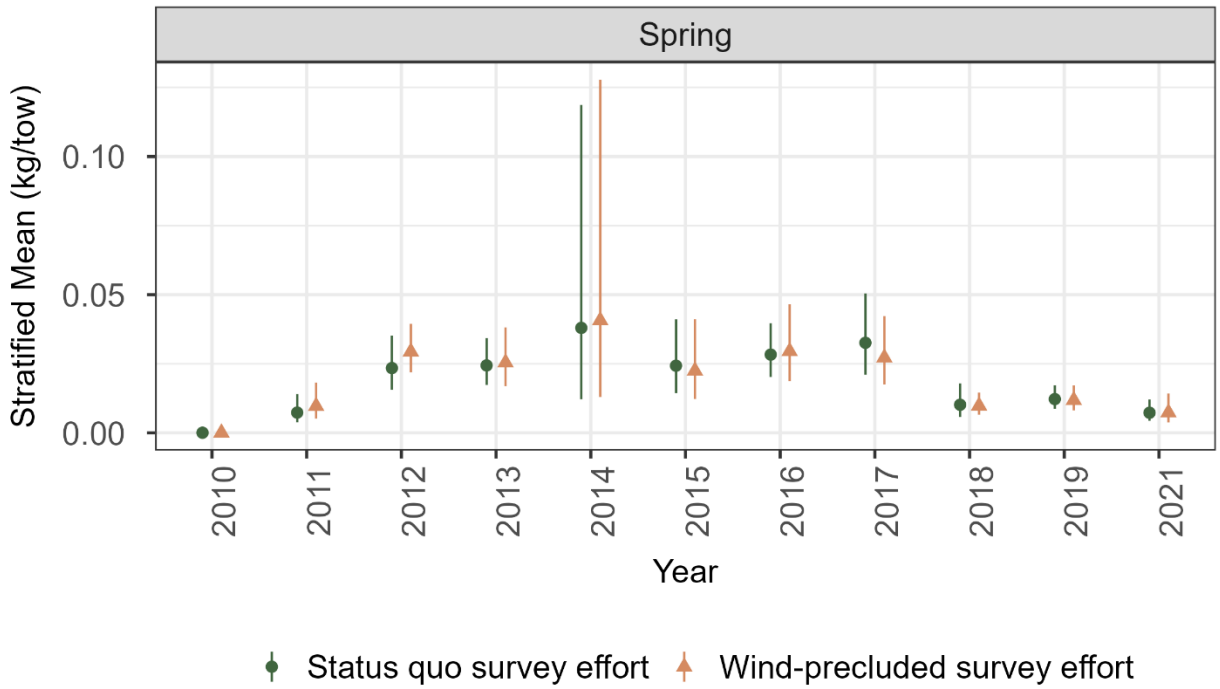

Figure A16. Spring estimates of annual abundance for unclassified etropus.

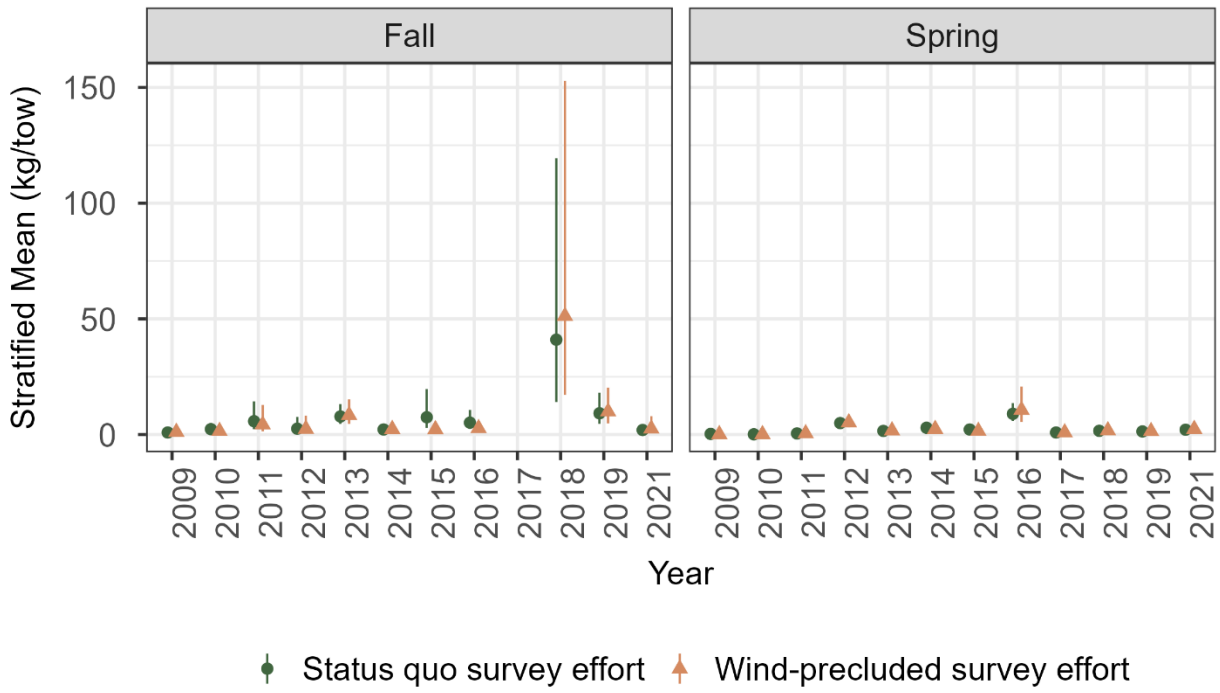

Figure A17. Fall and spring estimates of annual abundance for horseshoe crab.

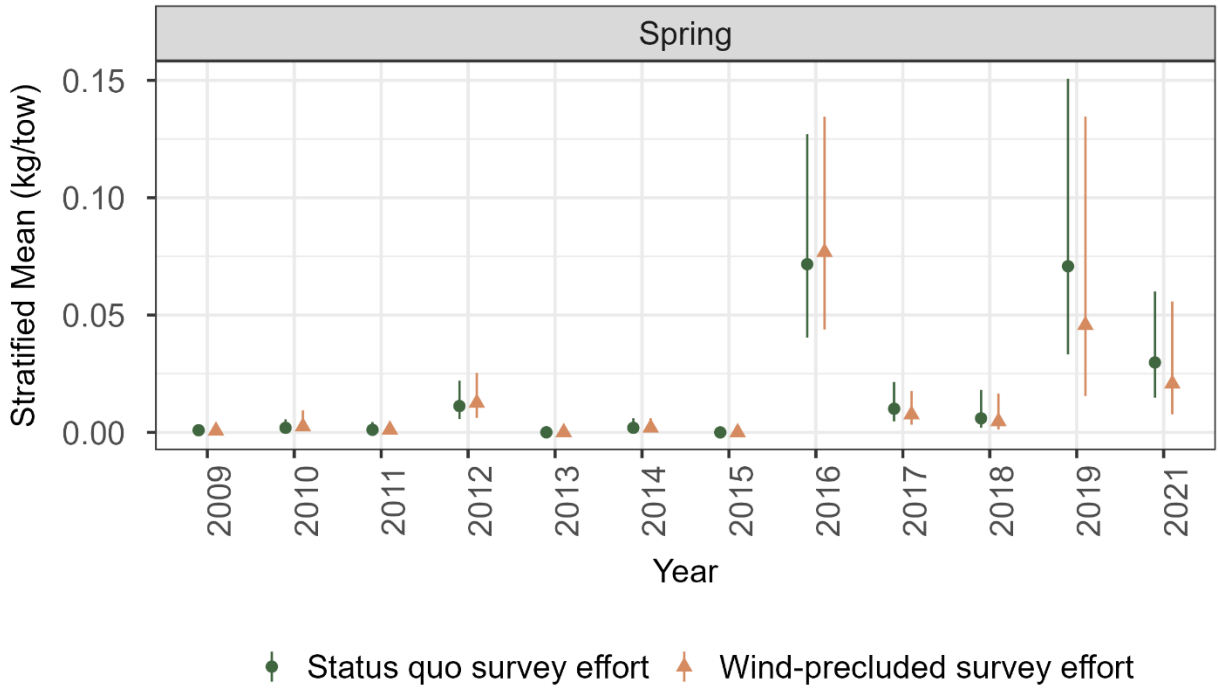

Figure A18. Spring estimates of annual abundance for lady crab.

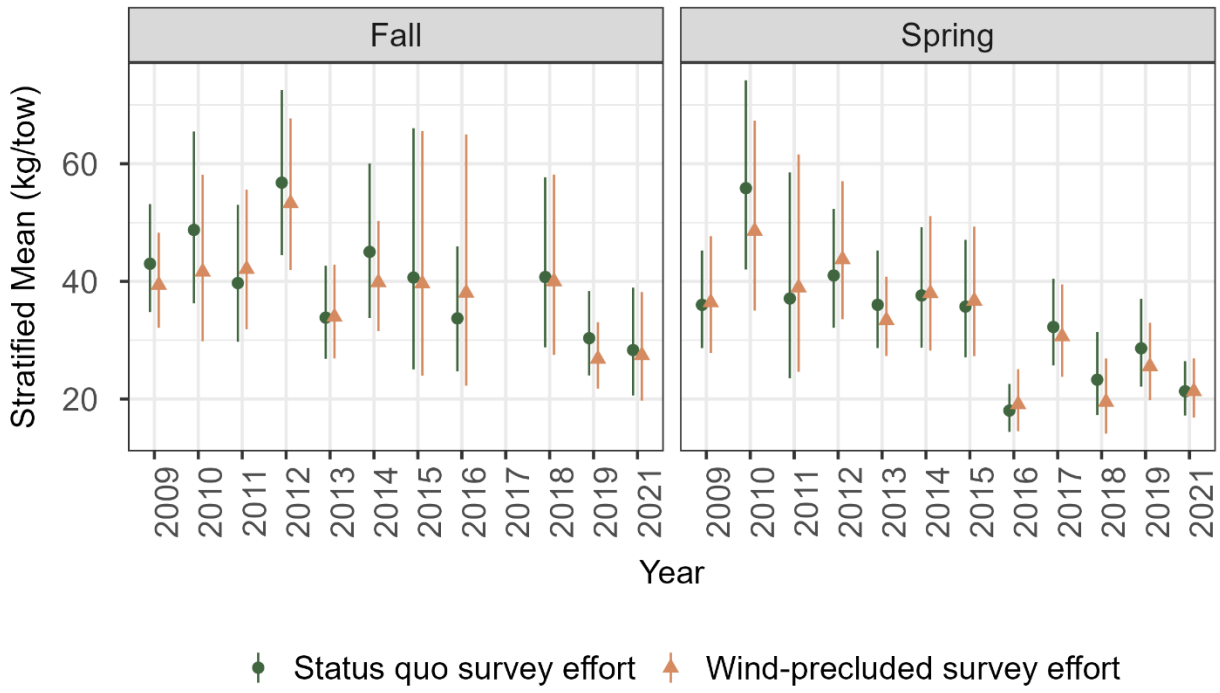

Figure A19. Fall and spring estimates of annual abundance for little skate.

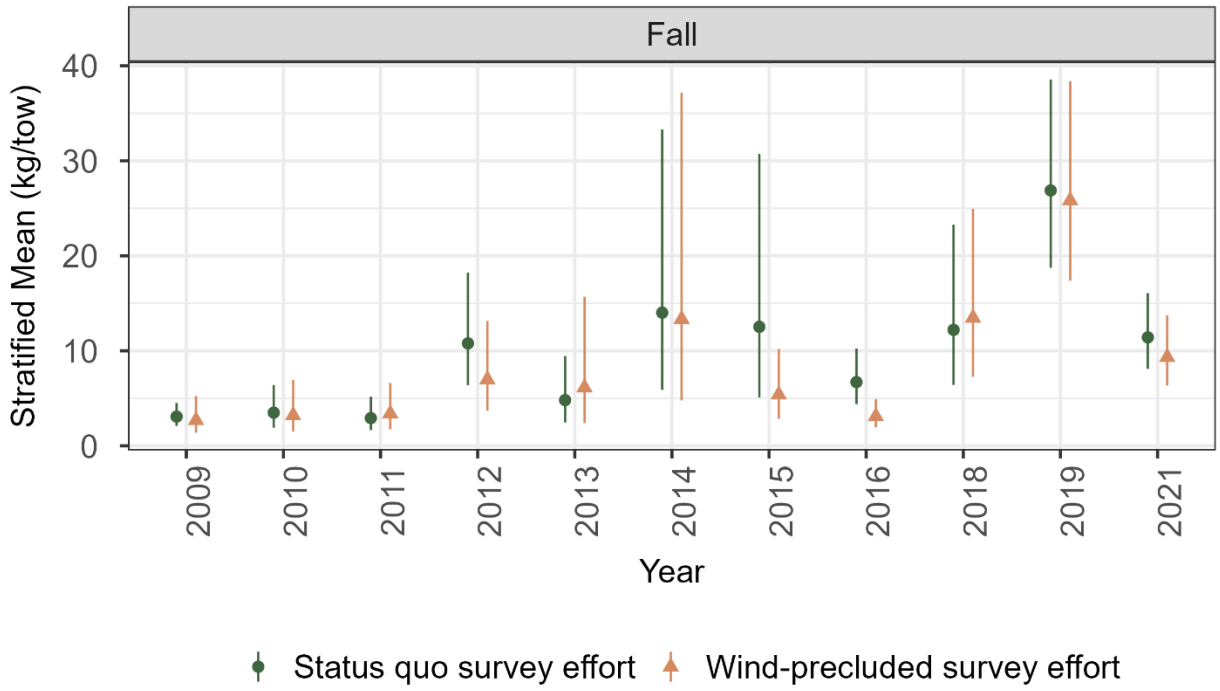

Figure A20. Fall estimates of annual abundance for northern searobin.

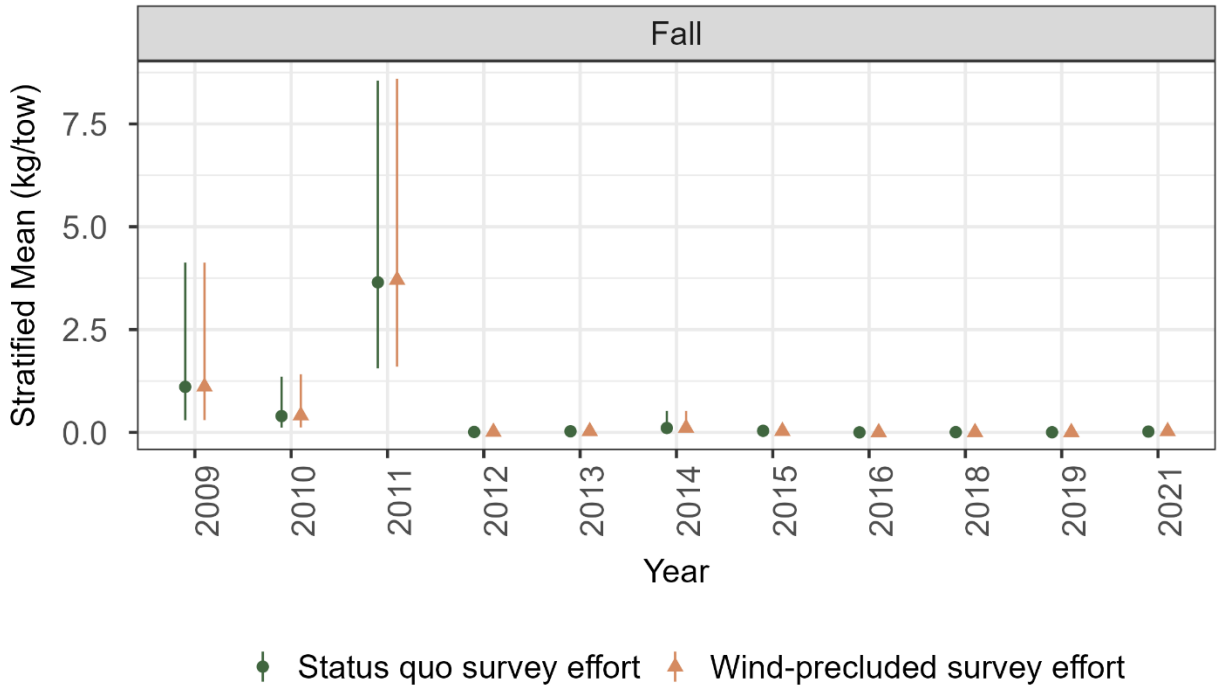

Figure A21. Fall estimates of annual abundance for rough scad.

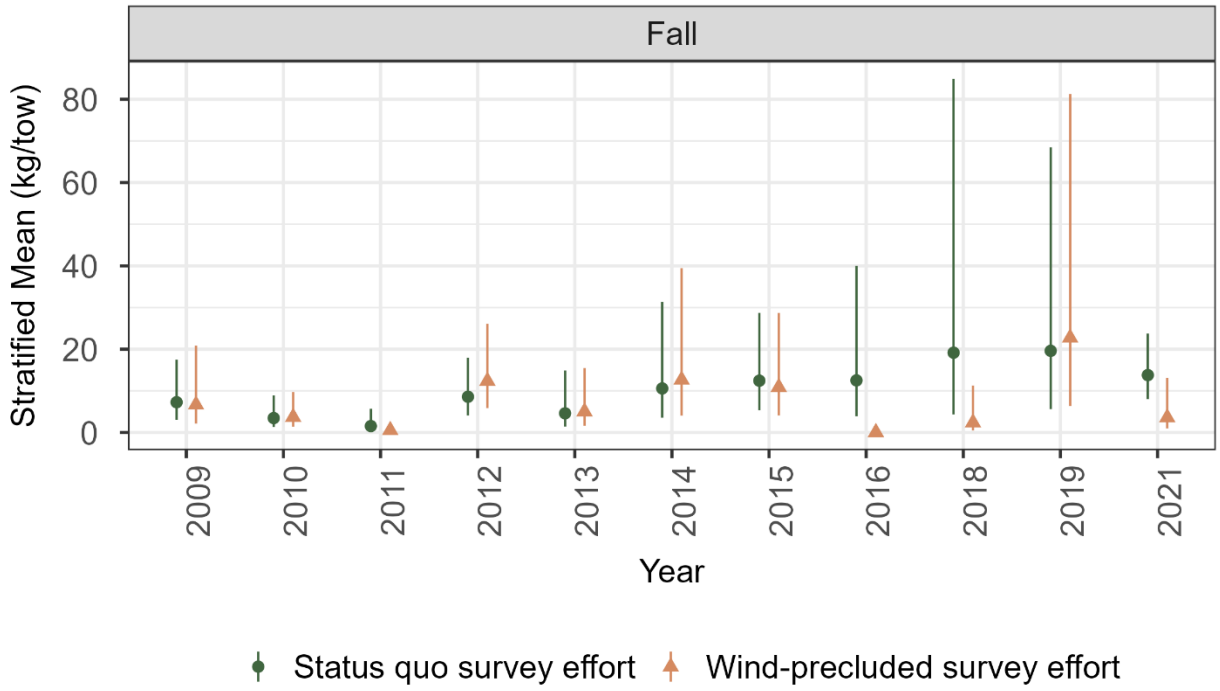

Figure A22. Fall estimates of annual abundance for roughtail stingray.

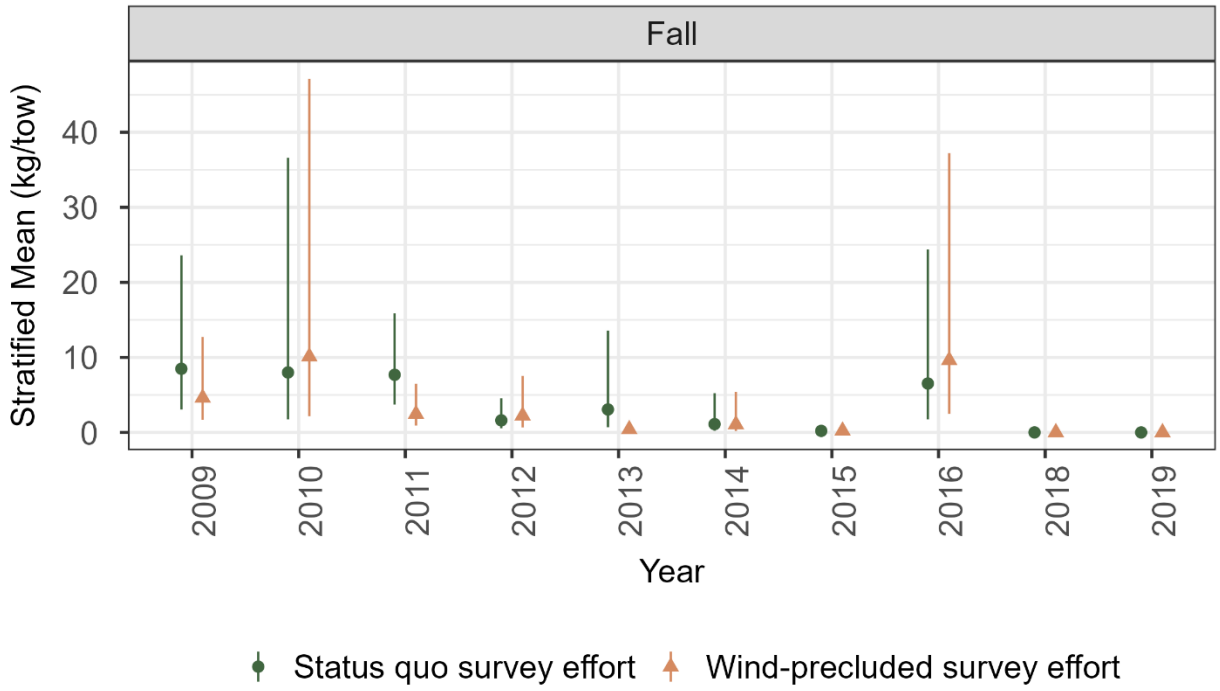

Figure A23. Fall estimates of annual abundance for round herring.

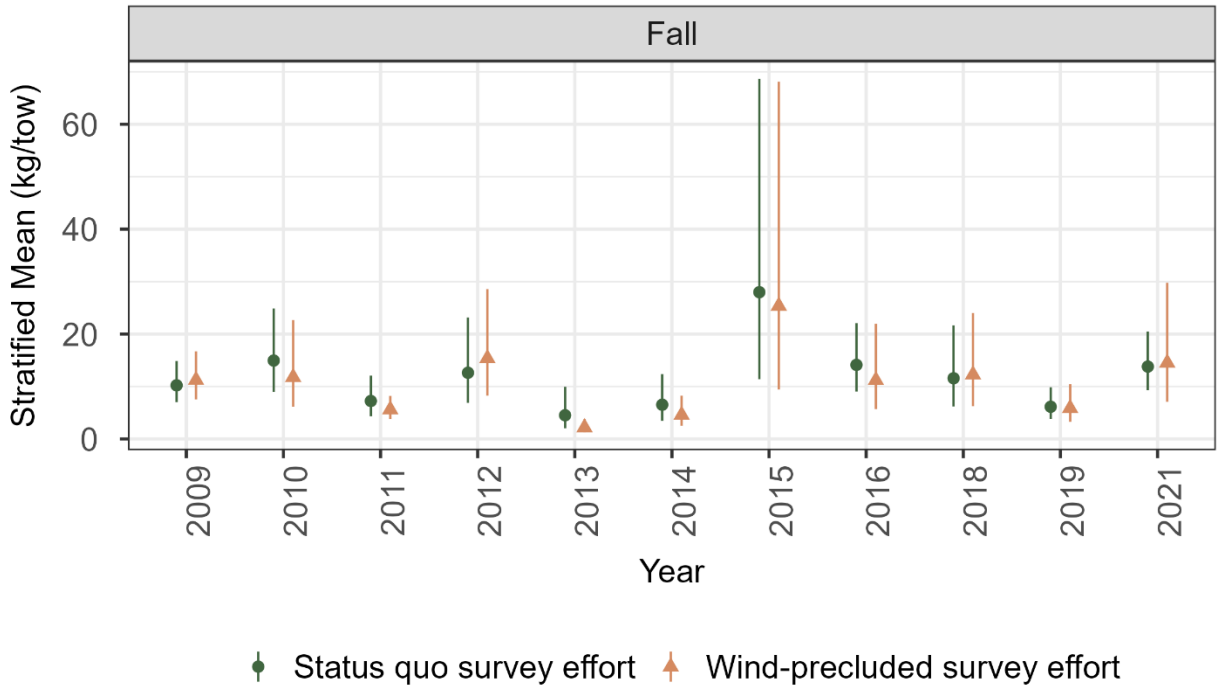

Figure A24. Fall estimates of annual abundance for scup.

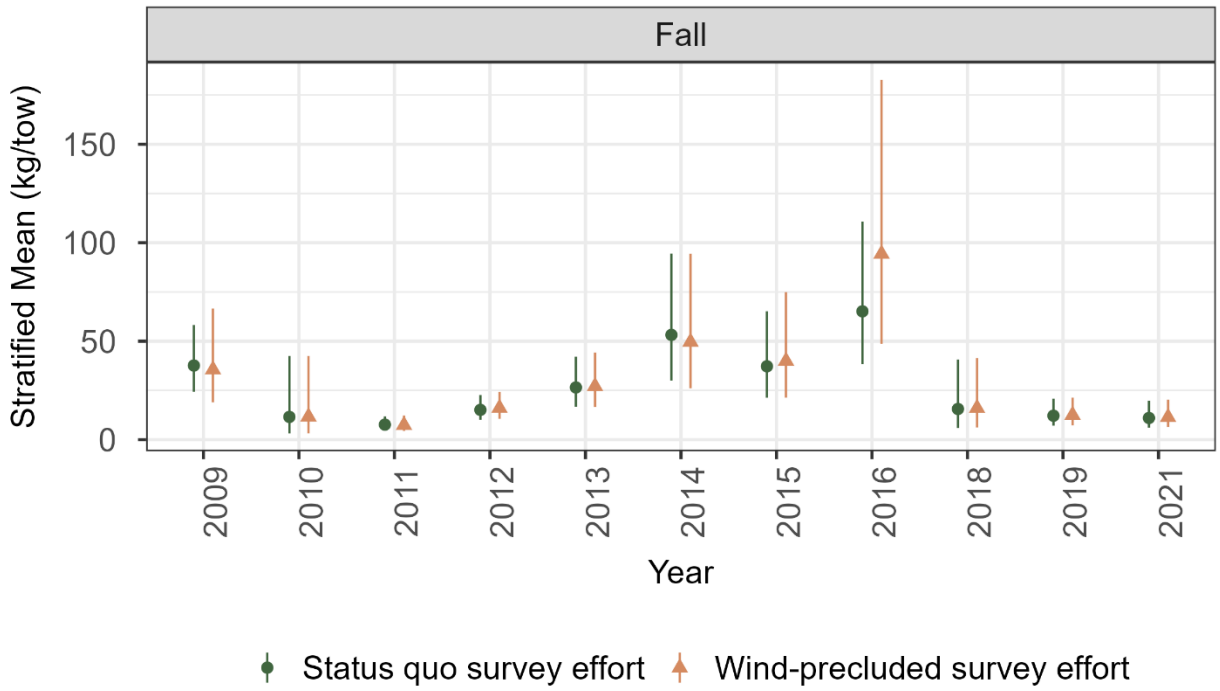

Figure A25. Fall estimates of annual abundance for sea scallop.

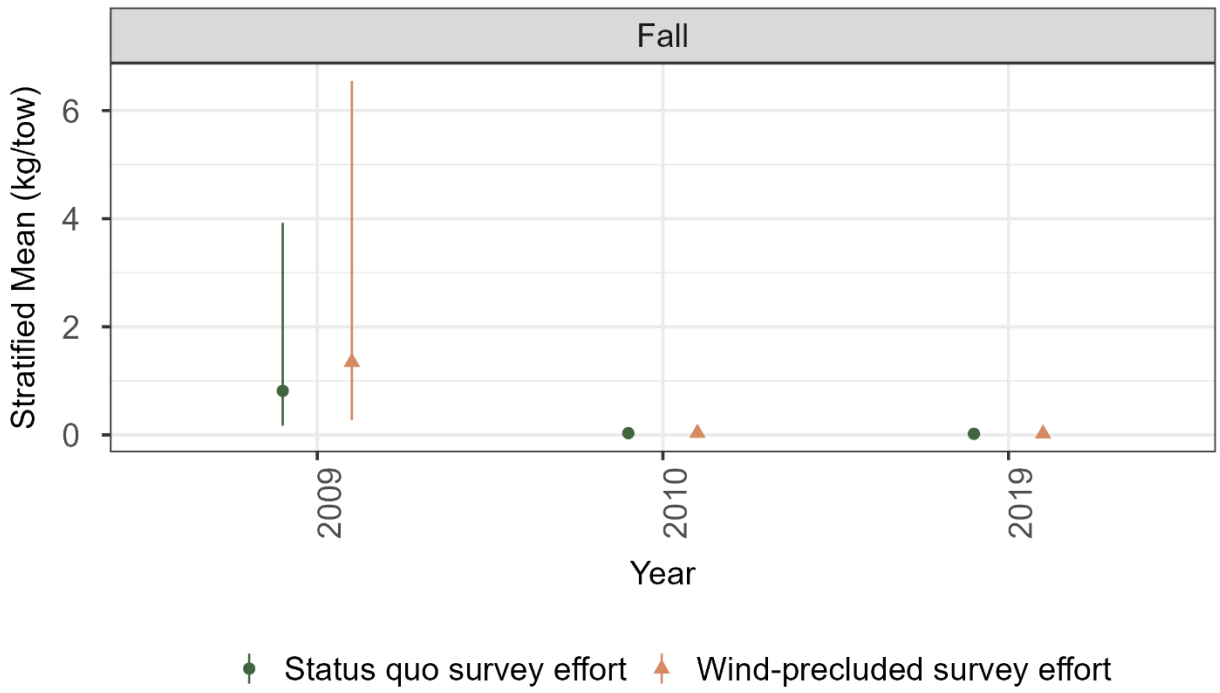

Figure A26. Fall estimates of annual abundance for pink, brown, and white shrimp.

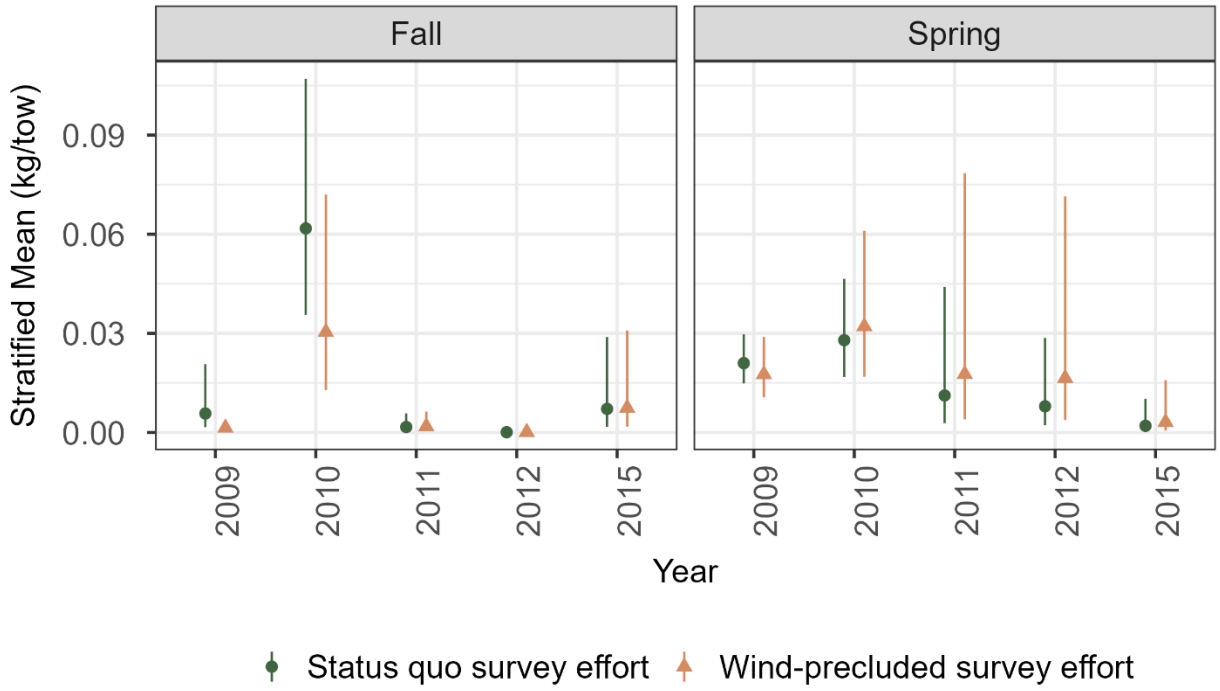

Figure A27. Fall and spring estimates of annual abundance for smallmouth flounder.

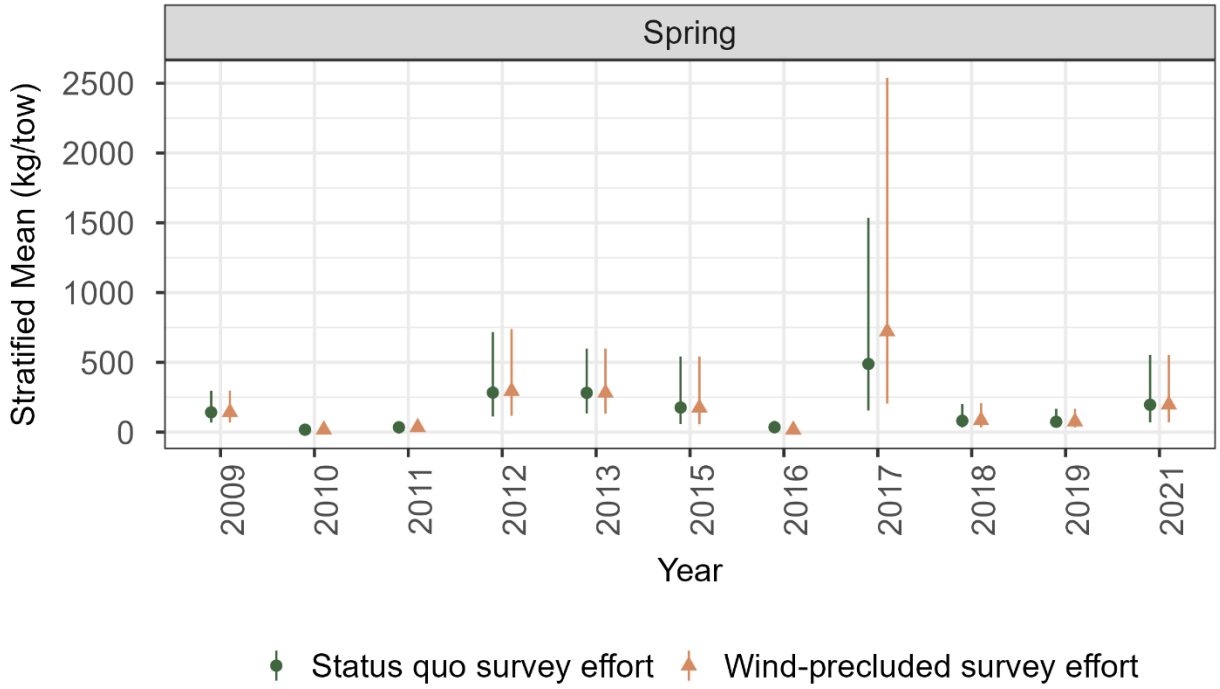

Figure A28. Spring estimates of annual abundance for smooth dogfish.

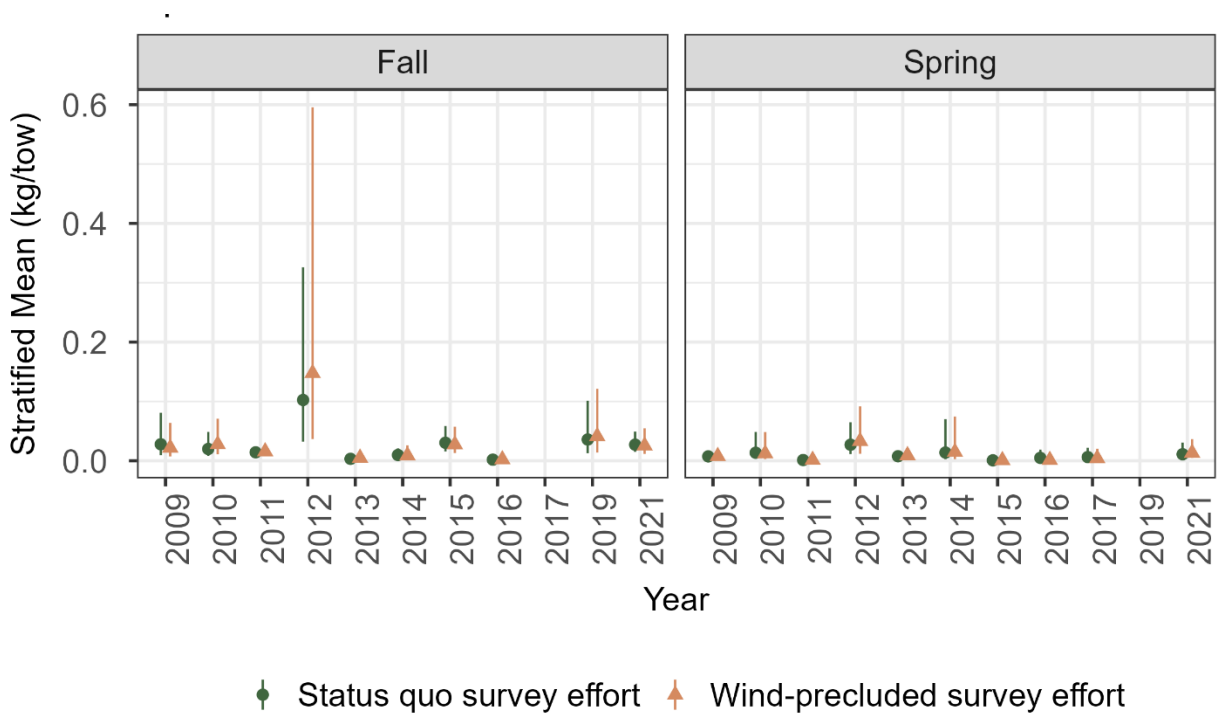

Figure A29. Fall and spring estimates of annual abundance for unclassified spider crabs.

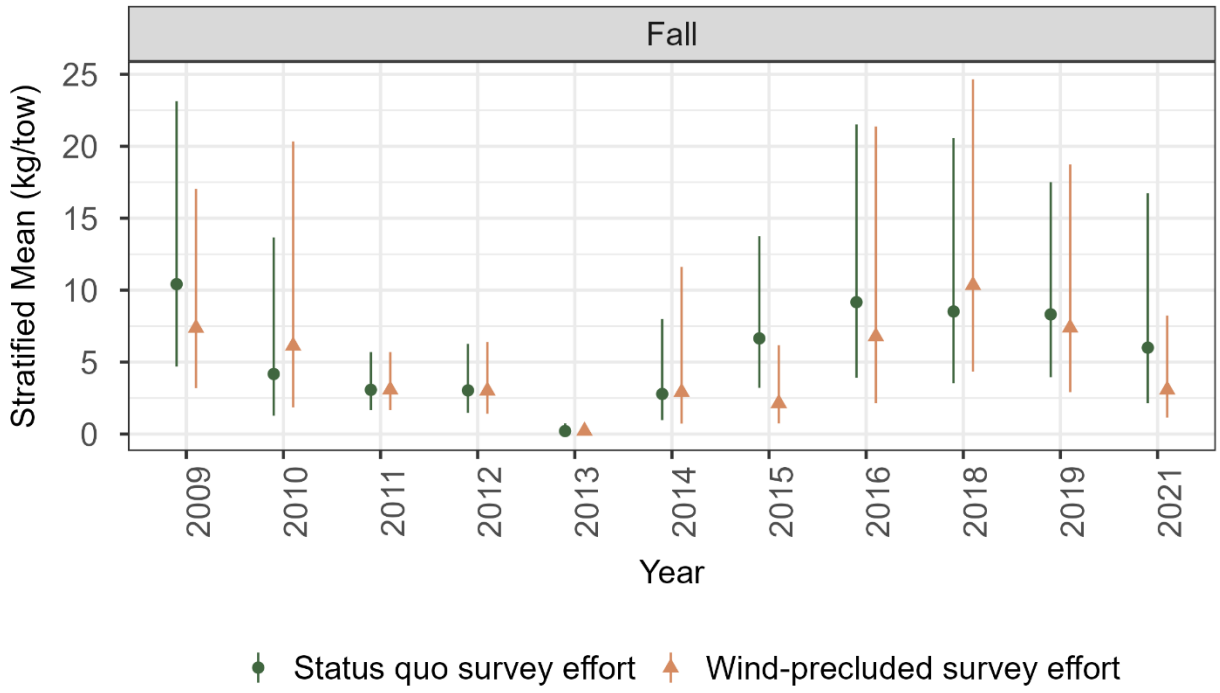

Figure A30. Fall estimates of annual abundance for spiny butterfly ray.

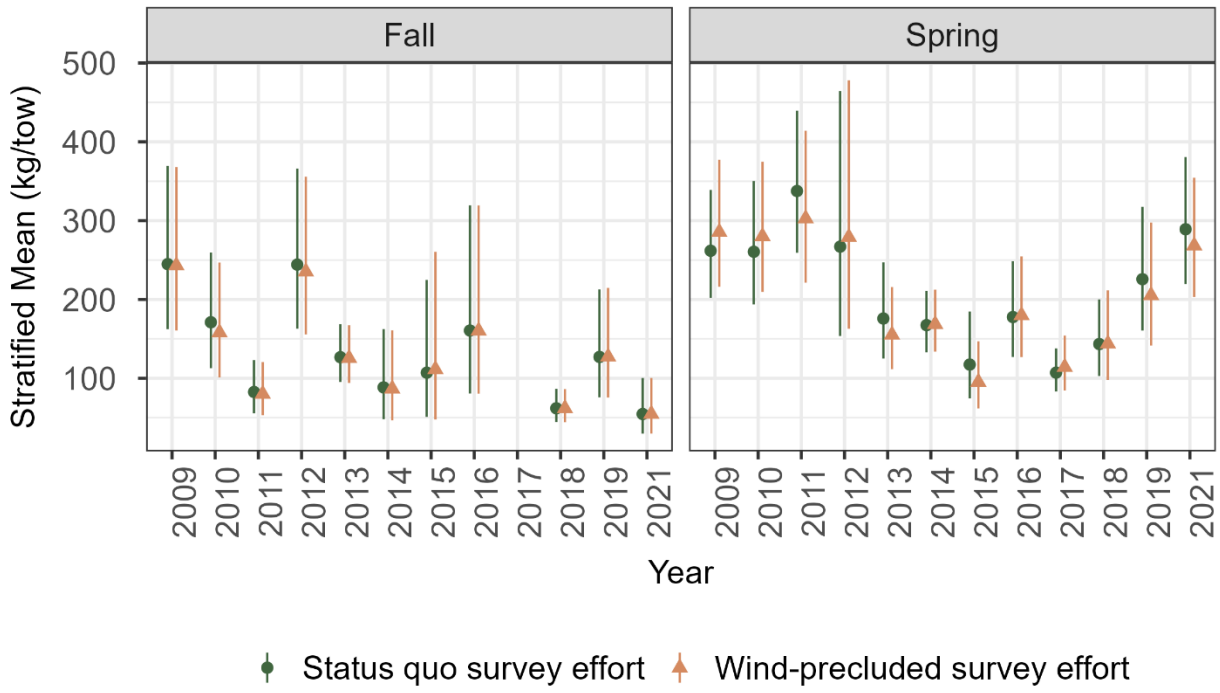

Figure A31. Fall and spring estimates of annual abundance for spiny dogfish.

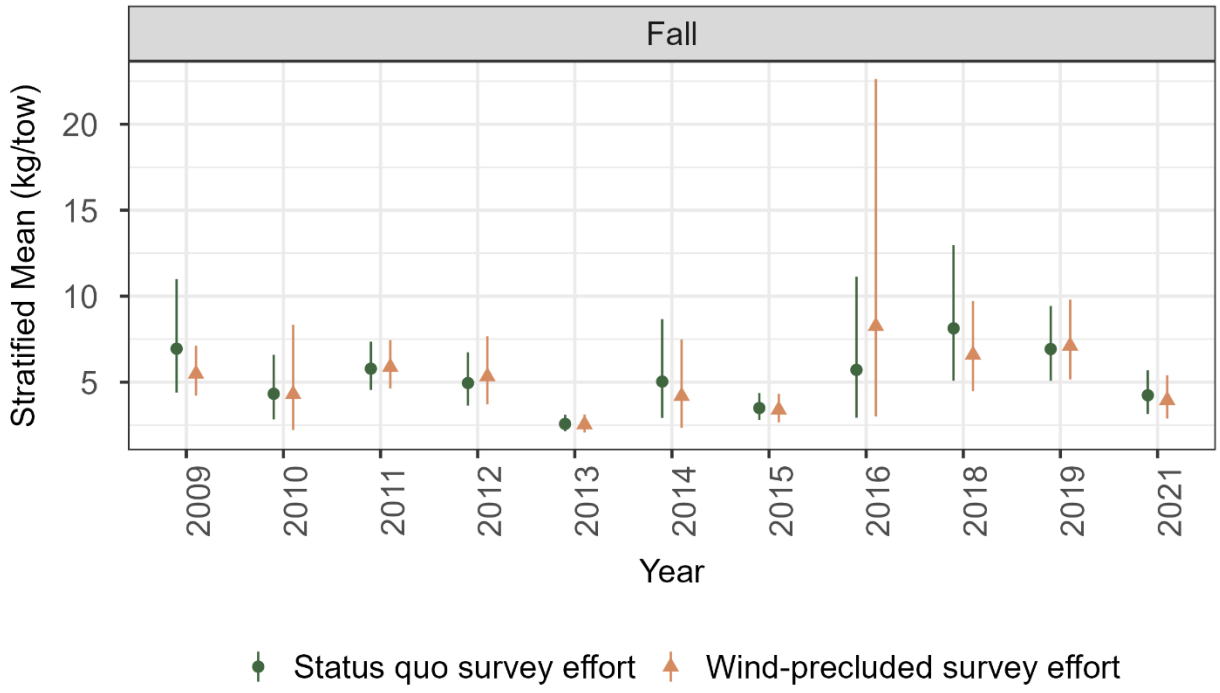

Figure A32. Fall estimates of annual abundance for spotted hake.

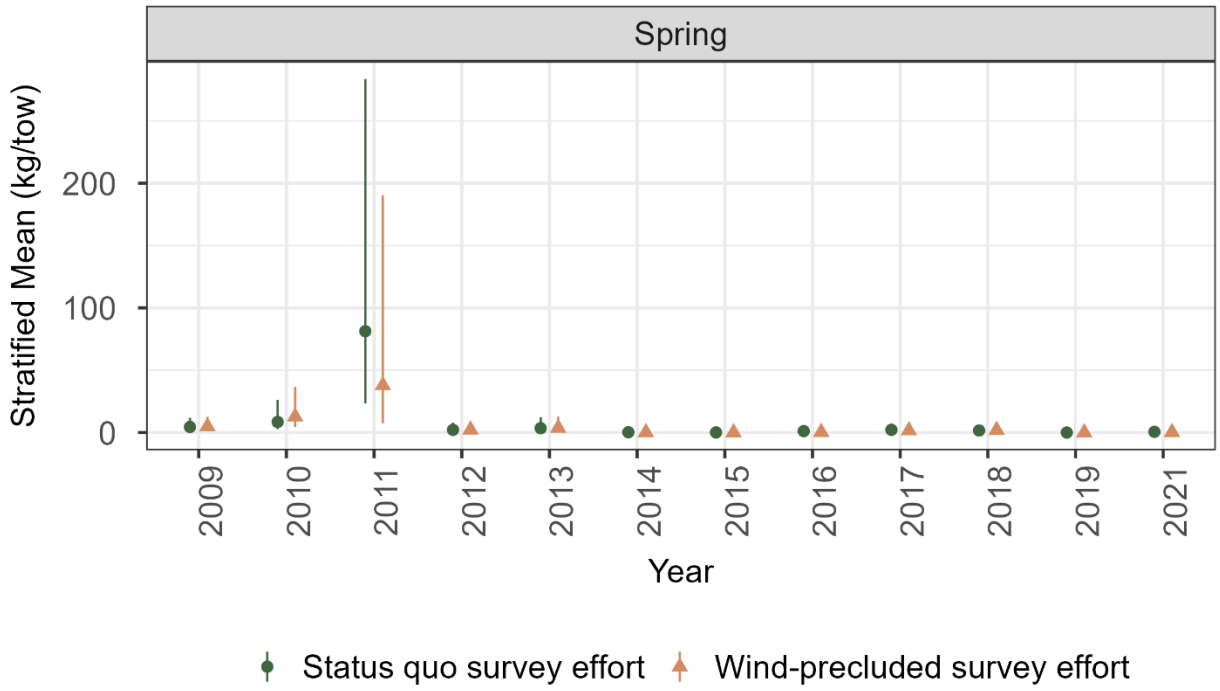

Figure A33. Spring estimates of annual abundance for striped bass.

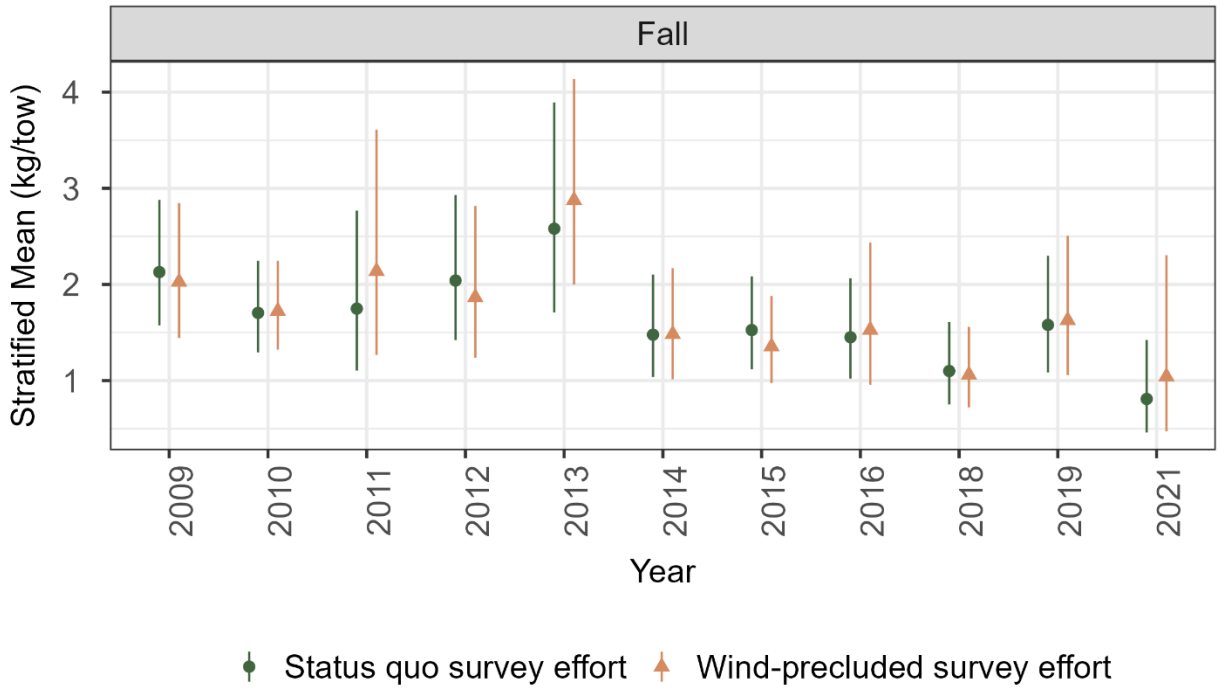

Figure A34. Fall estimates of annual abundance for windowpane flounder.

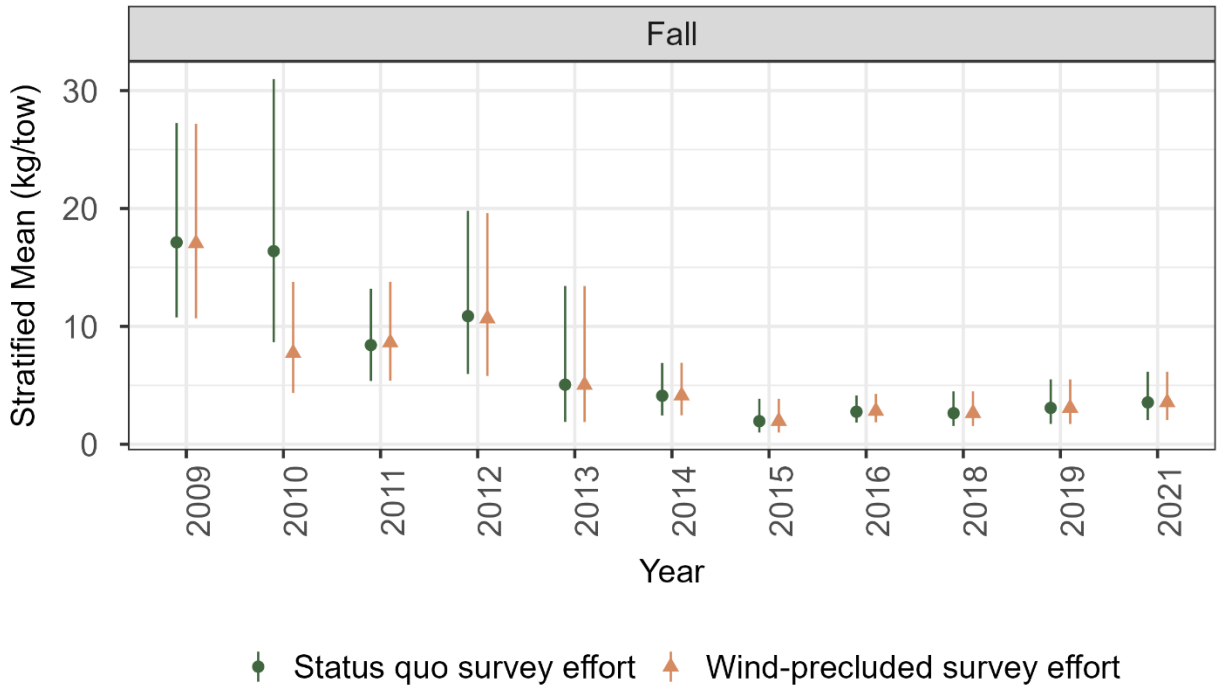

Figure A35. Fall estimates of annual abundance for yellowtail flounder.

A2. Stakeholder-selected Species

Seasonal annual abundance indices for each of the stakeholder-identified species from the SSEEP workshops under a status quo survey effort assumption (green) and a wind-precluded survey effort assumption (orange). The bars on each of the points represent the standard error around the stratified mean.

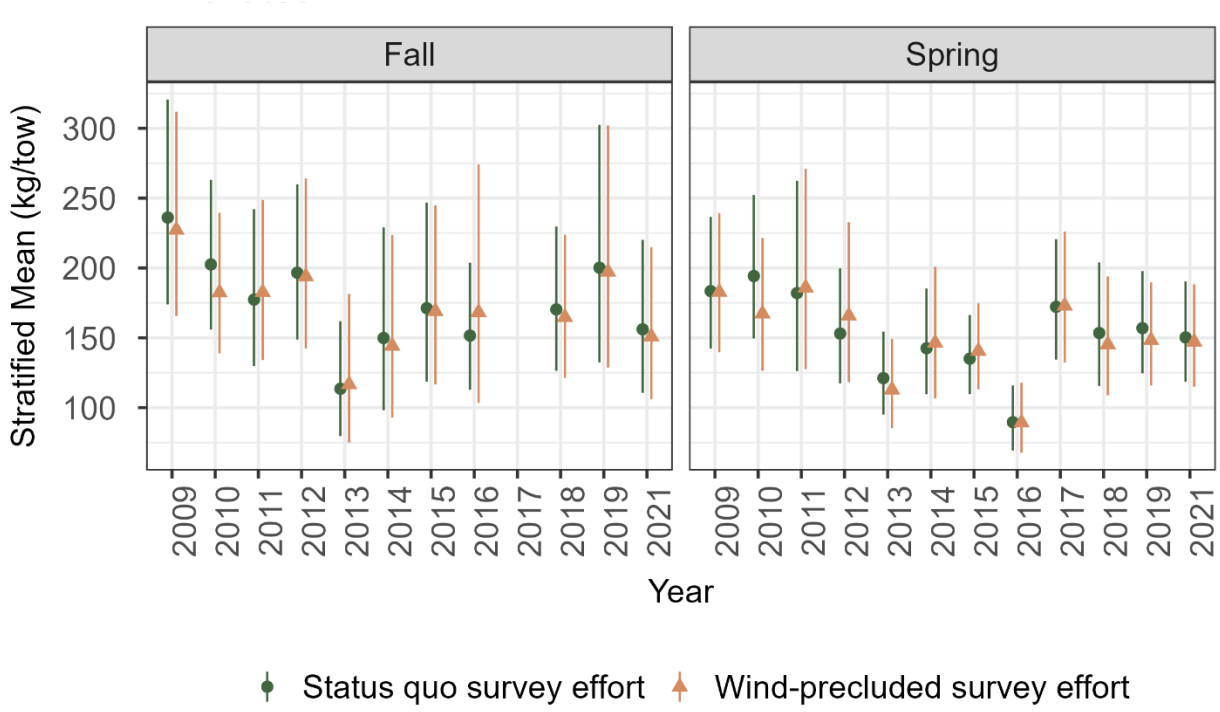

Figure A36. Fall and spring estimates of annual abundance for the skate complex.

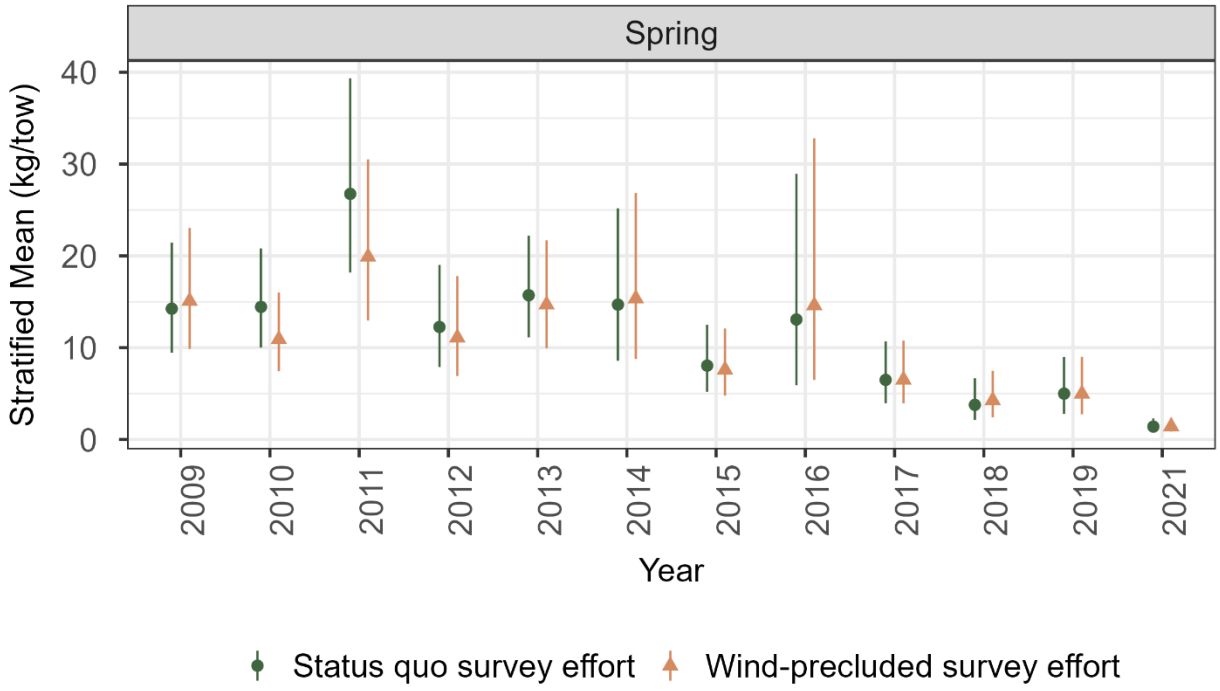

Figure A37. Spring estimates of annual abundance for Atlantic herring.

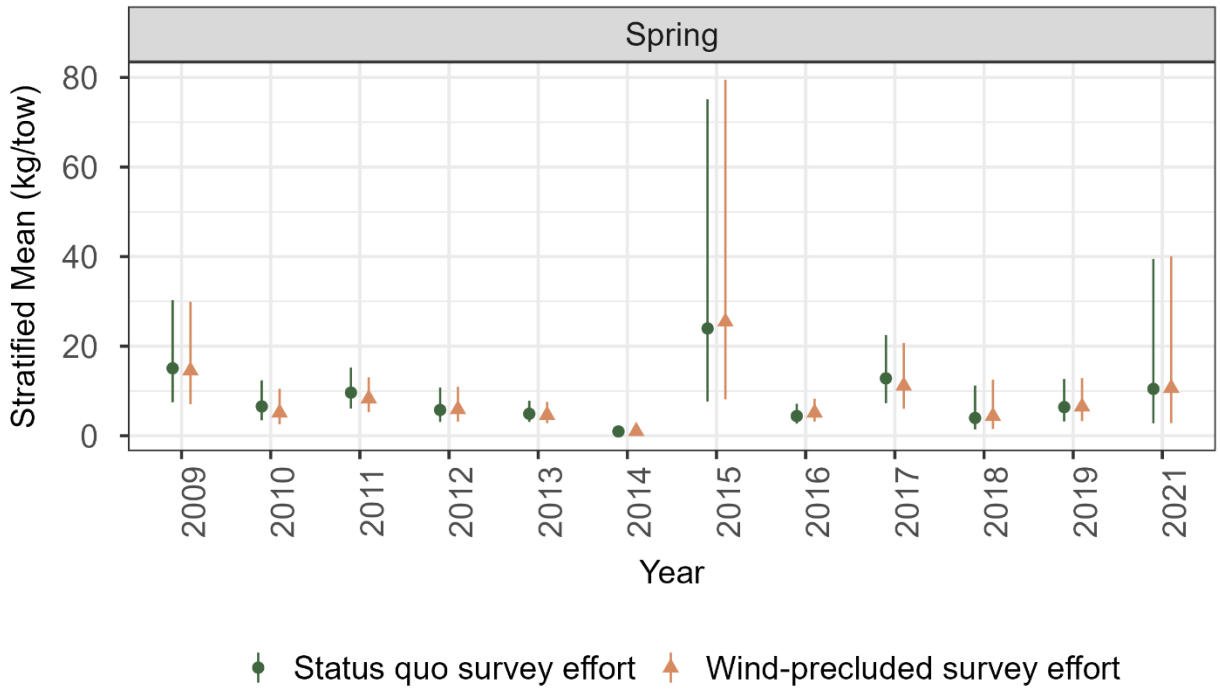

Figure A38. Spring estimates of annual abundance for Atlantic mackerel.

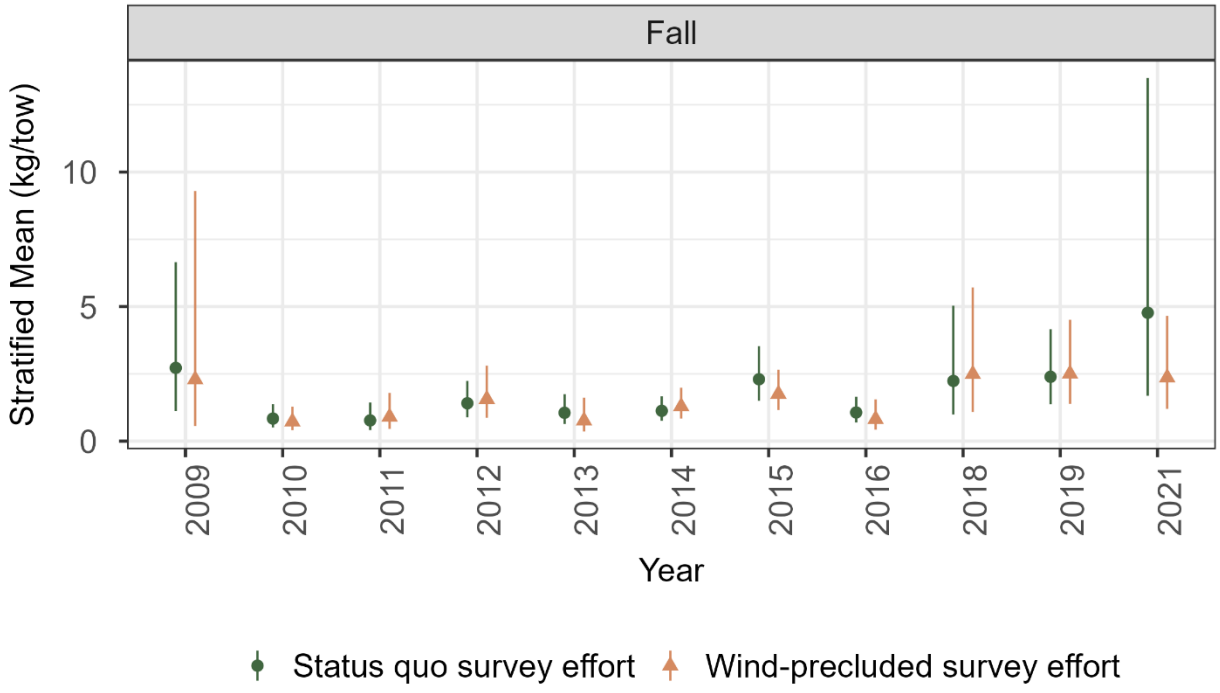

Figure A39. Fall estimates of annual abundance for black sea bass.

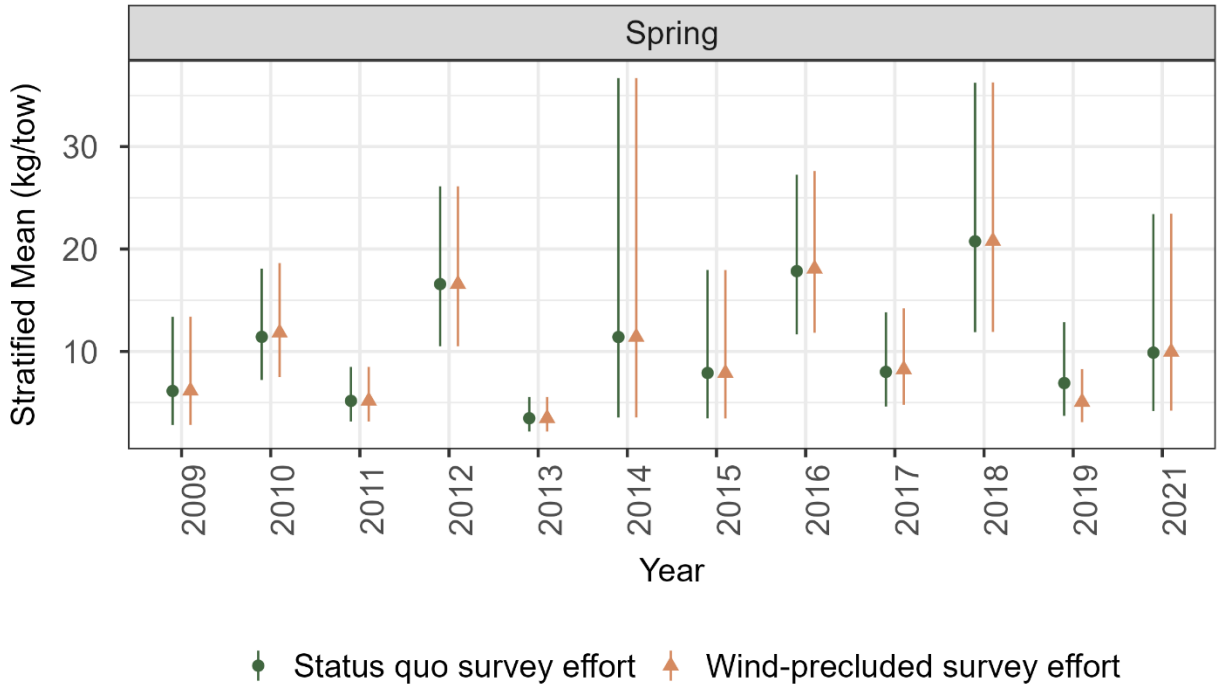

Figure A40. Spring estimates of annual abundance for butterfish.

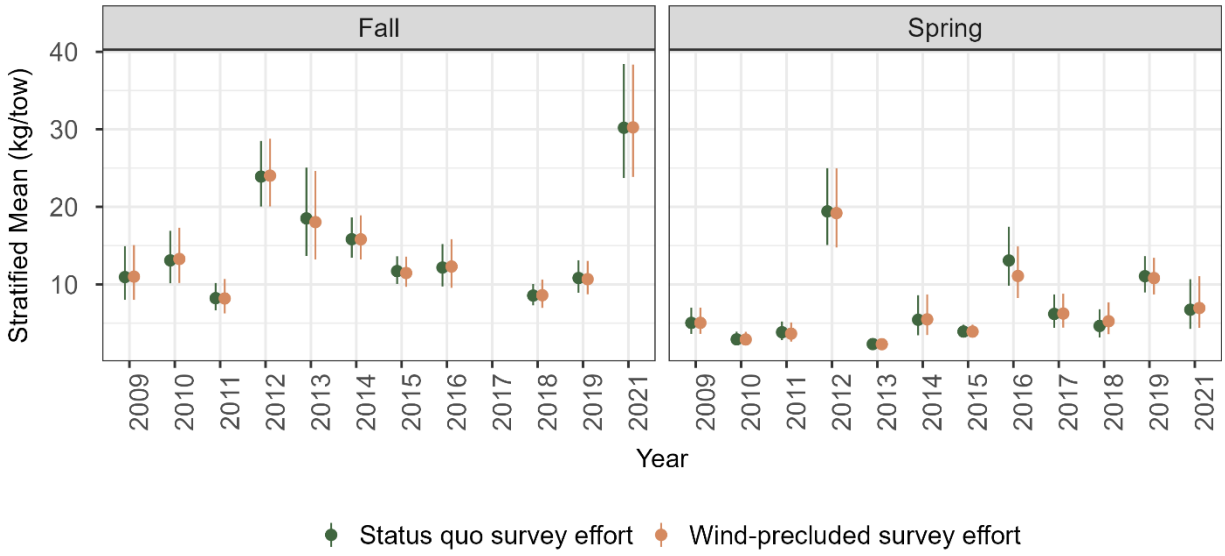

Figure A41. Fall and spring estimates of annual abundance for longfin squid.

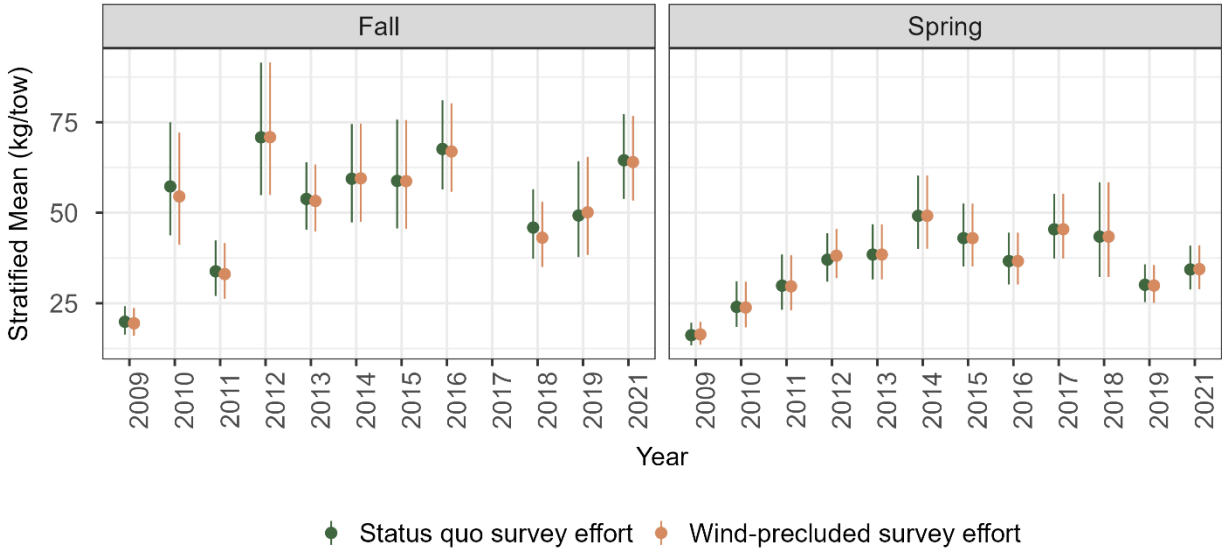

Figure A42. Fall and spring estimates of annual abundance for silver hake.

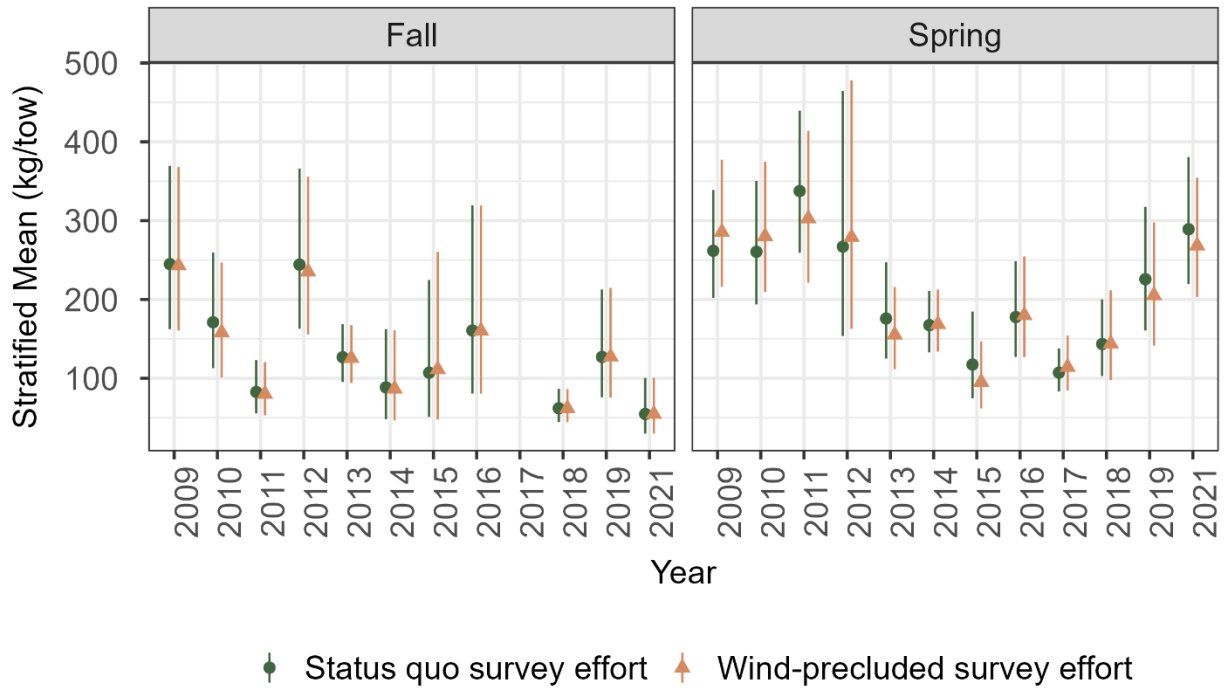

Figure A43. Fall and spring estimates of annual abundance for spiny dogfish.

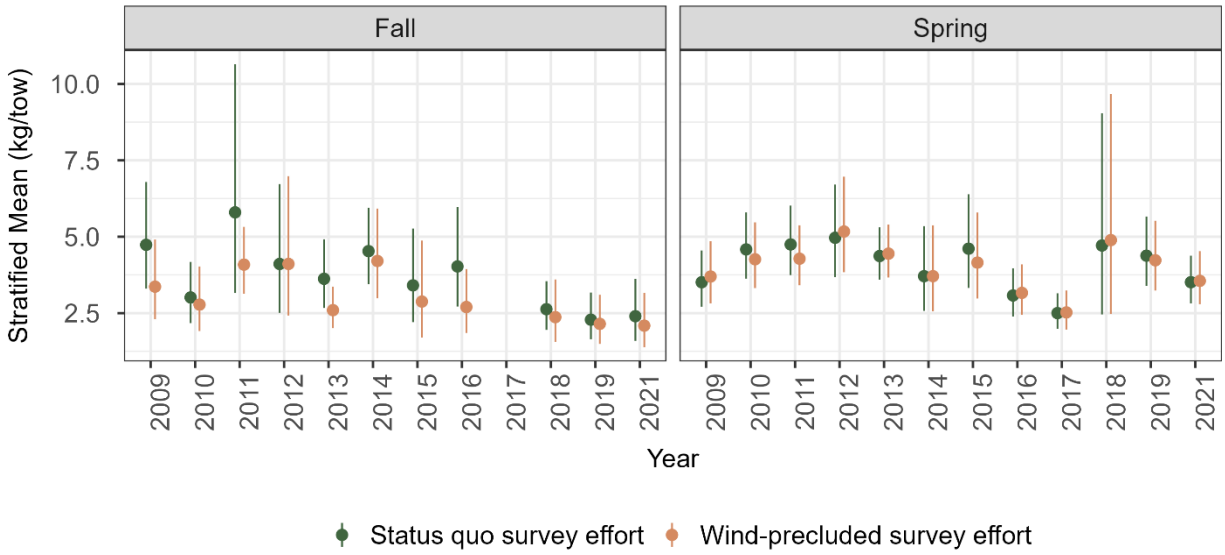

Figure A44. Fall and spring estimates of annual abundance for summer flounder.

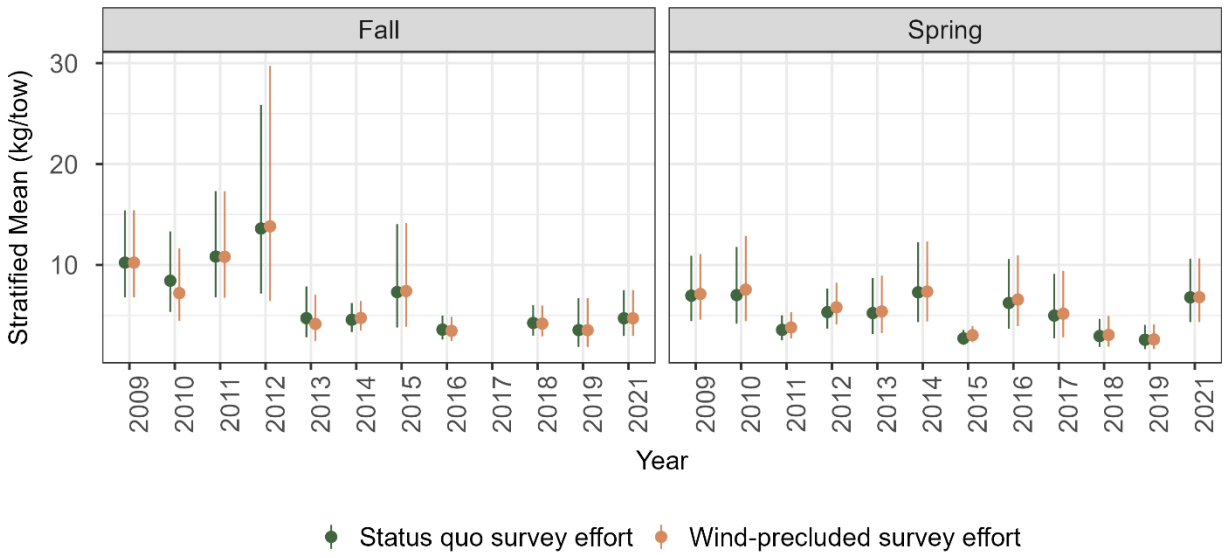

Figure A45. Fall and spring estimates of annual abundance for winter flounder.

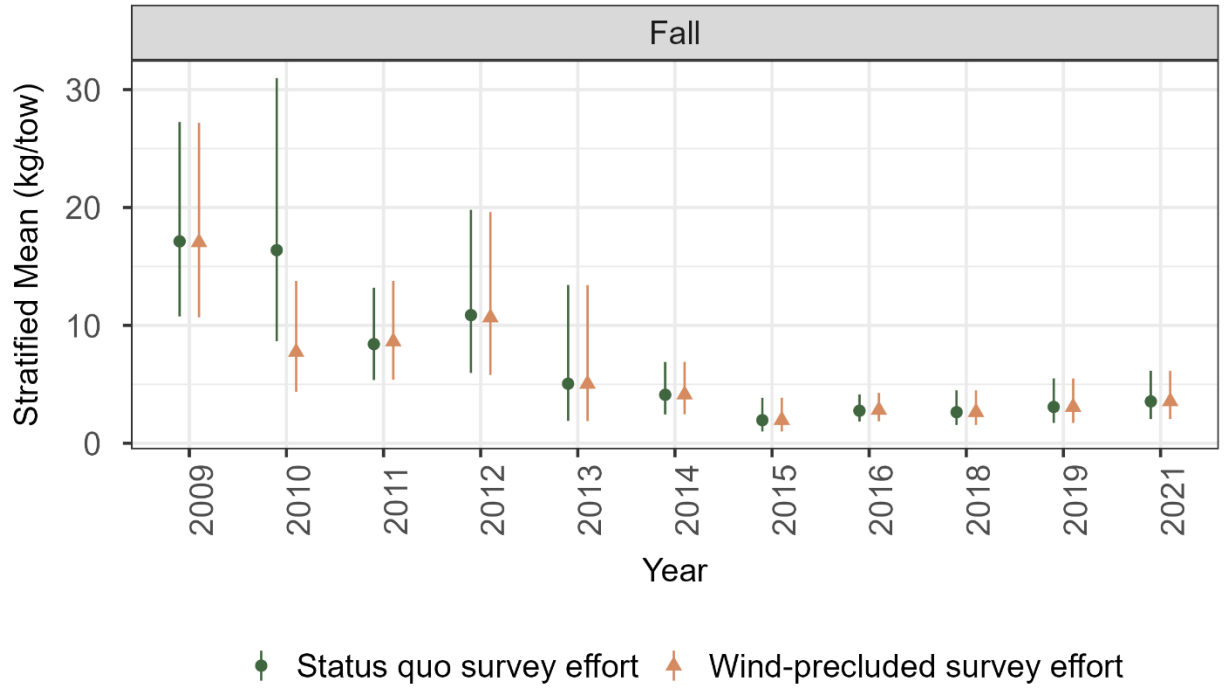

Figure A46. Fall estimates of annual abundance for yellowtail flounder.

A3. Species Distribution Models

Additional diagnostic plots for the fall and spring summer flounder models as well as the spring Atlantic mackerel model.

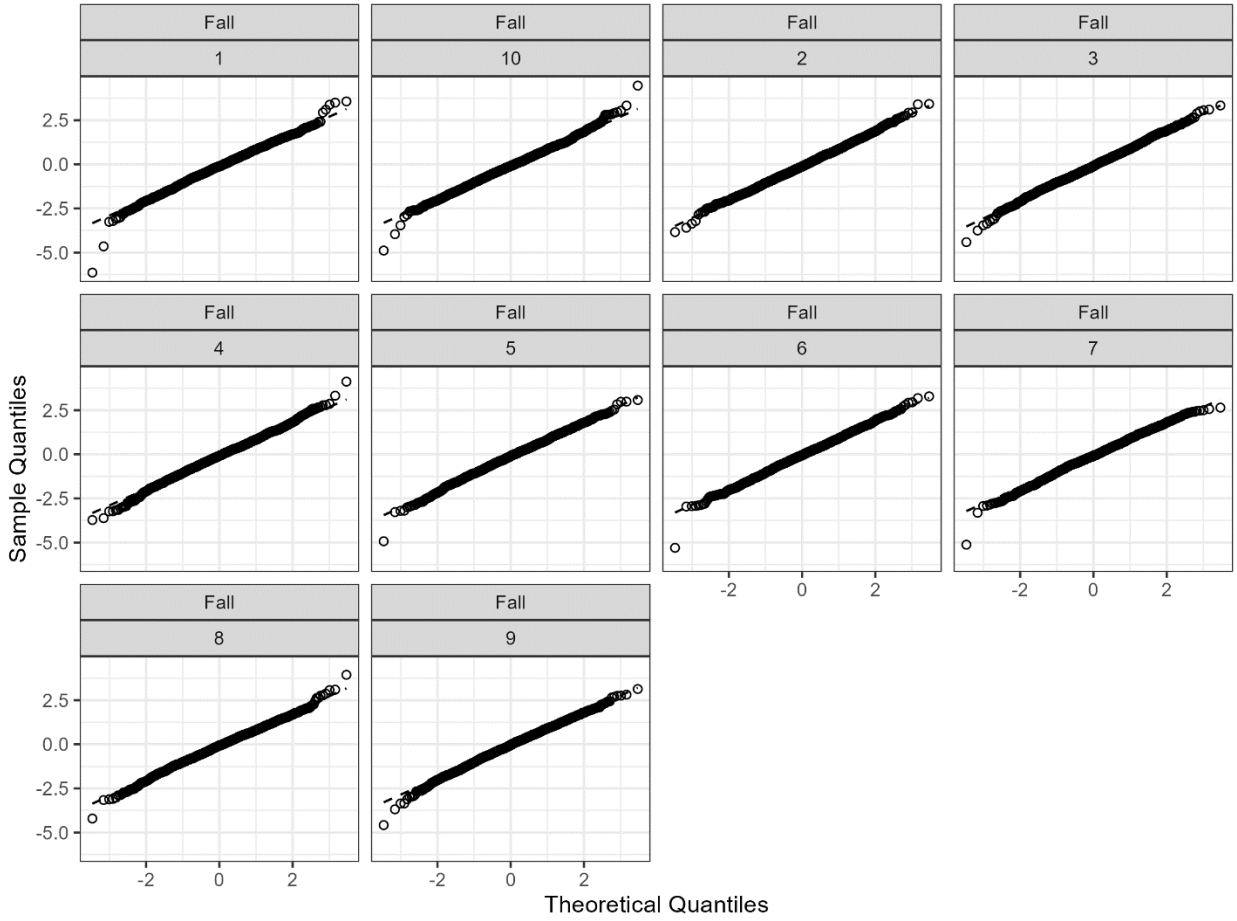

Figure A47. Quantile-quantile plots of observed quantiles across each simulation of MCMC-resampled residuals compared to the theoretical quantiles of residuals from the model fit to fall summer flounder survey data.

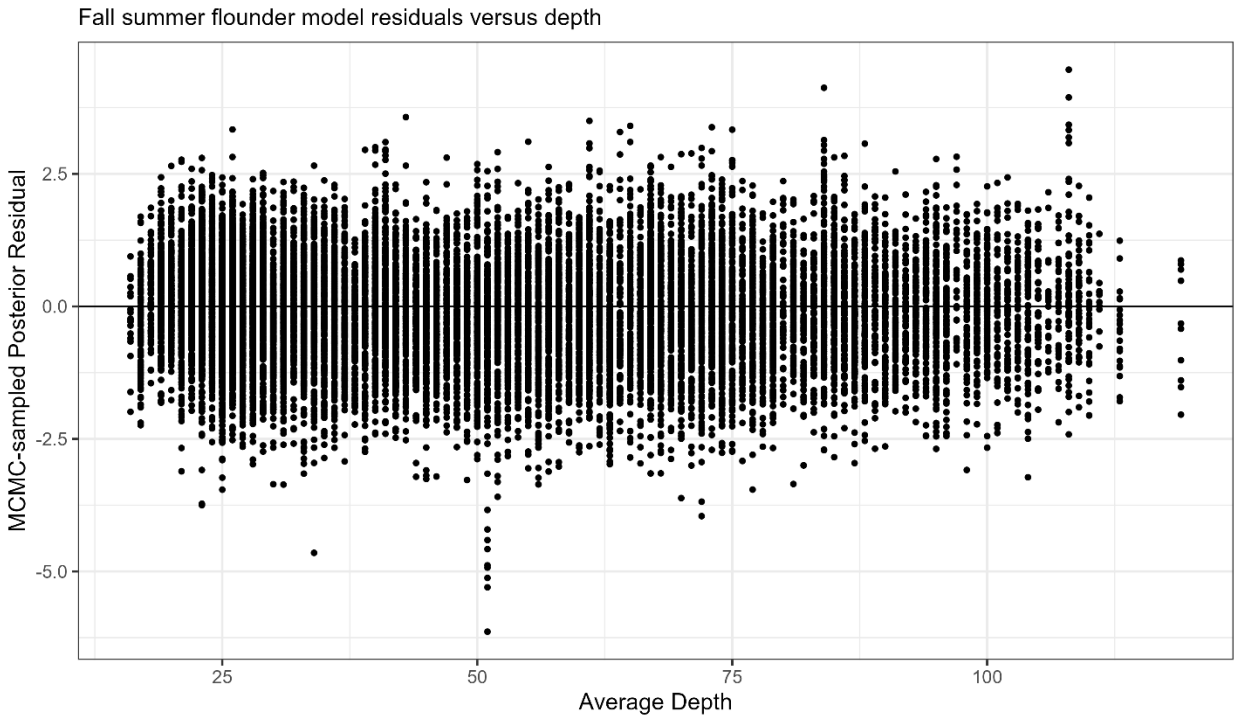

Figure A48. The distribution of MCMC-resampled residuals predicted over 10 simulations for summer flounder compared to the observed values of average depth fit to fall summer flounder survey data.

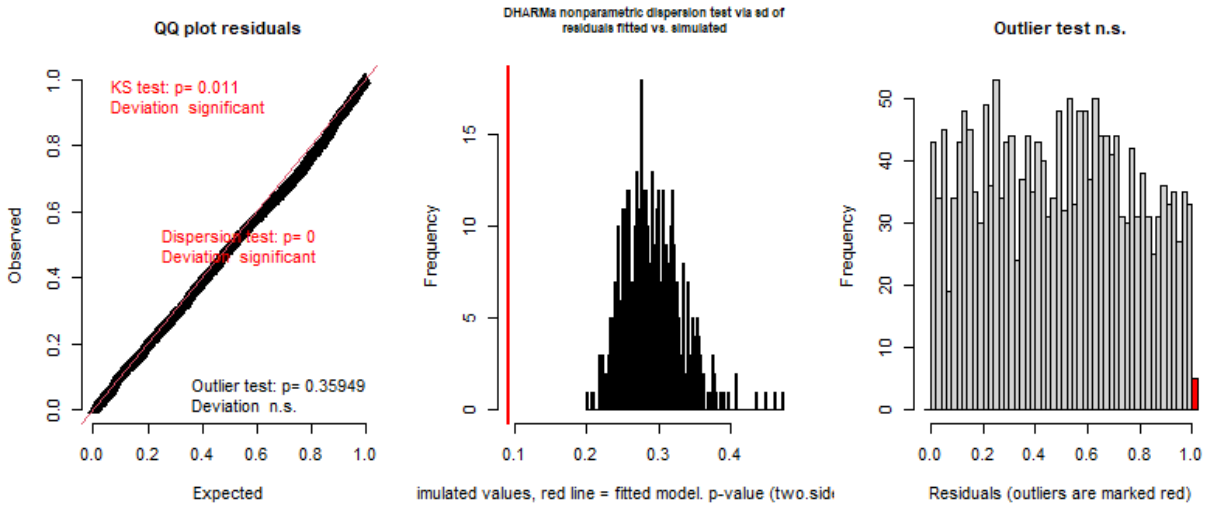

Figure A49. The quantile-quantile plot of DHARMa-simulated residuals (left plot) and the distribution of residuals plotted against the predicted values (right plot) from the optimal fall summer flounder model.

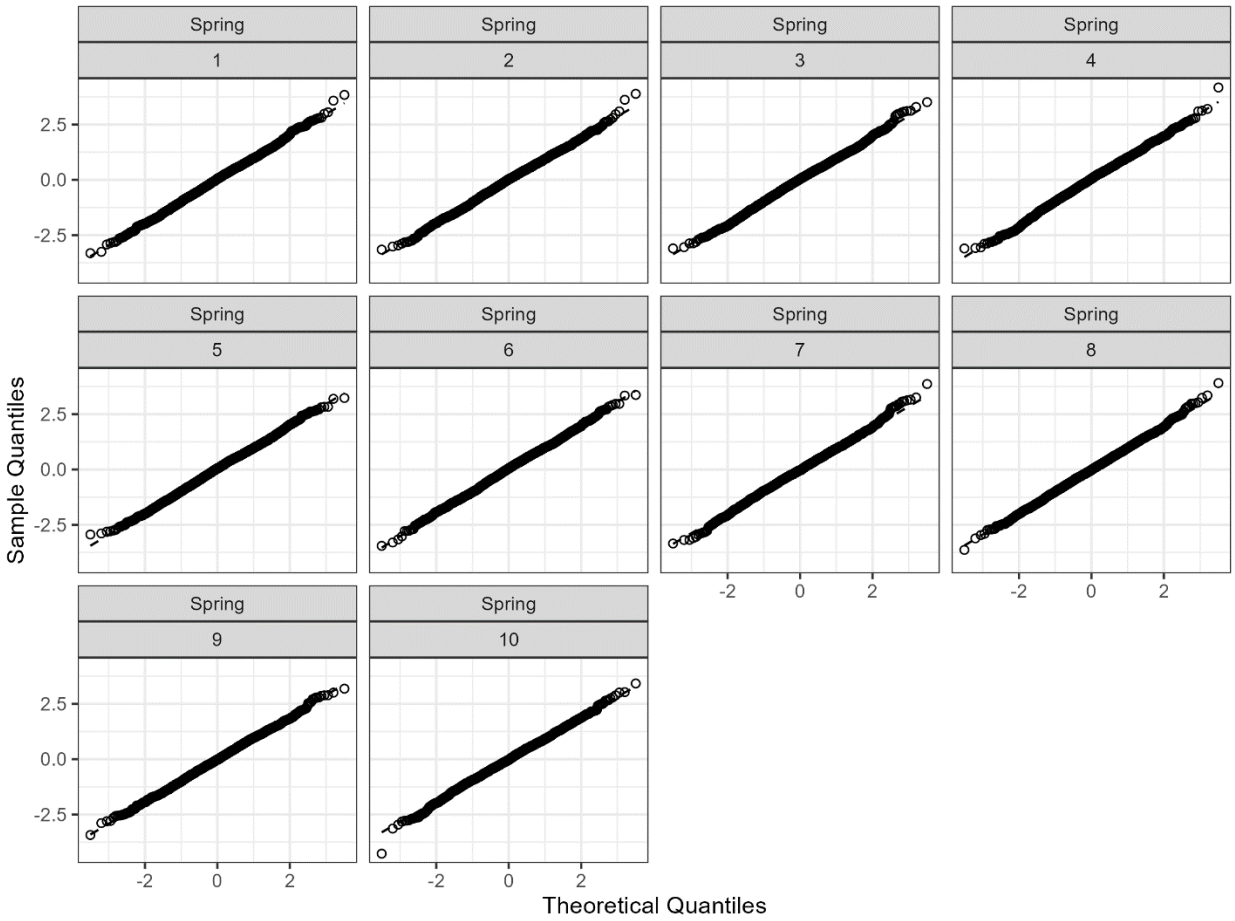

Figure A50. Quantile-quantile plots of observed quantiles across each simulation of MCMC-resampled residuals compared to the theoretical quantiles of residuals from the model fit to spring summer flounder survey data.

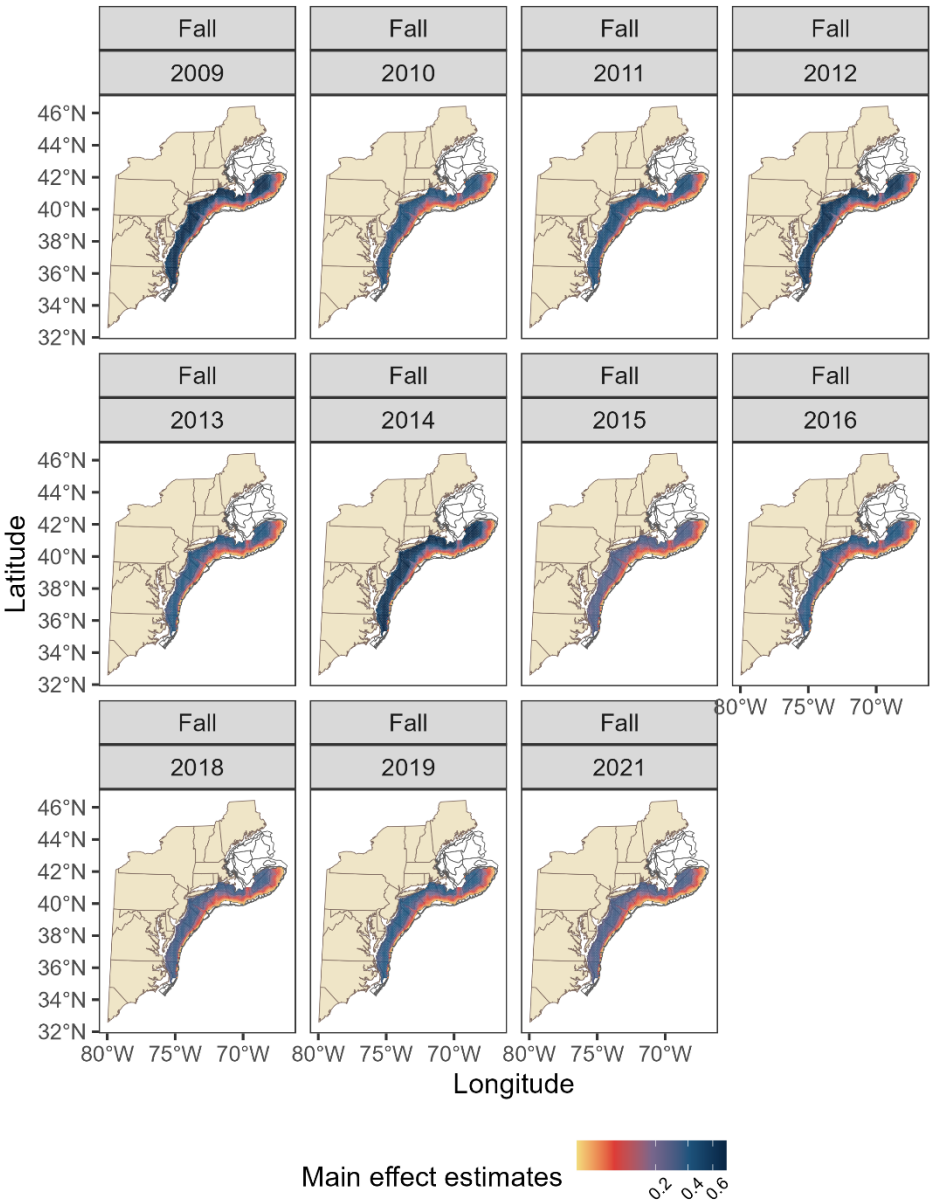

Figure A51. Estimates of the fixed effects across the full time series from the optimal fall model for summer flounder.

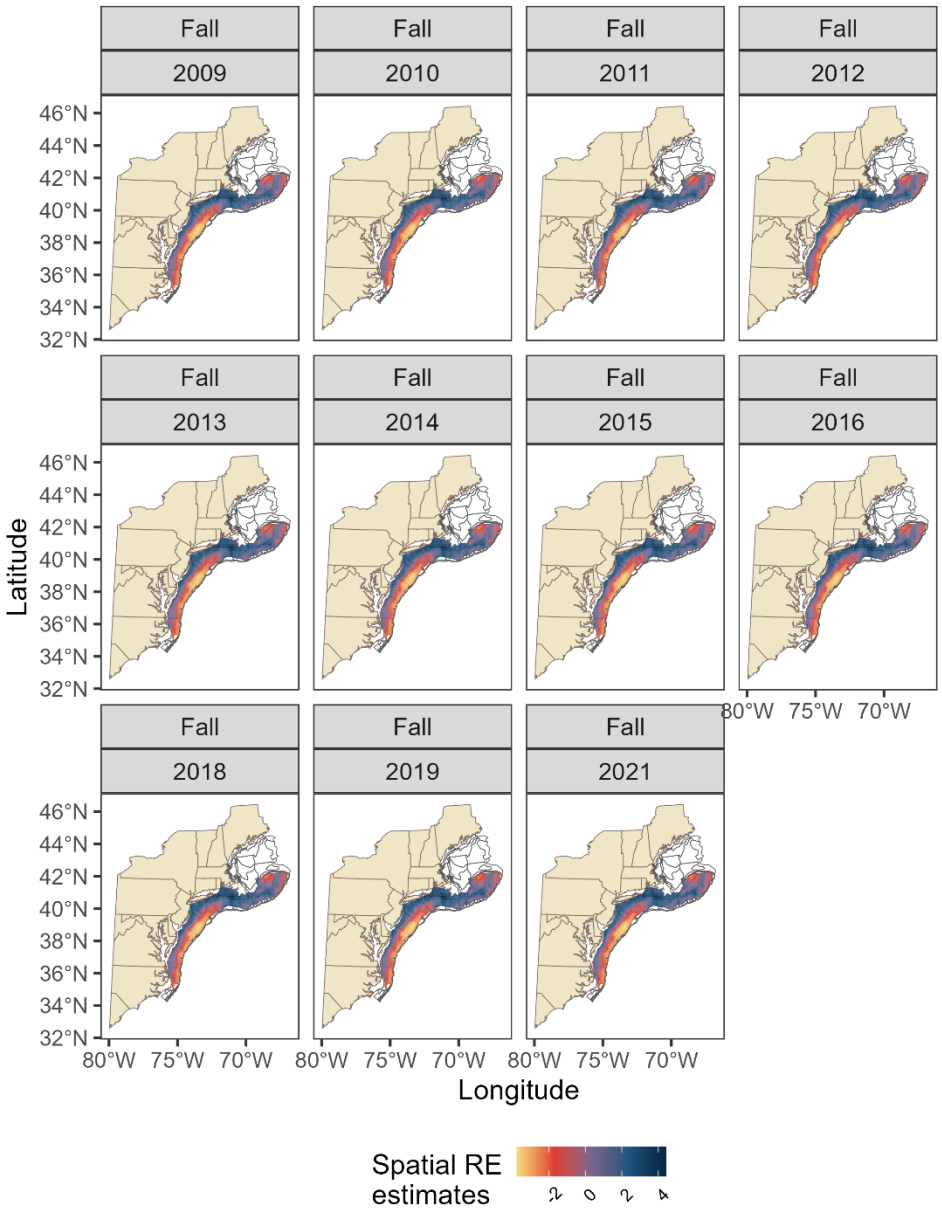

Figure A52. Estimates of the spatial random effects across the full time series from the optimal fall model for summer flounder.

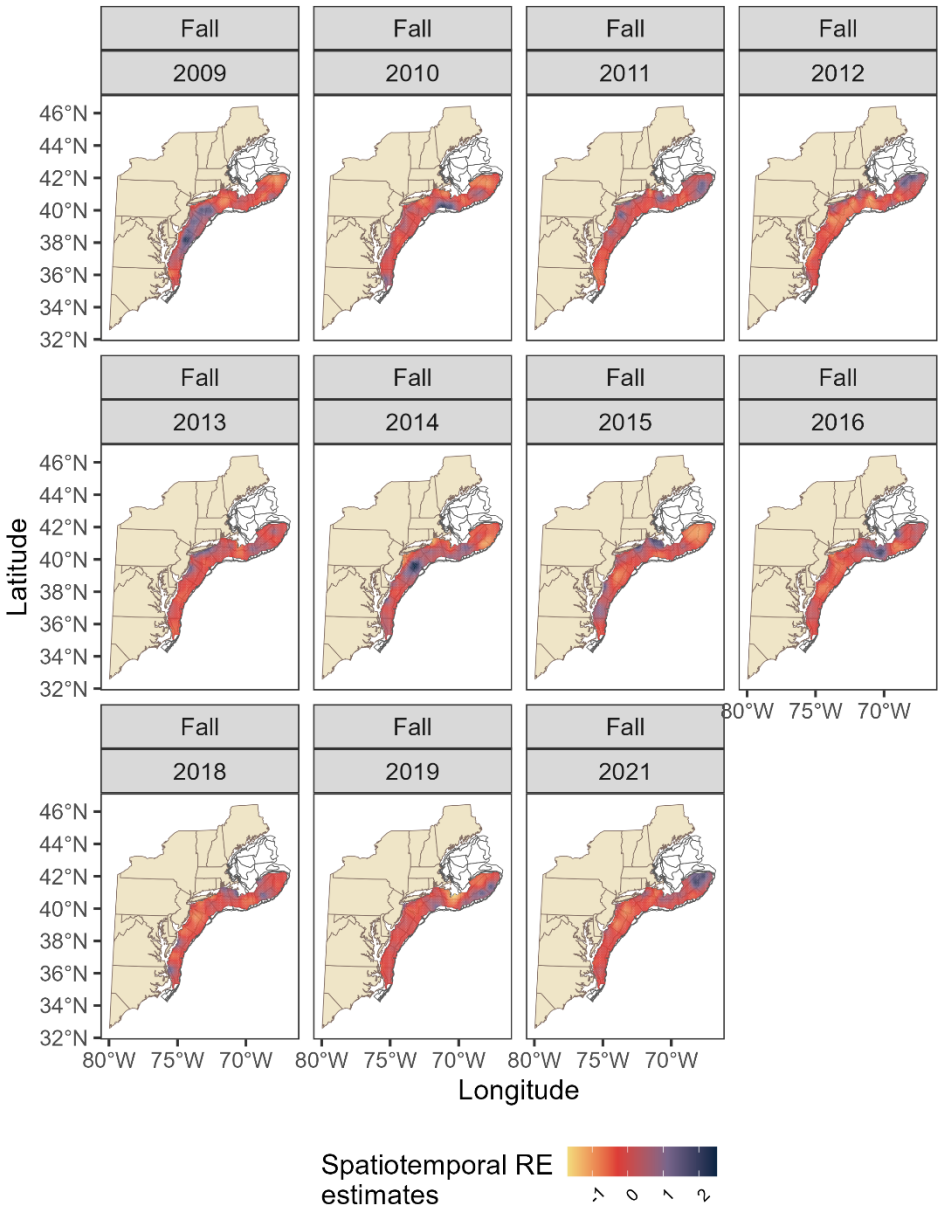

Figure A53. Estimates of the spatiotemporal random effects across the full time series from the optimal fall model for summer flounder.

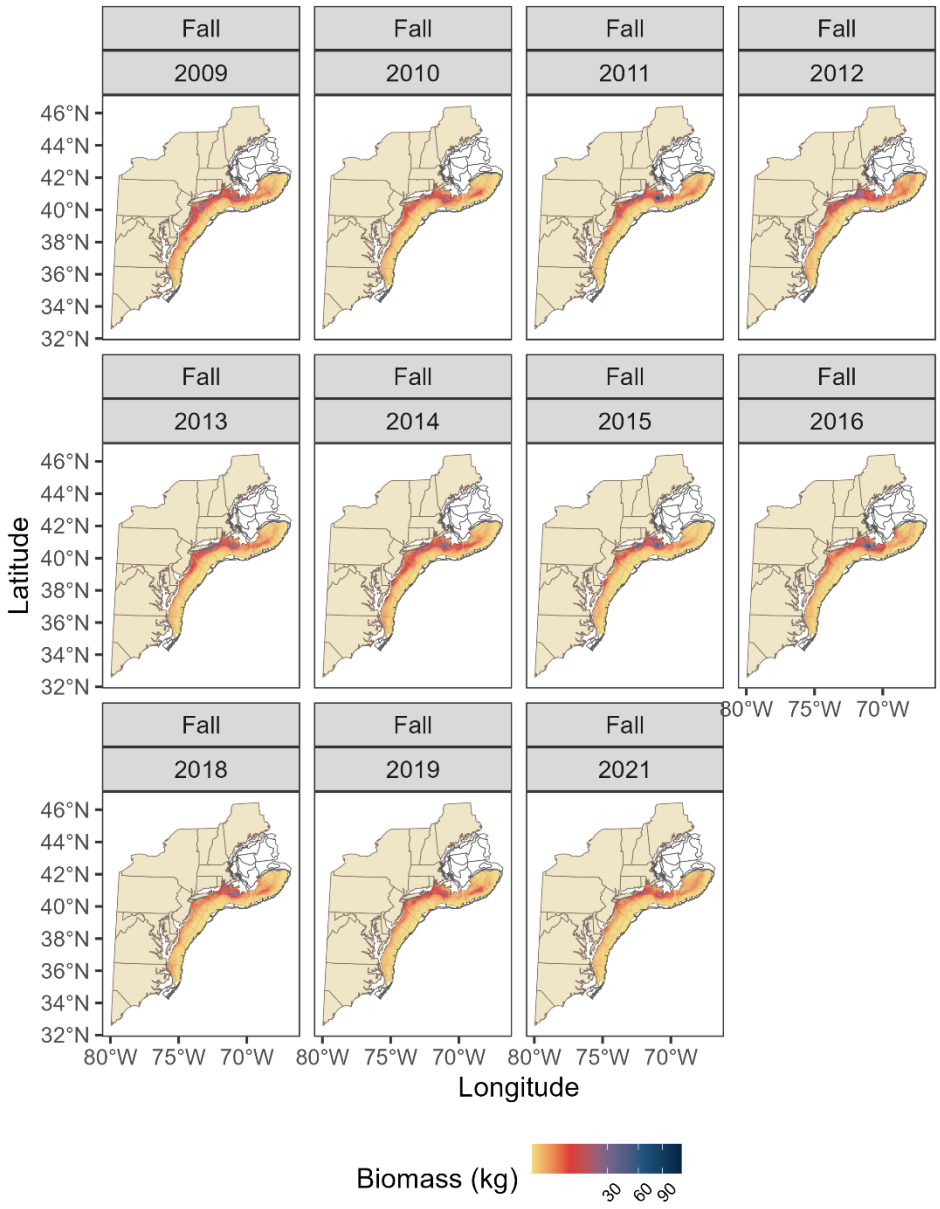

Figure A54. Estimates of biomass across the full time series from the optimal fall model for summer flounder.

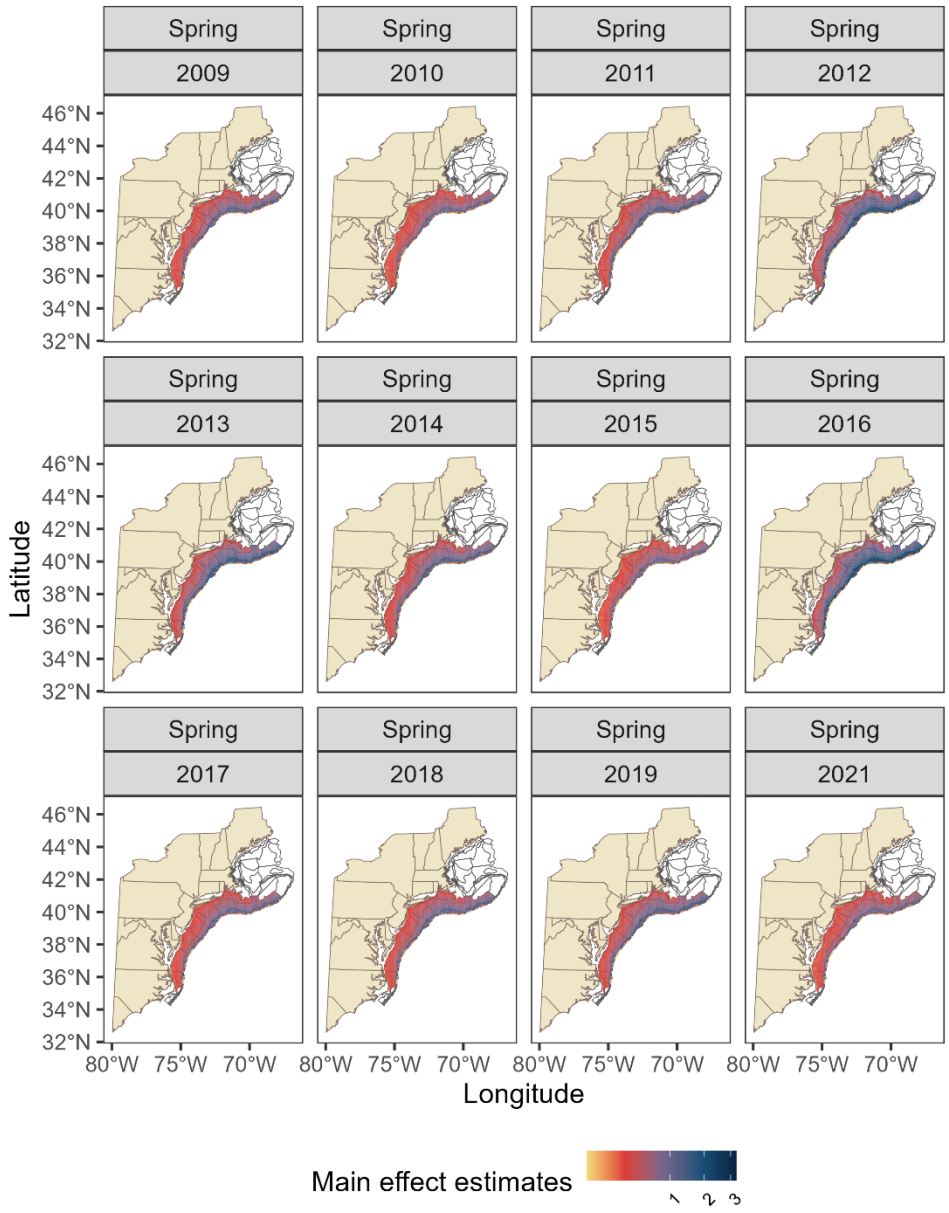

Figure A55. Estimates of the fixed effects across the full time series from the optimal spring model for summer flounder.

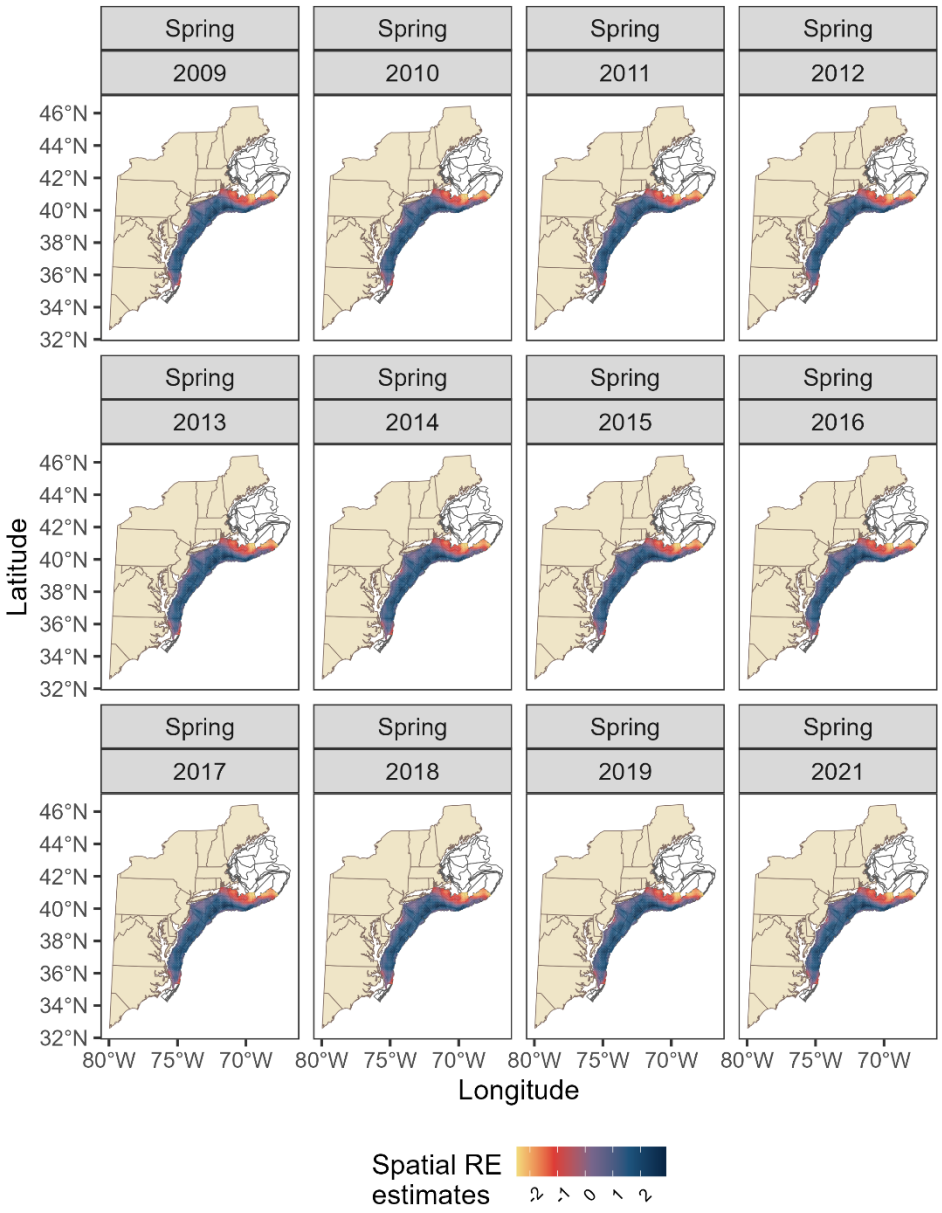

Figure A56. Estimates of the spatial random effects across the full time series from the optimal spring model for summer flounder.

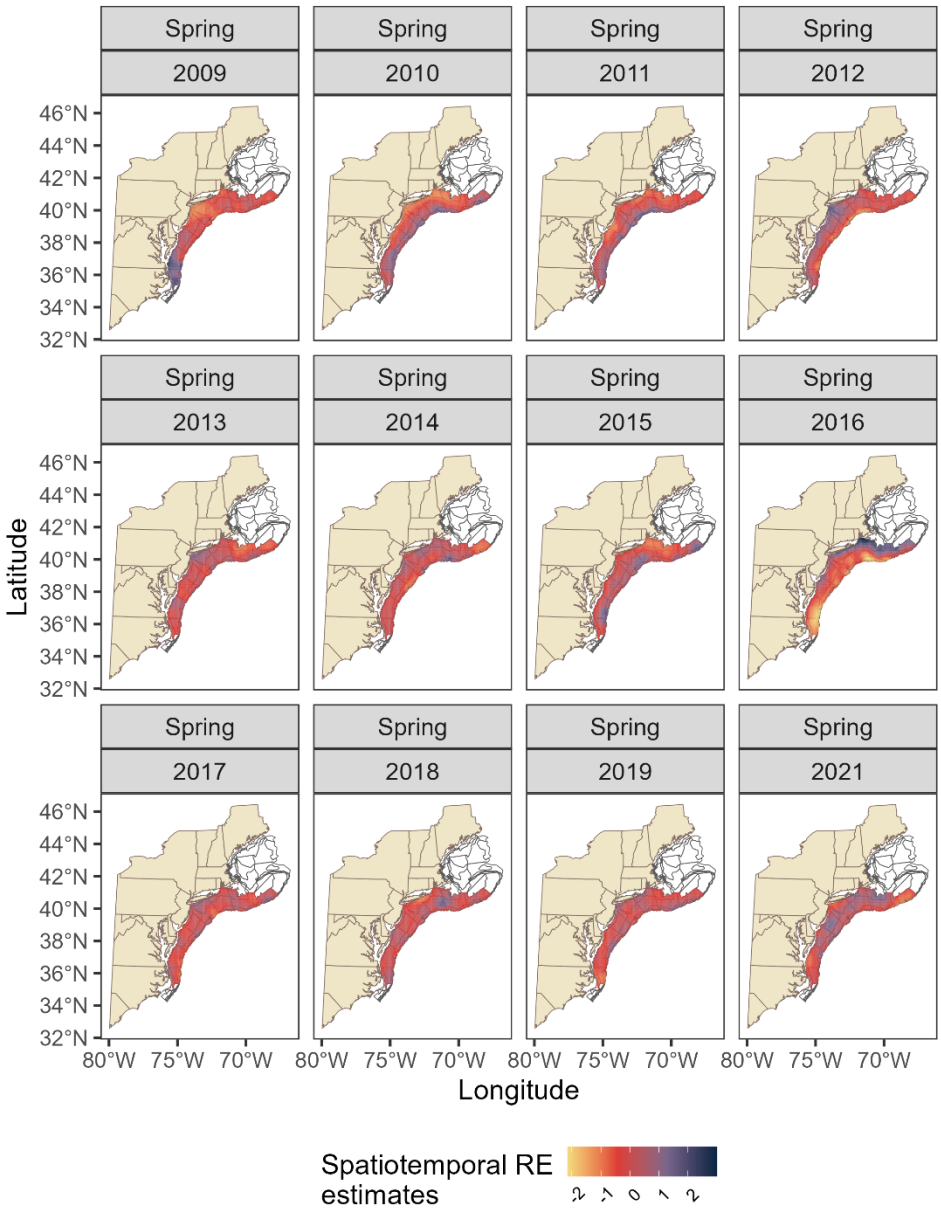

Figure A57. Estimates of the spatiotemporal random effects across the full time series from the optimal spring model for summer flounder.

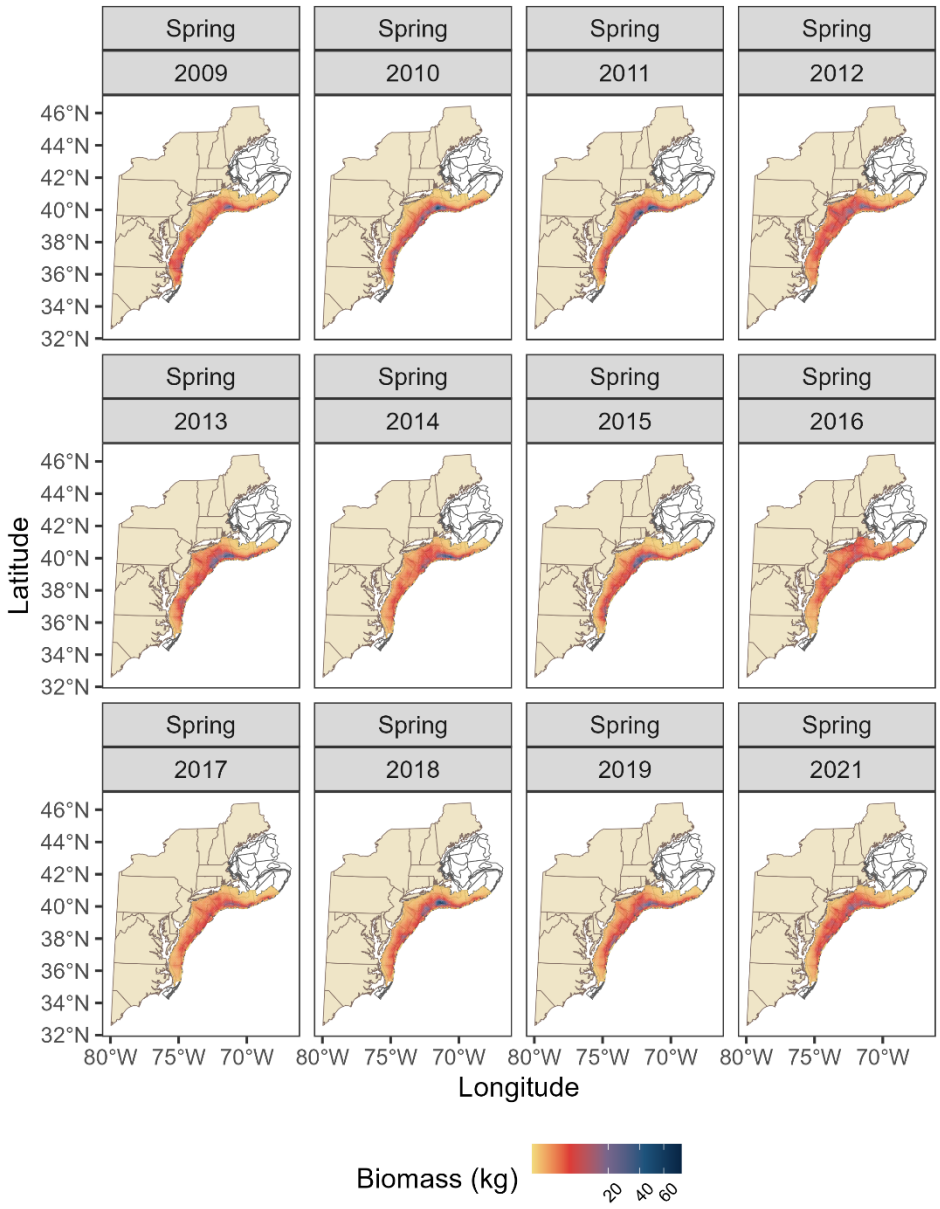

Figure A58. Estimates of biomass across the full time series from the optimal spring model for summer flounder.

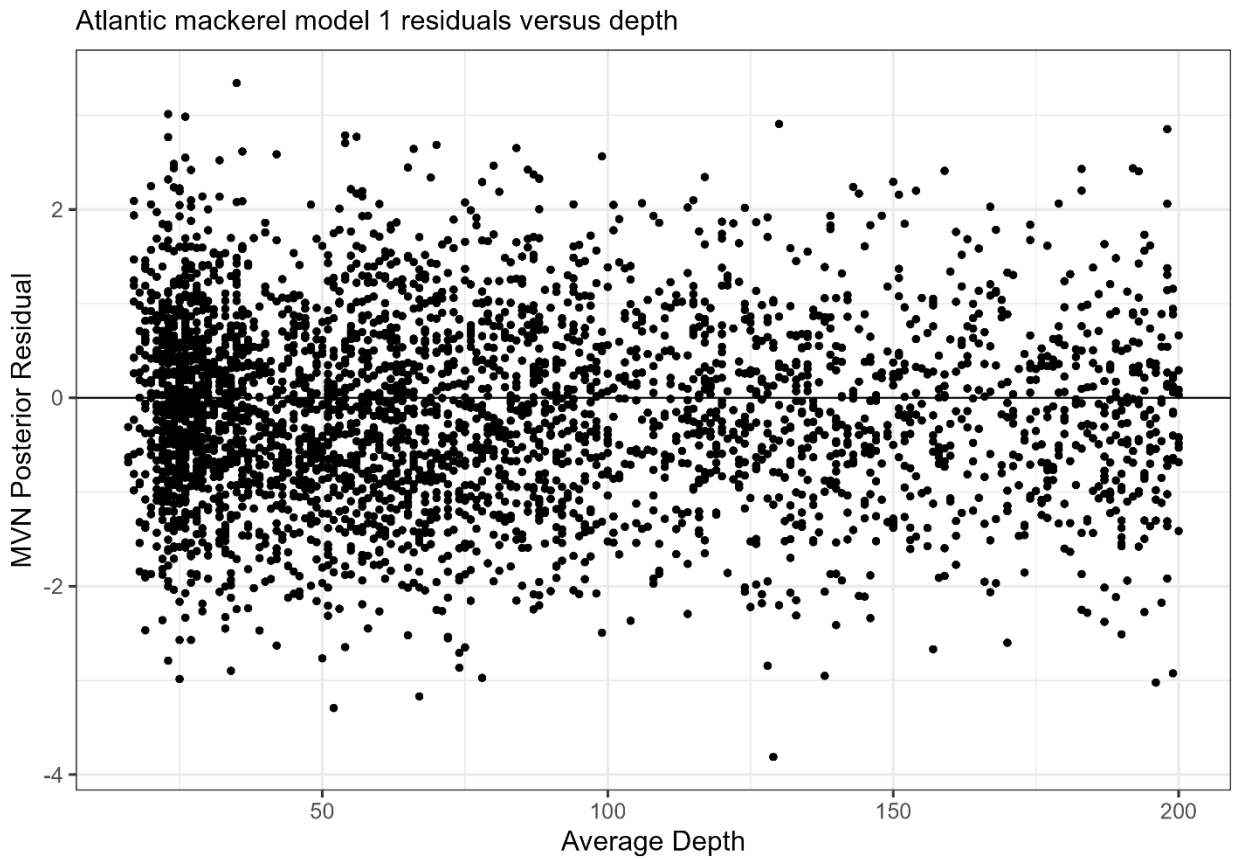

Figure A59. The distribution of MCMC-resampled residuals predicted from the presence-absence model component compared to the observed values of average depth fit to spring Atlantic mackerel survey data.

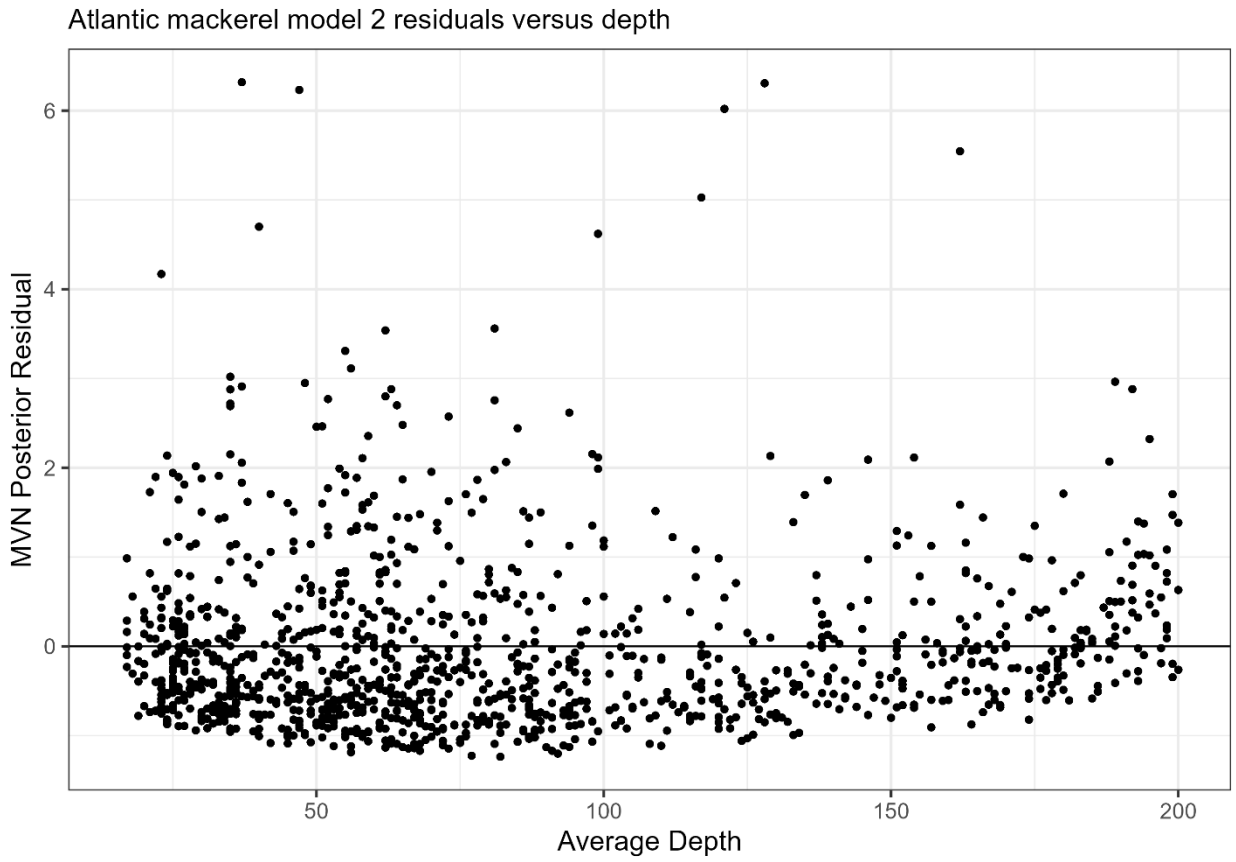

Figure A60. The distribution of MCMC-resampled residuals predicted from the positive encounter model component compared to the observed values of average depth fit to spring Atlantic mackerel survey data.

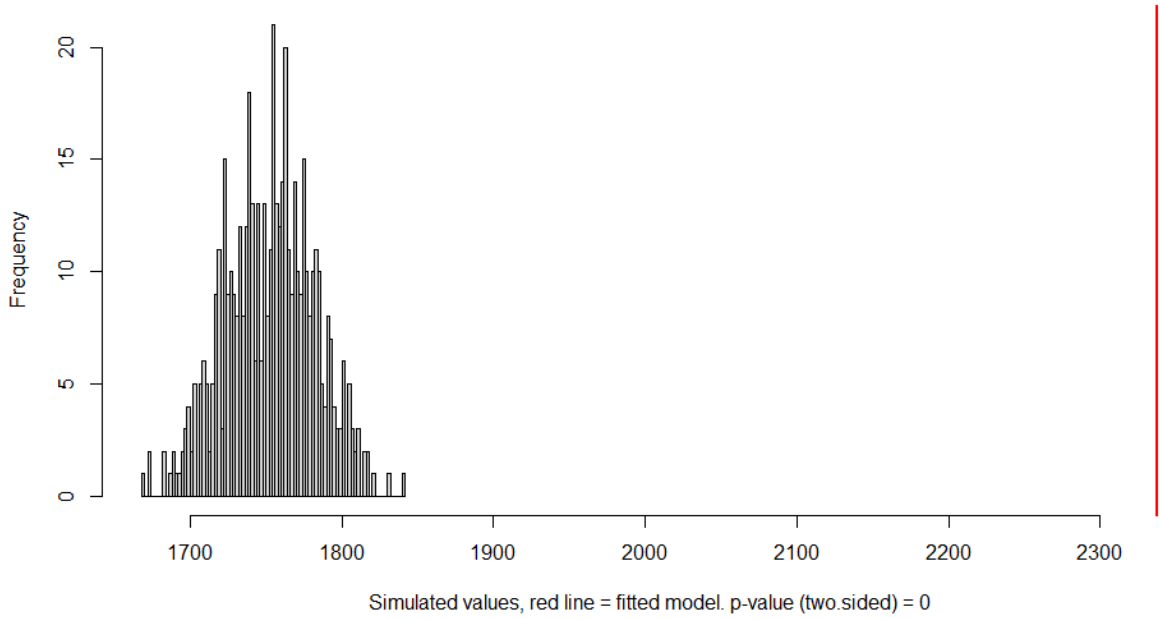

Figure A61. DHARMa zero-inflation test via comparison to expected zeros with simulation under the fitted model for spring Atlantic mackerel.

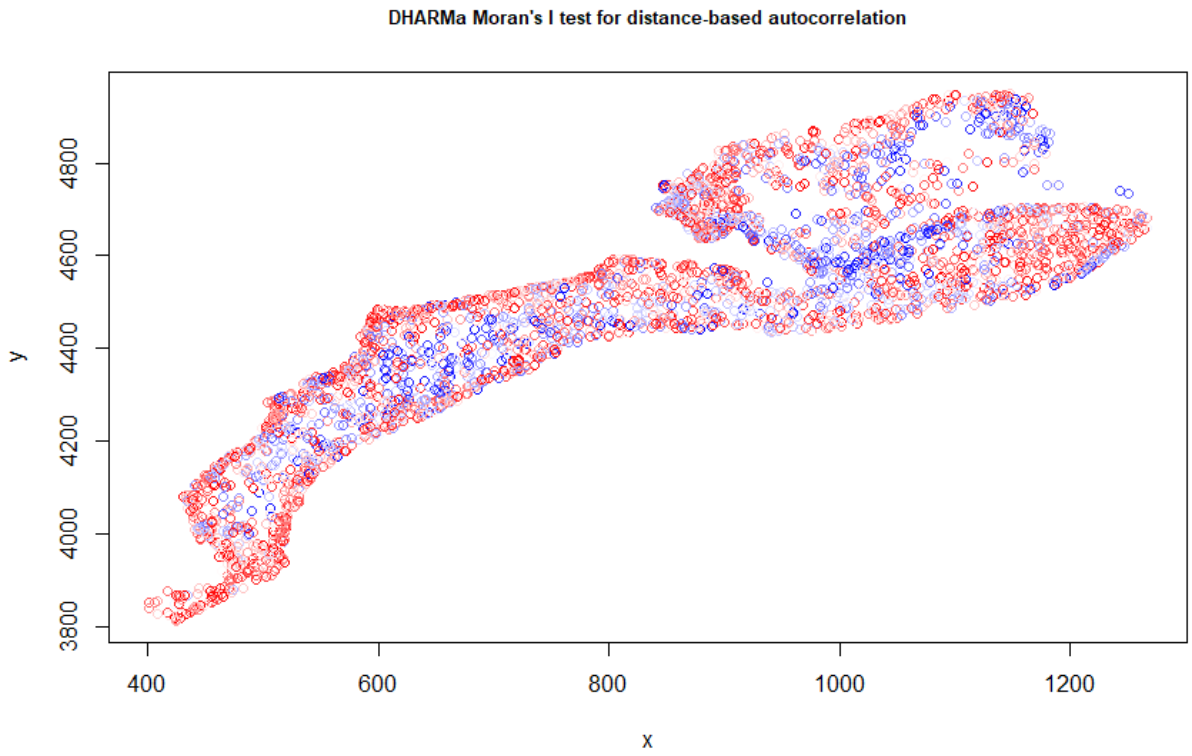

Figure A62. DHARMa Moran's I test for spatial autocorrelation for the spring Atlantic mackerel model.

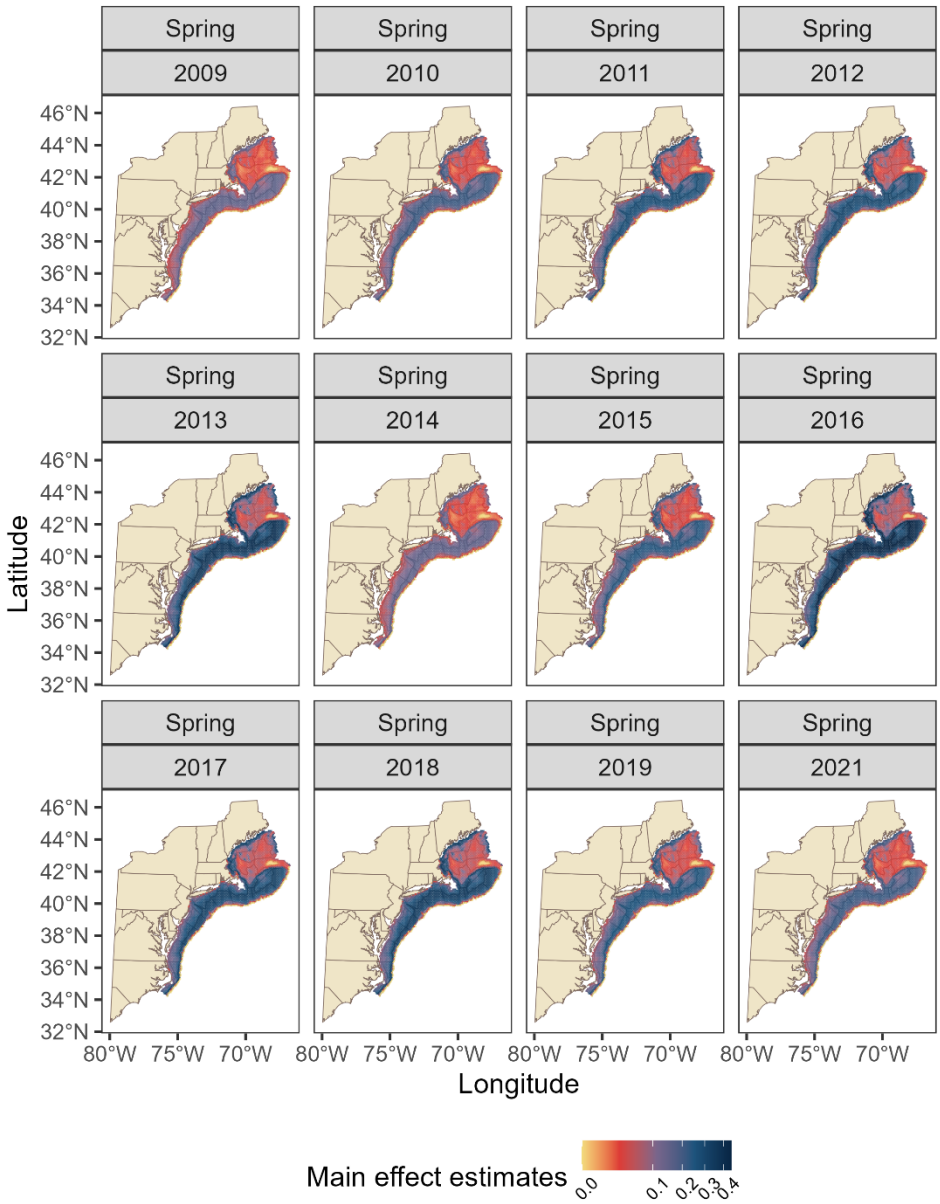

Figure A63. Estimates of fixed effects across the full time series from the optimal spring model for Atlantic mackerel.

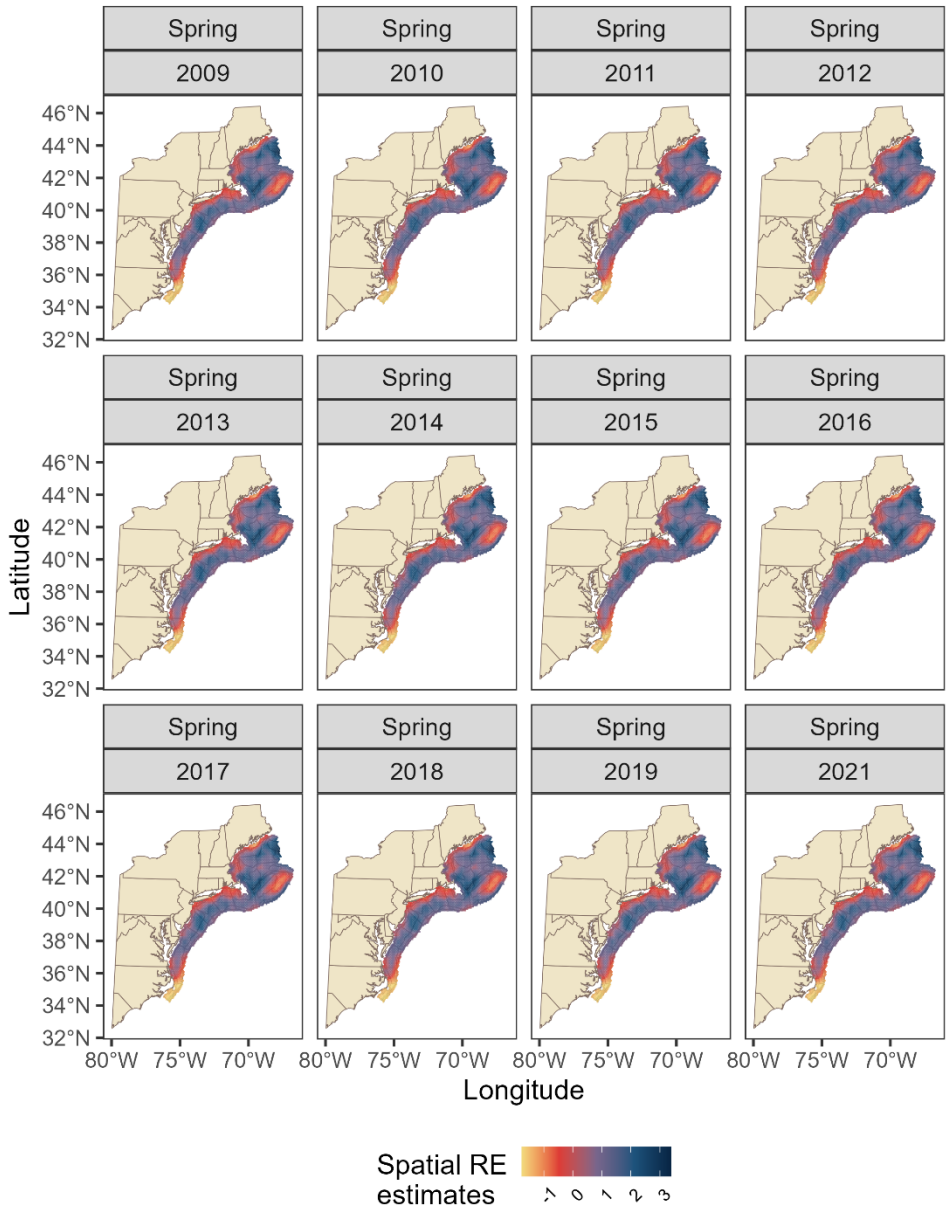

Figure A64. Estimates of spatial random effects across the full time series from the optimal spring model for Atlantic mackerel.

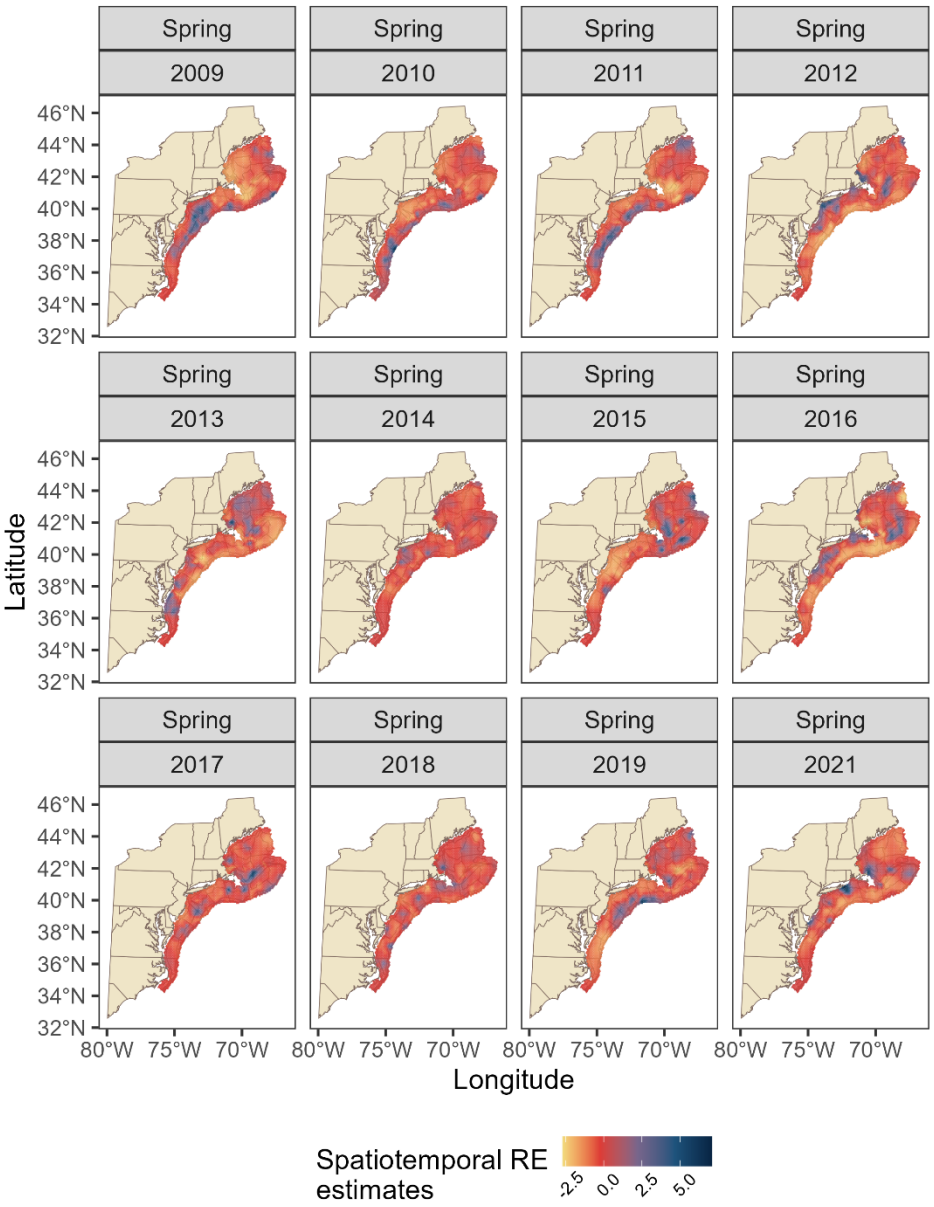

Figure A65. Estimates of spatiotemporal random effects across the full time series from the optimal spring model for Atlantic mackerel.

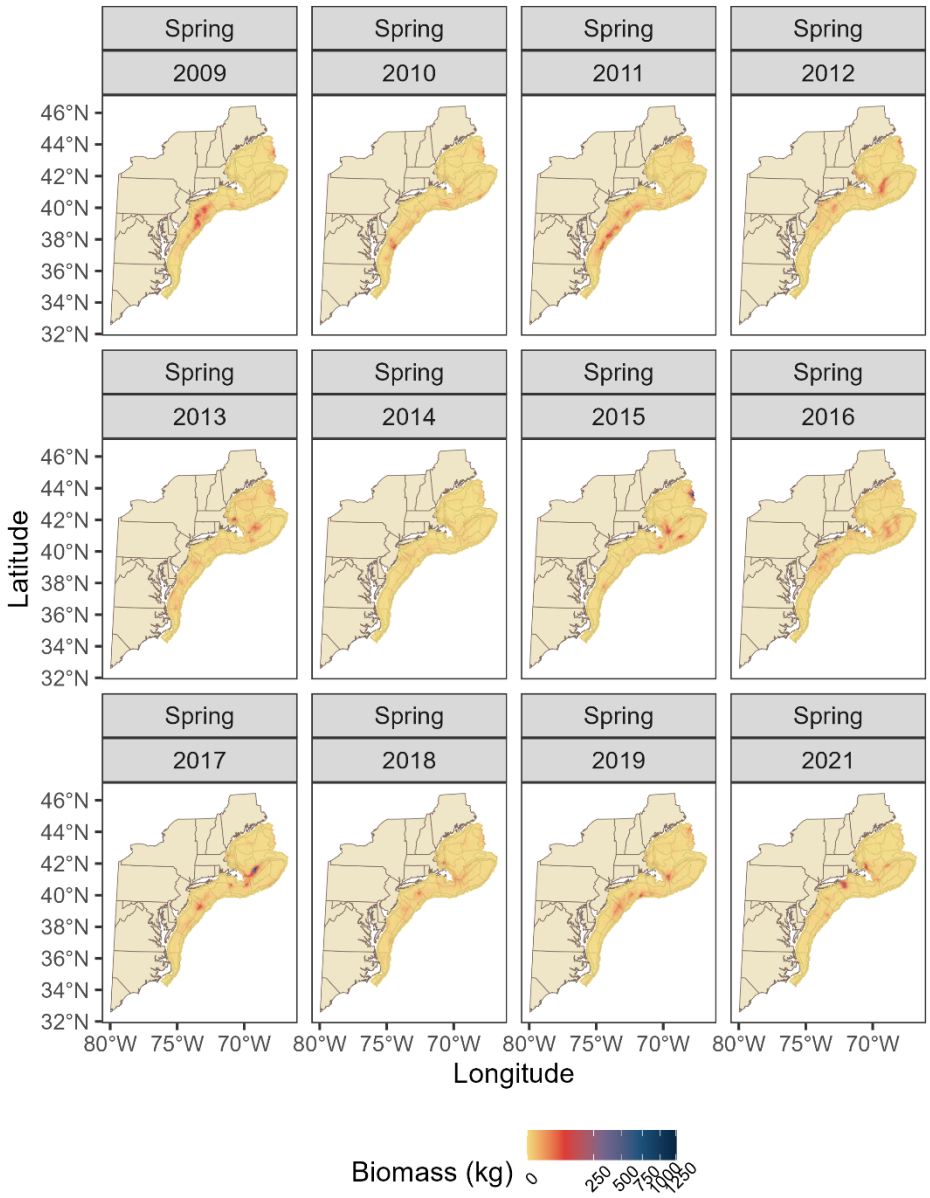

Figure A66. Estimates of biomass across the full time series from the optimal spring model for Atlantic mackerel.

APPENDIX B: TABLES

Table B1. Configurations used to fit the Tweedie observation models predicting Atlantic mackerel biomass catch rates. The candidate models are highlighted in red.

Models	Predictors	Spatial	Spatiotemporal	Time	Shared Range
All data present					
m1	Depth (Penalized spline) Year	-	-	-	Yes
m2	Depth (second-order polynomial) Year	-	-	-	Yes
m3	Depth (Penalized spline) Year Area	-	-	-	Yes
m4	Depth (second-order polynomial) Year Area	-	-	-	Yes
m5	Depth (Penalized spline) Year	On	-	-	Yes
m6	Depth (second-order polynomial) Year	On	-	-	Yes
m7	Depth (Penalized spline) Year Area	On	-	-	Yes

cont. on next page

Table B1 cont.

Models	Predictors	Spatial	Spatiotemporal	Time	Shared Range
All data present					
m8	Depth (second-order polynomial) Year Area	On	-	-	Yes
m9	Depth (Penalized spline) Year	On	IID	Year	Yes
m10	Depth (second-order polynomial) Year	On	IID	Year	Yes
m11	Depth (Penalized spline) Year Area	On	IID	Year	Yes
m12	Depth (second-order polynomial) Year Area	On	IID	Year	Yes
m13	Depth (third-order polynomial) Year	On	IID	Year	Yes
m14	Depth (fourth-order polynomial) Year	On	IID	Year	Yes
Biomass outliers >99th percentile removed					
m15	Depth (Penalized spline) Year	-	-	-	Yes

cont. on next page

Table B1 cont.

Models	Predictors	Spatial	Spatiotemporal	Time	Shared Range
Biomass outliers >99th percentile removed					
m16	Depth (second-order polynomial) Year	-	-	-	Yes
m17	Depth (Penalized spline) Year Area	-	-	-	Yes
m18	Depth (second-order polynomial) Year Area	-	-	-	Yes
m19	Depth (Penalized spline) Year	On	-	-	Yes
m20	Depth (second-order polynomial) Year	On	-	-	Yes
m21	Depth (Penalized spline) Year Area	On	-	-	Yes
m22	Depth (second-order polynomial) Year Area	On	-	-	Yes
m23	Depth (Penalized spline) Year	On	IID	Year	Yes
m24	Depth (second-order polynomial) Year	On	IID	Year	Yes

cont. on next page

Table B1 cont.

Models	Predictors	Spatial	Spatiotemporal	Time	Shared Range
Biomass outliers >99th percentile removed					
m25	Depth (Penalized spline) Year Area	On	IID	Year	Yes
m26	Depth (second-order polynomial) Year Area	On	IID	Year	Yes
m27	Depth (third-order polynomial) Year	On	IID	Year	Yes
m28	Depth (fourth-order polynomial) Year	On	IID	Year	Yes
Biomass at depths >200m removed					
m29	Depth (Penalized spline) Year	On	IID	Year	Yes
m30	Depth (second-order polynomial) Year	On	IID	Year	Yes
m31	Depth (third-order polynomial) Year	On	IID	Year	Yes
m32	Depth (fourth-order polynomial) Year	On	IID	Year	Yes

cont on next page.

Table B1 cont.

Models	Predictors	Spatial	Spatiotemporal	Time	Shared Range
Biomass at depths >200m removed					
m33	Depth (fourth-order polynomial) Year	On	IID	Year	No

Table B2. Diagnostic quantities for the spring Tweedie observation models fit for Atlantic mackerel. For each of the models, the following information is given: Akaike's Information Criterion (AIC), percent deviance explained, the total log-likelihood, the mean squared error across the folds of each cross-validation, and the model convergence. The final candidate models are highlighted in red.

Models	AIC	Deviance Explained	Sum log likelihood	Mean Squared Error	Model Convergence	Cross Validation Convergence
All data present						
m1	11,517.19	97.00%	-5,888.84	1,995.88	True	True
m2	11,663.04	98.23%	-5,936.78	1,945.46	True	True
m3	11,519.16	97.00%	-5,909.85	1,946.49	True	True
m4	11,664.85	98.23%	-5,940.14	1,969.45	True	True
m5	10,861.05	91.42%	-6,959.42	2,129.19	True	True
m6	10,860.20	91.42%	-7,080.82	2,118.72	True	True
m7	10,862.40	91.42%	-6,907.58	2,204.69	True	True
m8	10,861.64	91.41%	-6,974.92	2,170.60	True	True
m9	9,845.20	82.83%	-12,042.42	2,466.68	True	True
m10	9,852.66	82.89%	-12,835.69	2,235.19	True	True
m11	9,845.70	82.81%	-12,093.76	2,196.50	True	True
m12	9,853.19	82.88%	-13,845.91	2,167.77	True	True
m13	9,833.31	82.71%	-12,249.59	2,048.80	True	True
m14	9,833.47	82.69%	-12,083.44	2,114.91	True	True
Biomass outliers >99th percentile removed						
m15	9,858.75	97.76%	-4,942.90	36.07	True	True
m16	9,955.71	98.72%	-5,012.92	36.18	True	True

cont. on next page

Table B2 cont.

Models	AIC	Deviance Explained	Sum log likelihood	Mean Squared Error	Model Convergence	Cross Validation Convergence
Biomass outliers >99th percentile removed						
m17	9,859.63	97.75%	-4,942.15	35.71	True	True
m18	9,952.77	98.67%	-4,994.10	36.43	True	True
m19	9,384.16	93.00%	-5,031.67	37.27	True	True
m20	9,383.65	92.99%	-5,005.25	37.32	True	True
m21	9,385.22	92.99%	-4,955.16	36.97	True	True
m22	9,384.81	92.98%	-4,973.61	37.22	True	True
m23	8,607.62	85.25%	-7,073.02	56.22	True	True
m24	8,611.95	85.30%	-7,277.47	52.17	True	True
m25	8,615.95	85.32%	-7,070.21	42.35	False	False
m26	8,613.69	85.29%	-7,263.21	49.80	True	True
m27	8,597.89	85.14%	-7,038.54	46.81	True	True
m28	8,599.09	85.13%	-7,232.99	47.14	True	True
Biomass at depths >200m removed						
m29	8,942.61	83.43%	-11,557.58	2,696.41	True	True
m30	8,943.20	83.44%	-11,120.87	2,536.75	True	True
m31	8,933.66	83.33%	-11,031.87	2,371.88	True	True
m32	8,930.46	83.28%	-11,711.63	2,501.87	True	True
m33	8,912.83	83.10%	-	-	True	-

Table B3. Configurations used to fit the Delta gamma observation models predicting Atlantic mackerel biomass catch rates. The candidate models are highlighted in red.

Models	Predictors	Family	Spatial	Spatiotemporal	Time	Shared range
All data present						
m1	Depth (Penalized spline) Year	Binomial (*Component 1*)	-	-	-	-
		Gamma (*Component 2*)	-	-	-	-
m2	Depth (second-order polynomial) Year	Binomial (*Component 1*)	-	-	-	-
		Gamma (*Component 2*)	-	-	-	-
m3	Depth (Penalized spline) Year Area	Binomial (*Component 1*)	-	-	-	-
		Gamma (*Component 2*)	-	-	-	-
m4	Depth (second-order polynomial) Year Area	Binomial (*Component 1*)	-	-	-	-
		Gamma (*Component 2*)	-	-	-	-
m5	Depth (Penalized spline) Year	Binomial (*Component 1*)	On	-	-	-
		Gamma (*Component 2*)	On	-	-	-

cont. on the next page

Table B3 cont.

Models	Predictors	Family	Spatial	Spatiotemporal	Time	Shared range
All data present						
m6	Depth (second-order polynomial) Year	Binomial (*Component 1*)	On	-	-	-
		Gamma (*Component 2*)	On	-	-	-
m7	Depth (Penalized spline) Year Area	Binomial (*Component 1*)	On	-	-	-
		Gamma (*Component 2*)	On	-	-	-
m8	Depth (second-order polynomial) Year Area	Binomial (*Component 1*)	On	-	-	-
		Gamma (*Component 2*)	On	-	-	-
m9	Depth (Penalized spline) Year	Binomial (*Component 1*)	On	IID	Year	Yes
		Gamma (*Component 2*)	On	IID	Year	Yes
m10	Depth (second-order polynomial) Year	Binomial (*Component 1*)	On	IID	Year	Yes
		Gamma (*Component 2*)	On	IID	Year	Yes

cont. on the next page

Table B3 cont.

Models	Predictors	Family	Spatial	Spatiotemporal	Time	Shared range
All data present						
m11	Depth (Penalized spline) Year Area	Binomial (*Component 1*)	On	IID	Year	Yes
		Gamma (*Component 2*)	On	IID	Year	Yes
m12	Depth (second-order polynomial) Year Area	Binomial (*Component 1*)	On	IID	Year	Yes
		Gamma (*Component 2*)	On	IID	Year	Yes
m13	Depth (third-order polynomial) Year	Binomial (*Component 1*)	On	IID	Year	Yes
		Gamma (*Component 2*)	On	IID	Year	Yes
m14	Depth (fourth-order polynomial) Year	Binomial (*Component 1*)	On	IID	Year	Yes
		Gamma (*Component 2*)	On	IID	Year	Yes

cont. on the next page

Table B3 cont.

Models	Predictors	Family	Spatial	Spatiotemporal	Time	Shared range
Biomass outliers >99th percentile removed						
m15	Depth (Penalized spline) Year	Binomial (*Component 1*)	-	-	-	-
		Gamma (*Component 2*)	-	-	-	-
m16	Depth (second-order polynomial) Year	Binomial (*Component 1*)	-	-	-	-
		Gamma (*Component 2*)	-	-	-	-
m17	Depth (Penalized spline) Year Area	Binomial (*Component 1*)	-	-	-	-
		Gamma (*Component 2*)	-	-	-	-
m18	Depth (second-order polynomial) Year Area	Binomial (*Component 1*)	-	-	-	-
		Gamma (*Component 2*)	-	-	-	-
m19	Depth (Penalized spline) Year	Binomial (*Component 1*)	On	-	-	-
		Gamma (*Component 2*)	On	-	-	-

cont. on the next page

Table B3 cont.

Models	Predictors	Family	Spatial	Spatiotemporal	Time	Shared range
Biomass outliers >99th percentile removed						
m20	Depth (second-order polynomial) Year	Binomial (*Component 1*)	On	-	-	-
		Gamma (*Component 2*)	On	-	-	-
m21	Depth (Penalized spline) Year Area	Binomial (*Component 1*)	On	-	-	-
		Gamma (*Component 2*)	On	-	-	-
m22	Depth (second-order polynomial) Year Area	Binomial (*Component 1*)	On	-	-	-
		Gamma (*Component 2*)	On	-	-	-
m23	Depth (Penalized spline) Year	Binomial (*Component 1*)	On	IID	Year	Yes
		Gamma (*Component 2*)	On	IID	Year	Yes
m24	Depth (second-order polynomial) Year	Binomial (*Component 1*)	On	IID	Year	Yes
		Gamma (*Component 2*)	On	IID	Year	Yes

cont. on the next page

Table B3 cont.

Models	Predictors	Family	Spatial	Spatiotemporal	Time	Shared range
Biomass outliers >99th percentile removed						
m25	Depth (Penalized spline) Year Area	Binomial (*Component 1*)	On	IID	Year	Yes
		Gamma (*Component 2*)	On	IID	Year	Yes
m26	Depth (second-order polynomial) Year Area	Binomial (*Component 1*)	On	IID	Year	Yes
		Gamma (*Component 2*)	On	IID	Year	Yes
m27	Depth (third-order polynomial) Year	Binomial (*Component 1*)	On	IID	Year	Yes
		Gamma (*Component 2*)	On	IID	Year	Yes
m28	Depth (fourth-order polynomial) Year	Binomial (*Component 1*)	On	IID	Year	Yes
		Gamma (*Component 2*)	On	IID	Year	Yes
Biomass at depths >200m removed						
m29	Depth (Penalized spline) Year	Binomial (*Component 1*)	On	IID	Year	Yes
		Gamma (*Component 2*)	On	IID	Year	Yes

cont. on the next page

Table B3 cont.

Models	Predictors	Family	Spatial	Spatiotemporal	Time	Shared range
Biomass at depths >200m removed						
m30	Depth (second-order polynomial) Year	Binomial (*Component 1*)	On	IID	Year	Yes
		Gamma (*Component 2*)	On	IID	Year	Yes
m31	Depth (third-order polynomial) Year	Binomial (*Component 1*)	On	IID	Year	Yes
		Gamma (*Component 2*)	On	IID	Year	Yes
m32	Depth (fourth-order polynomial) Year	Binomial (*Component 1*)	On	IID	Year	Yes
		Gamma (*Component 2*)	On	IID	Year	Yes
m33	Depth (fourth-order polynomial) Year	Binomial (*Component 1*)	On	IID	Year	No
		Gamma (*Component 2*)	On	IID	Year	No
m34	Depth (fourth-order polynomial) Year	Binomial (*Component 1*)	On	IID	Year	Yes
		Gamma (*Component 2*)	On	IID	Year	No

cont. on the next page

Table B3 cont.

Models	Predictors	Family	Spatial	Spatiotemporal	Time	Shared range
Biomass at depths >200m removed						
m35	Depth (fourth-order polynomial) Year	Binomial (*Component 1*)	On	IID	Year	No
		Gamma (*Component 2*)	On	IID	Year	Yes
m36	Depth (fourth-order polynomial) Year	Binomial (*Component 1*)	On	IID	Year	No
		Gamma (*Component 2*)	-	IID	Year	-

Table B4. Diagnostic quantities for the spring Delta gamma observation models fit for Atlantic mackerel. For each of the models, the following information is given: Akaike's Information Criterion (AIC), percent deviance explained, the total log-likelihood, the mean squared error across the folds of each cross-validation, and the model convergence. The final candidate models are highlighted in red.

Models	AIC	Deviance Explained	Sum log likelihood	Mean Squared Error	Model Convergence	Cross Validation Convergence
All data present						
m1	11,278.55	95.43%	-5,730.74	1,956.96	True	True
m2	11,479.75	97.15%	-5,846.20	2,006.75	True	True
m3	11,281.93	95.43%	-5,768.61	2,056.36	True	True
m4	11,478.66	97.10%	-5,868.22	2,003.53	True	True
m5	10,438.92	88.22%	-7,178.20	2,088.47	True	True
m6	10,439.39	88.23%	-7,400.34	2,216.34	True	True
m7	10,442.09	88.22%	-7,080.00	2,170.32	True	True
m8	10,442.42	88.22%	-7,148.29	2,151.45	True	True
m9	9,660.76	81.57%	-10,457.93	1,999.92	True	True
m10	9,670.35	81.65%	-11,227.74	2,038.89	True	True
m11	-	-	-	-	-	-
m12	9,673.30	81.64%	-11,607.08	1,967.02	True	True
m13	9,647.24	81.42%	-10,838.71	2,045.53	True	True
m14	9,640.44	81.33%	-10,434.19	1,986.94	True	True
Biomass outliers >99th percentile removed						
m15	9,714.55	96.59%	-4,858.68	36.33	True	True
m16	9,827.79	97.73%	-4,941.02	36.50	True	True

cont. on the next page

Table B4 cont.

Models	AIC	Deviance Explained	Sum log likelihood	Mean Squared Error	Model Convergence	Cross Validation Convergence
Biomass outliers >99th percentile removed						
m17	9,714.54	96.55%	-4,854.76	35.80	True	True
m18	9,819.34	97.60%	-4,934.96	36.38	True	True
m19	9,073.31	90.10%	-4,827.97	36.17	True	True
m20	9,075.19	90.12%	-4,958.22	36.91	True	True
m21	9,073.55	90.06%	-4,880.65	36.58	True	True
m22	9,074.70	90.07%	-4,913.54	36.74	True	True
m23	8,480.28	84.13%	-5,882.63	36.33	True	True
m24	8,484.46	84.17%	-6,054.02	38.60	True	True
m25	8,483.98	84.12%	-5,827.27	37.89	True	True
m26	8,487.77	84.16%	-6,094.83	38.66	True	True
m27	8,467.82	83.96%	-5,852.50	38.49	True	True
m28	8,464.18	83.89%	-5,845.95	38.23	True	True
Biomass at depths >200m removed						
m29	8,818.24	82.54%	-9,211.70	2,251.81	True	True
m30	8,811.24	82.47%	-8,423.96	2,248.19	True	True
m31	8,808.24	82.40%	-8,344.62	2,213.10	True	True
m32	8,802.19	82.31%	-8,286.17	2,330.05	True	True
m33	8,803.62	82.29%	-8,690.88	2,311.10	False	False
m34	8,804.19	82.31%	-8,441.83	2,310.69	False	False
m35	8,801.62	82.29%	-8,092.74	2,324.47	True	True
m36	8,799.62	82.29%	-8,305.95	2,216.04	True	True